EXTRUSION OF ALUMINIUM-LITHIUM ALLOYS

A Thesis Submitted for the Degree of

Doctor of Philosophy of the University of London

by

NICHOLAS CHARLES PARSON

November 1984

John Percy Research Group
Department of Metallurgy and
Materials Science
Imperial College
London

ABSTRACT

Considerable interest has been shown in aluminium alloys containing lithium, primarily through their improvement in strength to weight ratio and specific modulus over existing aerospace alloys. The system is heat treatable to varying levels of strength dependent on the alloy additions. The present work is based on an aluminium - 2.5% Li - 3.5% Mg - 0.15% Zr ternary alloy and a quaternary with an addition of 0.8% copper, giving an alloy capable of higher strength levels.

Material was received as DC cast blocks and processed by the extrusion route consisting of three steps - homogenisation, extrusion and heat treatment. Having established suitable homogenisation practices, the first stage was an investigation into the variation of extruded structures with the process variables. Empirical relationships were derived for the dependence of extrusion pressure on the process conditions and the extrusion limits for both alloys were determined. Hot torsion testing was performed to simulate extrusion and to characterize the high temperature flow stress behaviour along with hot ductility.

The ageing characteristics were studied using mechanical property measurements, DSC and transmission electron microscopy and standard heat treatments were established. This enabled the variation of mechanical properties with extrusion conditions for the peak strength temper to be fully investigated.

The remaining section of the work concentrated on the more complex properties of toughness, stress corrosion resistance and corrosion resistance where high strength aluminium alloys are often susceptible. Again, variations with process parameters, together with the level of heat treatment were studied. In an attempt to improve toughness, a cold working operation was included in the heat treatment cycle.

In addition to the two initial compositions, several alloys were prepared by chill casting with varying levels of copper to further study the effects of this element.

TABLE OF CONTENTS

LIST OF FIGURES

LIST OF TABLES

CHAPTER ONE

LITERATURE SURVEY

1.1 High Strength Aerospace Materials

1.1.1 Conventional High Strength Aluminium Alloys

The Al-Cu, Al-Cu-Mg and Al-Zn-Mg-Cu heat treatable alloy systems were developed primarily for aircraft construction. General reviews on the literature concerning these alloys can be found in references 1-3.

Although the binary Al-Cu system shows good response to artificial ageing there are few commercial alloys based on it. The Al-Cu-Mg alloys are capable of higher strength levels and are widely used in aircraft structures. A typical example is 2014 where the response to ageing is raised by the high silicon content. The precipitation sequence in this system can proceed by a combination of two routes :

(a) The Al-Cu binary sequence, where θ' is the main strengthening agent and $CuAl_2$ is the stable product.

(b) The Al-Cu-Mg ternary sequence, where S' is the metastable semicoherent phase and the stable product is the S phase (Al_2CuMg).

Al-Zn-Mg-Cu alloys offer the greatest response to age hardening of any aluminium alloys, and 7075 is probably the best known of these. Low temperature ageing gives maximum hardening due to GP zone formation. However, a duplex ageing treatment, termed the T73 temper is often used to improve resistance to stress corrosion and exfoliation attack and this gives reduced strength. Here, an additional high temperature age is given to produce an even dispersion of M' ($MgZn_2$). Improved toughness in these alloys has been achieved by the removal of iron and silicon impurities and the alloy 7475 is an example of such a development

1.1.2 The Development of Aluminium - Lithium Alloys

The effects of lithium additions to aluminium alloys were studied as long ago as the 1920's when considerable effort went into producing heat treatable alloys similar to duralumin. Throughout the 40's and 50's the development of the Al-Cu-Mg and Al-Zn-Mg-Cu systems dominated aluminium alloy research, but in 1957 the commercial Al-Li-Cu alloy X-2020 was introduced in the U.S. This was produced with the targets of high specific strength and modulus, but only had one production application where it replaced 7075T651 in the wing skins of a U.S. Navy aircraft. However, it exhibited low ductility and toughness and was withdrawn from production. Work in the U.S.S.R. during the 1960's lead to the development of the commercial Al-Li-Mg alloy 01420 but the extent to which this has been used in service is unclear. Serious research in Great Britain and the U.S. began in the 1970's, with the incentive of reduced airframe weight and fuel consumption. Starting with the Al-Li-Mg and Al-Li-Cu systems, this has progressed along ingot and powder metallurgy routes and the most recent results point to the use of the Al-Li-Cu-Mg quaternary for high strength applications.

1.1.3 Aluminium - Lithium Alloys as Aircraft Structural Materials

A recent study[4] compared aluminium-lithium alloys with other contending airframe materials, i.e. titanium base alloys and carbon fibre reinforced composites (CFC). To be competitive, the alloys must be cheap, easy to fabricate and, of course, must possess adequate properties. The extra cost and difficulty in fabrication associated with titanium alloys makes their use unlikely except in those applications requiring high temperature or corrosion resistance. Fig. 1.1, from Peel et al[4], compares the specific strengths of the contending materials, in tension and compression, together with a standard 2014 alloy. The Al-Li alloy shown is that developed by RAE, DTDXXXA. CFC has the advantage in tension with a longitudinal fibre lay-up but the strength declines rapidly as the fraction of such fibres is reduced. The metals perform better in compression with Al-Li showing

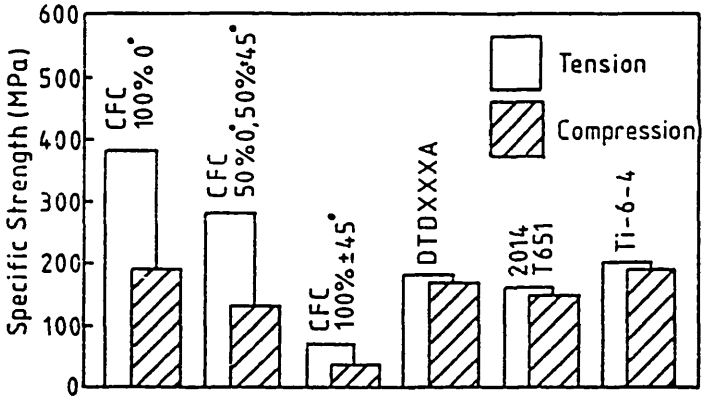

Fig 1.1 Specific design allowable strengths for candidate airframe materials (after Peel et al(4)).

Company/Sponsor	MFG Type	Low Strength	Medium Strength	High Strength	DADTA
LMSC/DARPA	PM		7075-T76 +30% E/ρ	7075-T76 +20% E/ρ +20% $\sigma y/\rho$	
Boeing/AFWAL	PM	2024-T3, T4 -10% ρ	7075-T73 +30% E/ρ	7075-T73 +20% E/ρ +20% $\sigma y/\rho$	
CALAC/NASA	PM,IM	2024-T3 -10% ρ +10% Fatigue		7075-T76 +10-20% σy +8% E +10% Fatigue	
Alcoa/Boeing	IM	2024-T3 -10% ρ		7075-T6 -7% ρ	2324-T39 -9% ρ
BACO, RAE ALCAN, RAE BRIT, Aerospace	IM	2024-T3 -10% ρ	2014-T6 -10% ρ	7075-T6 -10% ρ	
Alcoa/NAVAIR	IM	2024-T3 -8% ρ		7075-T6 -8% ρ	

Table 1.1 Targets of the various Al-Li development programs (after Quist et al(5)).

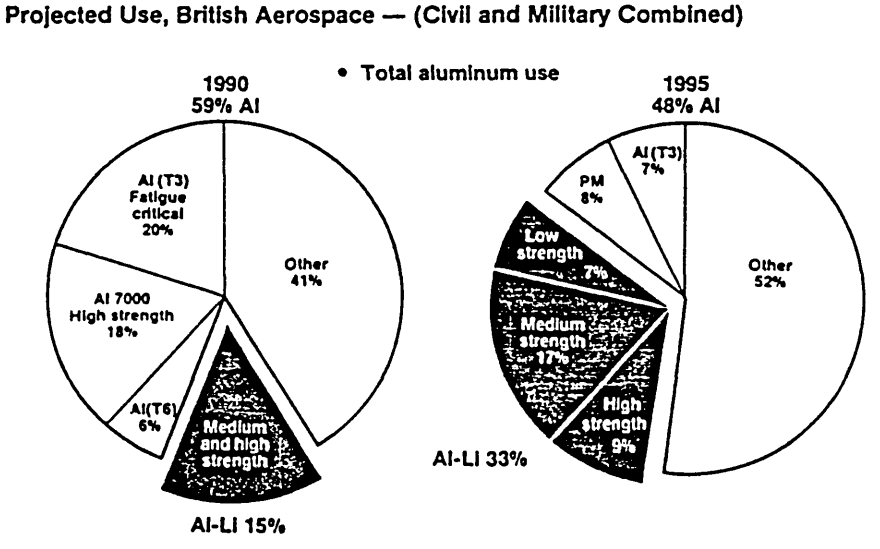

Fig 1.2 Predictions for Al-Li alloy usage (after Quist et al(5)).

a slight improvement over 2014. Peel also compared specific elastic and shear moduli. Here the tensile modulus of CFC with a 100% 0° lay-up was the highest, approximately double that of the Al-Li alloy, but this corresponded to the lowest shear modulus. To improve the latter, a larger proportion of fibres aligned at 45° was required which was accompanied by a serious strength loss. Thus, the metallic materials were at an advantage in shear and of these the Al-Li alloy had the highest moduli.

Quist et al have reviewed the various target property levels and predicted usage of Al-Li alloys set by the aluminium producers and manufacturers[5]. On the basis of weight saving they are expected to give at least a 10% reduction in airframe weight with the possibility of up to 15% by resizing and redesign, together with the use of new construction techniques. Values quoted for CFC are between 20-30%. The extent to which either of these materials is used will depend on whether or not the respective property goals are achieved.

The advantage of using the aluminium-lithium alloys is that they can be manufactured using current aluminium technology and can initially simply replace existing alloys in airframes. Table 1.1 lists the reported property goals set by the various Al-Li alloy development programs in the U.K. and the U.S. Most of the targets require improved modulus, density and specific strength over conventional alloys, whilst maintaining similar other properties. Fig. 1.2 shows projections made by British Aerospace as to the extent to which such alloys may be applied in civil and military aircraft. By 1995 it is anticipated that they will contribute one third of the total airframe weight.

1.2 The Metallurgy of Aluminium Alloys Containing Lithium

1.2.1 The Al-Li Binary

The addition of lithium to aluminium is initially attractive for aerospace applications, since each weight percent lithium reduces the density by 3% and increases the modulus by 6%[6]. The system is

also heat treatable, with the strength increasing with lithium content[7]. The mechanical properties are poor, however, in comparison with 2000 and 7000 series alloys.

The equilibrium structure in alloys of commercial interest is the aluminium based solid solution and the δ phase (AlLi). Up to 12 atom % lithium can be held in solid solution by quenching and the solid solubility curve exhibits the reduction in solute concentration necessary for age hardening response. The subsequent decomposition of the supersaturated solid solution through a low temperature ageing treatment leads to precipitation of the metastable phase δ' (Al_3Li), first identified by Silcock[8]. This possesses an ordered Ll_2 type structure[9] which consists of an FCC unit cell with aluminium atoms on the cube faces and lithium atoms at the corner sites. The lattice parameter of this structure is close to that of the aluminium matrix, resulting in a low misfit strain[9, 10] and interfacial energy[9]. The activation energy is therefore low and superlattice spots arising from the ordered structure have been observed in solution treated material[10,11]. Coarsening during ageing has been shown to follow Lifshitz-Wagner kinetics, that is the average particle size is proportional to the cube root of time, for a wide range of conditions. The metastable and stable solvi have been reported in fairly good agreement by several workers[9, 10, 12, 13].

Noble et al[14] investigated the effect of composition and heat treatment on the modulus of Al-Li and Al-Li-Mg alloys and obtained values in the range of 79 to 83 GPa for 2-3 wt.%Li. Although small increases occurred on ageing, they attributed most of the high modulus to the effects of lithium in solid solution. Magnesium additions reduced the modulus by 0.5 GPa per atom % but did not adversely affect the specific modulus.

1.2.2 The Al-Li-Mg Ternary

The ternary system offers improved strength over the binary alloy. Dinsdale et al[15] studied the effects of magnesium additions to an Al-2 wt.%Li alloy. Below 2 wt.%Mg they reported a hardening

rate of 50 MPa/wt.%Mg in aged material compared to that in binary Al-Mg alloys of 20 MPa/wt.%, indicating that this element is producing more than a solid solution strengthening effect. They proposed that magnesium was either affecting the density of Al_3Li nucleation sites or dissolving in the metastable phase to make the extra contribution. On this point, Gregson[16] showed that magnesium was dissolving in δ' by lattice parameter measurements.

Levinson and McPherson studied the phase relationships in the ternary system and produced several isothermal sections. Fig. 1.3 is such a section at 200°C which is close to typical ageing temperatures[15, 18]. The target composition of the ternary alloy in the present work is shown. Extra precipitation of the Al_2MgLi phase would appear likely and Thompson and Noble[11] determined the precipitation sequence in this system to be,

$$SSS \rightarrow \delta' \rightarrow Al_2MgLi$$

Thus, Al_2MgLi replaces AlLi formed in the binary alloy. It forms as rods or laths with <110> growth directions and is promoted by high ageing temperatures (> 170°C) or over ageing. The interface is incoherent and nucleation occurs at heterogeneous sites.

1.2.3 The Al-Li-Cu Ternary

Early work[7, 19] indicated that additions of copper considerably increase the strength of Al-Li alloys without a corresponding decrease in ductility. The old commercial alloy X-2020 (Al-4.5Cu-1.2Li-0.5Mn-0.2Cd) was based on this system and hence the literature here is more extensive. The phase equilibria of Al-Li-Cu alloys were investigated by Hardy and Silcock[20] who constructed isothermal sections. Fig. 1.4 is their section at 350°C where the ternary phases are coded as follows;

$$T_B = Al_{7.5}Cu_4Li,\ T_1 = Al_2CuLi,\ T_2 = Al_6CuLi_3$$

The quaternary alloy used in the present work is marked on this diagram and the possible phases from this ternary system are AlLi and T_2.

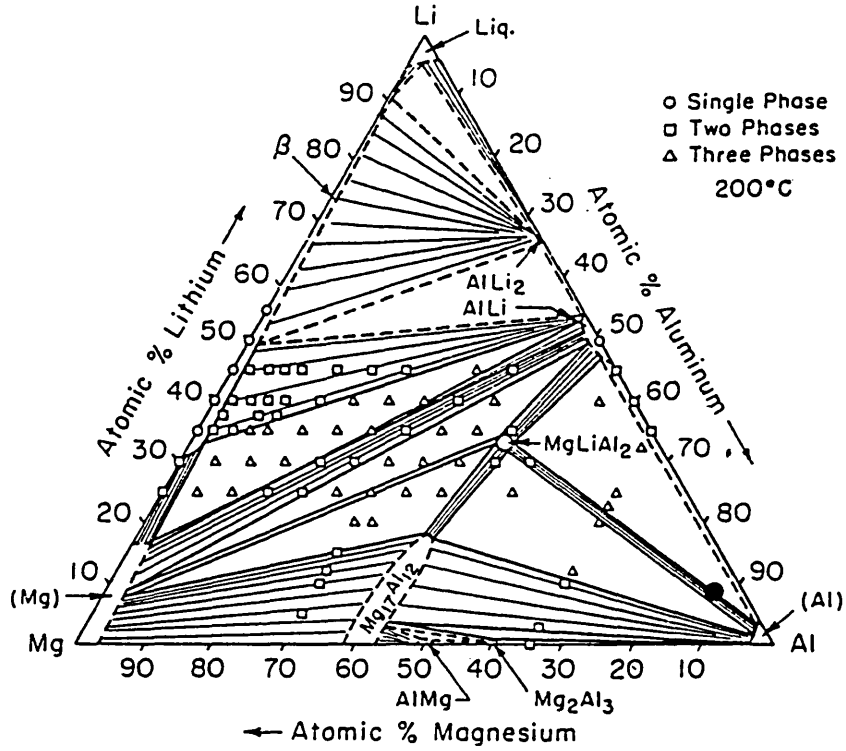

Fig 1.3 Isothermal section of the Al-Li-Mg system (after Levinson and McPherson(17)).

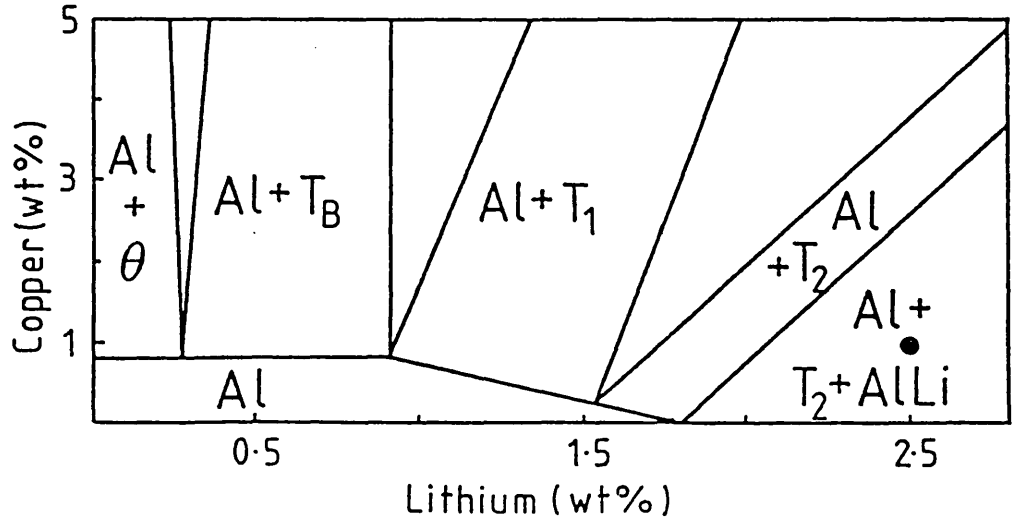

Fig 1.4 Isothermal section of the Al-Li-Cu system at 350°C (after Hardy and Silcock(20)).

Silcock[8] investigated the phases formed by ageing alloys from this system at 165°C and superimposed her results on the original isothermal section, which is reproduced in Fig. 1.5. The products of the binary Al-Cu and Al-Li systems are possible, together with ternary phases, and the precipitation sequences can be summarised as follows:

$$\begin{array}{lcccl} \text{SSS} & \rightarrow & \text{GP zones} & \rightarrow & \theta'' \rightarrow \theta' \\ & & T_1(Al_2CuLi) & & \\ & & \delta' & \rightarrow & \delta \end{array}$$

From reported ageing products in various alloys it would appear that θ' and T_1 are predominant in high copper low lithium alloys such as 2020[21], whereas at high Li:Cu ratios T_1 and δ' are the main products[22]. However, Noble and Thompson studied two compositions, Al-3.5 Cu-1.5 Li and Al-2.5 Cu-2 Li, and found T_1 to be the predominant precipitate[23]. This phase formed on {111} planes and they identified the orientation relationship.

The level of copper addition in the quaternary alloy in the present study is below any of the above values, but Silcock's results[8] suggest that δ' will be the main precipitate formed on ageing, with the possibility of T_1 formation.

1.2.4 The Al-Li-Cu-Mg Quaternary

Much of the recent work on Al-Li alloy development has centred on the Al-Li-Cu-Mg system[4, 24, 25, 26] and it would appear to offer the combination of high strength and toughness comparable with existing alloys. The quaternary is complex with an unknown phase diagram, but a combination of the two lithium ternary systems, together with the Al-Cu-Mg system is to be expected. Fig. 1.6 is an isothermal section through the latter at 190°C, from Polmear[27]. Again the composition of the alloy in the current investigation is marked and lies within the $S(Al_2CuMg)$ and $T(Al_6CuMg_4)$ phase region.

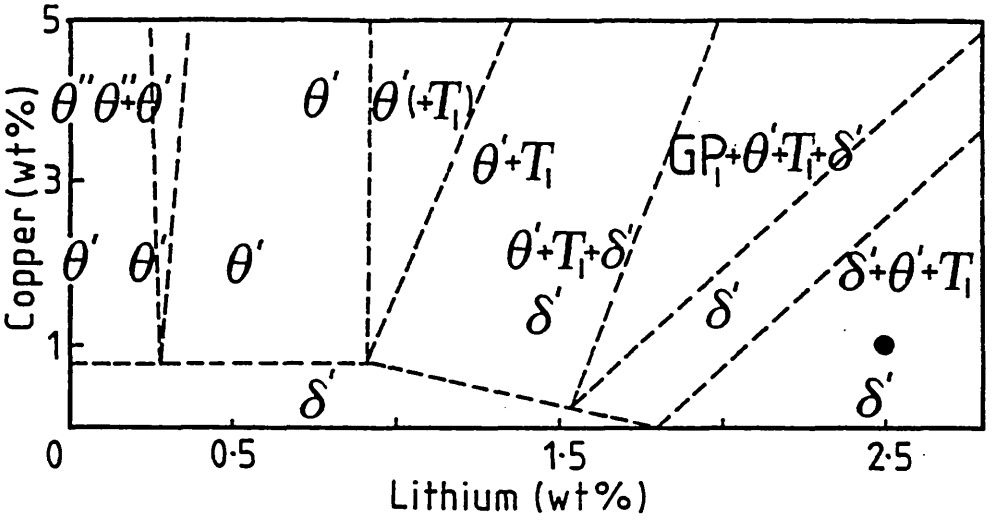

Fig 1.5 Precipitate phases in the Al-Li-Cu system after ageing at 165°C for 16 hours (after Silcock(8)).

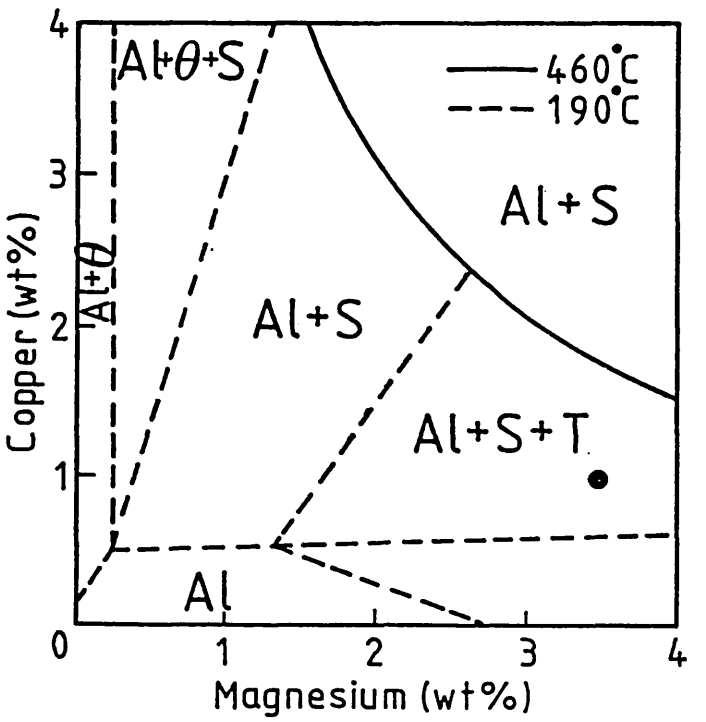

Fig 1.6 Isothermal sections of the Al-Cu-Mg system (after Polmear(27)).

Reported precipitation sequences in the quaternary alloys under development[4,25] are predominantly those producing δ', S' and T_1, where S' is the intermediate form of the S phase. Most of the strengthening arises from the Al_3Li phase and S' and T_1 act as slip dispersing agents. The latter are dislocation nucleated and special heat treatments have been developed to promote their formation[16]. Unlike δ', PFZs of these phases are not formed. Most of the compositions under investigation, such as the RAE-Alcan alloy DTDXXXA[4, 24], have low levels of magnesium addition, whereas in the present work this is quite high, approximately 4 wt.%, with a copper level of 1 wt.%. On a qualitative basis the high Mg:Cu ratio ought to promote the Al-Li-Mg and possibly Al-Cu-Mg sides of the system, rather than the copper and lithium containing phases. From this argument the most likely ageing products will be Al_3Li with the possibility of some S' formation. Al_2MgLi and Al_2CuMg are the probable equilibrium phases.

1.3 The Processing Route for High Strength Aluminium Alloys

The basic route for the production of a high strength aluminium alloy extrusion from DC cast material involves at least three separate processes;

1. Homogenisation
2. Hot Working (Extrusion)
3. Precipitation Hardening.

1.3.1 Homogenisation

As cast material is generally given a high temperature treatment prior to any working operation. This has several important effects with regard to the production of a more isotropic structure and alleviating cracking during working[28, 29]:

1. Relief of residual stresses induced during casting.
2. Reduction of segregation and breakdown of large intermetallics.
3. Removal of non-equilibrium low melting point eutectics.
4. Precipitation and redistribution of intermetallic dispersoids.

The last effect is particularly important for high strength alloys where dispersoid forming elements are added to control recrystallisation. They usually remain in supersaturation after casting and a high temperature treatment is necessary to allow precipitation. Once formed, the particles remain relatively stable at hot working temperatures.

1.3.2 Hot Working

1.3.2.1 Hot Deformation

Normally the term hot working is applied to deformation above 0.5 of the homologous melting temperature. It is characterised by a steady state flow stress, allowing very high strains, as opposed to the work hardening encountered during cold working operations. Available hot working flow stress data has been reviewed by several workers[30,31,32] and a general relationship has been established relating the flow stress to the strain rate and temperature. This can be rewritten in a more convenient form using the Zener-Hollomonn parameter (Z) which is a temperature compensated strain rate. The derivations of these expressions are outlined in section 2.1.

The steady state is a result of dislocation generation being balanced by dynamic softening processes. In aluminium alloys, where partial dislocation formation is limited due to the high stacking fault energy, dynamic recovery is the dominant softening mechanism. This region of the stress-strain curve is associated with a constant dislocation density and a subgrain structure of fixed dimensions, shape and misorientation, made possible by repolygonisation[33]. The substructure is sensitive to changes in temperature and strain rate, with higher Z values promoting smaller subgrains. A refinement of the subgrain size results in an increase in the room temperature yield stress and expressions based on Hall-Petch type relationships have been used to fit such data[34, 35]. The stored strain energy after deformation, in the form of the substructure, provides a driving force for static restoration processes which may destroy the hot worked structure if the product is not quenched. This can proceed by recovery and recrystallisation but the final structure is often still related to the process conditions.

1.3.2.2 Extrusion

Direct extrusion is simple in operation and has the advantage that complex shapes can easily be produced. For many sections it is the only possible production method. In a typical modern transport aircraft the use of this product form may be as large as 28%[5]. The main variables with regard to a material property investigation are the initial temperature, ram speed and extrusion ratio, although other factors such as lubrication and tooling temperature will affect extrudability. As with other mechanical working operations, extrusion exhibits a characteristic load displacement locus showing an initial peak, followed by a load drop to give a steady state region. The various aspects of the process have been extensively reviewed, together with the analyses developed to predict breakthrough pressure, temperature rise and strain rate[2, 36].

The extrusion of aluminium alloys produces a structure with marked directionality[37]. Original grains are elongated parallel to the extrusion direction, together with any inclusion particles present. As a result, material properties are strongly dependent on the test direction. The distribution of deformation is not uniform across the section and the surface layers undergo considerably higher strains. This can provide a driving force for static recrystallisation in these regions, giving rise to a recrystallised annulus. Extrusions also possess a marked fibre texture, if the hot worked structure is retained, which gives a strength contribution in the longitudinal direction.

1.3.3 Precipitation Hardening

The basic heat treatment given to aluminium alloys is a two stage process, consisting of a solution treatment followed by artificial ageing[38, 39, 40]. More complex treatments often include several ageing steps and intermediate cold or warm working.

1.3.3.1 Solution Treatment

The material is given a solution soak at a temperature within the single phase region, followed by a rapid quench, usually into cold water. This produces a supersaturated solid solution which provides the driving force for precipitation. In addition, the quench also retains the high temperature vacancy concentration. An excess above the equilibrium value can remain for significant times, in spite of the presence of vacancy sinks, due to entrapment by solute atoms and vacancy disc formation. The vacancy concentration can be raised by increasing the quench rate, although this is reported to have little effect on the subsequent ageing of Al-Li alloys[9]. The soak time given usually depends on the component thickness.

1.3.3.2 Ageing Treatment

Aluminium-lithium alloys do not produce a significant natural ageing response[4], although Al_3Li superlattice reflections have been observed in quenched material [11,41]. Nucleation and growth of the precipitating phase can be accelerated by holding at an elevated temperature within the two phase region. The driving force for this reaction is the volume free energy change which must overcome the energies associated with the formation of a new interface and misfit strain. An activation energy is therefore required and this corresponds to a critical particle radius. Metastable transition phases, such as δ', require a lower activation energy than the stable precipitates and their formation allows a more rapid free energy decrease. Nucleation is always heterogeneous and takes place at non-equilibrium defects such as point defects and dislocations. The density of precipitate nuclei is controlled by the ageing temperature with lower temperatures promoting a finer dispersion due to the increased driving force.

1.3.3.3 Strengthening Mechanism

The increase in yield stress on ageing Al-Li alloys is due to the interaction between glide dislocations and the Al_3Li precipitates.

In general precipitates can be divided into two groups[39], depending on the nature of this interaction;

1. Precipitates sheared by dislocations. These are generally coherent facilitating the transfer of slip.
2. Unshearable precipitates acting as obstacles to slip, causing dislocation looping.

In general, coherent precipitates produce the highest strength levels, and Al_3Li falls into this category. The level of their resistance to dislocation motion can be caused by the following factors;

1. The degree of order in the precipitate
2. Coherency strains
3. Modulus difference between the precipitate and matrix
4. Surface energy, chemical energy and stacking fault energy.

These are effectively energy terms which have to be balanced by the applied stress in order for a glide dislocation to pass through a precipitate. Since the lattice geometry of δ' is similar to that of the matrix, most of the above terms will be low. Noble and coworkers[42] calculated the contribution made by the different terms and concluded that order hardening could account for all strengthening, although modulus could also give a significant effect.

The passage of a single unit dislocation through an ordered lattice such as Al_3Li upsets the order on the slip plane creating an antiphase domain. A more stable dislocation configuration is that of two identical unit dislocations moving as a pair, so that the second one removes the order disturbance. This is termed a superlattice dislocation[43].

As ageing proceeds precipitate coarsening takes place and this is accompanied by a loss of coherency with the matrix, so that eventually a point is reached where it is more favourable for dislocations to bow round, rather than cut the precipitates. The yield stress then

becomes inversely proportional to the interparticle spacing so that further coarsening leads to softening. This condition is termed over-ageing. The change in the dislocation precipitate interaction gives rise to the classical yield stress versus time curve[38].

1.4 Factors Affecting the Properties of High Strength Aluminium Alloys

1.4.1 Toughness

The toughness of commercial aluminium alloys is strongly influenced by the distribution of second phase particles[28, 44]. There are basically three types of these present:

1. Large Fe and Si rich inclusions formed during casting, $\sim$ 0.1 - 10μ in size
2. Intermediate particles, usually containing Zr, Mn or Cr, which act as grain refiners and recrystallisation inhibitors
3. Small precipitates produced by heat treatment, $\leq$ 0.5 μ in size.

Crack extension in 2000 and 7000 series alloys is generally ductile, occurring by void initiation followed by growth and linkage. The coarser precipitates are nearly always harmful to toughness as they can crack and decohere to form voids soon after the onset of plastic flow. In wrought material these are elongated as stringers giving poor short transverse toughness. The intermediate particles are less likely to crack and their effect on toughness is mainly beneficial due to control of grain shape and homogenisation of slip.

The effect of the ageing precipitates on toughness depends on the level of ageing. In general, toughness falls with increasing yield stress due to the lower strain hardening capacity and the tendency for slip localisation. Also the minimum fracture toughness requirements become more demanding as the stress level is raised. Overageing may produce coarse equilibrium precipitates, but toughness is normally raised as a result of increased matrix plasticity. However, for this reason the underaged condition is usually tougher at the same yield stress[28, 45, 46].

1.4.1.1 The Toughness of Lithium Containing Alloys

Although conventional 2000 and 7000 series alloys show a tendency towards strain localisation upon ageing it is believed that ordered precipitates such as Al_3Li cause this to a much greater extent[6]. Once a superlattice dislocation has cut the precipitate, the effective radius of the obstacle on the slip plane is reduced, making it easier for following dislocations to move on that plane. In this way, intense slip bands can be formed, since crosslip is not normally a viable process for superlattice dislocations[43]. The stress concentrations produced when such bands meet grain boundaries have been held responsible for low ductility and toughness in several lithium containing alloys[18, 22, 42]. The magnitude of the stress concentrations produced by strain localisation will increase with the slip distance and therefore the production of an unrecrystallised wrought structure ought to delay crack formation. However, Peel[4] reported that in strongly textured unrecrystallised Al-Li-Mg-Cu sheet, slip bands were able to penetrate several grain boundaries, indicating that they are ineffective barriers to slip. Starke and Lin observed the same effect in an unrecrystallised 2020 type alloy[21] but regarded it as being beneficial to ductility by removing the grain boundary stress concentrations. Much of the reported work on different alloy systems is contradictory, but this is due to the wide range of precipitation reactions possible. Lin attributed low ductility in an Al-Li-Cu alloy to intersubgranular failure in unrecrystallised material and improved this by the production of an elongated recrystallised structure[47]. Here extensive T_1 precipitation along high and low angle boundaries was responsible for the failure mode.

Overageing to change from a precipitate cutting to looping mode can reduce strain localisation but in the commercially attractive Al-Li-Mg composition range this can lead to Al_2MgLi formation at the grain boundaries and their associated PFZs[11]. Harris et al[18] obtained reduced toughness as a result of this treatment due to strain localisation within such regions.

The addition of dispersoid forming elements is common practice in commercial alloys, and can have an important effect on the nature of slip. Manganese additions, forming Al_6Mn dispersoids, have been found to cause nucleation of stable phases within the matrix in Al-Li alloys[48, 49] and Mn containing inclusions have been responsible for reduced toughness in 2020 type alloys[50]. Zirconium is more effective at recrystallisation control[6, 51, 52] and small additions have improved the strength and ductility of Al-Li-Mg alloys[15].

Much recent work has indicated that Al-Li-Cu-Mg alloys offer toughness improvements through coprecipitation of the S phase and its effects on the distribution of slip[4, 24]. Treatments have been devised to produce the optimum dispersion of this phase[16].

There is some argument as to whether grain boundary segregation of impurity elements, such as Na and K introduced with lithium additions, contributes to the low ductility in Al-Li alloys. Relatively large concentrations of these have been detected on fracture surfaces[49, 53] and recently increasing the bulk Na concentration was shown to adversely affect the ductility of an Al-Li binary alloy[54]. However, Webster indicated from his results that there was no correlation between sodium content and ductility in either ingot or powder source material[55].

It has been suggested that hydrogen pick up may also lead to embrittlement by lithium hydride formation. Some work has been done in this area, but the results are inconclusive[56].

1.4.2 Stress Corrosion Cracking

SCC is an important problem for strong aluminium alloys under 'ambient' conditions and has received a great deal of attention. Kruger has listed the general features of this form of attack[57]:

1. The presence of a tensile stress
2. The alloy normally shows good corrosion resistance to the environment
3. SCC can occur more readily in specific environments and species present need only be present in small quantities.
4. Stress Corrosion fracture surfaces appear brittle, although the metal may have good ductility

5. A threshold stress level has normally to be exceeded.

Crack initiation can occur at a variety of sites which act as stress raisers, with the tensile stress frequently being provided by residual stresses. For this reason SCC is often encountered in thick sections[58]. Since SCC is virtually always intergranular the grain size and shape are important. The highly directional structure produced in wrought alloys makes them more susceptible to attack in the short transverse direction, where the large grain faces are directly stressed. The effect of environment on SCC is complex and not well understood, although several models have been proposed[57].

Alloy composition and heat treatment strongly affect susceptibility but there is no simple correlation between strength or toughness and the threshold stress. In general, underaged alloys exhibit the poorest resistance and the most important technique for SCC control is overageing[58]. The reasons for this are again not well understood, but factors such as homogeneity of slip, grain boundary precipitation and PFZ formation are thought to be responsible[59].

When looking at the SCC data on lithium containing alloys, it is important to compare test methods. However, the Al-Li-Mg system is generally regarded as being resistant to this form of attack[60, 61], together with the 2020 type alloy. Alloys containing magnesium and copper have shown susceptibility and Pizzo[62] indicated that this was greater than for 7075T6.

1.4.3 Corrosion Resistance

The literature on this subject is surprisingly limited. Heat treatable aluminium alloys can be susceptible to grain boundary attack in certain tempers, due to local electrochemical cells caused by precipitates and their associated PFZs. Generally the type of treatment given to impart stress corrosion resistance also produces general corrosion resistance. Wrought material can undergo a particular form of attack, that of exfoliation corrosion. Here corrosion attack takes place along elongated grain boundaries beneath the metal surface and the products of this reaction cause lifting of the overlying layer.

Al-Li binary alloys are reported to be susceptible to intergranular corrosion due to the anodic nature of the AlLi precipitate[63]. Magnesium additions alter the precipitation sequence and Al-Li-Mg[51] alloys have good resistance to general and exfoliation corrosion. Those alloys containing magnesium and copper appear to show some susceptibility to exfoliation[4, 24].

CHAPTER TWO

THEORY

In this chapter the constitutive equation is developed relating the flow stress with the process variables. Following this the analyses used to apply this theory to extrusion and torsion are described.

2.1 The Hot Working Equation

The interdependence of the steady state flow stress, strain rate and temperature in hot deformation has been extensively reviewed[30, 31, 32]. Available hot working data consists mainly of compression and torsion results and can be described by two types of expression depending on the stress level:

Low stress $\quad \dot{\varepsilon} = A'\sigma^{n'}$

High stress $\quad \dot{\varepsilon} = A'' \exp(B\sigma)$

Expressions of this form have also been applied to creep testing and this similarity has lead to the use of relationships, originally observed for creep, to analyse hot working even though they represent opposite extremes of strain rate. In this way a hyperbolic sine equation with Arrhenius dependence has been successfully used to correlate hot working data:

$$\dot{\varepsilon} = A\,[\sinh(\alpha\sigma)]^{n} \exp(-\Delta H/RT)$$

At high and low stresses this reduces to the respective power and exponential functions. The use of an Arrhenius term indicates that hot working is a thermally activated process where ΔH is the activation energy of the rate controlling mechanism. The last equation can be rewritten in the form of a temperature compensated strain rate, originally proposed by Zener and Hollomonn.

$$Z = \dot{\varepsilon} \exp(\Delta H/RT) = A[\sinh(\alpha\sigma)]^{n}$$

This parameter is a temperature compensated strain rate and can therefore be used to combine process variables in a single term when investigating material properties.

2.2 Strain Rate in Extrusion

A single value of strain rate for extrusion is difficult to calculate, since it varies with position in the deformation zone. In this work a single triangle axisymmetric upper bound computer model was used to give a mean strain rate. This allowed for energy dissipation due to velocity discontinuities, circumferential straining and container billet friction. Further details can be found in reference[36].

2.3 Temperature in Extrusion

Values of the temperature rise during extrusion were calculated using an integral profile model originally developed by Sheppard and Raybould[64] and are listed in appendix one. They are not totally satisfactory and are given mainly for reference. In the results sections the temperatures and values of lnZ quoted refer to the initial extrusion conditions, unless otherwise stated.

2.4 Torsion Analysis

It was shown in section 2.1 that the flow stress behaviour in hot working can be expressed mathematically using the constitutive equation providing the four constants are known. The following theory was used to derive these from an experimental torsion data matrix.

In order to make an accurate analysis of the test it is first necessary to allow for the heat generated within the specimen due to the work input. To this end, a finite difference model was used[3, 65], allowing for heat conduction and convection.

The torque generated by the deformation of a torsion specimen can be written:

$$M = (2\pi/\sqrt{3}) \int_0^r \sigma r^2 dr,$$

where r is the specimen radius. The flow stress substitution can be made by rewriting the constitutive equation and using the $\sinh^{-1}(x)$ expansion to give;

$$\sigma = (1/\alpha)\ln[(Z/A)^{1/n} + \{ (Z/A)^{2/n} + 1 \}^{\frac{1}{2}}] .$$

Z contains the mean equivalent surface strain rate which can also be substituted,

$$\dot{\varepsilon} = 2\pi r \dot{\theta} /(\sqrt{3}L),$$

where L is the gauge length and $\dot{\theta}$ the twist rate in revs/sec. Now the torque is related to the twist rate and temperature by the four constants. This was solved by minimising the difference between the torque calculated in this way and the measured torque[36, 66].

CHAPTER THREE

EXPERIMENTAL PROCEDURE

3.1 Extrusion Practice

The extrusion runs were performed on an Enefco vertical, direct acting 5 MN press with fast ram approach facility. Full details of press design and operation are described in reference 3.

A 75 mm diameter container liner was used for most of the experimental work with a billet length of 75 mm. The ram speeds used were in the range 3 - 15 mm/s and the extrusion ratio was varied from 10 to 100, giving exit speeds ranging from 30 to 1500 mm/s. Unless particular testpiece geometries required square or strip dies, all the extrusions were of round bar section and were performed unlubricated using square shoulder dies with a constant bearing length.

Preheating was carried out in a Banyard Metalheat induction furnace adjacent to the press and billets were transferred pneumatically, ready for extrusion. The heating rate up to the extrusion temperature was 125°C/minute and on reaching it the material was given a five minute soak. The container was electrically heated and kept at 50°C below the extrusion temperature to prevent excessive heating at the die face whilst avoiding significant heat loss from the billet prior to extrusion. All the extruded product, unless specified as air cooled, was given a water quench using a quench tube facility in the pit beneath the press, in order to retain the high temperature structure.

Extrusion data in the form of load and displacement-time traces was recorded using a Datalab DL 2800 transient recorder.

3.2 Torsion Testing

The testing machine was capable of surface shear strain rates of up to $50s^{-1}$ on the specimen used, which had a 10 mm gauge length and 5 mm gauge radius. Further information on machine design and operation can be found in references 67 and 68.

An induction coil around the gauge section heated the specimen to the test temperature using a Eurotherm programable controller. Where possible the heating practice used for the extrusion billets was followed. Some tests were stopped immediately after the peak torque

and quenched in situ to enable examination of the steady state structures, whereas in the hot ductility tests the specimens were strained to failure.

Testing conditions involved temperatures from 300 to 500°C and surface shear strain rates from 0.05 to 50s^{-1}. Data was recorded on UV paper in the form of a torque-time trace with markers for each tenth of a revolution.

3.3 Microscopy

Samples were taken from the extrudate at a position corresponding to a third of the ram stroke to ensure that the steady state regime had been reached and to compare the effects of different extrusion conditions at the same point in the extrusion cycle. For optical microscopy samples were mounted in slow setting resin, ground on silicon carbide papers and then final polished on 6 and 1 micron diamond cloths. A standard Kellars etchant was used to reveal precipitate distributions and this served to show up the grain boundaries in the heat treated condition. To study the as worked or solution treated conditions where the grain boundaries were not decorated by precipitation, Barkers electroetchant was used at 20 V.

TEM specimens were prepared with a Struers Tenupol jet thinner using a 25% nitric acid-methanol polishing solution at a potential of 15 V at temperatures below -30°C. The discs required for this technique were prepared in the conventional manner. Thin foils were examined using a Philips EM 301 and a JEOL JEM 120 cx Temscan, both operating at 100 kV. SEM work on fracture surfaces and corrosion testpieces was carried out using a JEOL T200 fitted with a Link EDX detector.

X-ray diffraction work for phase analysis was performed using a Philips wide range goniometer. Microprobe analysis was carried out on a Cambridge microprobe 5 at Alcan.

3.4 Heat Treatments

The high temperature treatments such as homogenisation were carried out in a large air circulating furnace capable of holding 1 metre length logs. After homogenisation the logs were scalped to remove the oxidised layer. For the lower temperature artificial ageing treatments, smaller fan driven ovens were used.

3.5 Material Properties

All testpieces were machined from the portion of extrudate behind the microscopy samples, again to ensure that corresponding steady state structures were being studied. The final 60 cm of the extrusion was never used, since this region usually remained unquenched.

Tensile testing was used to establish basic mechanical properties. An Instron universal testing machine was used at a crosshead speed of 0.5 mm/min with Hounsfield nō 12 testpieces. Elongation values were measured from the load-time traces and proof stress values quoted are for a 0.2% offset. Larger specimens with a cross sectional area of 100 mm^2 were tested on a Denison tensile testing machine, so that an extensometer could be fitted to make modulus measurements.

For rapid approximate property determination, for example in establishing ageing behaviour, the Vickers hardness test was used with a 10 kg weight.

Corrosion, stress corrosion and toughness testing were conducted according to the following standards. Details of these tests will be discussed in the relevant results sections.

Toughness	COD Test	BS5762 : 1979
Corrosion	NAWLT Test	ASTM G67-80
	EXCO Test	ASTM G34-79
Stress Corrosion	C-RING Test	ASTM G38-73

3.6 Materials

Material was received from the British Aluminium Company and later from Alcan International in the form of 80 mm diameter logs machined out of DC cast blocks. Two alloy compositions were supplied comprising of material from several casts. Chronologically the Al-Li-Mg ternary was provided first and the quaternary came two years into the project. Table 3.1 gives the target compositions for the two alloys, together with those actually used. In the ternary alloy the lithium level fell slightly below target and the magnesium was slightly raised, but both were generally consistent in all the casts. The targets were approached more closely in the copper bearing alloy and all three casts showed good agreement. No significant differences in behaviour between casts were found, but where possible a set of experiments was performed using a single composition.

ALLOY COMPOSITION WT %

CODE	Li	Mg	Cu	Zr	Fe	Si	Na
Target 1	2.5	3.5	-	0.15	-	-	-
QUD	2.17	3.82	-	0.17	0.12	0.10	0.001
QUE	2.14	3.74	-	0.12	0.12	0.12	0.001
QZX	2.24	3.64	0.02	0.14	0.10	0.04	0.001
QZT	2.3	3.53	0.02	0.17	0.11	0.05	0.002
RAA	2.22	3.75	0.02	0.16	0.11	0.05	0.004
Target 2	2.5	3.5	1.0	0.15	-	-	-
P5	2.4	3.46	0.86	0.15	0.12	0.02	-
P6	2.46	3.45	0.84	0.15	0.12	0.02	-
P7	2.43	3.47	0.82	0.13	0.12	0.02	-

Table 3.1 Target and Actual Alloy Compositions

CHAPTER FOUR

EXTRUSION DATA ANALYSIS

The variables recorded for each extrusion run are tabulated in appendix 1. The experimental program was carried out primarily to produce material for further structural and mechanical property investigations, hence the repetition of certain extrusion conditions. However, it is worthwhile at this stage to study the extrusion process itself, in particular the breakthrough pressure and the onset of hot shortness which determined whether or not an extrusion could be performed successfully. Although these extrusions were carried out on a small scale experimental press with small billet sizes and narrow section product, the results will give an indication of the extrusion behaviour at an industrial scale.

4.1 Pressure Displacement Curves

The variation of the extrusion pressure during the ram stroke results from the combination of the alloy's dynamic restoration characteristics and the external effects imposed by the process. Hot working theory predicts a true stress-strain curve for a given temperature and strain rate but in extrusion this is modified by the deformation geometry, frictional effects and temperature variations during the cycle. The frictional contribution is very significant in unlubricated extrusion as the friction at the container causes severe deformation of the outer layers of the billet. In this way the typical flat topped stress strain curve for a material undergoing dynamic recovery is transformed into the extrusion pressure displacement curves shown for the two alloys in Fig. 4.1.

Both alloys gave similar traces and exhibited similar trends with the extrusion variables. Fig. 4.1a shows the effects of extrusion temperature for the Al-Li-Mg alloy at a constant ram speed and ratio. At low temperatures the curves show the usual rapid rise followed by a levelling off and then a gradual decrease as the temperature rises and the billet length decreases to produce a peak. With increasing temperature, heat generation is reduced due to the lower work input, causing the difference between the maximum and minimum pressures to decrease, until at 500°C no peak is observed. In this situation the heat generated and the reduction in the frictional contribution balance the heat losses to the tooling. The same effect is shown by

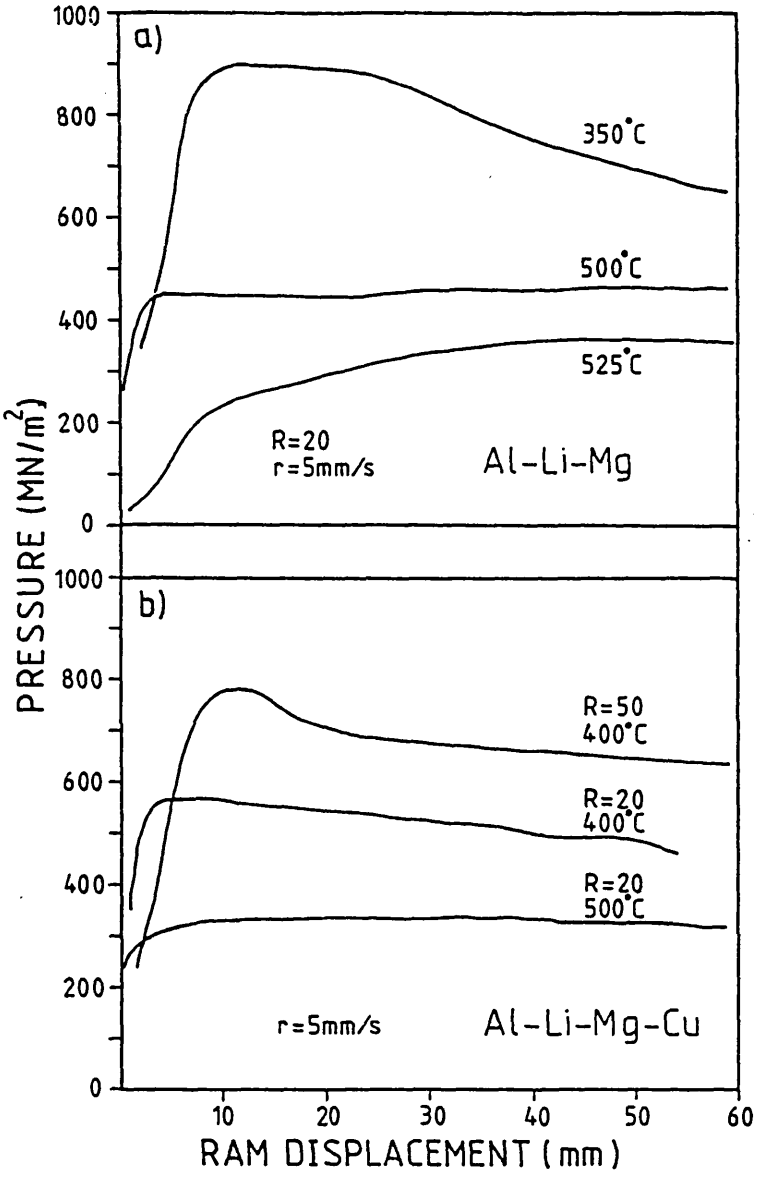

Fig 4.1 Pressure displacement curves.

the copper alloy at 500°C in Fig. 4.1b. However, billet lengths used in this work were very short and on larger size billets the larger friction contribution at the start of the process would probably still give a pronounced extrusion peak at 500°C.

Going up to a temperature of 525°C, shown by the lower trace in Fig. 4.1a, heat losses now outbalance heat generation and frictional effects, so the flow stress is raised and the extrusion pressure gradually increases. This shift in behaviour was not observed for the copper containing alloy as it could not be extruded above 500°C.

A pronounced peak is exhibited by the upper curve in Fig. 4.1b, where an increase in extrusion ratio has produced a greater temperature rise.

4.2 Variation in Breakthrough Pressure with the Process Variables

This section gives a brief account of the peak pressure variations with extrusion ratio, ram speed and temperature which are generally well established[69], as well as the influence of the copper addition.

Initially it is useful to remove the ram speed as a variable. Although it is accepted that raising the extrusion speed requires an extra increment in pressure, as hot working theory would predict, it was not found to have an appreciable effect in this work. For the range of speeds used, 3 - 15 mm/s, the value was only varied by a factor of 5 so that the greater heat generation associated with a shorter extrusion time compensated for any hardening due to the increased strain rate. In practice the highest speed was only used where it was necessary to achieve the maximum press capacity. All the relationships derived in this section use combined data from different ram speeds.

Fig. 4.2 shows the influence of initial billet temperature on extrusion pressure with a linear fit to the data. These plots are useful when trying to assess the minimum extrusion temperature for a given press capacity. Clearly the pressure decreases as the temperature is raised due to the reduction in flow stress. The rate at which the pressure falls is increased by higher ratios and also by the addition of 1% copper. The first effect is probably due to the

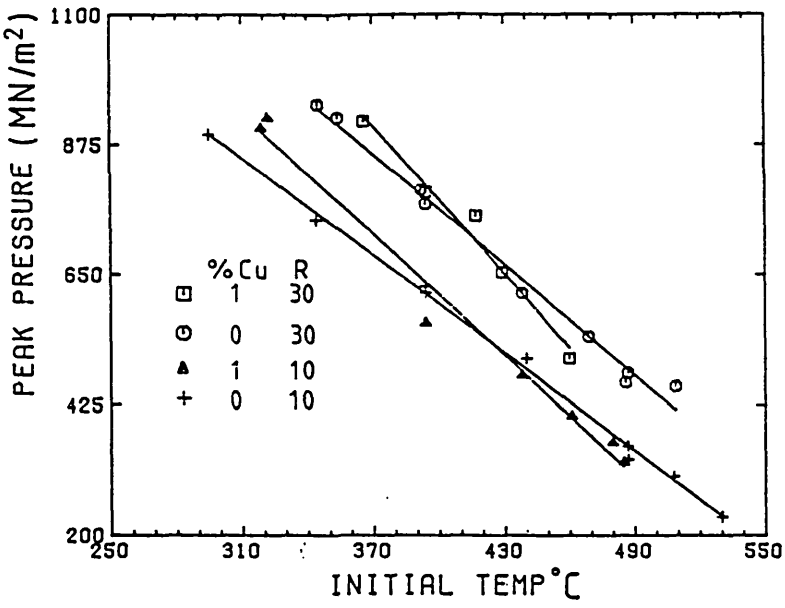

Fig 4.2 Variation in peak pressure with initial temperature.

$$P = A + B\,T$$

%Cu	R	A	B	cc
0	10	1743	-2·9	·99
0	30	2039	-3·2	·99
1	10	2013	-3·5	·99
1	30	2492	-4·3	·99

$$P = A + B \ln R$$

%Cu	T	A	B	cc
0	450	302	177	·98
0	350	319	187	·98

$$P = A + B \ln Z$$

%Cu	R	A	B	cc
0	10	-1190	56	·99
0	30	-1478	70	·99
0	50	-1396	69	·98
1	10	-1353	69	·99
1	30	-1625	84	·99

$$P = A + B \ln R + C \ln Z$$

Al-Li-Mg	$P = 125 \ln R + 62 \ln Z - 1658$	cc·98
Al-Li-Mg-Cu	$P = 137 \ln R + 69 \ln Z - 1687$	cc·98

Table 4.1 Regression data for pressure equations.

increased heat generation at higher reductions. The influence of copper is more complex as the alloy lines crossover at 400°C, indicating that the copper containing alloy is softer at higher temperatures and more difficult to extrude at low temperatures. Considering the effects of solid solution strengthening, the copper containing alloy did have a slightly lower level of magnesium (up to .25% less) which is a strong solution strengthener, but this would only account for a small difference. Vierod's results on 2000 series alloys[3] show that copper has a hardening effect during extrusion of approximately 30 MPa/wt%Cu. The difference between the two alloys at the extremes is of this order but so is the scatter at repeat points and with the lack of high temperature data points for the quaternary alloy, it is difficult to ascertain whether this is in fact a definite trend, although it is shown at both extrusion ratios. If it is, then a possible explanation for this behaviour could be that the strengthening effect of copper is additive at low temperatures but at higher temperatures this is reversed due to the influence of the copper atoms on recovery processes.

The regression data from the various fits of the pressure results attempted, including those in Fig. 4.2, and the development of a general equation are shown in Table 4.1. The linear fit with ln R, the strain in extrusion, is a well established relationship. Insufficient runs at constant temperature were performed to enable data for the quaternary alloy to be fitted but it is reasonable to assume that the relationship would be similar for both alloys. At this stage it was a logical step to combine all the extrusion variables in a single term. ln Z was chosen because it contains a temperature term and a strain rate term, which is in turn a function of the extrusion ratio and the ram speed. However, plots of this type still yielded individual lines for each ratio, with some improvement in the data fit, indicating that it is the strain and not the strain rate effect of varying the extrusion ratio which is more important here. Therefore, a more general expression for peak pressure including a ln Z and a ln R term was adopted. The individual constants were derived using a multiple regression computer package and they showed similarity for the two alloys as might be expected. Figs. 4.3 and 4.4 show the

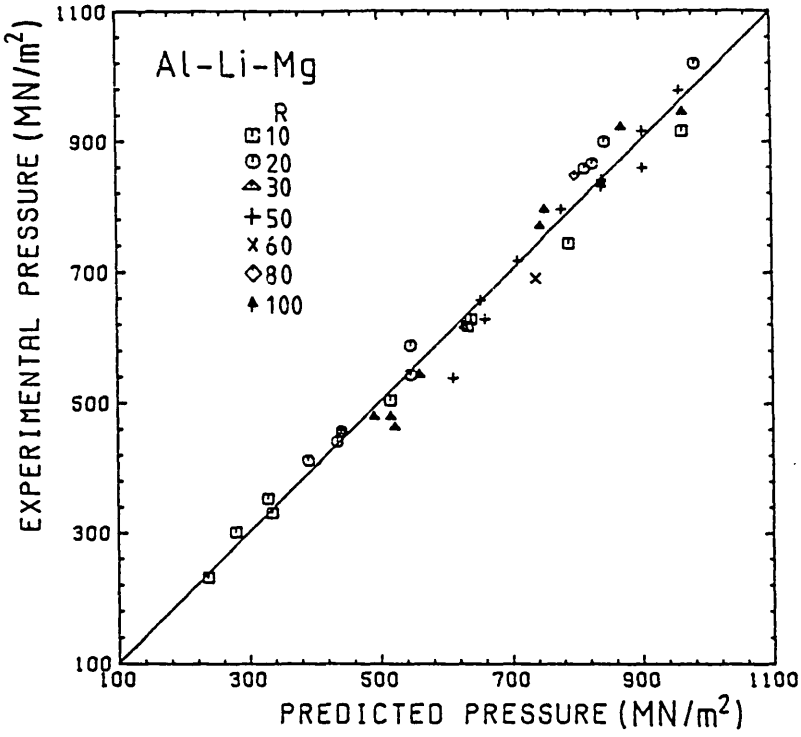

Fig 4.3

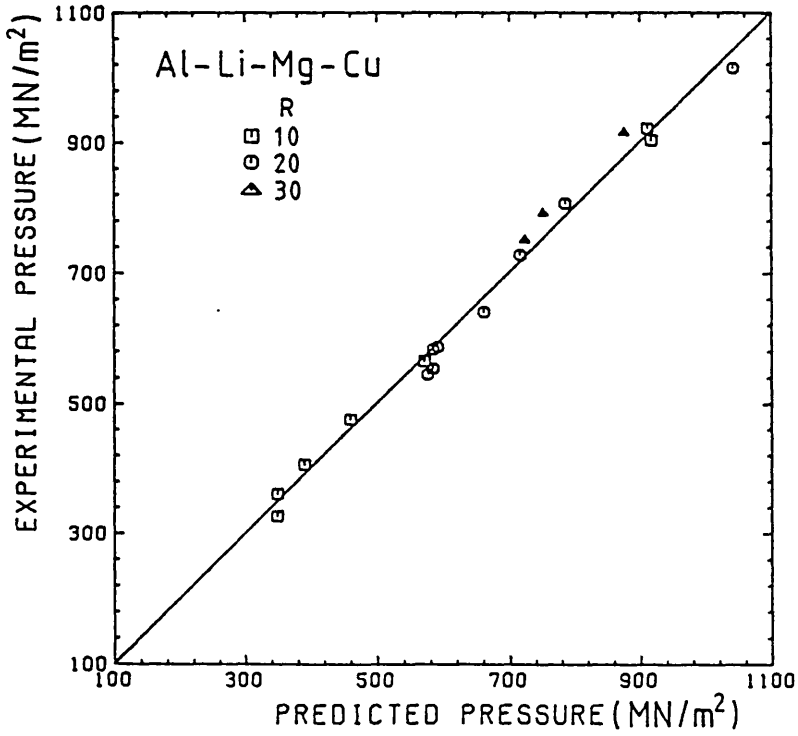

Fig 4.4

Comparison of experimental and predicted extrusion pressures.

accuracy of the fit where the measured pressure is plotted against the calculated value using data from all the extrusion runs. The points lie close to the line of gradient 1 drawn through the origin resulting in the good correlations achieved.

It is doubtful whether this expression could be applied directly to a larger scale operation, since the friction and temperature conditions are specific to this experimental set up. However, by compensating for these factors it may be possible to reach approximate pressure predictions.

4.3 Limit Diagrams

The range of conditions over which an alloy can be extruded successfully is determined by two factors; the available press capacity and the onset of surface defects. Figs. 4.5 and 4.6 are experimental extrusion limit diagrams constructed for each alloy. The pressure line is drawn for a press capacity of 1000 MPa using the pressure-temperature results from section 4.2. The upper limits are drawn for the onset of surface cracking at the extremes of ram speed used. Although other surface defects such as die lines, blistering and pick up can occur, cracking is the most serious and determines the upper limit to the working range. Care was taken in the experimental work to clean the dies and liner of aluminium regularly so as not to encourage any defect formation.

The most common cause of cracking is hot shortness, where excessive local surface temperatures are generated leading to liquation of non equilibrium low temperature phases. The stress distribution at the die mouth can then cause the cracks to open.

The diagrams have been constructed using a simple classification of extrusion finish:

A Acceptable surface

C Cracked surface

It was possible to distinguish between two types of cracking; extensive cracking due to hot shortness and a milder form confined to one point on the periphery. The latter effect is due to die pick up

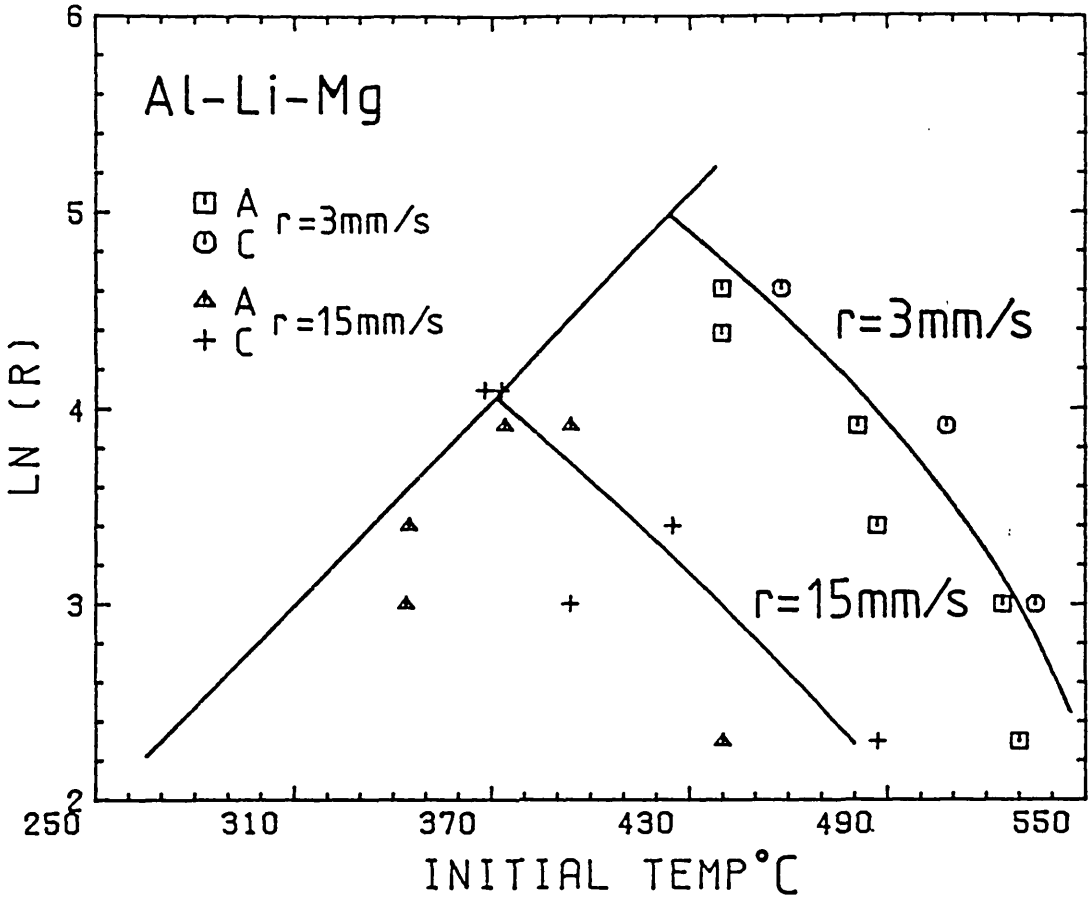

Fig 4.5

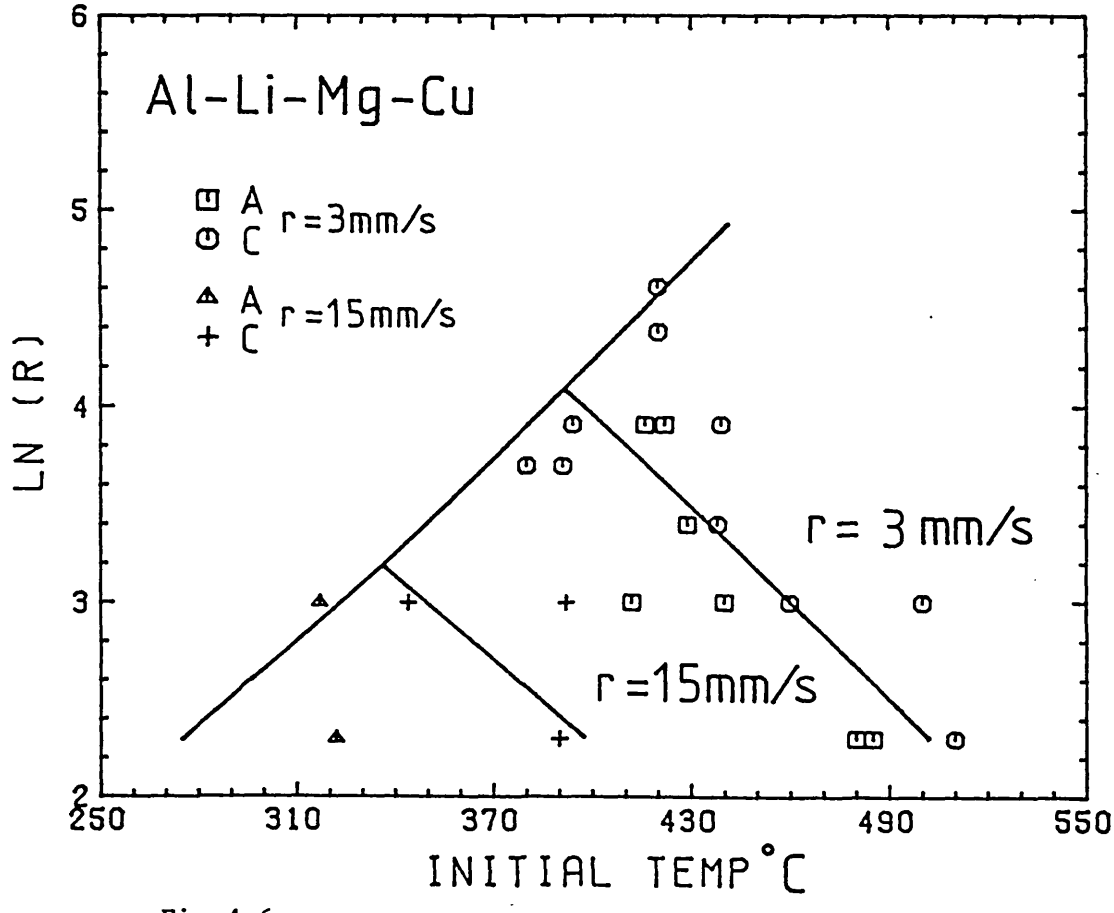

Fig 4.6

Extrusion limit diagrams.

where the metal alloys onto the die face and this often occurs close to the conditions causing hot shortness. To have included both types of cracking would have complicated the diagrams and so both types were classed together.

At low ram speed the generation of high local temperatures is suppressed to some extent by heat dissipation into the tooling and the surrounding material. At higher speeds and similarly at high ratios, where heat generation is usually greater anyway, dissipation is restricted so that local temperature rises cause either local melting or hot rupture. This explains the considerable narrowing of the working area when the speed is raised from 3 to 15 mm/s and the reduction ratio from 10 to 100.

Comparing the diagrams for the two alloys, the addition of copper narrows the working range dramatically, making it impossible to extrude this alloy at a ratio higher than 50, even at the slowest ram speed. The flow stress characteristics of the alloys have already been found to be very similar so the temperature rises can be assumed to be of similar magnitude, suggesting the effect is a constitutional one. The copper alloy proved difficult to homogenise (see section 6.1) and large amounts of S-type (Al_2CuMg) phases were carried over into the extrudate from the cast state. Differential thermal analysis (section 6.1) on the cast material indicated that liquation occurred at 523°C compared to 560°C for the copper free alloy. Therefore, the reduction in workability can be attributed to the liquation of this phase.

Finally, it is important to note that these limit diagrams relate to the particular homogenisation schedules given and the working area may be increased by improved homogenisation practice.

4.4 Summary

1. The extrusion pressures followed the expected trends with the process variables and could be related to them in a single simple expression.

2. The shape of the pressure-displacement locus was explained in terms of a balance between friction, heat generation and heat loss.

3. The addition of copper reduced the working range due to hot shortness brought about by a low temperature liquation reaction.

4. The two alloys required similar extrusion pressures but the addition of copper appeared to raise the pressure at low temperatures and to lower it at high ones.

5. For both alloys, increasing the ram speed from 3 to 15 mm/s considerably reduced the working area.

CHAPTER FIVE

HOT TORSION TESTING

The variables in a hot working process are usually complex and difficult to control and analyse. It is useful, therefore, to evaluate the hot working characteristics using a small scale testing technique with a known stress system. This chapter discusses the workability of the two alloys as determined by torsion testing.

5.1 The Torsion Test

The torsion test has the advantage that high strains can be applied at a constant surface strain rate. Also the temperature rise calculation is simplified by the small deformation volume. The main drawback is the strain and strain rate variation from zero at the centre to a maximum at the surface. It is usually assumed that the surface layer contributes the bulk of the measured torque and this value of strain rate is normally quoted. This can be justified by agreement with results from other hot working tests[31].

To counteract the tendency of aluminium specimens to contract during the test, the ends are normally constrained to maintain a constant geometry. Tensile axial stresses set up in this way can be ignored when calculating the flow stress, but they can influence hot ductility results by causing crack propagation[32].

Testpieces were machined from extruded material to reduce wastage. It had previously been straightened and given a twelve hour soak at 500°C followed by an air cool in an attempt to anneal the hot worked structure and simulate the starting structure for extrusion. In both alloys this proved unsuccessful in removing the recovered substructure but, in any case, the second phase particle distribution could never be returned to its as homogenised state. Hence the measured torque and ductility values reported here would be modified if extrusion billet material were used.

Test conditions were varied in the form of a 5 x 5 matrix using equivalent strain rates from 0.03 to 29 s^{-1} and a temperature range of 300 to 500°C corresponding to the range of extrusion temperatures used.

5.2 Torque - Twist Curves

It is convenient to discuss the stress strain behaviour of the alloys in terms of the torque-twist curves as the conversion from torque to flow stress requires an analysis to allow for strain rate dependency across the radius. Fig. 5.1 shows the effect of test conditions on the torque-twist curves for the Al-Li-Mg alloy, but the characteristics were very similar for the other alloy. Unlike extrusion where frictional effects dominate the pressure displacement locus, in torsion the curves can be explained directly by hot working theory, the only complication being the temperature rise. There is an initial period of microstrain during which the applied strain rate is reached and after this the torque rises as work hardening takes place. The gradient then falls off as recovery mechanisms - driven by the deformation energy - take an increasing effect. The peak torque corresponds to the steady state situation where dislocation generation and annihilation processes are balanced. Higher strain rates and lower temperatures increased the strain to reach this point which is consistent with hot deformation theory, since both of these factors slow down the rate at which recovery can balance hardening. The copper containing alloy showed much less sensitivity with strain rate in this respect, suggesting that recovery processes can be activated more rapidly here.

Where significant temperature rises took place, at low temperatures and high strain rates, the torque gradually fell beyond the peak. Little heat generation occurred at low Z conditions and the torque remained constant. At the highest temperatures it began to rise again presumably due to net heat loss.

In Fig. 5.2 the peak torque variation with initial temperature is shown for both alloys at the extremes of strain rate used. The ternary alloy produced consistently higher values of torque apart from at 300°C, 29 s^{-1}, i.e. the lowest temperature combined with the highest strain rate. This feature is interesting in that the same effect was encountered for the extrusion pressure variation in section 4.2 which corresponds to this level of strain rate, and suggests that this is a definite trend. There the two alloy lines crossed at 400°C and indeed here at the highest strain rate both alloys gave the same

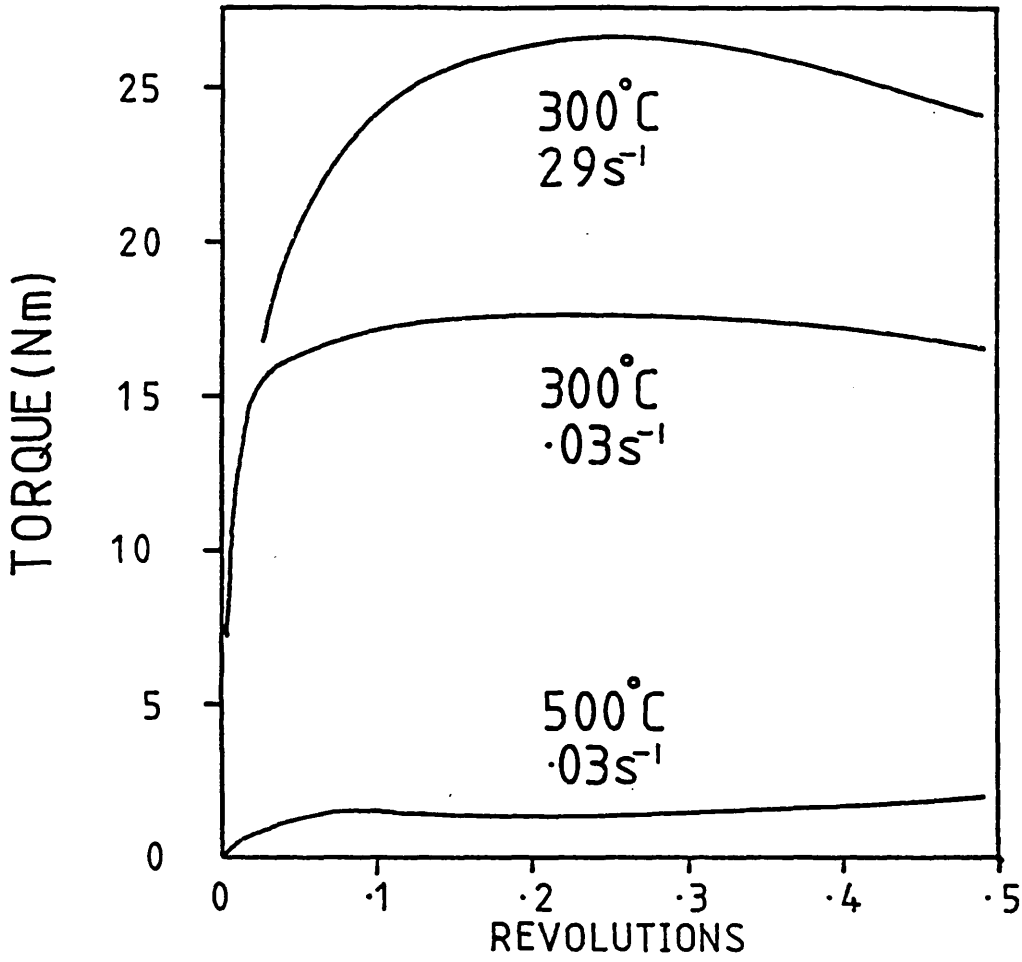

Fig 5.1 Typical torque twist curves for the Al-Li-Mg alloy.

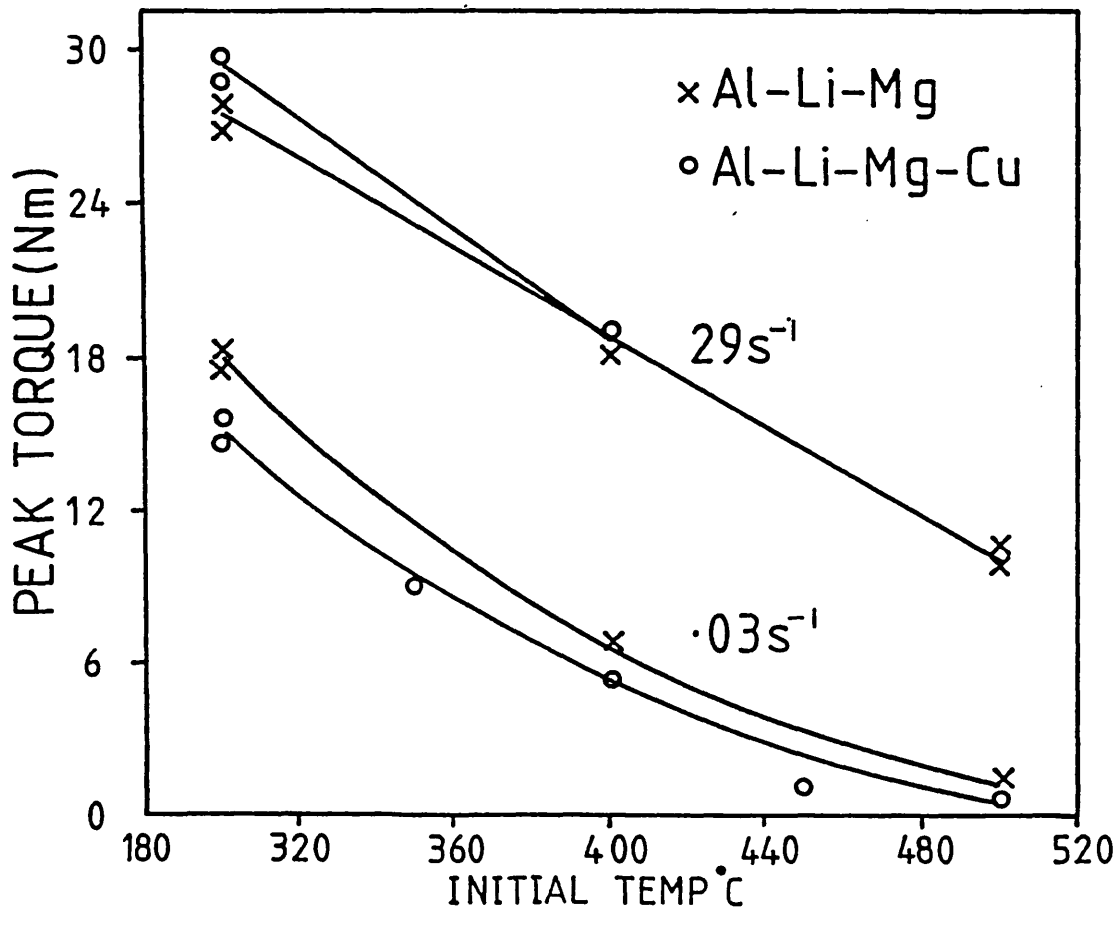

Fig 5.2 Variation of the peak torque with test conditions.

torque at this temperature. The next test temperature used was 500°C but the copper bearing alloy failed by incipient melting and the crossover of the torque lines could not be drawn. The fact that the copper addition is only effective in raising the flow stress at the highest strain rate suggests that the hardening effect is strain rate sensitive and that copper tends to aid recovery at lower strain rates.

A possible explanation for this behaviour could be that copper has two effects at what is a fairly low level of addition, a solution strengthening effect and a recovery effect, possibly through vacancy interactions. Copper atoms may be binding with vacancies allowing a higher overall concentration to be maintained and perhaps accelerating recovery events such as dislocation climb.

5.3 Flow Stress Characteristics

The flow stress behaviour with temperature and strain rate can be concisely described by the constitutive equation once the four constants have been established. This was carried out using the analysis described in section 2.4. The values, given below in Table 5.1 are effectively an average over the range of test conditions used.

	Al-Li-Mg	Al-Li-Mg-Cu	UNITS
ΔH	168	153	kj/mole
α	0.033	0.025	m^2/MN
n	2.15	2.29	-
ln A	24.49	24.01	s^{-1}

Table 5.1 The Hot Working Constants

Recalculation of the flow stress using these values gave similar trends between the two alloys as the torque results in the previous section. This indicates that the minimisation analysis used was successful. Comparing the two sets of constants the significant difference is in the value of activation energy ΔH, which is appreciably lower for the copper alloy. Both values are of a similar magnitude to that of 138 kj/mole[30] for self diffusion in aluminium, indicating the deformation mode is one of dynamic recovery but the difference between the two implies that softening processes are more easily activated in the presence of copper. Although all the hot working constants influence the value of flow stress, the similarity between the remaining values here ensures that the activation energy effect is carried through and supports the observations made on the different alloy behaviour on the torque-twist and pressure displacement traces.

n is effectively a measure of the strain rate sensitivity of the flow stress and has similar values for both alloys with the copper free being the slightly more sensitive. The other constants α and A are also similar. Their physical significance is not clear although they have been allocated some meaning by comparison[30] with rate theory equations.

5.4 Torsion Structures

All the quenched steady state structures consisted of well formed subgrains, typical of a material that undergoes dynamic recovery during hot deformation. Some static recrystallisation was observed but this was not extensive, due to the rapidity of the quench. The structures will be discussed further in Chapter six where they are compared with extruded substructures.

5.5 Hot Ductility

Ductility in hot working is dependent not only on the material but also on the process geometry so that simple tests such as torsion

and tension cannot accurately predict the behaviour during say extrusion. Having said this, the results can give useful indications and rankings between different alloys.

In torsion the axial tensile stress developed during the test means that the test is really a measure of crack propagation. Nucleation mechanisms are similar to those found in creep rupture, i.e. at triple points, grain boundary discontinuities and second phase particles. For materials undergoing dynamic recovery, which is the case here, failure often occurs by crack propagation from surface irregularities. At high temperatures there is also the possibility of failure by liquation of segregated phases.

The results in this section are from tests on extruded material. Using as homogenised material would have been desirable and would have reduced the values of ductility, since extrusion tends to break down segregation effects. Fig. 5.3 shows the effect of temperature on the strain to failure for the two alloys at equivalent strain rates of 3 and 29 s^{-1}. Increasing the strain rate reduces the ductility in both cases, due to the higher level of hardening. For the copper free alloy the ductility is not very temperature dependent, increasing only slightly as the flow stress falls. Although the quaternary alloy has a much higher second phase particle content, the addition of copper raises the low temperature ductility, particularly at low strain rates. This increases up to 400°C consistent with increased softening and then drops rapidly at 500°C when local melting took place. Usually failure took place normal to the specimen axis, but for these conditions specimens failed in a fibrous mode. Fig. 5.4 shows the intergranular nature of the failure due to second phase liquation along extruded grain boundaries. From Differential Thermal Analysis (section 6.1) this reaction is known to occur at 523°C. Failure occurred before a steady state peak was reached so either very rapid temperature rises were taking place, which is unlikely at 500°C, or the thermocouple reading in the specimen core was underestimating the surface temperature, even though this was calibrated. Melting was not encountered in the copper free alloy for this range of test conditions.

Comparing these results with the extrusion limit diagrams in section 4.3 indicates that cracking in extrusion is associated with the low ductility at high temperatures and not with the effects of hardening at low temperatures.

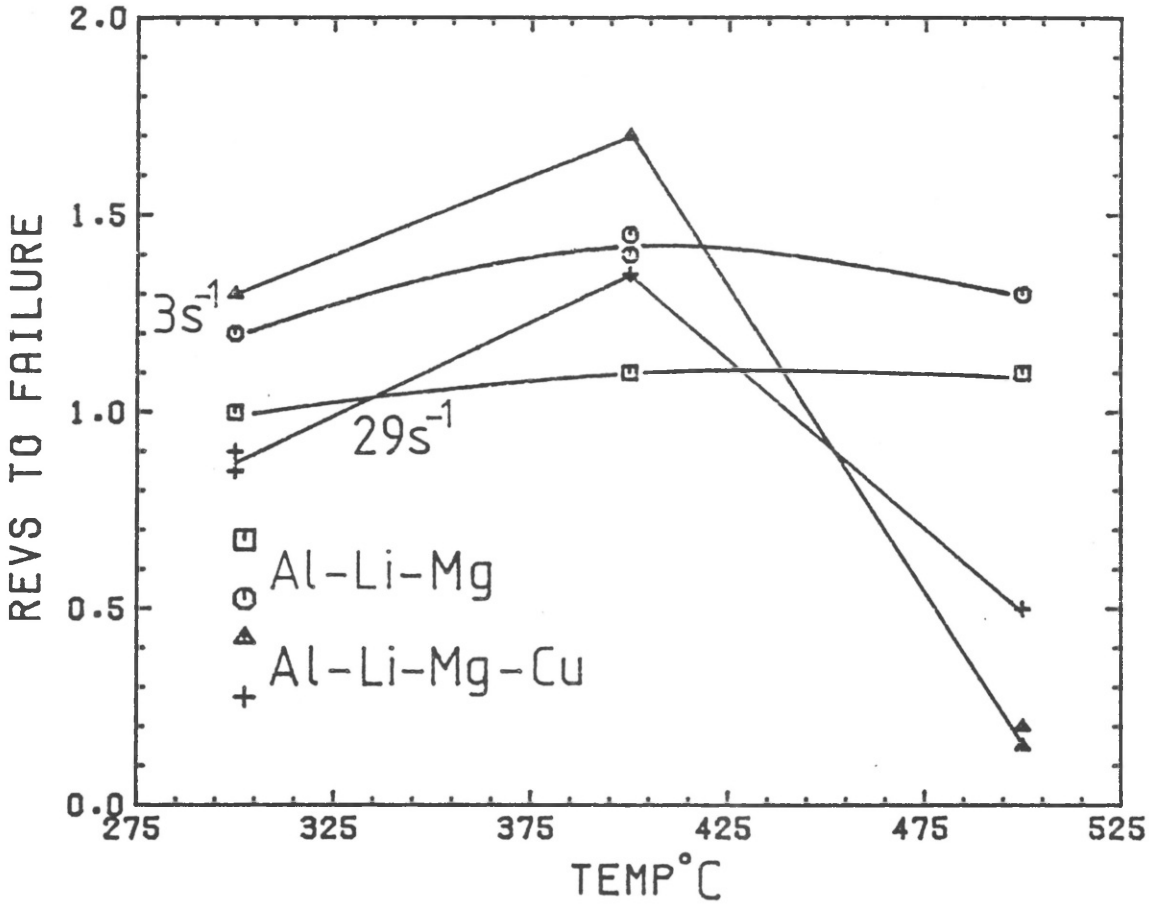

Fig 5.3 Variation in hot ductility with test conditions.

Fig 5.4 Al-Li-Mg-Cu torsion failure. 400X

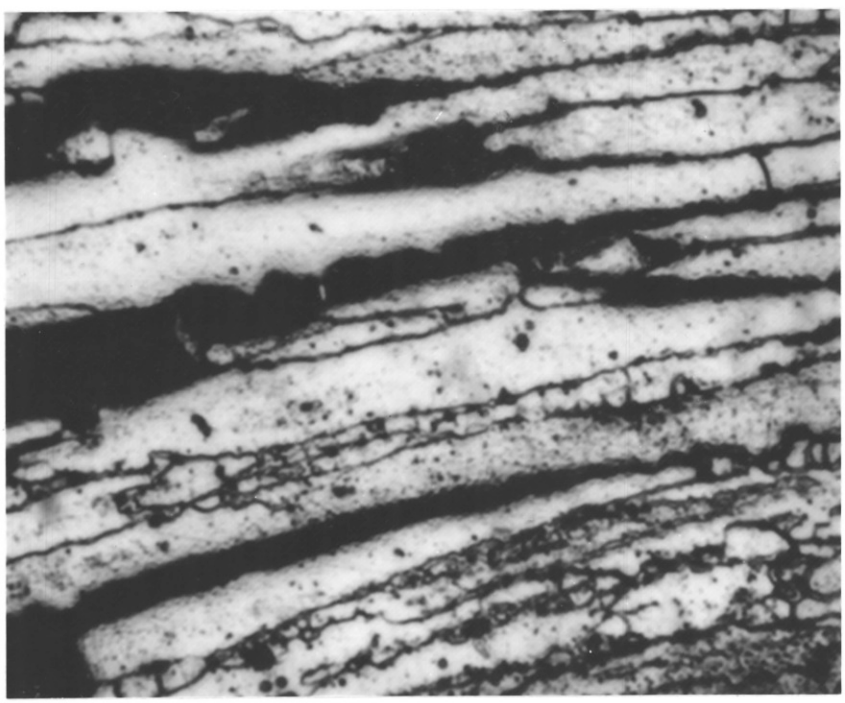

Finally, it is worth noting that at strain rates less than 3 s^{-1} the specimens from both alloys fractured at the radiused entry to the gauge length. At higher strain rates, where cracks are more easily nucleated in the microstructure, failure took place in the centre of the gauge length. Therefore, the mode of torsion failure can be related to the hot deformation processes.

5.6 Summary

1. Established hot working equations have been used to successfully characterise the flow stress behaviour of both alloys.
2. The stress strain variations in torsion can be explained simply by hot working theory.
3. Dynamic recovery is the operative restoration mechanism during hot torsion of these alloys.
4. The addition of copper lowers the activation energy for recovery processes and reduces the steady state torque at all but the highest strain rates.
5. The trends in the torque results with temperature at the highest strain rate agreed with those for extrusion pressure, in that copper raised the torque and pressure at low temperatures.
6. A theory was proposed to explain the effect of copper whereby it affects both hardening and softening processes to different degrees, depending on the conditions, due to vacancy-solute interactions.
7. The addition of copper reduces the hot torsion testing limits by the onset of second phase liquation at test temperatures of 500°C.

CHAPTER SIX

THE EFFECT OF EXTRUSION AND HEAT TREATMENT VARIABLES ON THE STRUCTURE AND TENSILE PROPERTIES OF THE TWO ALLOYS

6.1 Homogenisation Practice

6.1.1 The Effect of Homogenisation on the Extruded Structure of the Al-Li-Mg Alloy

The homogenisation of DC cast material is necessary in order to remove any undesirable structural features incurred by the rapid cooling rate during solidification. Its functions include removal of segregation and the break down of coarse intermetallic particles together with low melting point eutectics. The latter are a product of non-equilibrium cooling and can severely limit the working range by causing hot shortness. Homogenisation is also important where dispersoid forming elements, such as Mn, Cr and Zr are present; they remain in solution after casting and can precipitate out as intermetallics during high temperature treatments. As with most precipitation reactions the features of the dispersion can be influenced by the 'ageing conditions'. Both alloys in this work contained zirconium additions which form the dispersoid Al_3Zr, a strong recrystallisation inhibiting agent. Most of the elements involved have relatively low diffusivities in aluminium so that homogenisation is usually a lengthy high temperature treatment.

In this section of the work a standard soak time of 24 hours was adopted and the temperature was varied, since this can significantly alter diffusion rates. As cast billets of the copper free alloy were given soaks at 475, 500 and 550°C and then air cooled. Material from each cycle was extruded near the upper and lower extrusion limits at extrusion ratios of 10 and 20. No grain growth occurred during any of the treatments and also the soak temperature had no effect on the extrusion pressure. At the grain boundaries as cast particles were still present after the treatment and these were slightly smaller after the highest temperature soak.

All the extruded structures were partially recrystallised in the centre of the bar, being more so at lower extrusion temperatures. Table 6.1 lists the fraction recrystallised after the different treatments. Substantially more recrystallisation was produced after the 550°C homogenisation, particularly at the lower extrusion temperatures. The 475 and 500°C soaks gave virtually identical structures so no further work was done using the lowest temperature.

The tensile properties of the extrusions are given in Table 6.2. Figures quoted are for the fully heat treated condition but the extruded structure can be retained after solution treatment in these alloys (see section 6.4). Clearly there is a strength loss associated with increased static recrystallisation incurred by raising the homogenisation temperature. Although the level of recrystallisation increases at lower extrusion temperatures the strength loss is compensated for by substructural hardening.

This type of behaviour with homogenisation treatment has been reported for Al-Zn-Mg alloys containing Zr[71] and for an Al-Zn-Mg-Cu alloy containing Cr[28], where it was attributed to variations in the dispersoid distribution. Here the distribution of Al_3Zr is probably finer at the lower temperature since this is more likely to retard recrystallisation. Al_3Zr precipitates are reported to be very stable[72], showing little tendency to coarsen due to their low solubility and interfacial energy. They can affect recrystallisation by pinning the substructure as well as high angle boundaries. This suggests that it is the precipitation reaction and its frequency rather than coarsening during homogenisation which is controlling the dispersion. TEM work failed to produce evidence of an influence on the distribution of Al_3Zr in this context mainly because of the heterogeneity of size and distribution found in each thin foil. It did show, however, that the subgrain sizes were similar after different soak histories, indicating that the influence of the particle dispersion on recrystallisation is by way of a grain boundary mobility effect rather than through substructural refinement. The behaviour at the extrudate periphery would tend to support this argument. At the lowest extrusion temperature the 500°C soak gave a fully recrystallised surface layer with a grain size of 10 microns compared to 50 microns at 550°C.

Another possible explanation for the effect of soak temperature concerns the nucleation of recrystallisation at coarse second phase particles, but this must be rejected since the lower temperature soak produced slightly coarser particles which ought to give enhanced nucleation.

R	Extrusion Temp. °C	Homogenisation Temp. °C		
		475	500	550
20	500	10	10	20
20	350	33	31	82
10	500	-	5	4
10	325	-	13	70

Table 6.1 Effect of Soak Temperature on Recrystallisation %

Extrusion Temp. °C	Soak Temp. °C	P.S. (MPa)	U.T.S. (MPa)	%El
500	500	425	515	6.8
500	550	397	492	8.1
325	500	489	540	5.8
325	550	433	517	9.8

Table 6.2 Effect of Soak Temperature on Tensile Properties, R = 10

	Hardness HV_{10}							
Code	QUE	QUD	RAA	QZT	QZX	P5	P6	P7
Cast	80	95	75	91	80	133	134	132
Homogenised	119	120	115	110	112	145	142	144
			Al-Li-Mg			Al-Li-Mg-Cu		

Table 6.3 Comparison of Different Casts Before and After Homogenisation using the Hardness Test

In the choice of the homogenisation practice for further work the prevention of recrystallisation by the use of the 500°C soak was considered more important than the slight improvement in the breakdown of coarse particles using higher temperatures. Recrystallised product is generally regarded[28] to give lower toughness and stress corrosion resistance as well as reduced strength.

6.1.2 As Cast Structures

The etched as cast structures of the two alloys are shown in Figs. 6.1 and 6.2. The copper free alloy contained two main types of phase, the coarse grain boundary type 5 - 10 μ in size and the finer phase, .5 - 1 μ in size, segregated in the matrix near the boundaries. The former were shown to contain the impurities iron and silicon by microprobe work on extruded stringers. X-ray diffraction work on the cast material showed strong Al_2MgLi peaks which can be attributed to the finer particles.

The copper bearing alloy contained very large amounts of a dark coarse grain boundary phase, up to 10 μ wide and 40 μ long, which was almost continuous in some areas. Energy dispersive X-ray analysis showed it to contain copper and magnesium and microprobe work gave a Mg/Cu ratio of unity so they are probably S phase (Al_2CuMg). The other phase present in appreciable amounts was similar in size and distribution to Al_2MgLi in the previous alloy.

6.1.3 Homogenised Structures

Initially incipient liquation points of the alloys were determined by optical microscopy to give an upper limit for the homogenisation treatment. They were found to be 565°C and 520°C for the copper free and copper containing alloys respectively. The early onset of melting in the latter can be attributed to the eutectic in the Al-Cu-Mg system at 518°C[73] involving the S phase (Al_2CuMg). Homogenisation was therefore limited to 510°C, with a 10°C safety margin, making an investigation of soak temperature on the extruded structure unnecessary. A 24 hour treatment proved inadequate to

remove the grain boundary phase and so this was extended to 36 hours.

To summarise, the homogenisation practices used were:

Al-Li-Mg - 24 hours at 500°C, air cool

Al-Li-Mg-Cu - 36 hours at 510°C, air cool.

The heating rate up to the soak temperature was nominally 150°C/hour. Air cooling was given in order to retain as much solute in solution as possible.

Homogenised structures of the alloys are shown in Figs. 6.3 and 6.4. In the ternary alloy the Al_2MgLi precipitates have been redistributed but the coarse grain boundary particles still remain. Similarly, in the second alloy, the finer precipitates were redistributed but the coarse grain boundary phase still remains. This feature was responsible for the early onset of cracking in extrusion and torsion. It is also undesirable because it ties up copper and magnesium, reducing possible strengthening effects, and will probably also lead to reduced toughness in the final product.

Table 6.3 shows the hardness values of the various casts before and after homogenisation. Differences between casts are probably due to varying amounts of solute in precipitate form. The results show that homogenisation gives rise to similar structures in the different casts for each alloy. Any residual difference can be attributed to slight variations in grain size and composition.

Difficulty in homogenisation and subsequent fabrication of quaternary alloys has been reported[24] by other workers. Alloys containing at least 1% copper could not be homogenised if the magnesium level was greater than 1% of if the sum of the two elements was greater than 4%. Clearly in the present work both of these conditions were satisfied. Later in the project Differential Thermal Analysis (DTA) was used to determine the liquation points of the two alloys accurately. The method and theory associated with this technique are similar to those for Differential Scanning Calorimetry, described in section 6.5.4, only the apparatus is modified to allow for specimen melting. This gave values of 565°C for the ternary and 523°C for the quaternary. With this information it may have been possible to increase the homogenisation temperature of the latter, perhaps reducing the amount of eutectic, but it is unlikely that it could have been removed completely.

As Cast Structures

Fig. 6.1

Al-Li-Mg

Fig. 6.2

Al-Li-Mg-Cu

Homogenised Structures

Fig. 6.3

Al-Li-Mg

Fig. 6.4

Al-Li-Mg-Cu

Etchant : Kellars Reagent

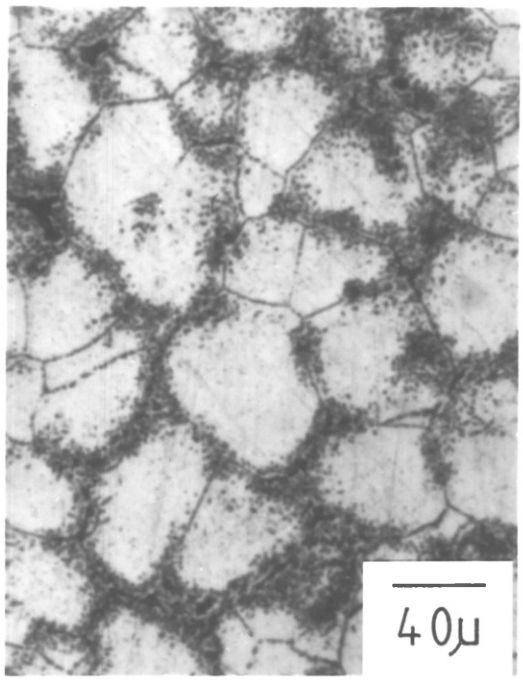
40μ

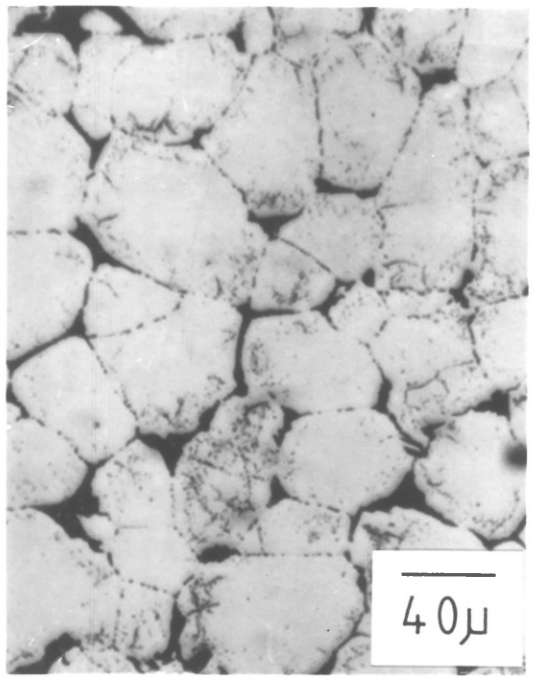
40μ

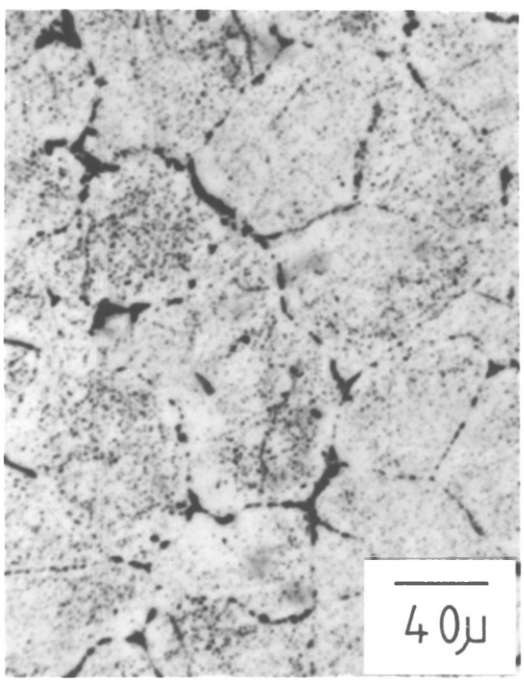
40μ

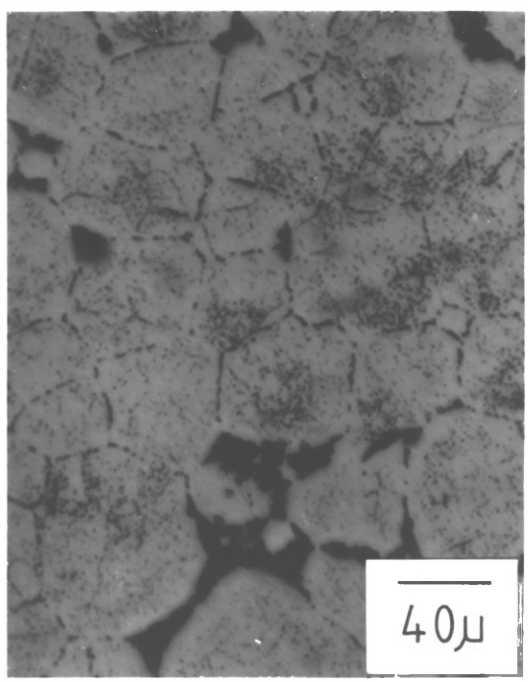
40μ

6.2 Structural Variations with the Extrusion Conditions

The extruded sections were all composed of two distinct zones:

a) An outer layer composed of heavily deformed material originating from the outer regions of the billet. This metal had travelled across the face of the dead metal zone and was subjected to the highest strains and strain rates, giving rise to complete recrystallisation at the product surface.

b) An inner core consisting of material from the centre of the billet which had travelled straight on through the die and as a result underwent less deformation than the outer layers.

Towards the end of extrusion the metal in the centre of the billets became used up and the more fibrous outer layer took up an increasing proportion of the section. All the structures examined in the following investigation were taken from a position in the extrudate corresponding to one third of the ram stroke where the core type structure was extensive.

Before looking at the effects of heat treatment on these alloys a preliminary study was carried out on both alloys in order to investigate the dependence of the extruded structure on the extrusion conditions. Figs. 6.5 to 6.8 show typical core and surface structures produced in the Al-Li-Mg alloy for a ratio of 20:1. Similar variations in structure were observed in the copper containing alloy.

6.2.1 Extrudate Core Structures

The structure in the centre of the extrusion is important with regard to final properties as it usually takes up the bulk of the section. It is therefore worth discussing the variations in structure observed in this region in order to relate them later on to mechanical properties.

In these alloys the core structures were partially recrystallised to some extent for all conditions. At the highest extrusion temperatures, as in Fig. 6.5, very little static recrystallisation occurred and when it did this took the form of small equiaxed grains, less than 5 μ in size, sited near original grain boundaries.

As Extruded Structures, Al-Li-Mg, R = 20:1

Extrudate Core

Fig. 6.5

Initial Temp = 500°C
ram speed = 5 mm/s

Fig. 6.6

Initial Temp = 325°C
ram speed = 15 mm/s

Extrudate Surface

Fig. 6.7

Initial Temp = 500°C
ram speed = 5 mm/s

Fig. 6.8

Initial Temp = 325°C
ram speed = 15 mm/s

Etchant : Barkers Reagent

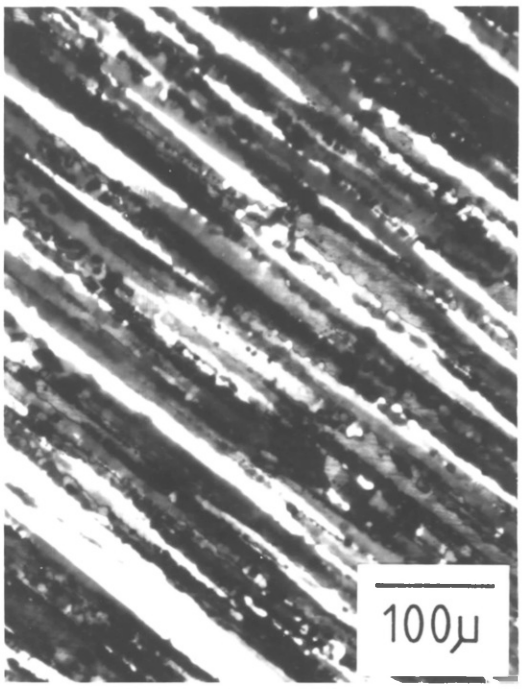
100μ

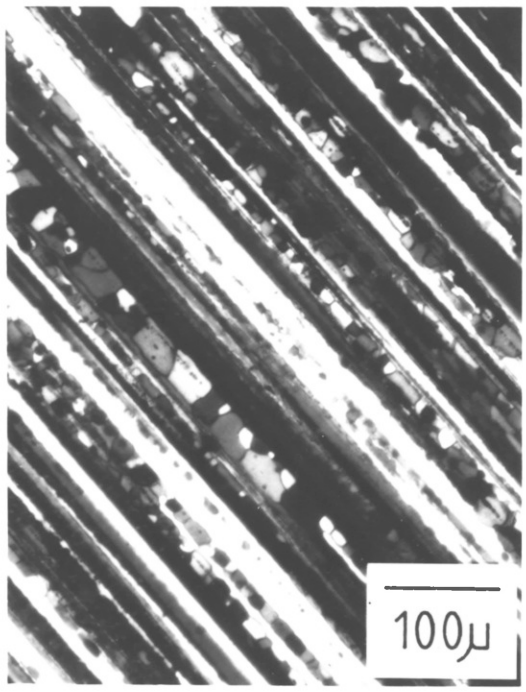
100μ

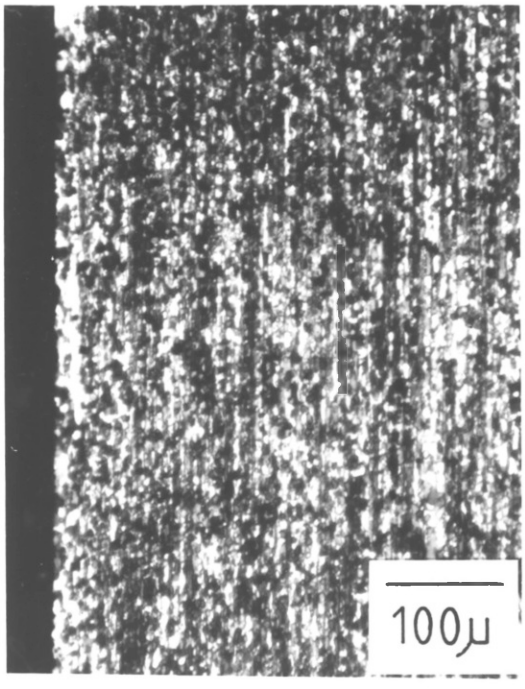
100μ

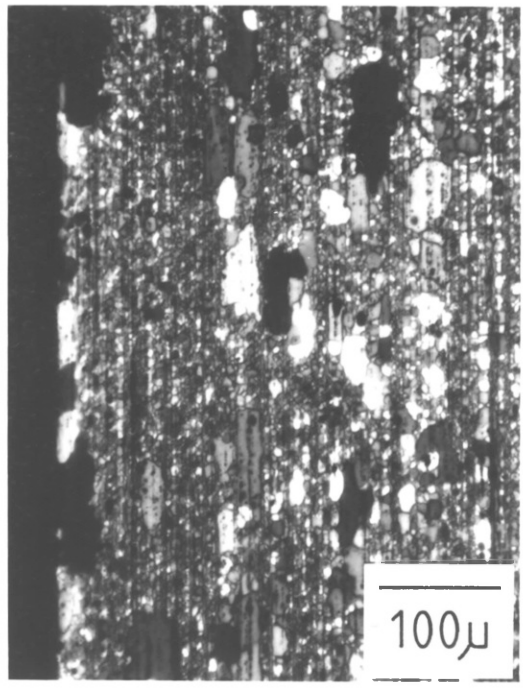
100μ

Effectively this structure could be classed as unrecrystallised. Nucleation took place preferentially near grain boundaries due to the greater level of deformation there, associated with accommodation of the shape change. Reducing the temperature increased the extent of recrystallisation, as illustrated in Fig. 6.6, together with the recrystallised grain size, here about 40 μ. A similar trend was shown as the extrusion ratio was increased. However, fully recrystallised structures were never produced. Figs. 6.9 and 6.10 demonstrate graphically the variation in the extent of core recrystallisation with process conditions. Here measurements were made on as extruded material but the results are identical to those after heat treatment, since negligible further recrystallisation and grain growth occurred during solution treatment. This would indicate that the press quench is not in fact preventing static recrystallisation which was verified by producing identical structures without using water cooling.

The effect of decreasing the extrusion temperature and raising the level of recrystallisation was shown by both alloys at all ratios. However, raising the extrusion ratio had a more dramatic effect on the copper free alloy. At an extrusion ratio of 30, extrusions below 500°C produced very substantial levels of recrystallisation (> 50%), significantly greater than at 20:1. Raising the reduction ratio further gave even more softening.

A similar trend with working temperature has been reported for an Al-Li-Cu-Zr alloy[47]; at all but the highest rolling temperatures the structures were partially recrystallised and,in addition, great difficulty was experienced in producing full recrystallisation.

The important factor in determining the level of static recrystallisation then appears to be the degree of stored energy. Comparison of the high and low temperature grain structures suggests that nucleation still occurs near original grain boundaries in the latter, but here there is a driving force for the boundaries to advance, in the form of a higher dislocation density. Thermal activation at high temperatures does not appear to promote high angle boundary migration in these alloys.

Typical low and high temperature substructures for both alloys are shown in Figs. 6.11 to 6.14. They are generally highly recovered containing well formed equiaxed subgrains. The internal dislocation

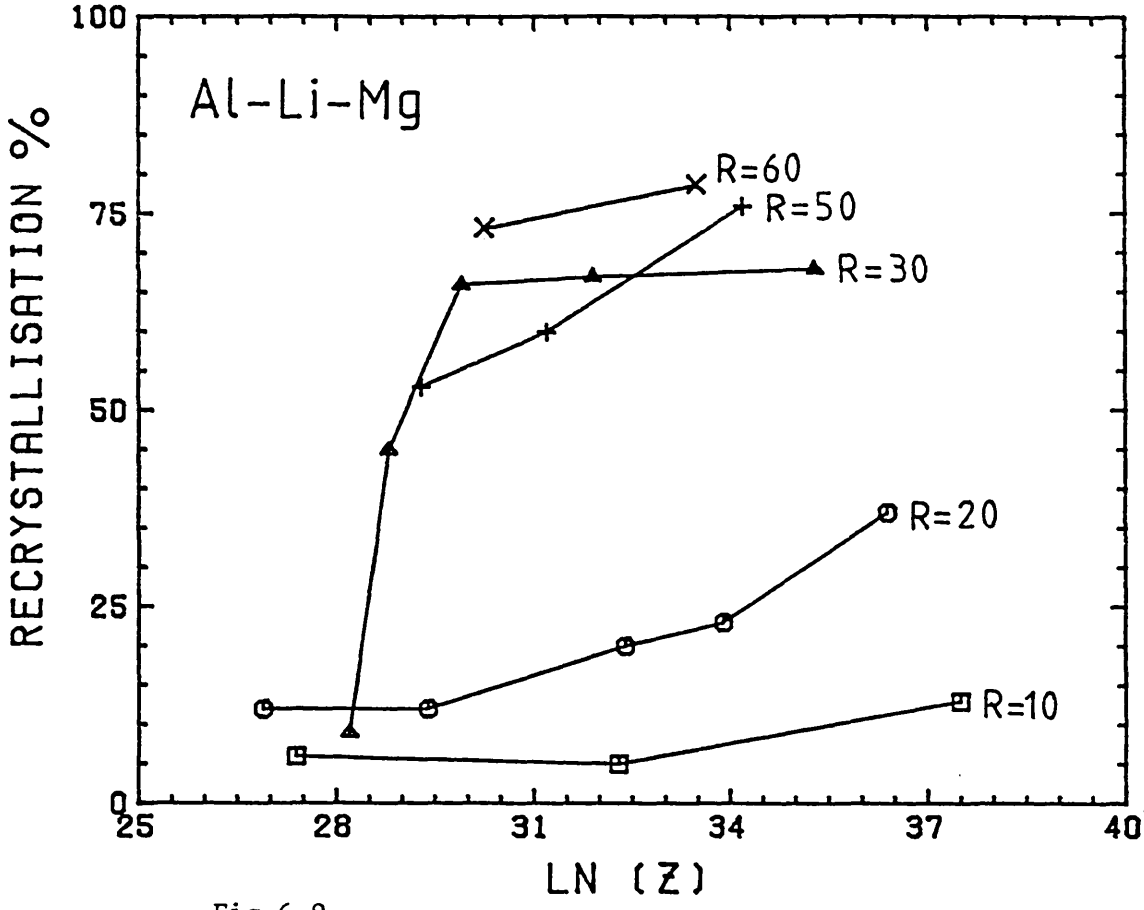

Fig 6.9

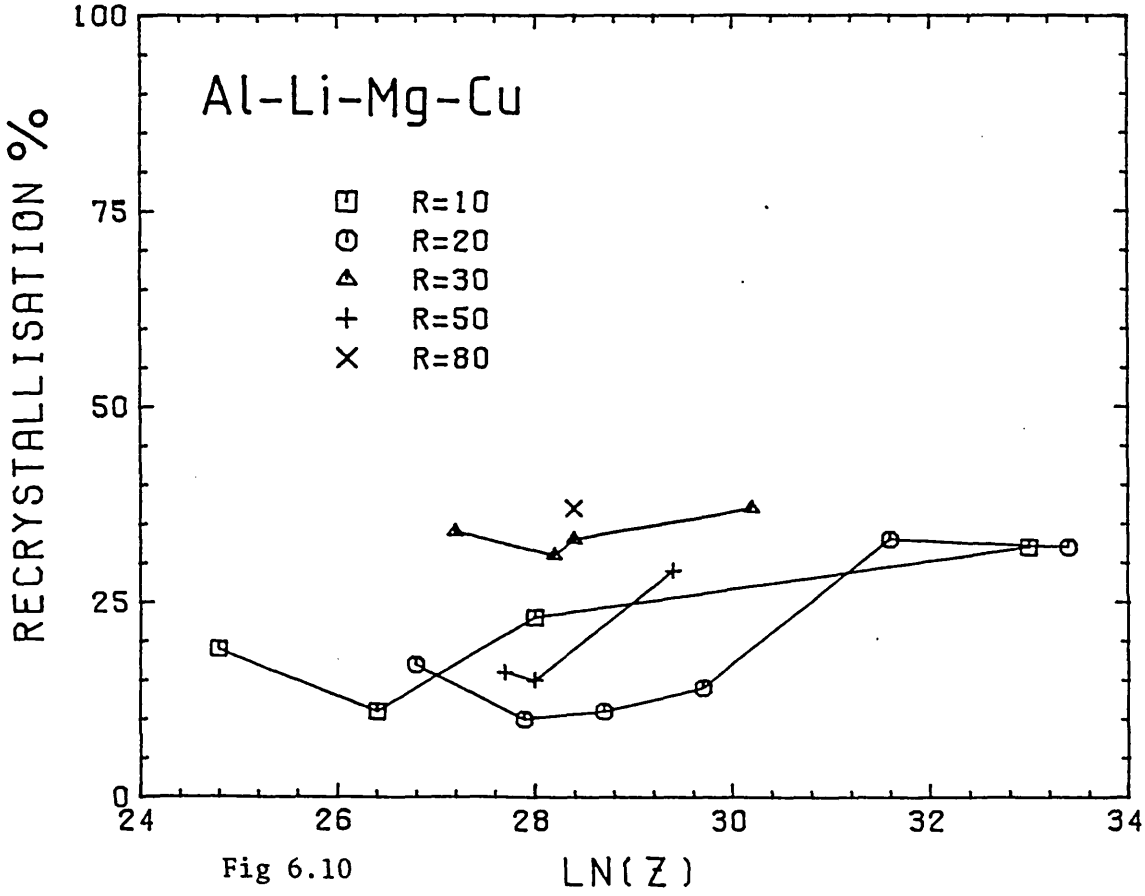

Fig 6.10

Variation in the level of recrystallisation with the extrusion conditions.

As Extruded Substructures, R = 20:1

Al-Li-Mg

Fig. 6.11

Initial Temp = 500°C
ram speed = 5 mm/s

Fig. 6.12

Initial Temp = 325°C
ram speed = 15 mm/s

Al-Li-Mg-Cu

Fig. 6.13

Initial Temp = 450°C
ram speed = 5 mm/s

Fig. 6.14

Initial Temp = 325°C
ram speed = 5 mm/s

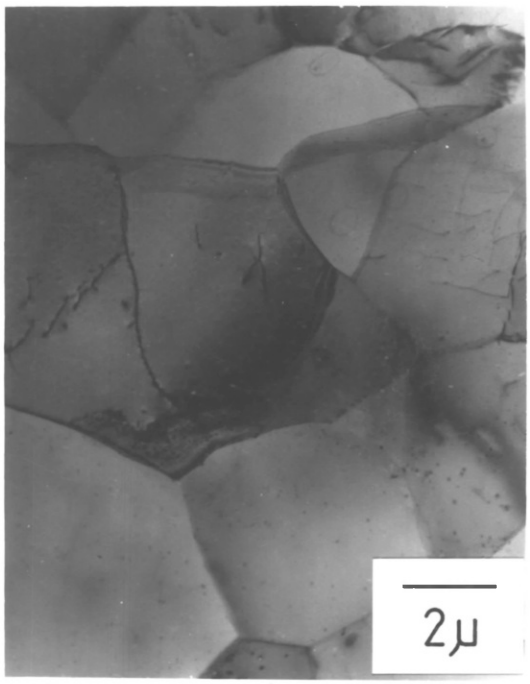
2μ

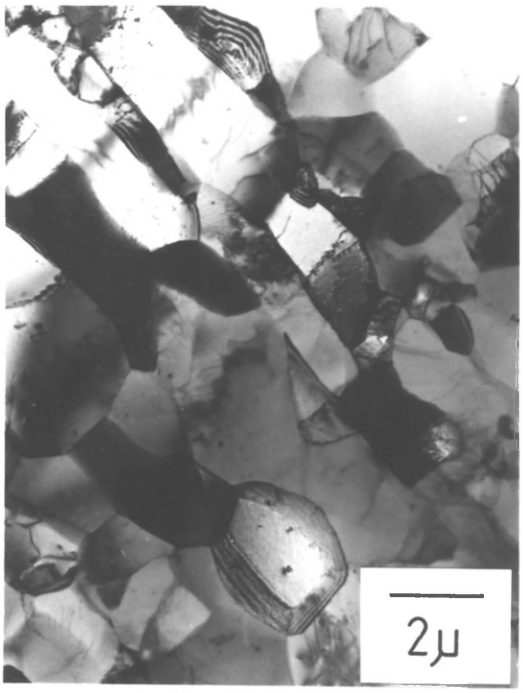
2μ

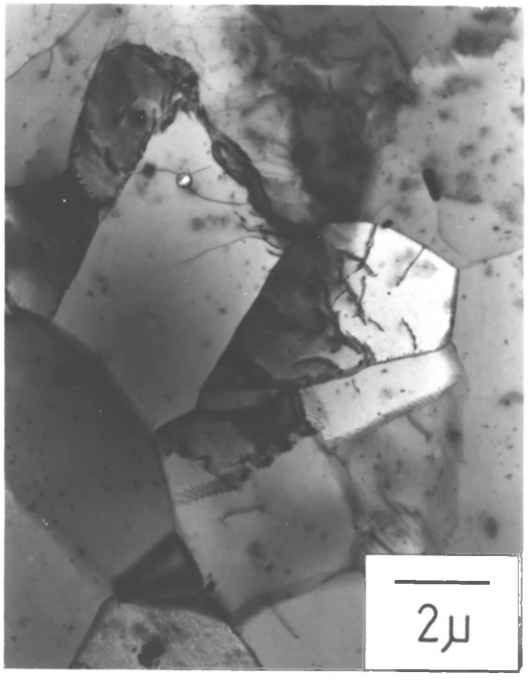
2μ

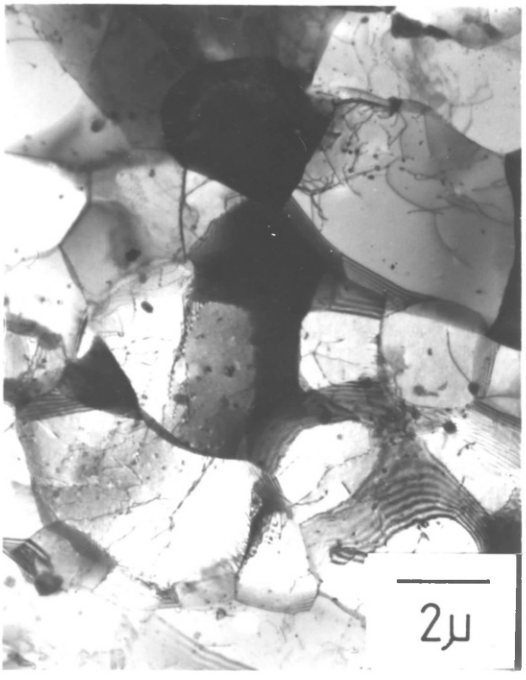
2μ

densities are low but increase at lower temperatures coinciding with the reduction in subgrain size. There is no evidence of any of the lithium containing phases and these must have been taken into solution by the process heating, that is the induction preheat and extrusion temperature rise. Differences in the scale of the substructure will be discussed in a later section, but what can be noted here is the increased submicron particle content in the Al-Li-Mg-Cu alloy. The finer of these are probably Al_3Zr, but the coarser ones may be remnants of coarse as cast particles. At the lower temperatures both alloys tended to produce a more elongated substructure due to reduced recovery, as seen for the Al-Li-Mg alloy in Fig. 6.15.

As the structures of the two alloys are generally well recovered the most likely mechanism for nucleation of recrystallisation is subgrain coalescence, where high misorientations are produced by merging of adjacent subgrains. In some instances, as in Fig. 6.16, statically recrystallised grains were observed adjacent to stringer particles. Here it would appear that nucleation occurred at the line of micron-size particles originally on a grain boundary. Humphreys[74] explained this mechanism in terms of the lattice rotations adjacent to large particles, which are necessary to allow for the strain discontinuity in the matrix. His review of the literature showed that this effect was not observed for particles below 1 micron in size for aluminium. This is not the main mechanism in these alloys, however, otherwise the copper containing alloy would have exhibited a greater level of recrystallisation due to its higher inclusion content.

An interesting feature of recrystallisation in these alloys below 500°C is its banded nature. Fig. 6.6 shows this effect, together with the electron micrograph Fig. 6.17. The newly formed grains occur in rows between what appear to be two original grain boundaries and are unable to migrate past them. This is probably due to the alignment of particles in the extrusion direction, as seen in Fig. 6.16, although the texture difference across a grain boundary is also reported to have an effect on recrystallisation[37]. Both the coarse as cast particles and the submicron Al_3Zr particles are strung out in this way but whereas the former are usually in a single line corresponding to an original grain boundary, the latter are present in the matrix in bands separated by particle free regions. The fine intermetallics will be more effective in this respect as Al_3Zr is reported to be a

Features of the Extruded Structure

Fig. 6.15

Al-Li-Mg
350°C, 5 mm/s, 20:1

Fig. 6.16

Al-Li-Mg
400°C, 5 mm/s, 30:1

Fig. 6.17

Al-Li-Mg
430°C, 5 mm/s, 30:1

Fig. 6.18

Al-Li-Mg
325°C, 14 mm/s, 20:1

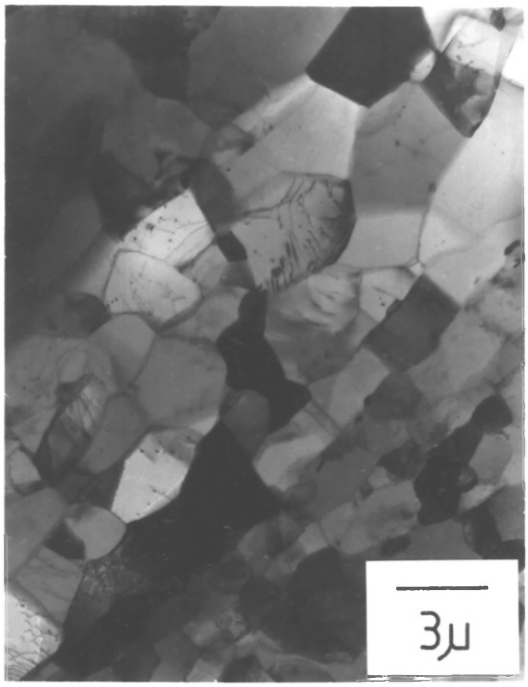
3μ

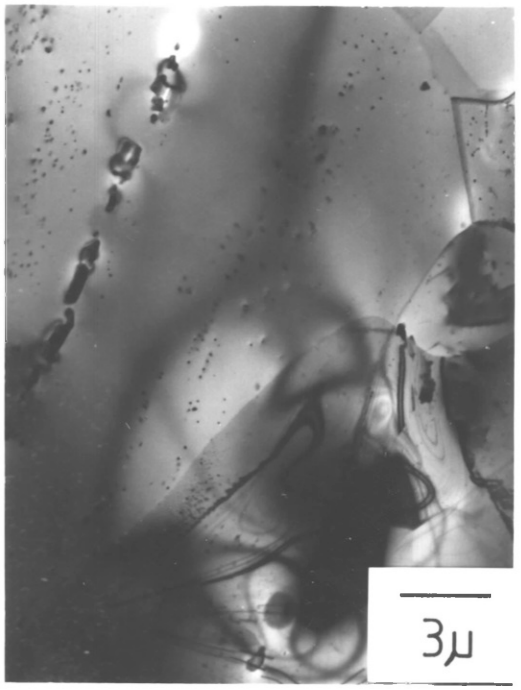
3μ

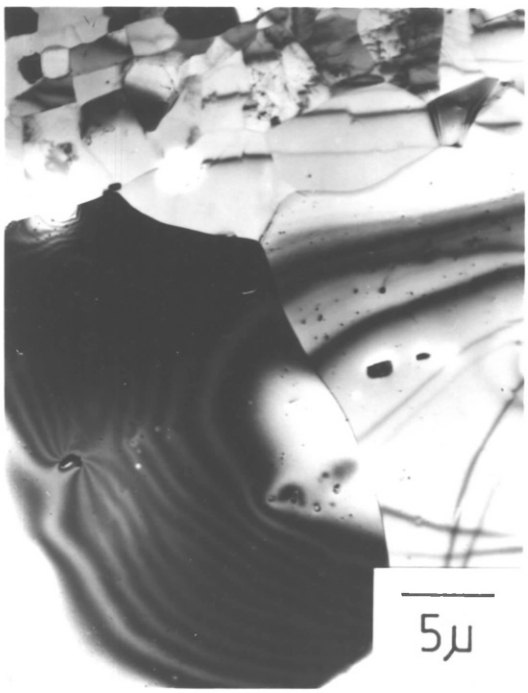
5μ

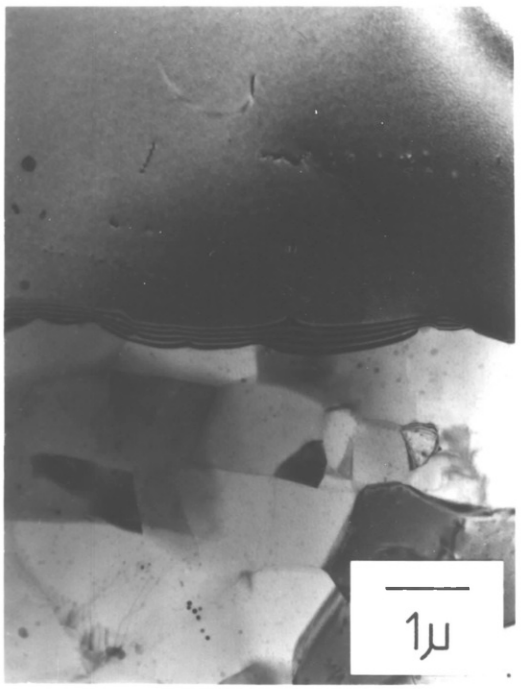
1μ

Features of the Extruded Structure

Fig. 6.19

Al-Li-Mg
400°C, 5 mm/s, 30:1

HVEM in situ
ageing experiment

Fig. 6.20

Al-Li-Mg
360°C, 15 mm/s, 30:1

Fig. 6.21

Al-Li-Mg T6
450°C, 5 mm/s, 80:1

Fig. 6.22

Al-Li-Mg T6
450°C, 5 mm/s, 100:1

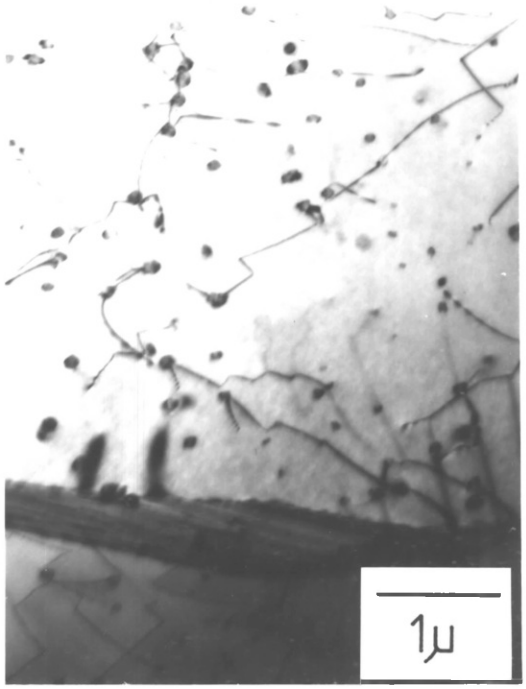
1μ

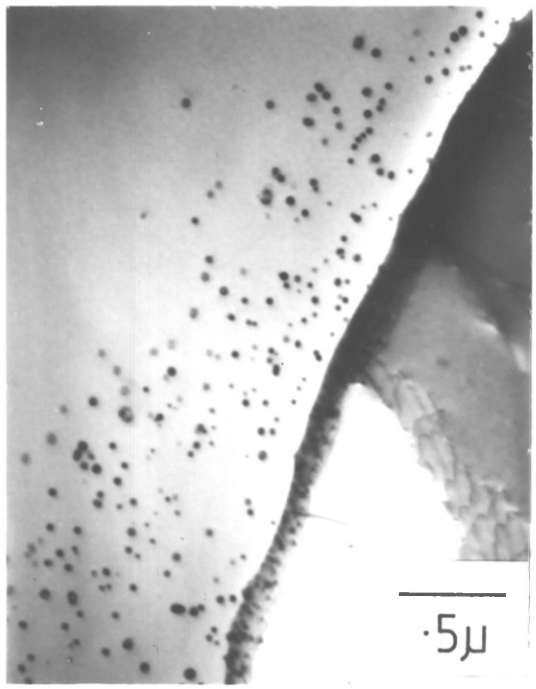
·5μ

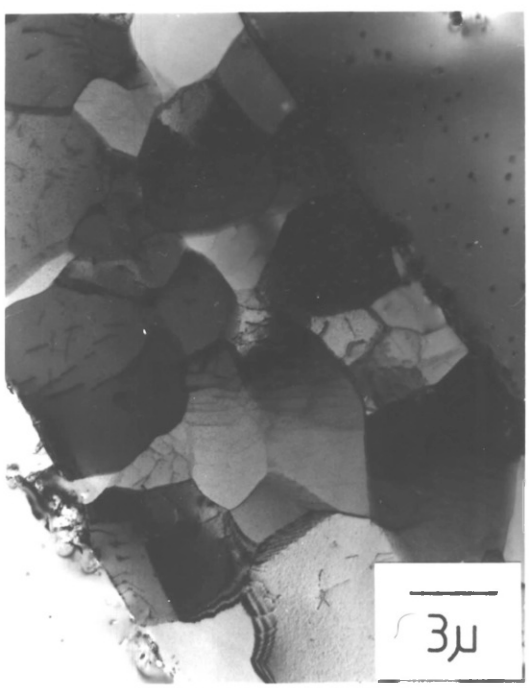
3μ

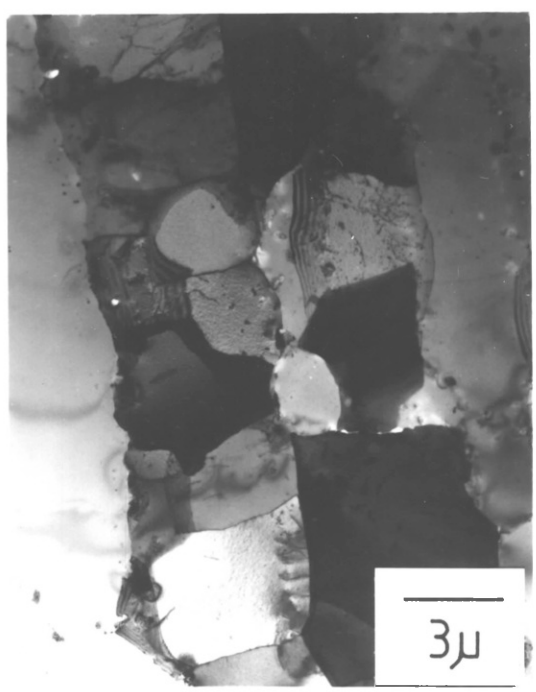
3μ

powerful grain boundary pinning agent[72] due to the semicoherent nature of its interface. They were observed to have two functions in these alloys, pinning high angle boundaries, Fig. 6.18, and pinning dislocation arrays, Fig. 6.19. The last micrograph was taken during an in situ HVEM ageing experiment. Dislocation motion due to thermal stresses was observed to be impeded by the Al_3Zr particles. Also, the particles can be positively identified here by the lines of zero contrast shown. The effectiveness with which both of the above functions are performed is responsible for a virtually identical structure being retained through subsequent heat treatment. However, as shown above, the Al_3Zr distribution was somewhat heterogeneous and was often found in very high particle densities. Such an area is illustrated in Fig. 6.20. It is possible that the Al_3Zr distribution could give rise to a nucleation mechanism. Substantial dislocation tangles may build up during extrusion in regions of high particle density and if a significant misorientation can be produced then migration into the adjacent particle free area might occur.

The banded nature of the grain structure and the substructure is emphasised at higher ratios. Figs. 6.21 and 6.22 are from the Al-Li-Mg alloy extruded at 80 and 100:1. (The extrudate was fully heat treated, explaining the lighter phase on the grain boundaries). The higher strain has resulted in alternate bands of recrystallised and unrecrystallised material. This effect made it difficult to show any clear trend with recrystallised grain size.

In summary, the extruded structures in these alloys were nearly always partially recrystallised. The extent to which static recrystallisation took place could be related to the process conditions and was promoted by lower temperatures and high ratios, i.e. an increase in the stored strain energy. The fact that these structures can be retained during heat treatment, due to the Al_3Zr distribution, would indicate that control of the extrusion parameters could influence final properties.

6.2.2 Extrudate Surface Structures

A recrystallised periphery was present in all the extrusions due to the high levels of deformation at the surface. In general, only the layer immediately adjacent to the surface was fully

recrystallised and the subcutaneous fibrous zone was partially recrystallised, merging in with the core structure. Again the form that the surface layer took varied with the extrusion conditions. Referring back to Figs. 6.7 and 6.8, these micrographs show the effect of extrusion temperature on the recrystallised structure for a ratio of 20, in the Al-Li-Mg alloy. At the higher temperatures, above 450°C, a very fine equiaxed grain structure was produced with grains of about 5 microns in diameter. This was stable on subsequent heat treatment, presumably because of the very even distribution of Al_3Zr in this region. At lower temperatures this structure coarsened by discontinuous grain growth giving rise to a range of grain sizes. The trend shown here also supports the observation made for the core structures, that larger recrystallised grain sizes are promoted by high dislocation densities in these alloys, rather than by thermal activation. Substantial coarsening of the structure was encountered at higher ratios giving surface grain sizes of up to 50 microns. However, measurements became erratic as large variations were observed in short distances along the extrude length and periphery.

The copper containing alloy showed similar trends but the grain sizes were larger and the measurements even more erratic. The fine equiaxed structure could be produced at 500°C with a ratio of 10:1, but at all other conditions the structure was coarser than for the copper free alloy. Often the surface layer was 2-3 grains thick with a maximum grain size of the order of 100 μ. These structures may be partly due to the higher coarse particle content which will be broken down near the surface giving rise to more nucleation sites.

Recrystallised depths increased with higher ratios and lower temperatures but these were trends rather than fixed relationships. The depth was a difficult variable to measure, since there was rarely a definite recrystallised surface layer like that found in 5000 series extrusions. Instead, recrystallised and recovered material were present together in the fibrous outer layer and this gradually merged into the core structure which was usually partially recrystallised anyway.

Most of the surface structures were retained after solution treatment, although discontinuous grain growth sometimes occurred locally.

6.2.3 Structural Variations in Torsion and Extrusion

In order to compare torsion and extrusion substructures, torsion tests were stopped shortly after the peak torque was reached and water quenched. This ensured that the steady state structure was being studied and not that due to temperature rise effects specific to the torsion test.

All the extrusion and torsion substructures consisted of well formed subgrains with low internal dislocation densities. The tendency towards subgrain banding found at low extrusion temperatures was not observed in the torsion structures and also no evidence of static recrystallisation was found. The latter effect may have been due to the rapidity of the quench in the torsion test but it is more likely that both of these effects are associated with the elongated nature of the extruded structure. Similarly, no recrystallised surface layer was produced in torsion, since this is a result of the severe surface strains in extrusion.

Subgrain size measurements were made using the linear intercept method on micrographs taken in the longitudinal plane. Strictly the torsion structures at the surface should have been examined to correspond with the calculated strain rate. However, this was not practical and structures were examined from as close to the surface as possible.

Subgrain size data for each alloy in the two modes of deformation is presented in Figs. 6.23 and 6.24. The torsion results are from a wide range of temperatures and strain rates and those from extrusion are for ratios of 20, 30 and 50. The two types of results are plotted as reciprocal subgrain size against ln Z. This relationship is generally accepted as giving a good correlation for this sort of data[30, 75], although several alternative types of expression can be used due to the inherent scatter in subgrain size results.

The scatter in the torsion data is considerably greater than that for extrusion due to the positional effect outlined earlier. Comparing the linear fits for the two types of data, those for the torsion results are slightly higher in both alloys. This can be explained by the higher temperature rises in extrusion giving lower actual values of Z. The broken line in Fig. 6.24 was constructed using temperature corrected ln Z values for extrusion and is very close

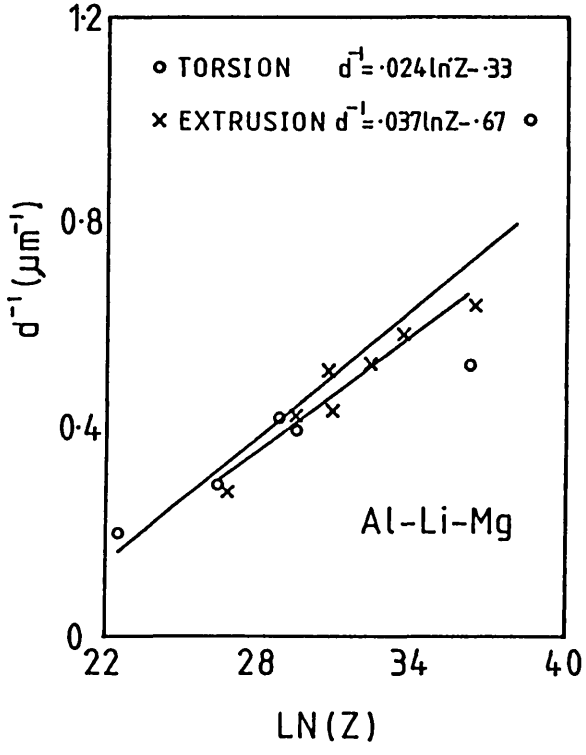

Fig 6.23

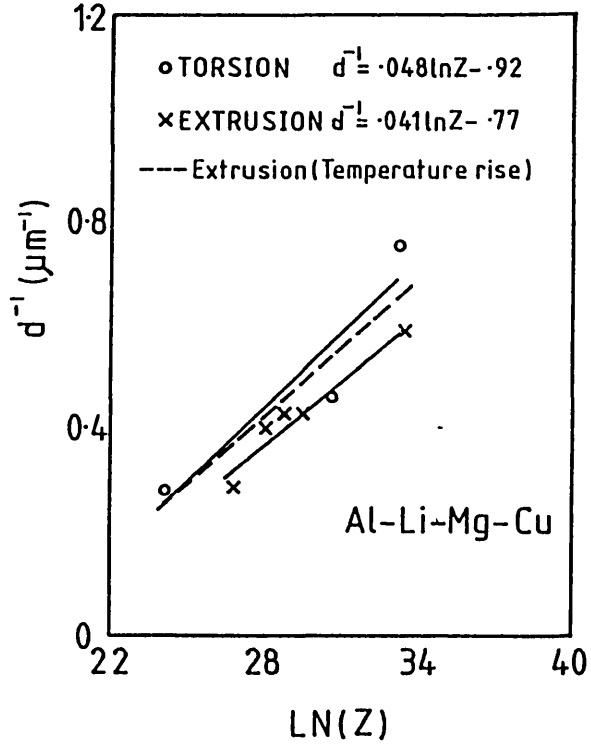

Fig 6.24

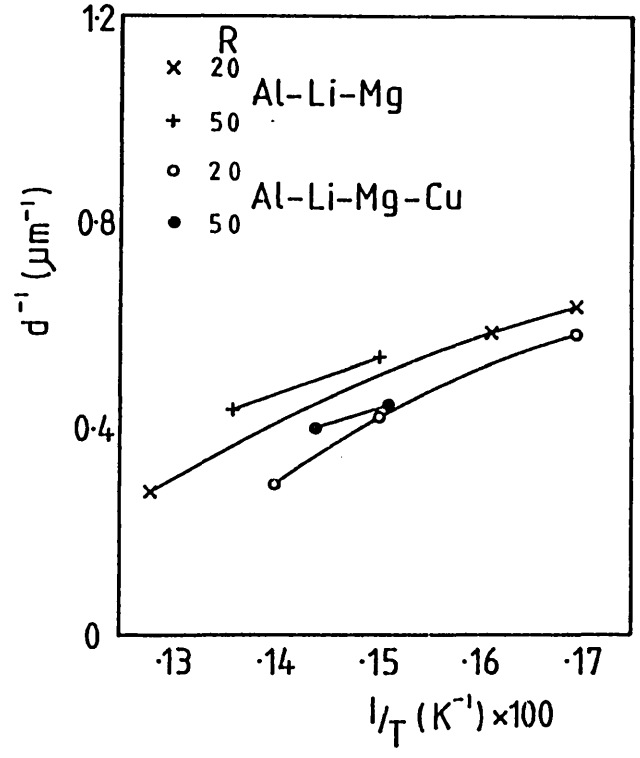

Fig 6.25

Subgrain size variations in torsion and extrusion.

to the fit to the torsion data. Calculated torsion temperature rises were small and only gave minor changes in ln Z.

Thus, these results show that the torsion test may be used as a model to predict the substructural variation in extrusion. Its use is limited, however, when trying to predict the effect of extrusion ratio, particularly on recrystallisation effects, as these appear to be controlled by the elongated nature of extruded structures. The linear fit of the extrusion data with ln Z suggests that substructural hardening can be varied with the process conditions in both alloys.

Fig. 6.25 compares extruded subgrain size data for both alloys in the form of reciprocal subgrain size against reciprocal temperature at ratios of 20 and 50. Subgrain size was reduced by higher ratios in association with the banding effect and this corresponds to the increased level of recrystallisation. The addition of copper increases the size of the substructure by roughly 6-14%, indicating recovery is made easier by the presence of copper. This is to be expected from the lower activation energy and flow stress reported in Chapter Five. If recovery is made easier then the subgrain walls might be expected to be less tangled and hence offer less resistance to glide dislocations giving reduced hardening in this alloy.

6.2.4 Two Stage Extruded Material

Extruded lengths of the Al-Li-Mg alloy were provided by Alcan International Ltd, in order to investigate the effects of further extrusion on the structure. They had been processed at 460°C with a container temperature of 400°C and a ram speed of 24 mm/s. The bar diameter was 54 mm so extrusions were performed using the 57 mm liner. Combining the initial extrusion ratio of 17 with those used in this work gave overall reduction ratios of 100, 380, 580 and 960. Billet heating was performed in an air circulating furnace as an induction coil of the appropriate size was not available. The length of billet used was increased to 100 mm to produce reasonable extrude lengths at low ratios.

Extrusion pressures were higher than for the 75 mm extrusions at corresponding conditions, but this was probably due to the greater

frictional contribution rather than the strength of the worked structure. With the lower loads due to the reduced ram diameter it was possible to extend the lower extrusion limit.

The as received material was almost unrecrystallised initially, apart from very fine grains at original grain boundaries, i.e. identical to the structure observed for similar extrusion conditions earlier. All the structures produced by further extrusion were again partially recrystallised, similar to those found earlier, but the high levels previously produced at ratios of 30 and above were never attained. This is initially surprising since even higher levels of recrystallisation might be expected at these very high net ratios. However, by splitting the deformation into two steps recovery is made easier, since the strain rate is reduced. Also from hot working theory the starting substructure should not influence the final substructure if a steady state is reached. Even so, the highest ratio used in the second stage was 55:1 and a strain of this order ought to have produced substantial levels of recrystallisation. A possible explanation for this may be that as the grain boundaries are already aligned in the extrusion direction then the strains in their vicinity will be comparatively less giving a smaller number of nucleation sites.

Again the structures were stable during heat treatment and so using two stage extrusion may be a method of reducing the high levels of recrystallisation produced after large reductions.

Surface recrystallisation was generally coarser than for previous extrusions, due to the accumulated surface deformation, although some of this can be attributed to the large amount of upset that occurred with this billet size. It was possible to extrude down to 225°C at the lowest ratio and here it was interesting that the very fine surface structure found at the highest extrusion temperatures reappeared. This then coarsened considerably on solution treatment, indicating that at this extrusion temperature grain boundary mobility is restricted. Another feature of the low temperature extrusions was that the original grains were bent back in an 'arrow' shape at the surface, indicating a change in the metal flow characteristics due to increased metal stiffness.

To summarise, this work would indicate that large reductions are possible in these alloys without incurring extensive recrystallisation, by applying the deformation in stages.

6.2.5 Recrystallisation Experiments

It has been reported in previous sections that the extruded substructure could be retained during the solution treatment step, an hour's soak at 500°C, with very little change in subgrain size. Experiments were now conducted to further investigate the effects of annealing time and temperature on recrystallisation behaviour using the 225°C extrusion produced from two inch bar in section 6.2.4. This ought to have the least recovered substructure of all the extrusions and therefore should be the most likely to recrystallise.

Initially sections were given an hour's soak at various temperatures up to 560°C, close to the liquation point, using an air circulating furnace. Even at this temperature the core structure only showed slight coarsening of the recrystallised grains present, with very little further nucleation. Any changes that occurred were mainly at the surface. The fine grains present after extrusion underwent grain growth and above 500°C the layer began to advance inwards. However, this was slow and even at 560°C the depth of this layer was only 3 mm.

These results are a further indication of the effectiveness of the Al_3Zr dispersoids as recrystallisation inhibitors. Difficulty in annealing zirconium containing alloys has even been reported for cold worked material[52].

A further experiment was conducted, increasing the soak time at 560°C, but after five hours the core structure was still predominantly unrecrystallised. The surface recrystallised layer broadened to a depth of 5 mm in this period. A high temperature extrusion given similar treatments showed virtually no effect apart from limited grain growth at the surface.

In summary, it appears that even for the highest stored energy levels and the highest soak temperatures this alloy still shows a high resistance to recrystallisation.

6.3 The Effect of Extrusion Conditions on the Room Temperature Tensile Properties

6.3.1 As Extruded Properties

Mechanical testing on the 20:1 extrusion matrices for each alloy was carried out in the as extruded condition in order to look at the contribution to the final properties without this being masked by the effects of heat treatment. The results are shown in Fig. 6.26 for the ternary alloy and in Fig. 6.27 for the quaternary.

Starting with the copper free alloy, the proof stress increased linearly with ln Z showing an improvement over the extrusion range of 40 MPa. This trend was also reflected in the UTS results. Any softening associated with the increased level of recrystallisation at low temperatures is clearly being outweighed by the strengthening due to the reduction in subgrain size.

In contrast the copper containing alloy exhibited only a very slight variation in strength with Z. The proof stress was higher than for the ternary alloy at low Z conditions due to solid solution strengthening but the ternary was capable of this strength level at high Zs. Using a reported figure for the solid solution strengthening effect of copper in aluminium[42], the level of addition here should give an increment of 15 MPa which corresponds to the difference at low Z values. The UTS was also raised by the addition of copper, but now it showed a slightly downward trend with Z. Elongation values for both alloys showed considerable scatter without any real trend and were centred around the 15% level.

The lack of proof stress variation with ln Z for the copper alloy can be partly attributed to the smaller working range, but significant subgrain size variations were still observed. However, the subgrains were generally larger for the same conditions which may explain this effect. It is possible that the copper addition is influencing the nature of the low angle boundaries and perhaps reducing their misorientation and effectiveness as obstacles to glide.

Hardness measurements were also taken in the as extruded condition but this was not found to be particularly sensitive to sub-structural strengthening and no clear trends were detected with

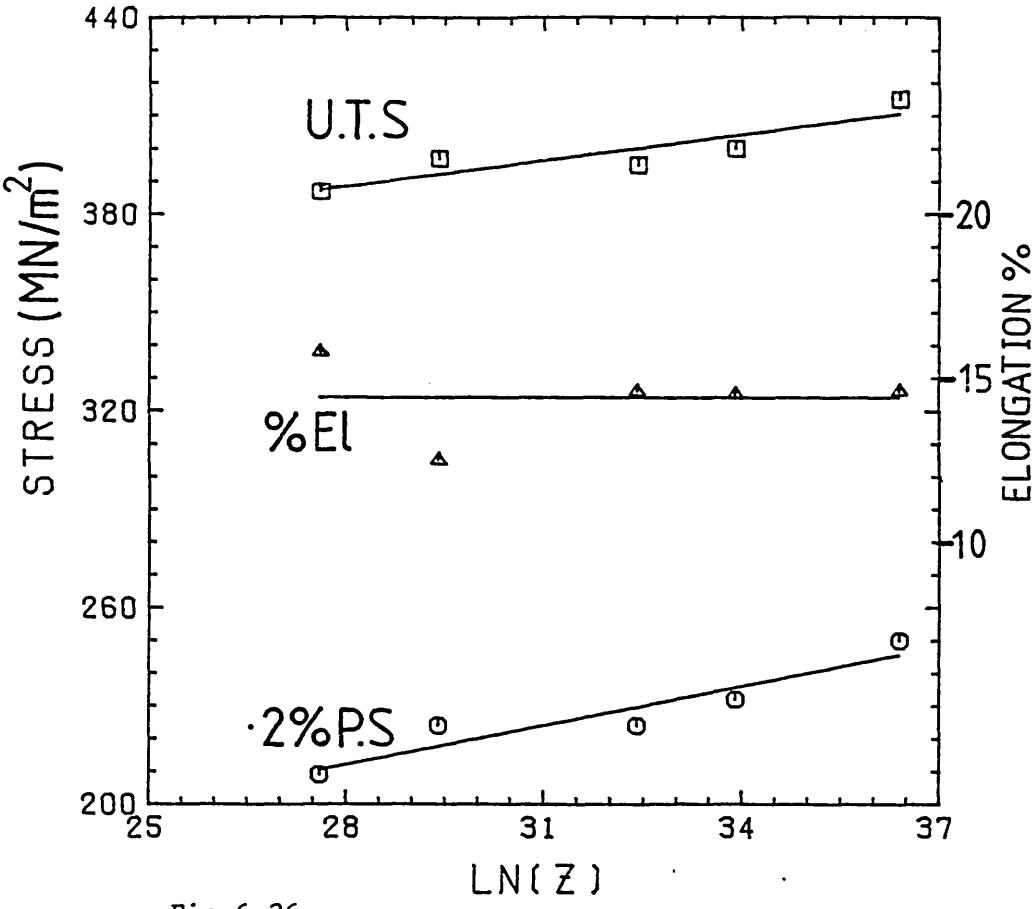

Fig 6.26

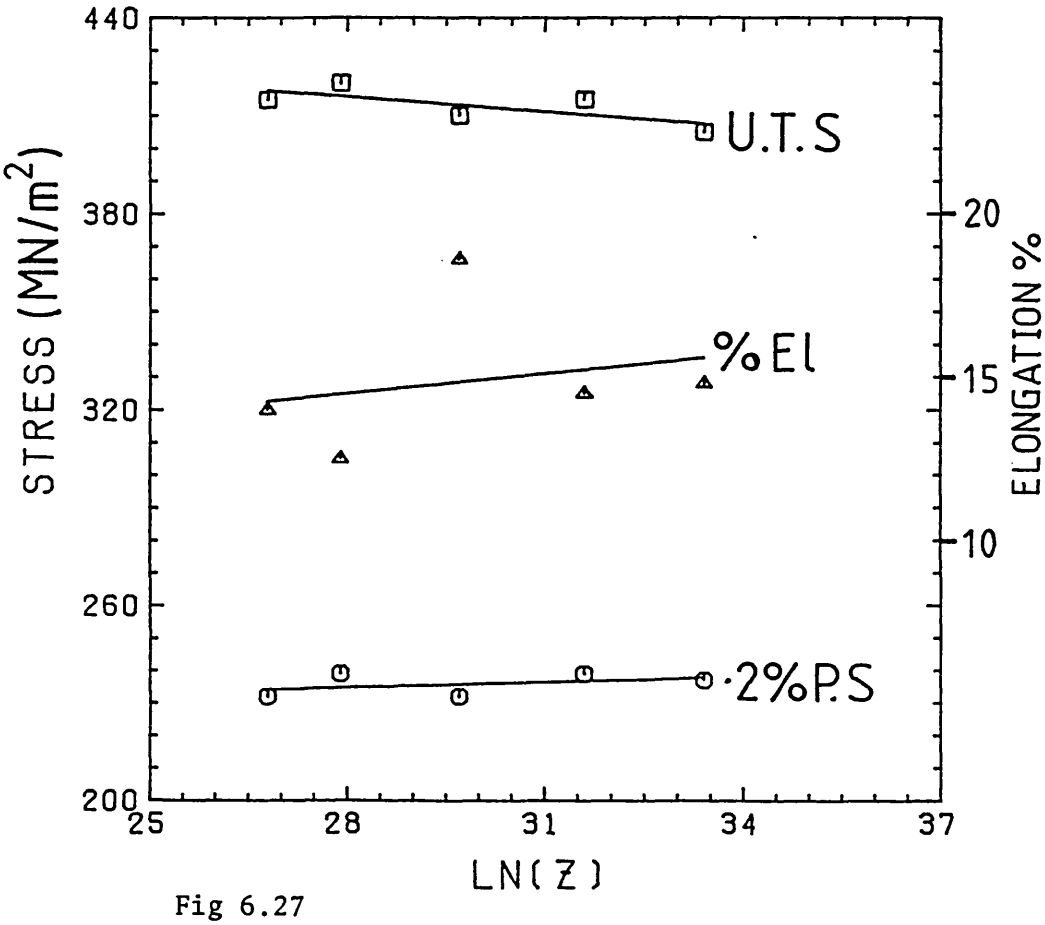

Fig 6.27

Variation of as extruded tensile properties.

extrusion temperature or ratio. In general for similar conditions the copper alloy was 5 VPN harder. The extruded hardnesses were all lower than for the homogenised state because press quenching prevented any precipitation hardening. Finally, no natural ageing was detected in either alloy in measurements made regularly over a six month period.

6.3.2 Fully Heat Treated Properties

Ageing practices for the peak strength temper were established by first following the ageing behaviour using hardness testing. Further details of this are given in Section 6.4.2. For heat treated properties the full extruded section thickness was heat treated and tensile specimens were machined from the centre in the longitudinal direction.

The variation in the tensile properties with ln Z and R is shown for the ternary alloy in Figs. 6.28 - 6.30 and in Figs. 6.31 - 6.33 for the quaternary. These will be discussed separately as the observed trends are quite different.

It has already been reported that in these alloys the extruded structure can be retained after heat treatment and for the copper free alloy the tensile results reflect this. The proof stress shows a linear increase with ln Z at low reduction ratios corresponding to the substructure strengthening observed in the as extruded condition. Over the range of extrusion temperatures the strength varies by 30 MPa, 7% of the minimum strength level. At higher ratios the influence of recrystallisation becomes important and the trend in the proof stress is the opposite of that for core recrystallisation, i.e. it decreases with ln Z and R. The level of softening at the higher ratios is quite considerable; at a ln Z value of 34 the proof stress falls from 460 MPa at 10:1 to 350 MPa at 60:1. Not all of this 110 MPa difference is due to subgrain strengthening, however, other contributions come from fibre strengthening and also texture strengthening. Generally extruded aluminium alloys have a strong fibre texture whereby 75% of the grains are aligned with their [111] directions parallel to the extrusion direction and the remainder have a [100] orientation. Strengthening is derived from the fact that in FCC metals the maximum applied stress: critical resolved shear stress ratio occurs in <111> directions.

T6 tensile property variations , Al-Li-Mg.

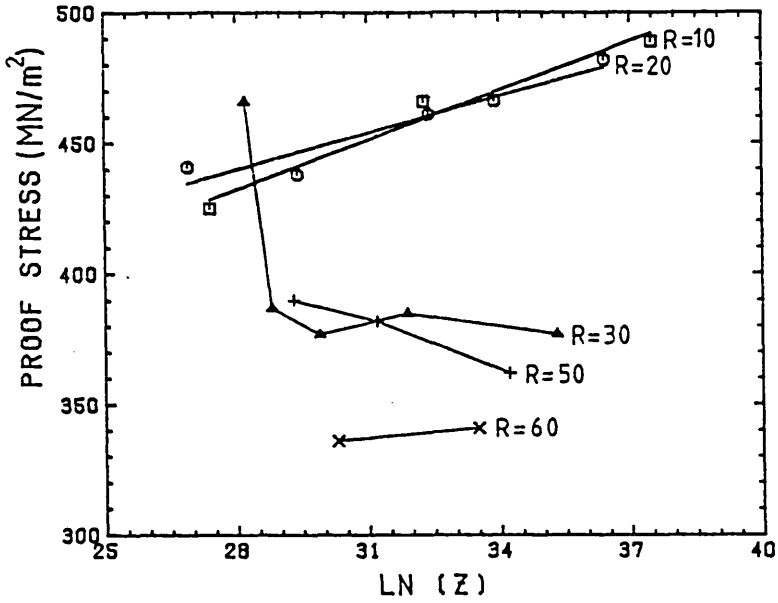

Fig 6.28

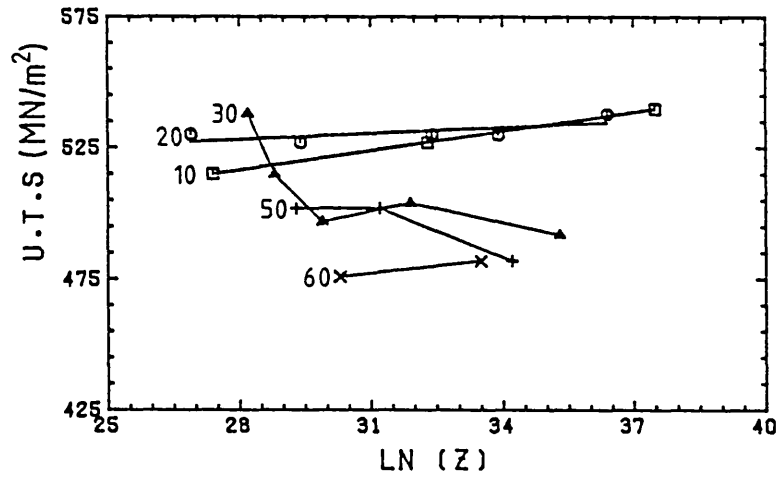

Fig 6.29

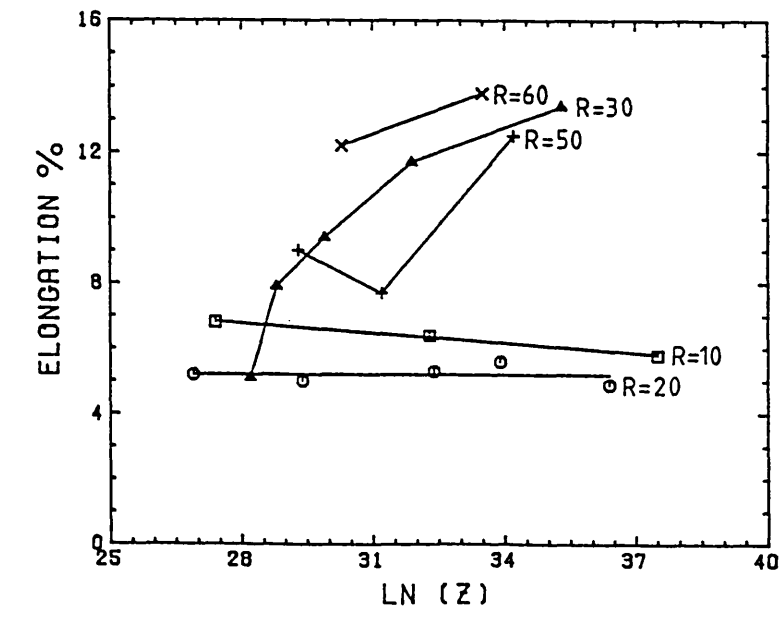

Fig 6.30

Static recrystallisation usually destroys this contribution.

The proof stress results were arrived at using up to three of the different casts and although the compositions were similar it is worth discussing any variations in properties this may have caused. Using the results from Miller et al[24], where the properties of several different ternary alloy compositions are given, slight variations in the magnesium levels can be ignored. Over all the ternary compositions in the present work the lithium level only varies by a maximum of 0.13 wt.% which by comparison can be expected to produce a difference in proof stress of only 7 MPa. The difference in lithium content between the quaternary and ternary alloys is greater and can be expected to give up to a 20 MPa increase over the latter in some cases.

The UTS varied with ln Z in a similar manner to the proof stress but the range of values was narrower. This occurred because more work hardening is possible in the lower yield stress structures. Elongation results followed an opposite trend to the proof stress which is not surprising, since the yield stress is a measure of the difficulty of deformation whilst ductility is a measure of its ease. However, it is worth noting that at low reduction ratios where recrystallisation is limited, strength can be increased by subgrain refinement without ductility loss.

Looking at the Al-Li-Mg-Cu results now, the proof stress varies in a completely different manner. Whereas for the ternary, the final strength was the sum of a fixed age hardening contribution and a variable substructure term, here both of the terms appear to vary with processing. (It should be noted that the stress scales have been expanded for this alloy by a factor of two). It has been reported already that the levels of recrystallisation in this alloy are lower, but softening was still associated with the higher extrusion ratios. In addition, for all ratios, even at 10:1, the proof stress increases as the extrusion temperature is raised. In the as extruded condition substructural hardening did not vary with the extrusion temperature for this alloy. Therefore this effect is due to a feature of the hot worked structure, other than the subgrain size, carried over through the heat treatment and in particular the solution treatment step. The most likely explanation for this trend is that the

T6 tensile property variations , Al-Li-Mg-Cu.

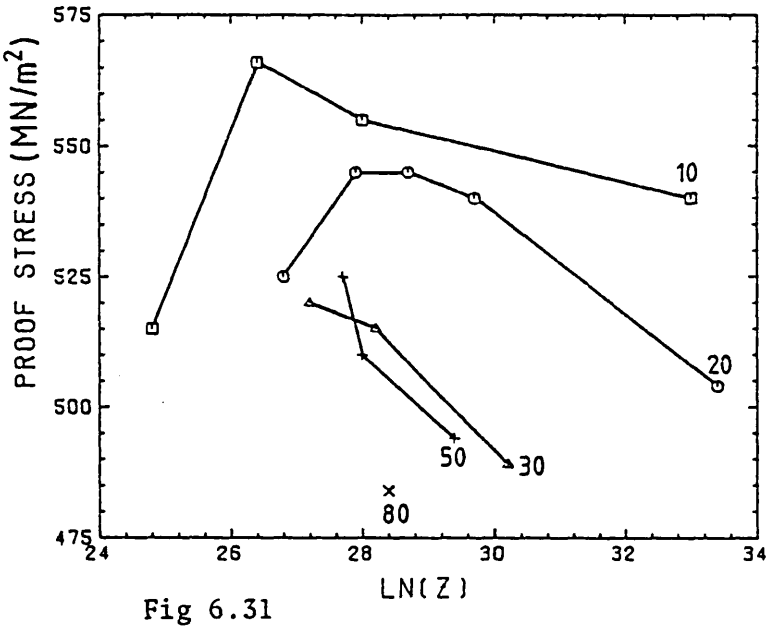

Fig 6.31

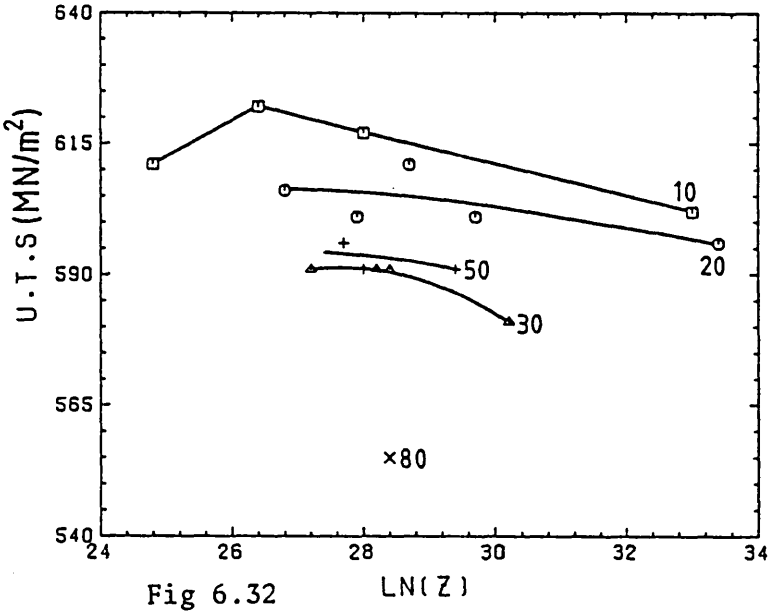

Fig 6.32

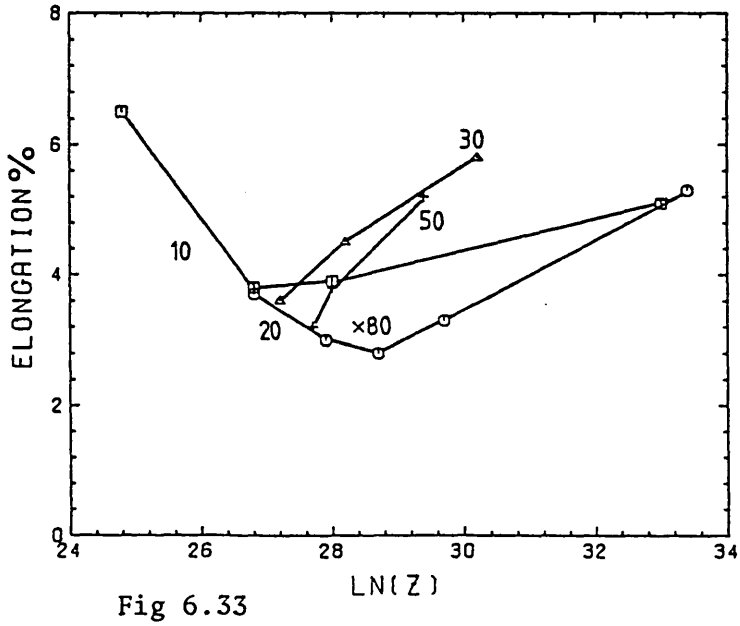

Fig 6.33

process heating is helping to solutionise more of the S phase present in this alloy. Higher extrusion temperatures will take more magnesium and copper into solution, producing a greater ageing response. This in turn implies that the solution treatment used was inadequate.

A further complication occurs at the highest extrusion temperatures; above 450°C at a ratio of 10:1 and above 425°C for a ratio of 20:1 the strength drops off very sharply. This feature is difficult to explain as TEM did not reveal any marked changes in the substructure at these temperatures and the proposed solutionising mechanism ought to be enhanced by these conditions. The UTS followed the proof stress trends, whilst elongation followed the reverse.

The 80:1 data point was included,even though the extrusion showed surface cracking,in order to give an indication of the effects of the highest ratios. The strength is reduced due to recrystallisation and possibly as a result of the high temperature effect seen at 10 and 20:1, since the temperature rise will be greater here. The elongation is not raised, however, but the variation of this parameter with grain structure appears fairly weak in this alloy. The overall spread of the data is only 4% which is produced by the temperature spread at each ratio, indicating that precipitation effects are controlling the ductility here.

The range of properties produced by varying the extrusion conditions, whilst still maintaining a sound product, are given in Table 6.4 for both alloys. The proof stress was raised by at least 50 MPa by the addition of copper at the conditions where the ternary alloy was at its strongest. This increased to 100 MPa in some instances but the strengthening was associated with a loss in ductility. Precipitation effects are primarily responsible for the hardening, as solid solution and substructural strengthening have already been shown to have little effect on the as extruded properties. Additional precipitation may be promoted by the copper addition or possibly the existing precipitation sequence may be affected. Whatever the mechanism, it is not improving the ductility of the system. For the lowest strength conditions in the copper alloy the ductility levels are similar to those of the first alloy in the high strength condition, suggesting a strong similarity between hardening mechanisms.

Alloy	Proof Stress (MPa)	UTS (MPa)	%El	Condition
Al-Li-Mg	490	540	5	R=10, T=325°C
	340	475	14	R=60, T=380°C
Al-Li-Mg-Cu	565	620	4	R=10, T=450°C
	490	580	6	R=30, T=350°C

Table 6.4 The Variation in T6 Temper Properties with the Extrusion Conditions

These alloys are candidate aerospace materials and therefore it is useful at this stage to compare their properties with those of alloys currently in use. The usual targets set in this respect[24] are 2014 T6 and 7075 T76 property levels. Minimum tensile properties quoted by the Aluminium Association for extrusions are listed in Table 6.5. Before making a direct comparison with these values it should be noted that they were determined using much larger specimens than in the present work and this factor can affect ductility results.

The Al-Li-Mg alloy is capable of 2014 T6 strength levels at low extrusion ratios but the ductility here is 2% lower. With increased substructural strengthening it is also capable of the 7075 T76 proof stress but again with reduced ductility. The copper containing alloy exceeds the 2014 T6 strength level at all conditions along with that for 7075 T76 but even at the lower strength conditions the ductility values are never reached.

The most attractive property of aluminium-lithium alloys is their low density giving high strength to weight ratios compared to other alloys. Density measurements were made by weighing samples in air and in water, giving a value of 2.51 g/cm^3 for both alloys. The copper addition had no effect and was probably compensated for by a slightly higher lithium level in the sample used. The density of a sample of 2014 extrudate was also measured to check the accuracy of the technique and this gave 2.79 g/cm^3, the value quoted by the Aluminium Association. The two alloys showed a density reduction of 10% over this which was the minimum target set by Peel[4]. Strength to

weight ratios of 2014 and 7075 are given in Table 6.6. In these terms the range of proof stress shown by the ternary alloy is 135-195, so that above 380 MPa the 2014 T6 strength to weight ratio is exceeded. At these strength levels the elongation of 7% can also be matched.

Alloy	Proof Stress (MPa)	UTS (MPa)	%El
2014 T6/T651	414	469	7
7075 T76	448	517	7

Table 6.5 Target Values for Tensile Properties

	[MPa/(g/cm^3)]	
Alloy	Proof Stress	UTS
2014 T6, T651	148	168
7075 T76	161	185

Table 6.6 Target Values for Specific Strengths

To summarise, the fully heat treated tensile properties in these alloys have been shown to vary with extrusion conditions. In the Al-Li-Mg alloy, strength is purely a function of the subgrain size and the level of recrystallisation, whereas in the copper containing alloy the extrusion temperature appears to influence age hardening behaviour. The alloys are easily capable of target strengths in this product form but ductility is still generally below that for conventional alloys.

6.4 The Effect of Heat Treatment Variables on Room Temperature Tensile Properties

This section reports the response of the two alloys to a simple two stage heat treatment. Finally, the effects of the incorporation of a cold stretch are discussed.

6.4.1 Solution Treatment

Unless otherwise stated, all the heat treated material was given a solution treatment consisting of a solution soak followed by a cold water quench. This was performed even though the process heating and press quenching ensured that a high level of supersaturation already existed. The soak time used normally depends on the section thickness. Here the largest extrusion diameter was 25 mm and a standard time of one hour was used.

The Al-Li-Mg alloy was not very sensitive to the solution treatment conditions and a soak temperature of 500°C was adopted. No property advantages were found in exceeding this. The properties of the Al-Li-Mg-Cu alloy have already been shown to be sensitive to the extrusion temperature, presumably through its solutionising effect. Therefore, the maximum temperature possible was used for the solution treatment but due to S phase liquation it was not safe to exceed the homogenisation temperature, 510°C.

In many commercial alloys, the hot worked structure is destroyed by recrystallisation during this treatment, but this has already been found not to be the case here. Subgrain size measurements made before and after solution treatment showed remarkably little change and the only difference in structure appeared to be a reduction in the internal dislocation density.

All solution treatments were carried out in air, resulting in a lithium depleted layer near the surface, approximately 20 μ deep. This became significant in the investigation of corrosion resistance later in the project (Chapter 8).

6.4.2 Artificial Ageing

Initially the effects of ageing time and temperature were investigated using hardness testing as this is a rapid method for characterising alloy behaviour. In tests made at times ranging from immediately after solution treating up to three months, no natural ageing response was detected in either alloy. Figs. 6.34 and 6.35 show the ageing response of both alloys at temperatures of 150, 170 and 190°C. In both cases the general shapes of the curves are similar showing classical ageing behaviour for a system producing metastable coherent precipitates. The maximum hardness was raised at lower ageing temperatures due to the promotion of finer precipitation. However, with the reduced diffusion rates at these temperatures the time taken to achieve this is also increased quite considerably. At 150°C no softening due to coarsening, which relies on diffusion, was found even after 200 hours, whereas at 190°C it occurred after 20 hours.

Comparing the two alloys, the early stages of ageing are very similar with a rapid initial hardness increase being shown. This is due to the interaction of glide dislocations with the δ' precipitates by a shearing mechanism. Continued ageing leads to coarsening and a gradual loss of coherency with the matrix, together with an increase in the interparticle spacing, which changes the mechanism to one of dislocation looping. This is accompanied by a gradual loss in hardness. Both alloys began to soften after similar times, but also gave broad flat peaks because of the slow coarsening rate of δ' due to its low interfacial energy. On overageing the copper containing material underwent a more rapid loss in properties.

The addition of copper raised the peak hardness by roughly 20 VPN, an increase of 14%, although 10 VPN of this was present in the solution treated condition. Even so this represents an increase in precipitation strengthening, either through additional precipitation reactions or by modification of the Al_3Li reaction.

Heat treatment practices for further work on material properties, such as corrosion resistance and toughness, were established using these results. A standard temperature of 170°C was adopted so that peak hardness could be achieved in practical times without a significant sacrifice in strength. Underaged and overaged conditions were

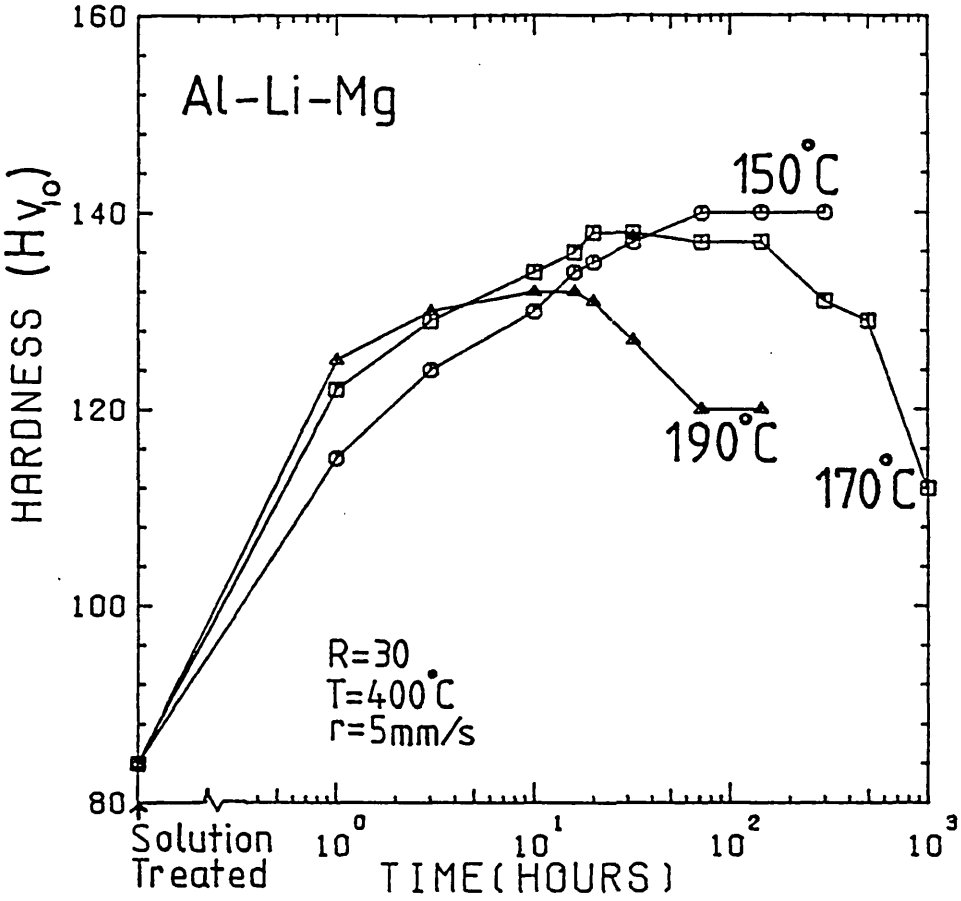

Fig 6.34

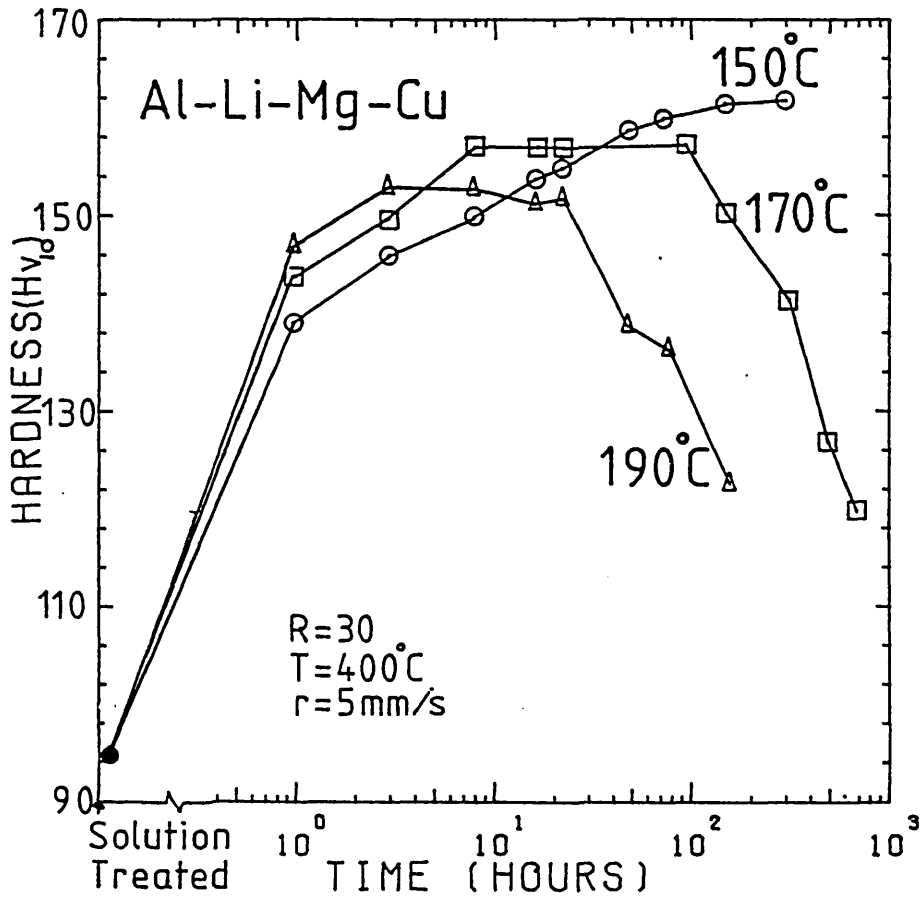

Fig 6.35

Hardness vs. time ageing curves.

produced by heat treating to give 80% of the peak hardness increment. The ageing times used are listed in Table 6.7. Clearly the overaged times are industrially impractical but it was thought better to maintain a constant ageing temperature in this work.

	Ageing Time (Hours)		
Alloy	U/A	P/A	O/A
Al-Li-Mg	3	16	300
Al-Li-Mg-Cu	4	32	150

Table 6.7 Ageing Practices

At a later stage the ageing behaviour was investigated using tensile testing to check the levels of strengthening associated with the heat treatment conditions chosen. The results are presented in Figs. 6.36, 6.37 and 6.38. The three Al-Li-Mg lines show the substructural effect seen earlier, where raising the extrusion temperature raised the proof stress, although this is not borne out by the solution treated values.

The addition of copper raised the maximum proof stress by roughly 80 MPa ($\sim$20%) but reduced the ductility. In the solution treated condition the difference in strength was much smaller so the additional effect can be attributed to enhanced precipitation hardening.

Again the initial hardening rate is rapid for both alloys and softening commences after 100 hours, the latter occurring more rapidly for the quaternary. The copper containing alloy still showed a flat-topped peak similar to the hardness curve, but the Al-Li-Mg alloy gave an additional local peak after 48 hours. This gave a strength increase of approximately 30 MPa over the condition chosen for the peak strength temper meaning that the treatment used gave a slightly underaged structure. UTS values showed a similar trend to the proof stress results and again elongations showed the reverse.

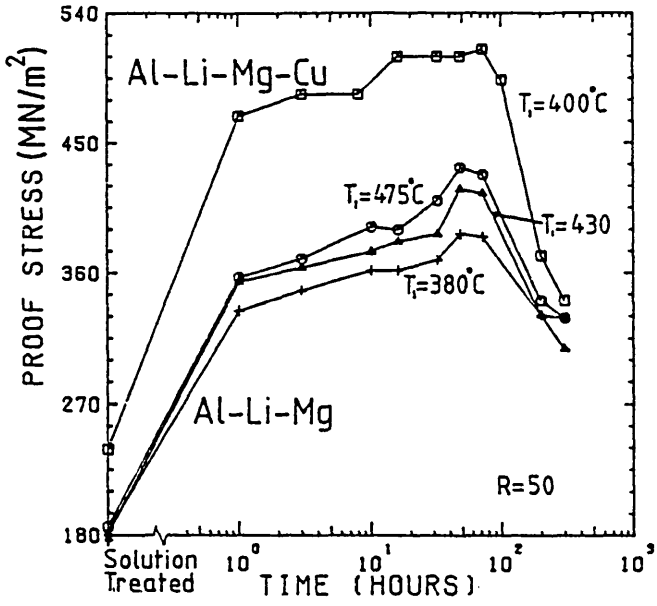

Fig 6.36

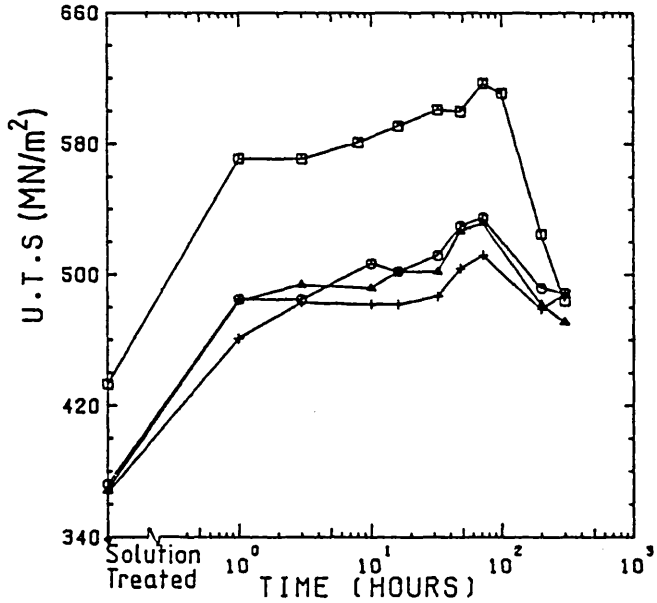

Fig 6.37

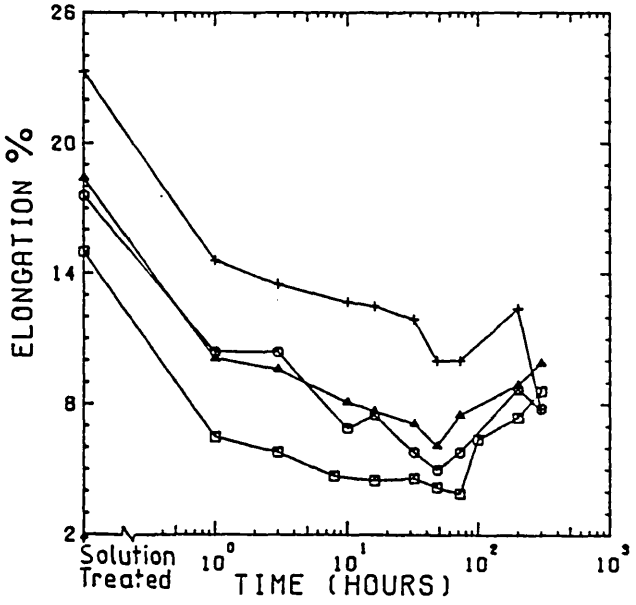

Fig 6.38

Variation of tensile properties with ageing time.

The elongation values are generally higher in the underaged condition than after overageing to the same strength level and this may be a method of improving ductility without sacrificing too much in the way of strength. The ageing curve for the copper alloy suggests that 7075 T76 strength and elongation values may be reached in this way. Similarly, underageing the Al-Li-Mg ternary in the substructurally hardened condition will give elongation values on 2014 T6 levels, while still allowing adequate strength to be maintained. However, it should be noted that elongation is not a direct measure of toughness, although it can give useful indications and is really specific to tensile deformation.

From these results the levels of strengthening for the heat treatment practices established by hardness testing were calculated and are given in Table 6.8. In all the tempers the copper free alloy was underaged compared to the copper containing system due to the inaccuracy of the hardness test in predicting small proof stress variations.

	% Maximum Hardening		
Alloy	U/A	P/A	O/A
Al-Li-Mg	70	90	50
Al-Li-Mg-Cu	90	100	70

Table 6.8 Levels of Strengthening for the Heat Treatments Used

Figs. 6.39 and 6.40 show typical true stress-true strain curves from the tensile tests which produced the results in Figs. 6.36-6.38. True stresses were calculated using the standard conversion[76] and at low strains engineering and true strain can be assumed to be identical. The calculation of true stress breaks down when tensile instability in the form of necking occurs but in these alloys little necking was encountered. It never occurred in the copper alloy, presumably because failure occurred at the first signs of any instability. This was the case for the Al-Li-Mg alloy, apart from in the softest condition,

i.e. solution treated or recrystallised underaged material, but not in the overaged condition. When it did occur it was limited to an engineering strain of 0.01. The curves are drawn for similar extrusion conditions but the ternary alloy was softened by heavy recrystallisation. The main feature apparent when comparing both sets of curves is the extent of work hardening. In the solution treated condition the two are similar, as expected, but on ageing the copper bearing alloy shows a reduction in the extent of work hardening in all the tempers. Upon overageing the copper free alloy showed a sufficiently high work hardening rate to approach the 'peak-aged' curve, whereas in the high strength alloy all the conditions had similar hardening rates. In precipitation hardening alloys the rate of work hardening is not normally increased by the formation of coherent precipitates and remains constant until peak strength is reached when it undergoes a sharp rise[38]. This transition is due to the change in the dislocation particle interactions.

A common feature in both alloys was the occurrence of serrated yielding. This is often found in aluminium alloys containing magnesium in solid solution and is also referred to as the Portevin Le Chatelier effect. It is due to the interaction of magnesium solute atom atmospheres with the stress fields of glide dislocations. They repeatedly attach themselves to the dislocations which can break free as the applied stress is raised. The effect was prevalent in the ternary alloy in the solution treated condition and for short ageing times. In the former, the cycles were continuous with a stress amplitude of 5 MPa but this increased to 12 MPa on ageing with a correspondingly larger strain per cycle. As ageing continued, the serrations became less frequent and disappeared on overageing, indicating that magnesium was being lost from solid solution. The fact that this effect was seen to a lesser extent in the second alloy is perhaps due to the influence of copper atoms on the magnesium diffusion rate. Serrated yielding has been observed in other Al-Li-Mg-Cu alloys[62].

From the true stress-true strain curves it is possible to evaluate the strain hardening exponent, n, assuming a stress strain relationship of the form;

$$\sigma = A \varepsilon^{n}.$$

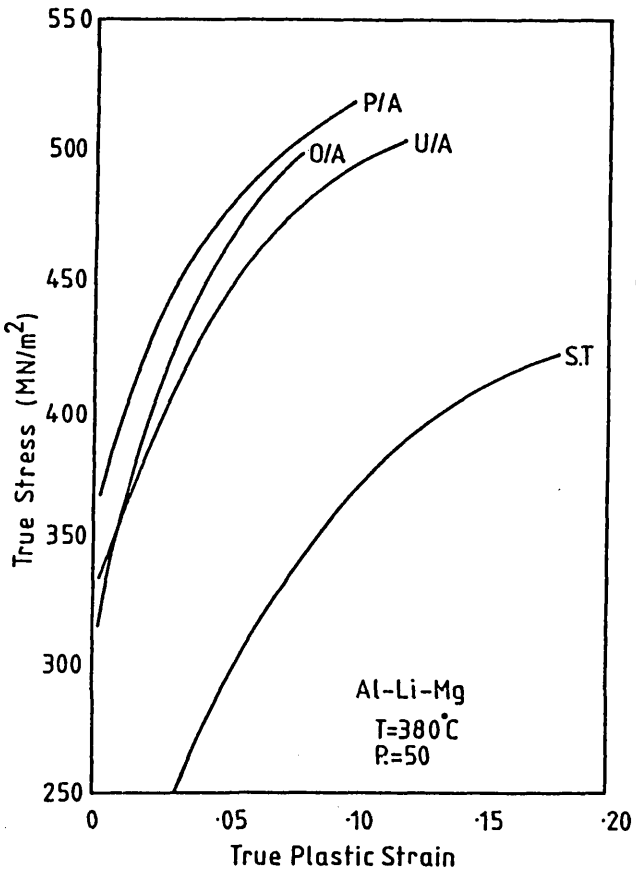

Fig 6.39

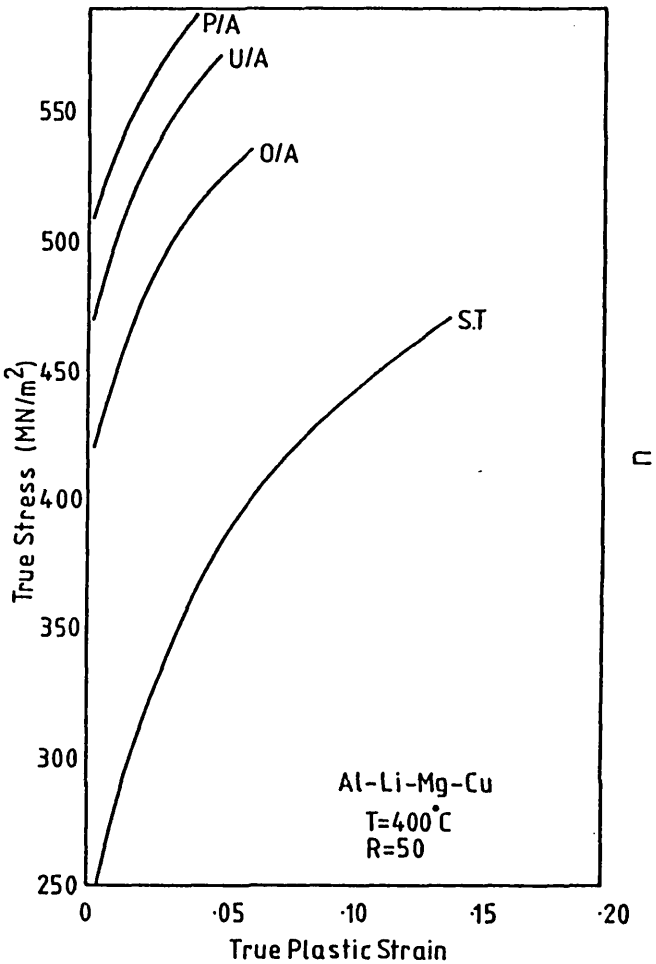

Fig 6.40

True stress-true strain curves.

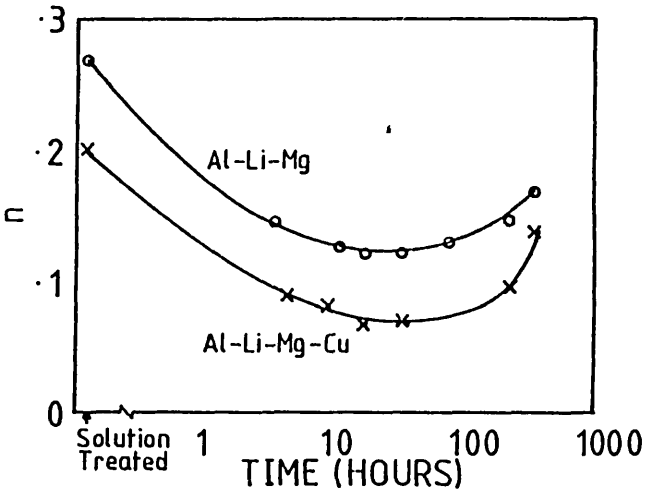

Fig 6.41

Variation of n with ageing time.

n is effectively a measure of the capacity for work hardening and as such it has been used in theories for predicting toughness from tensile properties[77]. It can also be shown that n should be equivalent to the plastic strain to instability[76] which, in the case of these alloys, is the plastic elongation.

Work hardening exponents for the two alloys are shown in Fig. 6.41 as the ageing time is increased. The data came from the tensile tests used to construct Figs. 6.39 and 6.40. Values for the copper free alloy are consistently higher even in the solution treated condition due to a combination of substructural and ageing effects. The n values are highest in the solution treated condition where the main dislocation barriers are dispersoid particles so that considerable bowing and subsequent generation takes place. On ageing dislocations are forced to cut through precipitates leading to restriction of their motion and strain localisation. This condition is at its most severe in the peak strength condition. Overageing is associated with a change from cutting to bowing, as the precipitate interface loses coherency, giving the final increase in n. The copper alloy shows a particularly rapid rise in n here, corresponding to the rapid strength loss seen earlier. Clearly, the n values here are not equivalent to the strain to failure and are significantly higher.

Thus, from this section of work it would appear that the addition of copper to the Al-Li-Mg alloy is producing further hardening during artificial ageing. However, this is achieved at the expense of ductility and work hardening capacity.

6.4.3 Elastic Modulus Measurements

Youngs modulus measurements were made with a clip on extensometer using large tensile specimens with a gauge length of 50 mm. The results,shown in Table 6.9, are the average of several tests in the elastic region. For comparison purposes standard values for conventional alloys are quoted.

	Modulus (GPa)			
Alloy	ST	U/A	P/A	O/A
Al-Li-Mg	-	75.8	76.5	76.4
Al-Li-Mg-Cu	78.1	77.2	79.5	78.1
2014 T6			73	
7075 T76			72	

Table 6.9 Measured Modulus Results Compared with Standard Values for Conventional Alloys

The lithium containing alloys clearly have increased modulus values with the addition of copper giving a further improvement. Noble et al[14] attributed most of the modulus increase in Al-Li alloys to the presence of lithium in solid solution. They also noted a slight increase during ageing caused by δ' precipitation, but this effect is not shown by the results here. Most elements, magnesium being an exception, raise the modulus of aluminium. The difference between the two alloys here is due to the beneficial effect of copper in this respect which is reported to give a modulus increment of 2.25 GPa/atomic %[14]. For the quaternary alloy this should give an increase of 0.7 GPa.

The technique used in this work was fairly crude, but the results agree with typical values quoted for these alloys[14, 24]. A figure of 78 GPa was adopted for use later in calculating the stress intensity factors for toughness measurements. This value is compared with that for 2014 and 7075 in specific modulus terms in Table 6.10. The lithium containing alloys are at an even greater advantage in this respect and also the effect of magnesium on the modulus is balanced by its beneficial influence on density.

Alloy	Specific Modulus (MNm/kg)
Al-Li-Mg(Cu)	31.08
2014 T6	26.16
7075 T76	25.81

Table 6.10 Comparison of Specific Moduli

6.4.4 Alternative Ageing Treatments

Extruded product is usually given a cold stretch of a few percent in order to straighten it and relieve residual stresses. Where the alloy is age hardenable this is often incorporated into the heat treatment cycle prior to ageing and this is termed the T8 temper. The dislocations and point defects introduced in this way can affect the precipitation kinetics and alter mechanical properties. In this section the effect of an intermediate stretch on tensile properties is examined.

To include structural variations the 30:1 extrusion matrices were used. Lengths of extrudate were solution treated using the same conditions and then stretched using a Denison tensile testing machine before ageing. Figs. 6.42 and 6.43 show the difference in proof stress between the T6 and T8 tempers produced in this way. Additionally, the properties of directly aged extrusions are shown (T5 temper), which were aged within 48 hours of extrusion without a separate solution treatment. In this way the effectiveness of the process heating and press quench as a substitute for this step can be seen. Typical UTS and elongation values for each temper are given in Table 6.11.

Starting with the copper free alloy in Fig. 6.42, all three tempers showed the same trend with ln Z. The 2% stretch raised the proof stress by approximately 20 MPa but some strengthening is to be expected here due to work hardening. UTS values were very similar, indicating that the final level of work hardening was not affected, but the elongation dropped by 2-3%. Therefore this level of stretching does not appear to be influencing precipitation and merely introduces slip dislocations. Other workers have reported that an intermediate stretch is not particularly beneficial to Al-Li-Mg alloys[24, 51]. Harris et al[18] claimed to have increased strength in Al-Li-Mg alloys of similar composition by cold stretching, without serious loss in ductility, but as the initial T6 ductility was only 5% any reduction is a significant percentage loss.

The copper alloy was given stretches of 2 and 4%. Here the effects were expected to be more promising as cold work has been reported to promote S phase precipitation with its beneficial effect on the slip dispersion[4]. However, the strength

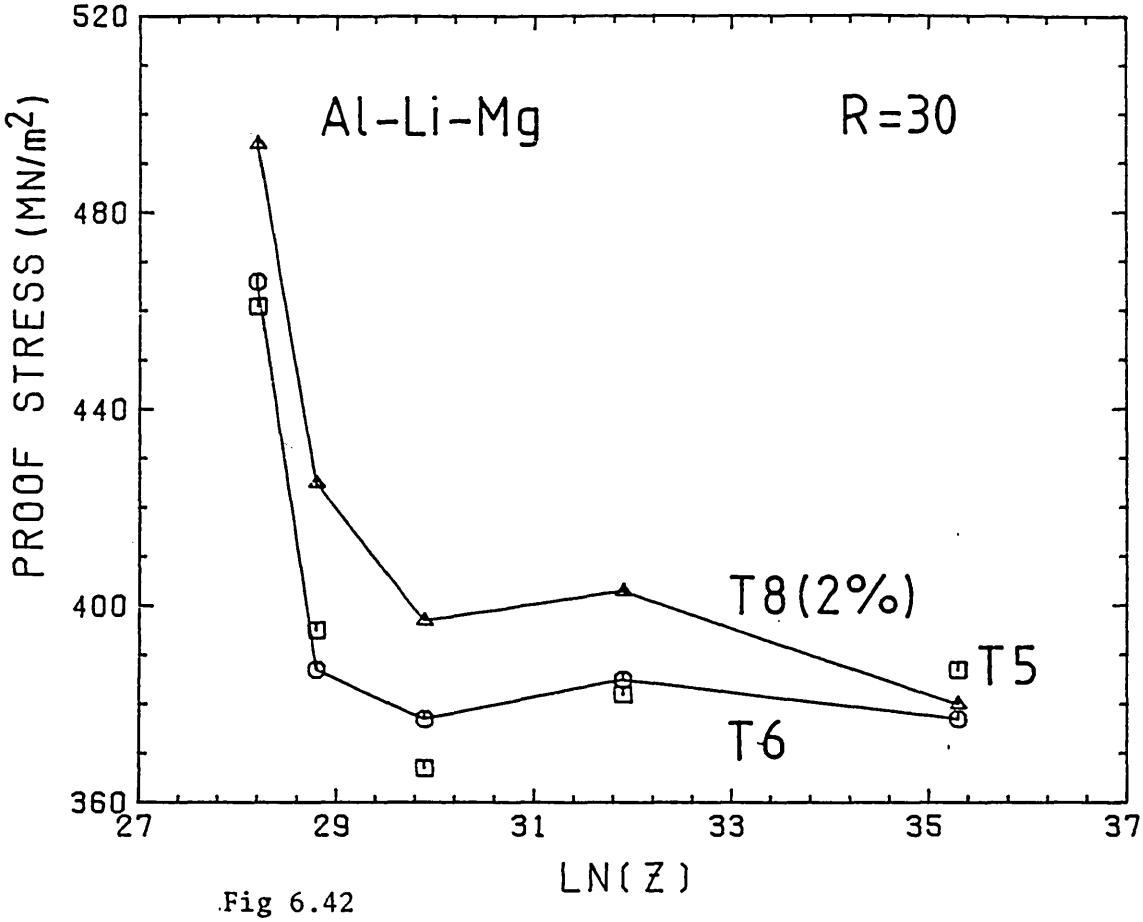

Fig 6.42

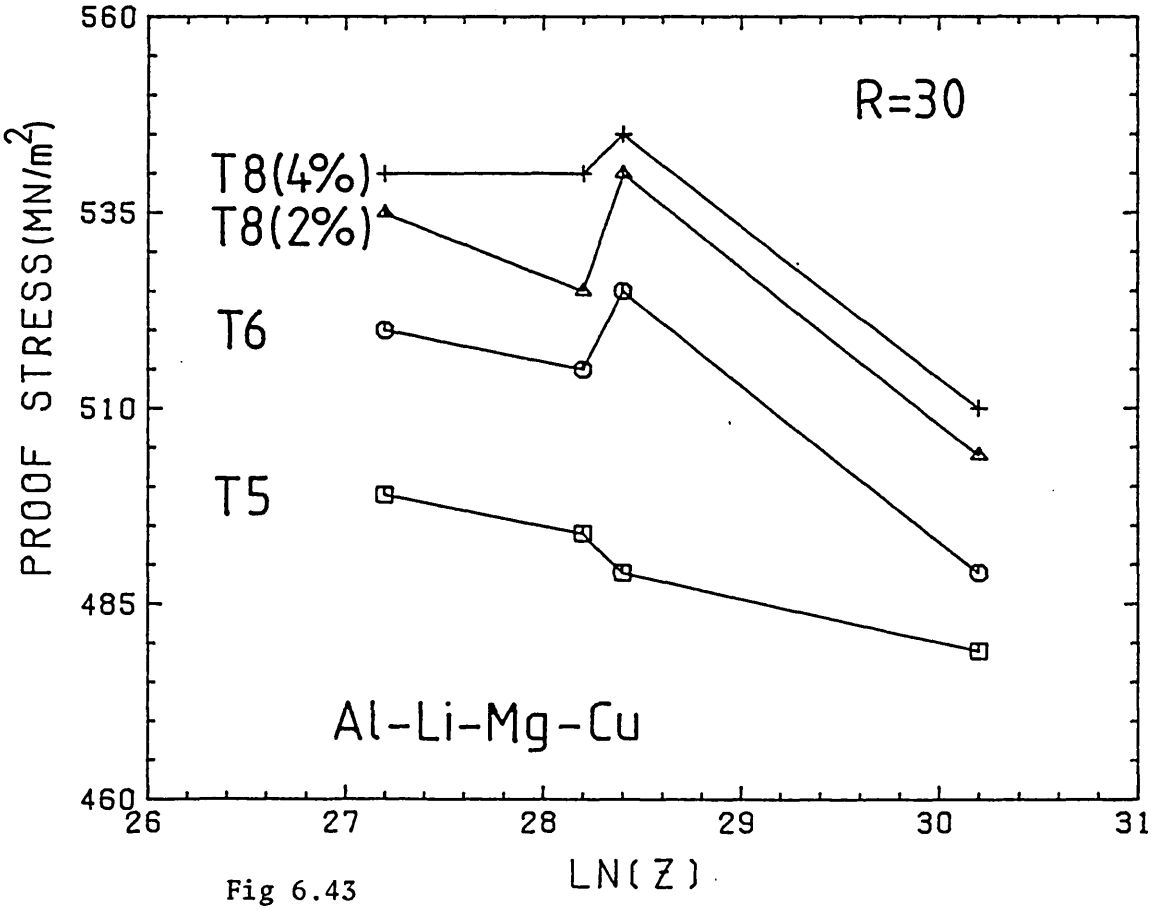

Fig 6.43

Proof stress variations in the T5,T6 and T8 tempers.

increases produced by these treatments were 15 and 25 MPa respectively, lower than that for the first alloy. The UTS results showed a lot of scatter, but in general the T8 values were raised over the T6 by roughly 15 MPa for both levels of stretching. Elongation was slightly lowered by these treatments, although the whole data set lay between 3 and 4%. Again these effects are so minor as to make it unlikely that the precipitation sequence is being significantly altered.

Returning to the effects of ageing on S phase precipitation, most of the reported work on quaternary alloys has concentrated on low magnesium levels. This includes the DTDXXXA type composition 2.5%Li, 1.2%Cu, 0.7%Mg, which was tailored to give maximum S phase precipitation[4, 16]. It is possible, with the high levels of magnesium in the present alloys, that S phase precipitation is not favourable and the tensile results tend to support this. In the next chapter the effect of stretching on toughness will be examined which should be improved if significant S phase precipitates out.

The responses to direct ageing are quite different for the two alloys. For the Al-Li-Mg alloy the T5 and T6 proof stress results were almost identical along with those for tensile stress and elongation. It can be concluded therefore, that for the section thicknesses used here, the process heating was effective as a solution treatment even down to an extrusion temperature of 350°C. Sanders found almost the same effect for Al-Li-Mg alloys, with extrusions which were air cooled afterwards[78]. A similar experiment using hardness testing gave identical T5 and T6 hardnesses down to 325°C.

There was a strength loss of up to 30 MPa associated with direct ageing. the Al-Li-Mg-Cu alloy. In all three tempers in Fig. 6.43 the importance of extrusion temperature on solutionising is shown and this must also occur during solution treatment explaining the difference between the T5 and T6 conditions. Alternatively this alloy may be more sensitive to the vacancy concentration present on ageing, which will be increased by a separate solution treatment. No natural ageing occurred in either alloy but quench sensitivity was a feature not investigated and could be an additional factor for the copper alloy.

	Proof Stress (MPa)	UTS (MPa)	%El
Al-Li-Mg			
T5	461	543	5.0
T6	466	538	5.1
T8	494	543	2.5
Al-Li-Mg-Cu			
T5	499	581	4.5
T6	520	591	3.6
$T8_2$	535	611	4.0
$T8_4$	540	606	3.8

Table 6.11 Tensile Properties of High Temperature Extrusions in T5, T6 and T8 Tempers

6.5 Structural Variations with the Ageing Conditions

In this section the changes in structure are described that occur on ageing at 170°C, together with a DSC investigation of the precipitation reactions.

6.5.1 Peak Aged Structures

There was a significant difference between the microstructures viewed optically in the solution treated and heat treated conditions. Even after short ageing times precipitation occurred along the grain boundaries enabling them to be seen when etched with a reagent such as Kellars. The grain structures of the two alloys in the fully heat treated condition are shown in Figs. 6.44-6.47, for an extrusion ratio of 50:1 at similar extrusion temperatures. The longitudinal and transverse sections illustrated here define the grain structure of a round bar extrusion. This 3-D view of the grain shape is particularly important when considering corrosion and stress corrosion resistance.

Fully Heat Treated Structures

Al-Li-Mg

Fig. 6.44

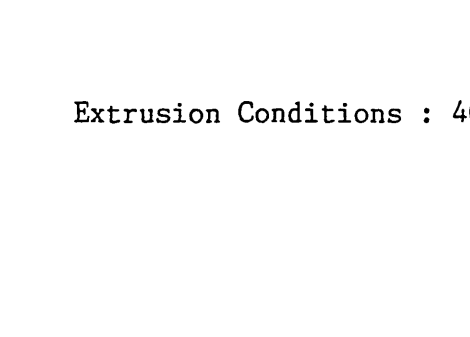

longitudinal

Fig. 6.45

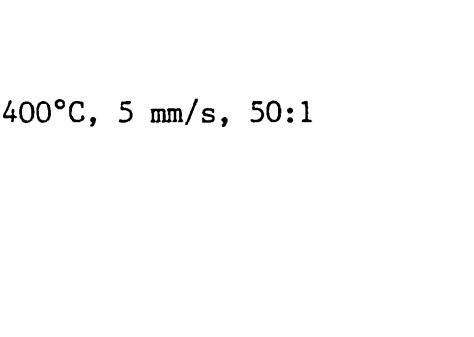

transverse

Extrusion Conditions : 400°C, 5 mm/s, 50:1

Al-Li-Mg-Cu

Fig. 6.46

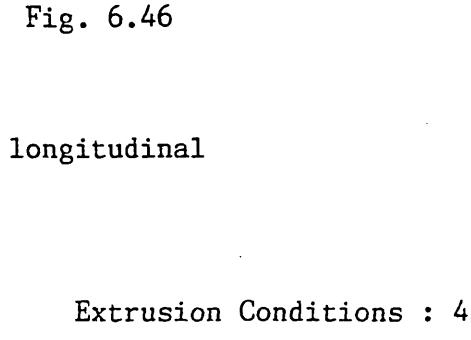

longitudinal

Fig. 6.47

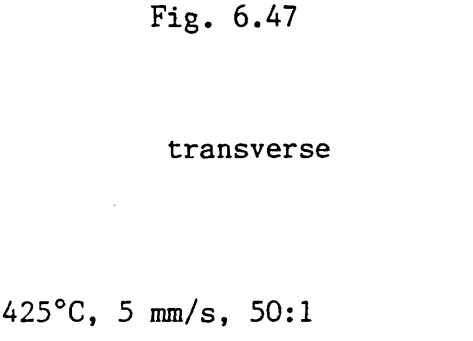

transverse

Extrusion Conditions : 425°C, 5 mm/s, 50:1

Etchant : Kellars Reagent

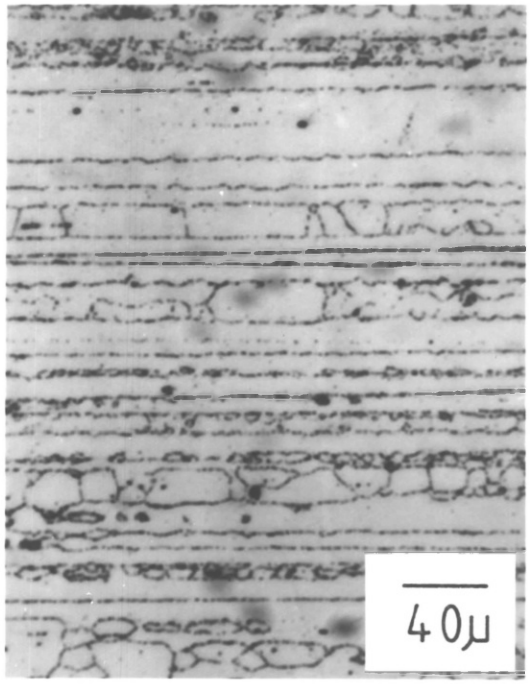
40μ

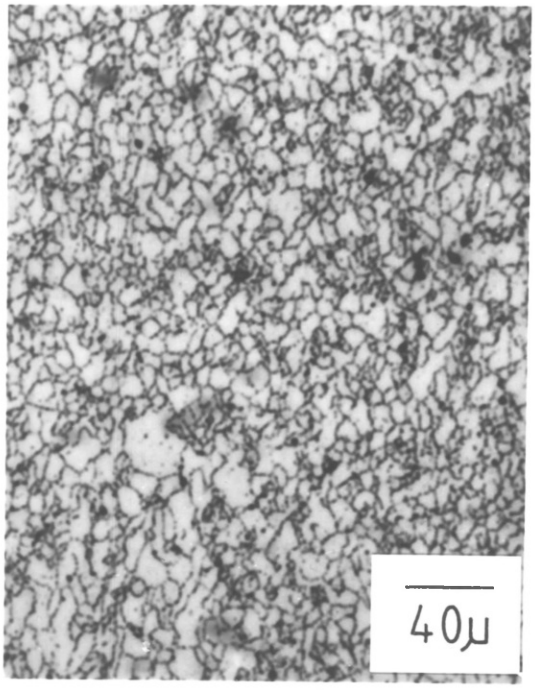
40μ

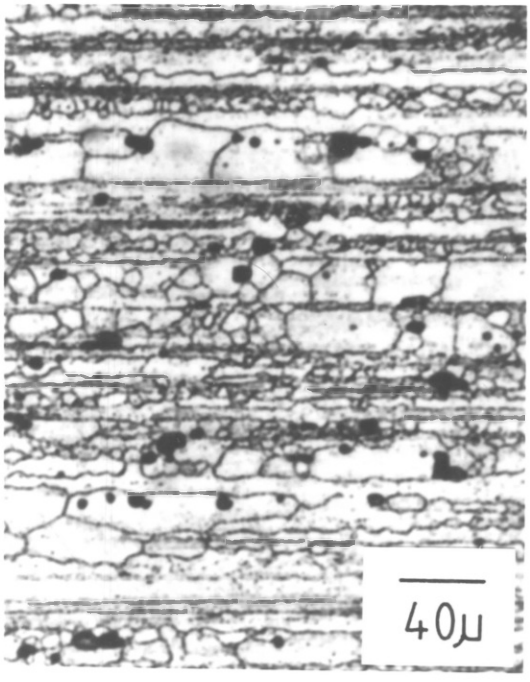
40μ

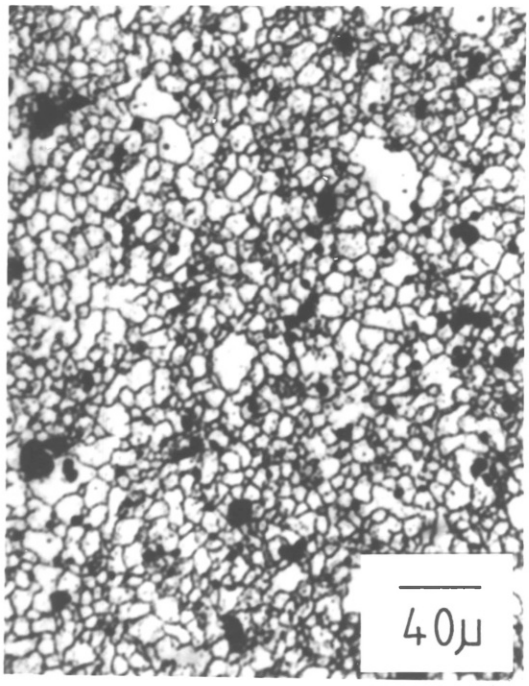
40μ

Comparing the two sets of micrographs, there are two noticeable differences between the alloys; firstly the copper containing alloy appears to have a higher level of grain boundary precipitation, outlining the grains more clearly, and secondly the same alloy has a much higher inclusion content. The latter is to be expected from the pre-extrusion structures, but the increased amount of ageing product must be due to the influence of copper on the ageing response.

6.5.2 Ageing Response of Al-Li-Mg

In the solution treated condition, which is essentially the same as that seen earlier in the as extruded micrographs, no precipitation was observed. However, weak superlattice reflections were detected indicative of the early stages of Al_3Li formation. Consistent with the rapid change in mechanical properties upon ageing, rapid δ' precipitation was observed. After three hours at 170°C, i.e. the UA temper, a fine dispersion was present throughout the matrix. Even at this early stage, precipitation of what was presumably the equilibrium phase began to occur. This was restricted to high angle boundaries, as in Figs. 6.48 and 6.49, indicating that nucleation in the matrix was difficult at this stage. Fig. 6.49 shows this product at a higher magnification together with Al_3Zr dispersoids on a boundary. The ageing particles are 0.1 μ in size and are amorphous in shape, which is to be expected for growth on grain boundaries as the usual energy considerations are relaxed.

Figs. 6.50, 6.51 and 6.53 are from material aged for a longer time, to produce peak strength, and show the typical structural features observed in this condition. Grain boundary precipitates had now grown to approximately 0.2 μ in diameter and were in evidence on some subgrain boundaries. In general, the interparticle spacing on the grain boundaries was of the order of a micron. Another feature of high angle boundaries, recrystallised and original, typical of age hardening aluminium alloys was the presence of precipitate free zones (PFZ), approximately 0.06 μ wide. There are two possible mechanisms by which they could occur; either by dissolution of matrix precipitates by growth of stable grain boundary precipitates (essentially producing

Features of the Heat Treated Structure

Al-Li-Mg

Fig. 6.48

UA temper

325°C, 15 mm/s, 10:1

Fig. 6.49

UA temper

325°C, 15 mm/s, 10:1

Fig. 6.50

PA temper

400°C, 5 mm/s, 50:1

Fig. 6.51

PA temper

400°C, 5 mm/s, 100:1

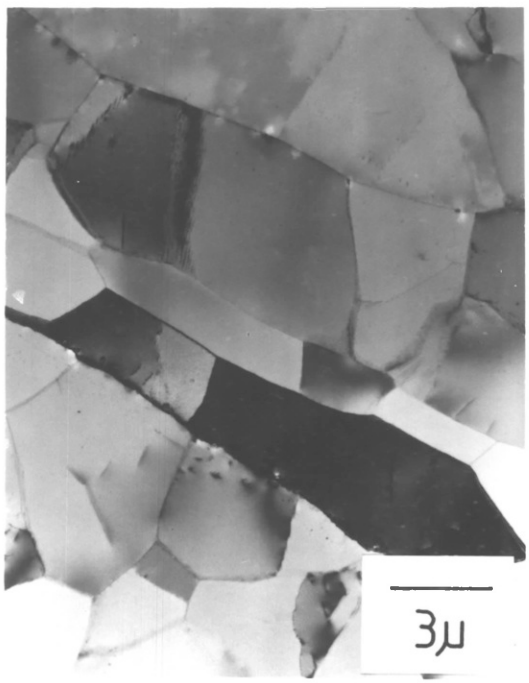
3μ

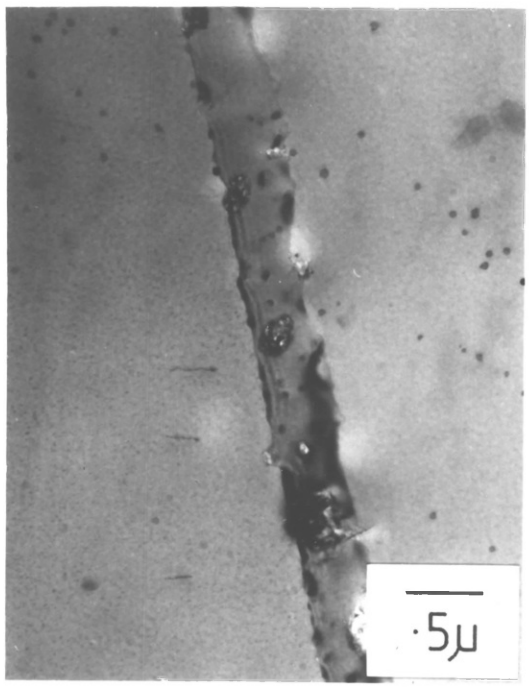
·5μ

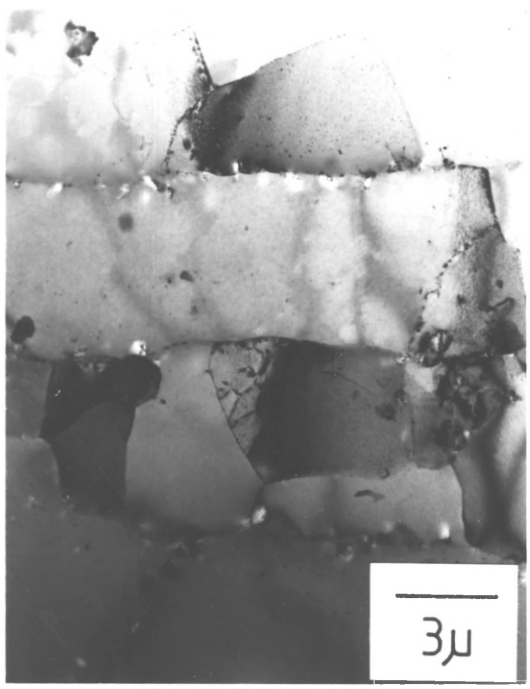
3μ

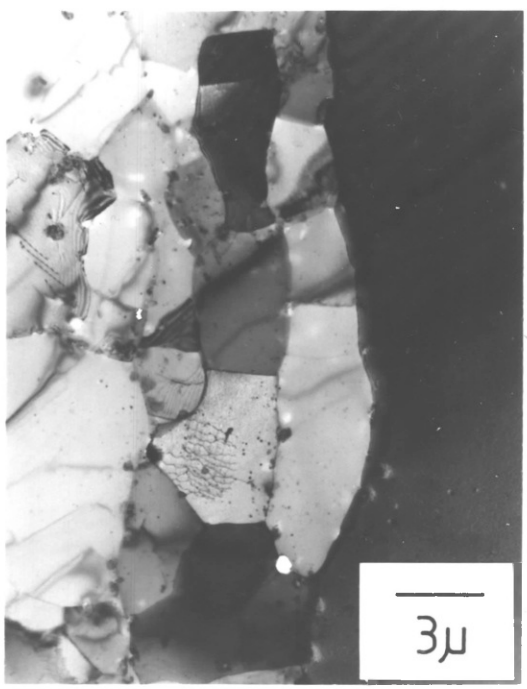
3μ

Features of the Heat Treated Structure

Al-Li-Mg

Fig. 6.52

T8 temper

(2% stretch)

400°C, 5 mm/s, 30:1

Fig. 6.53

PA temper

325°C, 15 mm/s, 10:1

Fig. 6.54

OA temper

325°C, 15 mm/s, 10:1

Fig. 6.55

OA temper

325°C, 15 mm/s, 10:1

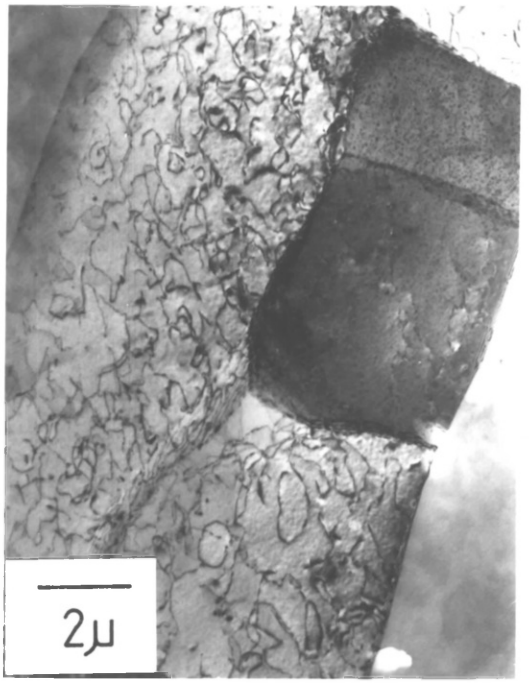
2μ

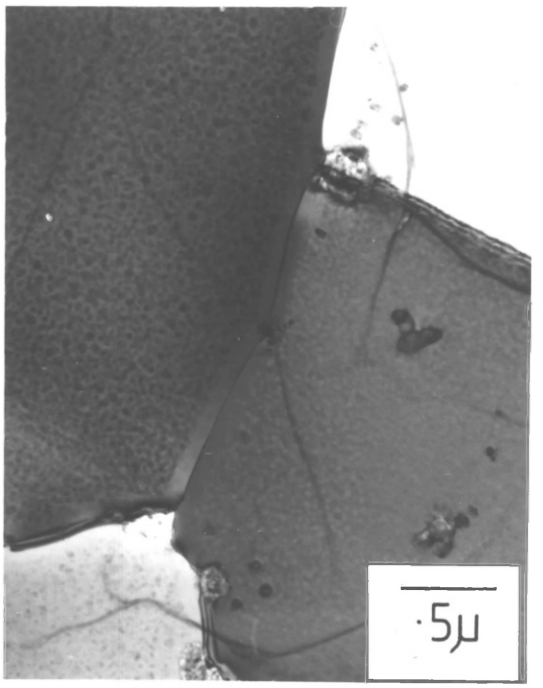
·5μ

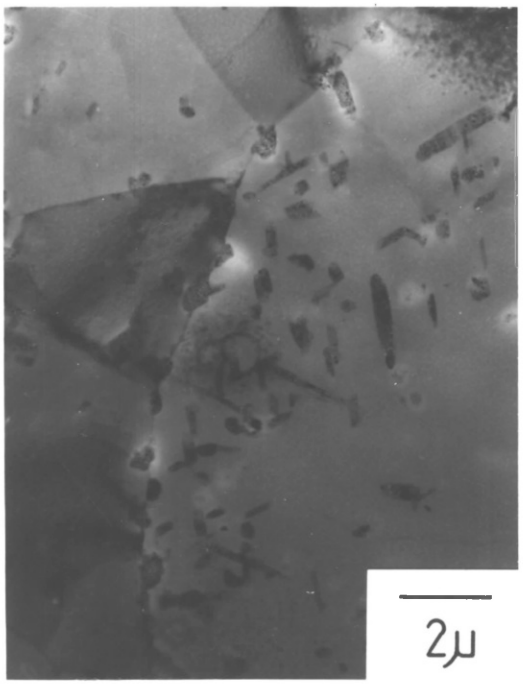
2μ

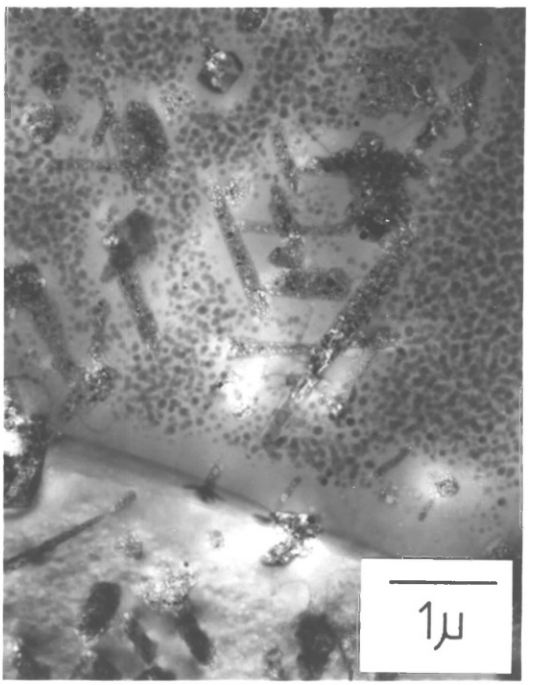
1μ

a solute depleted zone) or by retardation of matrix precipitate nucleation due to the reduced vacancy concentration adjacent to such boundaries. From Fig. 6.53 the latter mechanism appears to be the main cause of such zones in this alloy as the particle density on the boundaries is not high enough to produce a continuous zone. Having said this, the grain boundary precipitates did widen the zone when they extended past the normal width, indicating they are lithium containing.

The overaged condition chosen for this alloy, 300 hours at 170°C, would be best described as heavily overaged, with the strength loss encountered being greater than anticipated. The structure produced by this treatment (see Figs. 6.54 and 6.55) is best discussed in terms of matrix and grain boundary events. At high angle boundaries the precipitates had now grown to roughly half a micron in size. At the same time further nucleation took place at these sites, giving rise to a large range of particle sizes. (The fact that further nucleation can occur indicates that the PFZ is not depleted in solute). In the matrix the δ' precipitates coarsened but the main feature here was the nucleation and growth of coarse particles with a rod type morphology. They were formed up to 2 μ in length and on certain crystallographic orientations. The more equiaxed type shown in Fig. 6.54 are probably sections through rods lying near to the normal to the foil. Fig. 6.55 indicates they are lithium containing because of the extensive δ' PFZs surrounding them. In some areas they were present in such a high density that the PFZs from adjacent particles overlapped. Softening on overageing was therefore accelerated due to the solution of δ' in these areas. In addition to lithium these particles were almost certainly magnesium bearing because of the disappearance of the discontinuous yielding effect on overageing. This effect, described in section 6.4.2, is due to magnesium in solid solution the level of which must be decreasing at long ageing times. As a result, some of the softening on overageing can be attributed to the loss of the solid solution strengthening contribution made by this element. It is unlikely that the phase observed here had any effect on strength because of its coarse nature.

From the survey of the literature concerning phase equilibria and precipitation reactions in the ternary system (section 1.2.2),

the products of ageing were expected to be δ', together with either Al_2MgLi or to a lesser extent AlLi. Thompson and Noble identified precipitates with a similar rod morphology to those seen here, as Al_2MgLi, by electron diffraction pattern analysis and also identified the <110> growth directions[11]. The grain boundary precipitates are similar in appearance to those in the matrix and are probably also Al_2MgLi but were formed at an earlier stage due to the difficulty in matrix nucleation. As the formation of δ(AlLi) may also be possible thermodynamically, some of the latter may be of this composition. However, Niskanen et al, working on a very similar alloy composition and heat treatment, argued against AlLi formation on the grounds of electrochemical parameters[63]. AlLi has a very marked effect in this respect whereas Al_2MgLi has little or no effect.

The speckled nature of all the coarse precipitates was due to etching and oxidation, which could not be avoided by varying the polishing conditions and in many cases the particles simply dropped out of the foil. A combination of the strong superlattice reflections shown by δ', together with oxide rings on the diffraction patterns made it difficult to obtain information in this way to identify individual particles.

Generally, grain boundary precipitation and PFZ formation are regarded as being detrimental to material properties such as stress corrosion resistance and toughness. The PFZs are softer than the matrix and can undergo high local deformation, giving rise to stress concentrations. Similarly, grain boundary precipitates can act as void nucleation sites giving a tendency towards intergranular fracture. These two factors are often associated and it is difficult to separate their effects. In addition, the inhomogeneity in potential between the matrix and the boundary can lead to intergranular corrosion and stress corrosion attack. In other aluminium alloys, attempts are sometimes made to remove PFZs[38] using either cold working or trace element additions to promote precipitation within them. This can have the additional effect of promoting equilibrium phase formation in the matrix, rather than on the boundaries. However, the 2% stretch given to this alloy had neither of these effects, indicating that precipitation is not dislocation nucleated. Fig. 6.52 shows the structure

produced in the T8 temper. The grain boundary precipitates have dropped out during thinning, but their formation has not been promoted in the matrix. The stretch would appear to have merely introduced glide dislocations which have interacted with the Al_3Zr dispersoids.

6.5.3 Ageing Response of Al-Li-Mg-Cu

The structural changes produced on ageing this alloy were very similar to those for the ternary system. Superlattice reflections were detected in the solution treated condition and short ageing times produced a fine Al_3Li dispersion together with grain boundary precipitation, as shown in Fig. 6.56. Here the precipitates are roughly 0.1 μ in diameter and similar in appearance to those seen previously. However, their average spacing along the boundaries is reduced to 0.5 μ, half of that in the Al-Li-Mg alloy.

In the peak aged condition the boundary precipitates grew to an average size of 0.2 μ, similar to those in the first alloy and δ' coarsening also continued. Figs. 6.57 - 6.60 show the main matrix and grain boundary features in the peak strength temper. Precipitation of the equilibrium phase was still restricted to high angle boundaries and no further nucleation appeared to occur in this respect. The interparticle spacing remained at 0.5 μ. Again PFZs were found at all high angle boundaries and at the larger grain boundary precipitates, the width being of the order of a tenth of a micron. In this and the previous alloy no precipitate free zones were found at subgrain boudnaries, often reported for Al-Cu-Li alloys[22]. Some of the precipitates were more regular in shape than others, as in Fig. 6.60, and these were usually the coarser of the population.

Typical overaged structures are shown in Figs. 6.61 - 6.63. This condition was not as overaged as that for the ternary alloy and corresponded to a reduced level of softening, but the structural features are very similar. The δ' and grain boundary particles coarsened further and coarse rod shaped precipitates formed in large numbers in the matrix. The latter appeared identical to the Al_2MgLi precipitates seen earlier, having the preferred orientation and being surrounded by a δ' PFZ. The S phase precipitation expected with the

Features of the Heat Treated Structure

Al-Li-Mg-Cu

Fig. 6.56

UA temper

450°C, 3 mm/s, 10:1

Fig. 6.57

PA temper

450°C, 5 mm/s, 20:1

Fig. 6.58

PA temper

450°C, 3 mm/s, 10:1

Fig. 6.59

PA temper

450°C, 5 mm/s, 20:1

·5μ

3μ

·5μ

·5μ

Features of the Heat Treated Structure

Al-Li-Mg-Cu

Fig. 6.60

PA temper

450°C, 3 mm/s, 10:1

Fig. 6.61

OA temper

325°C, 15 mm/s, 10:1

Fig. 6.62

OA temper

325°C, 15 mm/s, 10:1

Fig. 6.63

OA temper

325°C, 15 mm/s, 10:1

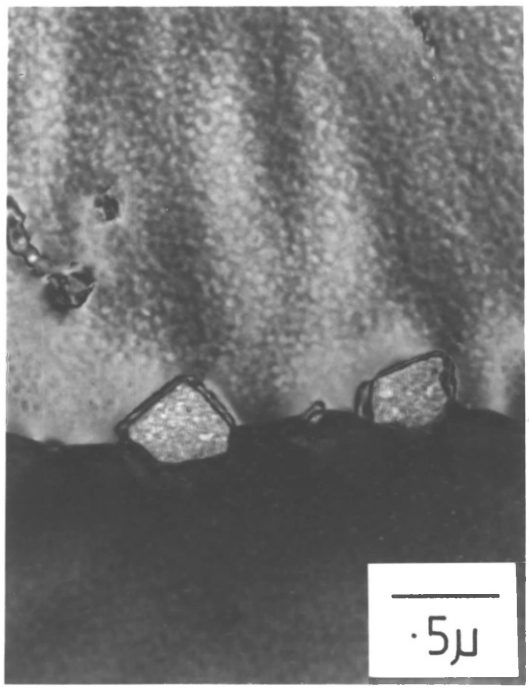
·5μ

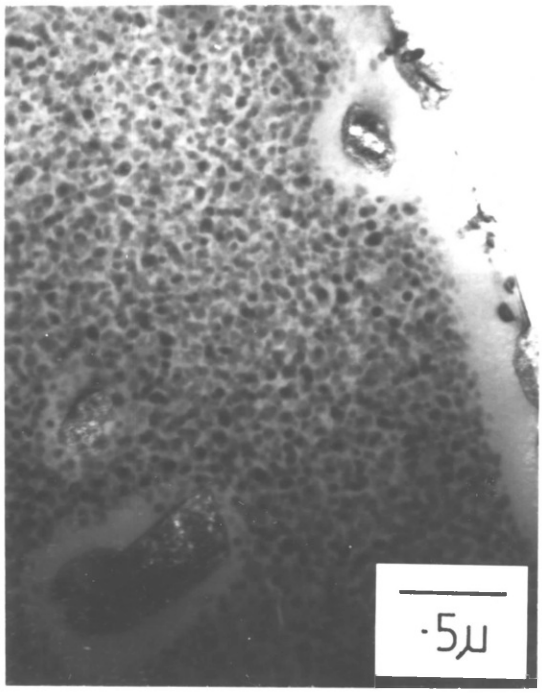
·5μ

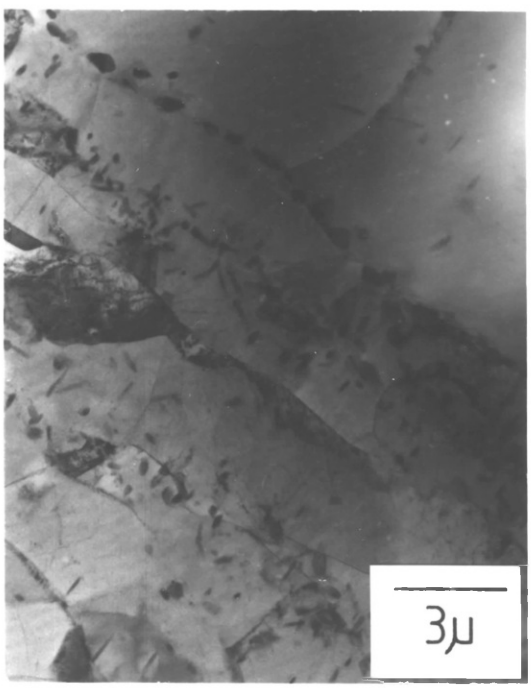
3μ

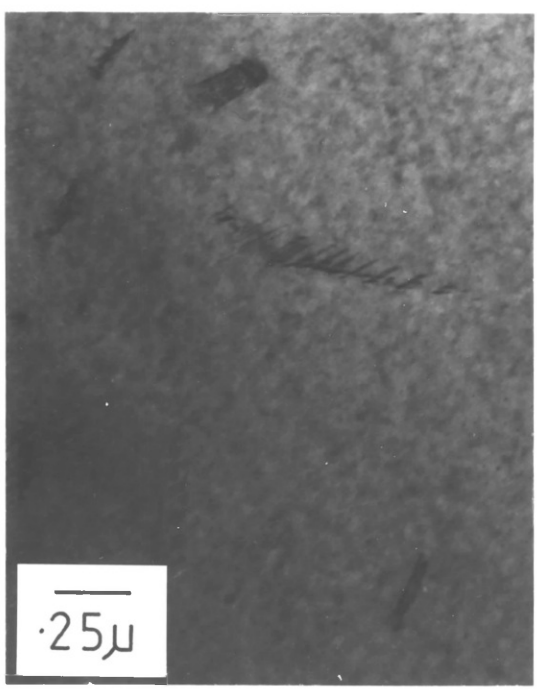
·25μ

addition of copper was not seen in the peak aged condition, but on overageing some fine needle-like precipitates were observed in 'rafts' on dislocations as shown in Fig. 6.63. However, these structures were infrequent and well dispersed and could not account for the strength increase produced by the addition of copper.

From this investigation the products of ageing in the two alloys appear to be identical except for the slight S phase formation due to the addition of copper. The Al-Li-Mg ternary system would seem to dominate the reactions occurring on ageing, although the formation of grain boundary precipitates is clearly enhanced in the copper containing alloy.

An interesting difference between the two alloys was found in all the heat treated conditions. In certain areas the quaternary alloy contained bands of what appeared to be precipitates at low magnification but on closer inspection were revealed to be dislocation loops. This was verified by tilting the foil until a position was reached where they became invisible. These features were observed in extruded and press quenched material, together with solution treated and heat treated material, but they were very scarce in the ternary alloy. The rows were usually aligned in the extrusion direction, as in Fig. 6.64. Fig. 6.65 shows the same area at a higher magnification. Often the rows of loops were associated with dislocation helices, as in Fig. 6.66.

All of these configurationsare the result of vacancy condensation processes. The high temperature vacancy concentration retained after solution treatment is always reduced to some extent by diffusion of vacancies to sinks, such as dislocations, interfaces and grain boundaries (giving PFZ formation). However, this loss can be reduced by the formation of stable vacancy structures. Dislocation loops can be formed by the association of vacancies into a vacancy disc, followed by a collapse of the lattice and this was probably the source of most of the loops in Fig. 6.65. Another mechanism that can occur during this period is the formation of helical dislocations. Vacancies can diffuse to a pinned dislocation segment and assist climb of the edge component to produce helices. Hull gives an outline of the theory of this mechanism[43]. During ageing the helices can break

up by recovery to give rise to dislocation loops, which explains the association of loops and helices in Fig. 6.66. Helical dislocations have been observed to act as nucleation sites for θ' in aluminium copper alloys along with other dislocation configurations[38]. This is probably due to the concentration of solute atoms in the portion of distorted lattice surrounding them.

Dislocation loop and helix formation were observed by Thompson and Noble[23] in Al-Li-Cu alloys and such features are common in Al-Cu alloys[38]. However, Gregson[16] noted the lack of vacancy condensation effects in both of the ternary lithium systems, together with the Al-Li-Mg-Cu system and suggested that vacancies were being bound to lithium atoms making them unavailable to form such structures. The addition of copper to the ternary alloy in the present work would appear to have the reverse effect, increasing the available vacancy concentration and allowing the formation of condensation structures. Comparison of available solute atom vacancy binding energies is not very helpful in explaining this behaviour as there is considerable scatter in the data from different sources and also the values for lithium and copper atoms are very similar[73].

At this stage, the significance of these structures on the strength increment produced by the addition of copper is unclear. They are not giving enhanced S phase precipitation so possibly the effect is connected with the overall vacancy concentration and its influence on the Al_3Li reaction. If copper is raising the level of available vacancies then this may be affecting the δ' reaction kinetics. Alternatively the strength increase may be unconnected with the vacancy distribution, since in Al-Li binary alloys the rate of the solution quench is reported to have little effect on subsequent δ' precipitation[9].

Relating the vacancy condensation structures to the ageing sequences observed, they were prime sites for nucleation of the small amounts of S-phase formed and also probably assisted in Al_2MgLi nucleation in the matrix, giving rise to its accelerated formation in this alloy.

Finally, a feature of the precipitation in both alloys was the formation of two δ' size populations. Fig. 6.67 shows the existence of coarse Al_3Li particles, in some cases surrounded by PFZs. Although

Features of the Heat Treated Structure

Al-Li-Mg-Cu

Fig. 6.64

PA temper

325°C, 15 mm/s, 20:1

Fig. 6.65

PA temper

325°C, 15 mm/s, 20:1

Fig. 6.66

UA temper

325°C, 15 mm/s, 20:1

Fig. 6.67

PA temper

450°C, 5 mm/s, 10:1


3μ

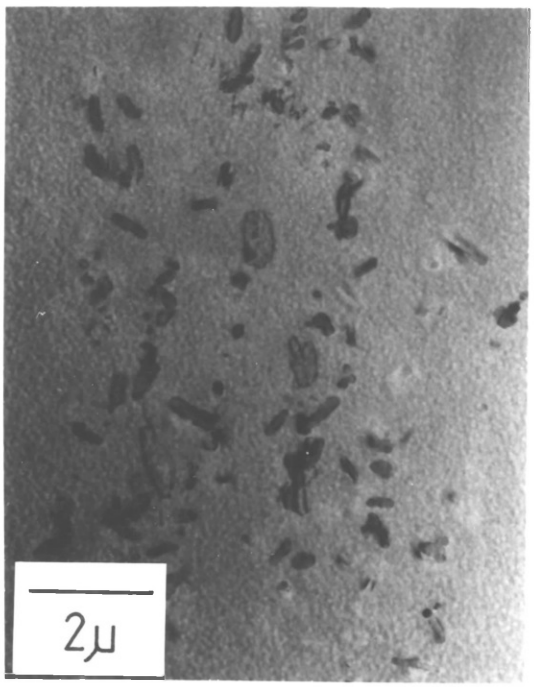
2μ

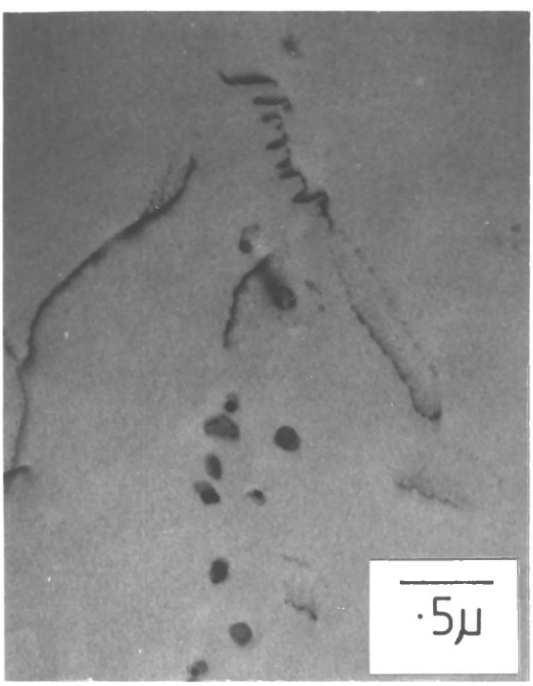
·5μ

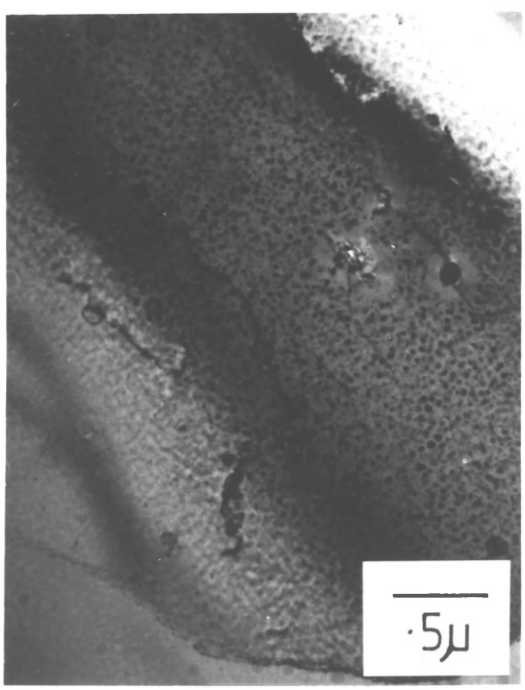
·5μ

they appear to have been dislocation nucleated they have probably formed on Al_3Zr particles which also happen to be pinning a dislocation line. This is energetically favourable in terms of the misfit strains of the two precipitate types and this mechanism has been discussed at length elsewhere[16, 79].

6.5.4 Differential Scanning Calorimetry

With there being some ambiguity as to the precipitation reactions occurring in these alloys, it was decided to study them using the Differential Scanning Calorimetry (DSC) technique. This is a method of characterising the phase changes that can occur by measuring the level of the various heats of reaction as the temperature of the sample is raised at a fixed rate. It has been used to some extent in published studies of the Al-Li binary system[79, 80]. In this work a Dupont 990 programmer/recorder was used with a 910 DSC system.

Samples of material extruded at 400°C were solution treated for one hour at 500°C a few days before the test. Specimens were then prepared by turning the rod down to 6 mm in diameter and slicing off sections a few millimetres thick. For the actual test one of the discs, together with a reference sample of super pure aluminium, of the same weight, was placed inside the furnace section of the apparatus over a small thermocouple. The heating cycle was started below 0°C, using liquid nitrogen to cool down the apparatus, so that thermal equilibrium was reached by the time the sample was at room temperature. A heating rate of 20°C/min was used in all of the runs. Argon gas was bubbled past the specimens throughout the test to prevent excessive oxidation, although this proved to be difficult due to the reactive nature of these alloys.

Output traces plotted the difference in the rate of heat output between the two samples against temperature. On undergoing an exothermic precipitation reaction the test sample becomes slightly hotter than the reference sample giving a rise on the trace. As the reaction proceeds the maximum reaction rate is reached followed by a gradual decrease in the rate of heat evolution as it nears completion to give a peak on the output graph. Conversely, an endothermic solution reaction gives rise to a trough. In theory when no reactions occur

the trace should be a horizontal straight line, but in practice the base line will be a shallow curve upwards which is a function of the apparatus. The area enclosed between the baseline and a reaction peak or trough is a measure of the overall heat of reaction. So in this way differences in precipitation sequences can be seen, together with the extent to which they occur. It is important to note that this test is not isothermal and the reactions occurring,and in particular their kinetics, may be different during a low temperature artificial age.

The traces produced for the two alloys are shown superimposed in Fig. 6.68. Repeat tests were run and the features of the curves were found to be highly reproduceable. Table 6.12 gives the various temperatures of points of interest. In order to relate features on the curves with structural developments TEM specimens were taken at the points indicated. Samples were held isothermally for five minutes once the appropriate point had been reached, to allow the structure to stabilise and were then water quenched.

	Observed Temperatures °C			
Alloy	δ' Peak	δ' Solvus	2^{nd} Peak	Solvus
Al-Li-Mg	192.5	270	337.5	420
Al-Li-Mg-Cu	170	285	332.5	475

Table 6.12 Temperatures of DSC Trace Features

Both alloys gave the same types of feature on the trace; a low temperature reaction due to Al_3Li precipitation and resolution, followed by a higher temperature reaction associated with stable precipitate formation. Finally, oxidation gave a continuous rise. In the case of Al-Li-Mg-Cu the incipient melting reaction was also encountered.

On the Al-Li-Mg trace the first reaction to occur was Al_3Li precipitation, peaking at 192°C. TEM confirmed that this was the sole product and that it was present in the form of a fine dispersion similar to that observed in the underaged tempers. The reaction took

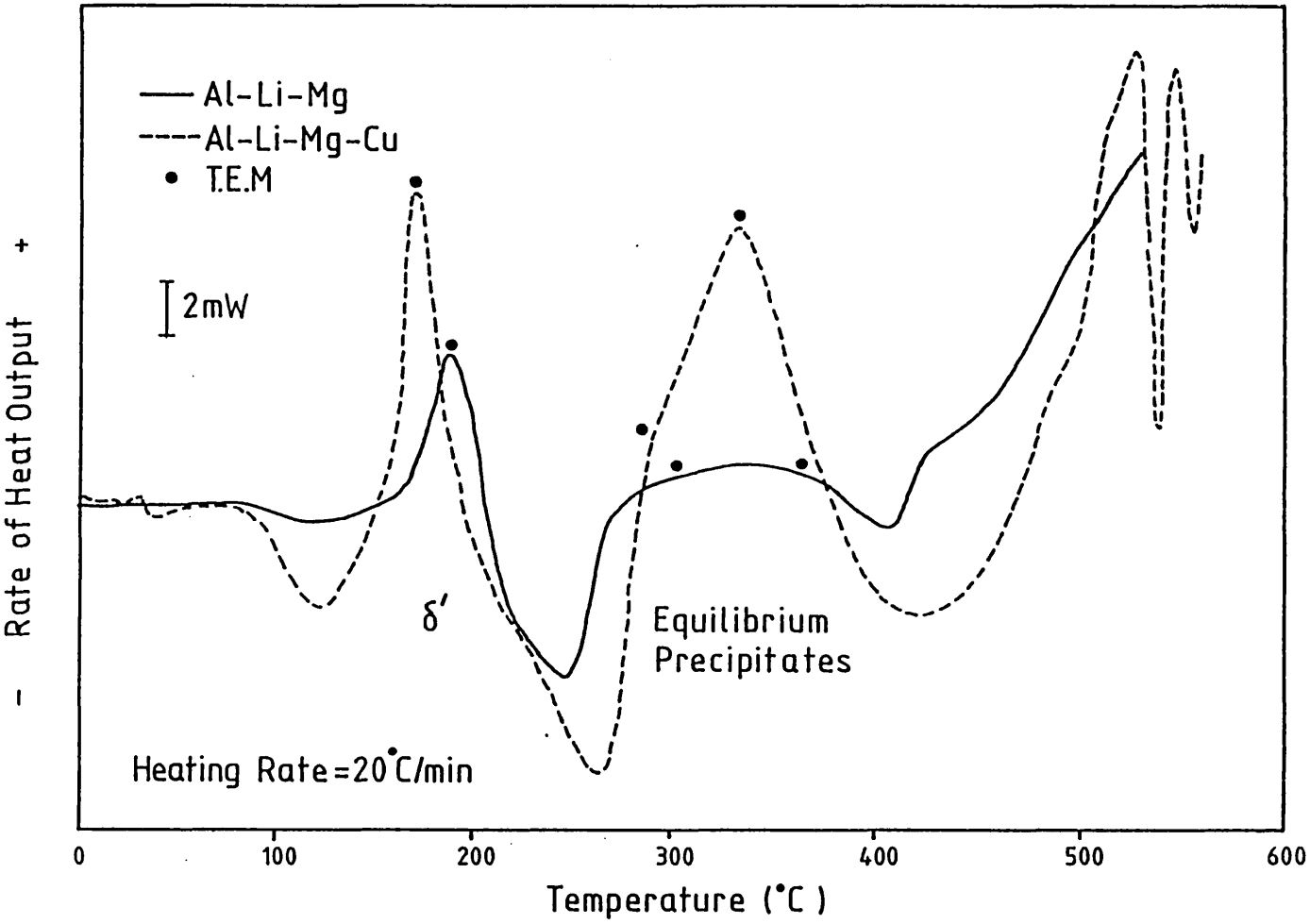

Fig 6.68 DSC Thermograms.

place over a temperature range of 40°C and was immediately followed by the δ' solution reaction. By 270°C, at which temperature the baseline was crossed again, all the precipitates should have dissolved, although this was not verified by TEM. Stable precipitate formation probably took place while this was still occurring, giving rise to the slow change in gradient at this point. The second peak was broader than the first, extending over 100°C, and was also slightly asymmetrical. This may have been due to the superposition of two reaction curves and to investigate this point TEM was carried out on either side of the peak. During the rise to the peak the predominant reaction appeared to be the formation of precipitates at the grain boundaries. Some rod type precipitates were present but most grain interiors were devoid of them, as in Fig. 6.69. On the high temperature side of the peak, Fig. 6.70, the rod morphology Al_2MgLi precipitates were in evidence throughout the matrix and the structure was similar in appearance to that observed on overageing at 170°C. Therefore, there are two reactions occurring but they correspond to the two modes of nucleation of Al_2MgLi. Throughout the period of the reaction the boundary precipitates continued to coarsen. The solution reaction took place over a comparatively short temperature range and was complete by 420°C.

The addition of copper still produced the metastable and stable reactions, but their characteristics were changed dramatically, as shown in Fig. 6.68. In addition, at low temperatures from 25 to 50°C a small peak and trough occurred, giving the appearance of a precipitation-solution reaction. This may possibly have been a G.P zone reaction associated with the Al-Cu side of the system but no TEM was done at this point. It is clearly not great in magnitude and as it was complete by 50°C it is unlikely that it affected 170°C ageing. Another result of the copper addition is the endothermic reaction prior to the δ' peak. Looking back at the Al-Li-Mg alloy this was also shown, but to a lesser extent. This feature suggests that a reversion reaction is occurring, probably of Al_3Li formed during the quench and in the subsequent delay before testing at room temperature, explaining the weak superlattice reflection seen in quenched material. The larger area enclosed by this trough suggests that more precipitate was present in the Al-Li-Mg-Cu alloy, contributing to the increased strength seen in the as extruded condition.

The nature of the metastable reaction peak also changed considerably. The maximum reaction rate now occurred at 170°C, i.e. it was depressed by 20°C, and the peak height increased, together with the area beneath the curve, indicating that the overall heat of reaction was increased. This is partly to be expected as a result of the greater driving force in terms of free energy at lower temperatures. What is interesting is the fact that the reaction can now occur more easily at lower temperatures and this ought to influence the δ' distribution produced. TEM again showed Al_3Li was the sole product but it was difficult to compare the size and number densities of the precipitates in the two alloys due to their extremely fine nature. The shift in peak temperature may be a result of enhanced δ' nucleation due to the effect of copper on the vacancy concentration in association with the vacancy condensation structures seen to be promoted by this element. If this is the case, then a finer δ' dispersion would explain the strength increase after ageing produced by 0.8%Cu. In Chapter 9 this is discussed more fully when various other copper levels are examined.

The exothermic reaction corresponding to stable precipitation was also larger in this alloy, with a much more pronounced peak, although it did occur at a similar temperature. There was a change in the gradient up to the peak suggesting that two reactions were also occurring here. TEM specimens were prepared at the peak and at the point where the gradient changed. Figs. 6.71 and 6.72 are from the latter position. The coarse grain boundary precipitates, together with the rod shaped matrix precipitates were both present (Fig. 6.71) indicating the latter are more easily nucleated this time. At higher magnification (Fig. 6.72) rafts of fine lath shaped precipitates were resolved, formed on dislocations. They were apparently present as two size distributions but this was probably due to the orientation of the needles - the narrower precipitates being the end on variant. From Gregson's analysis[16] of the precipitation reactions in Al-Li-Mg-Cu alloys these structures compare well with those of the S phase (Al_2CuMg). Therefore, the composition here is capable of producing S phase but only under favourable nucleation conditions and perhaps not during the normal peak strength ageing treatment. Not all regions contained such high S phase densities as that shown in Fig. 6.72 and

TEM Investigation on the DSC Trace

Fig. 6.69

Low temperature side of the equilibrium precipitate exotherm

Fig. 6.70

High temperature side of the equilibrium precipitate exotherm

Al-Li-Mg

Fig. 6.71

Low temperature side of the equilibrium precipitate exotherm (290°C hold)

Fig. 6.72

Al-Li-Mg-Cu

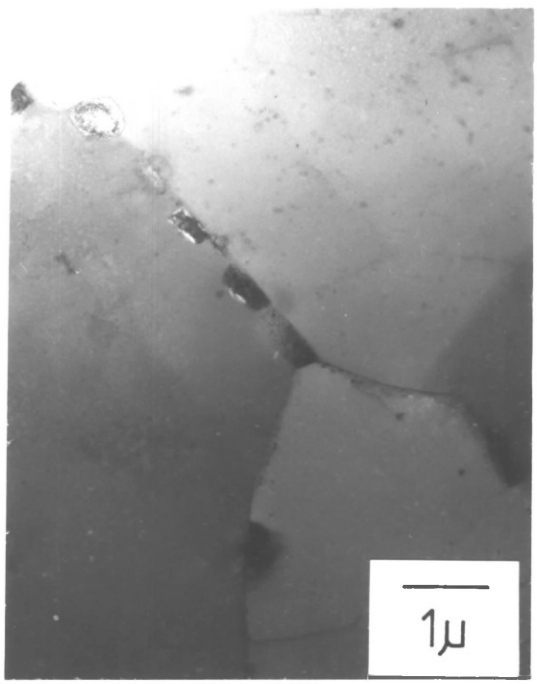
1μ

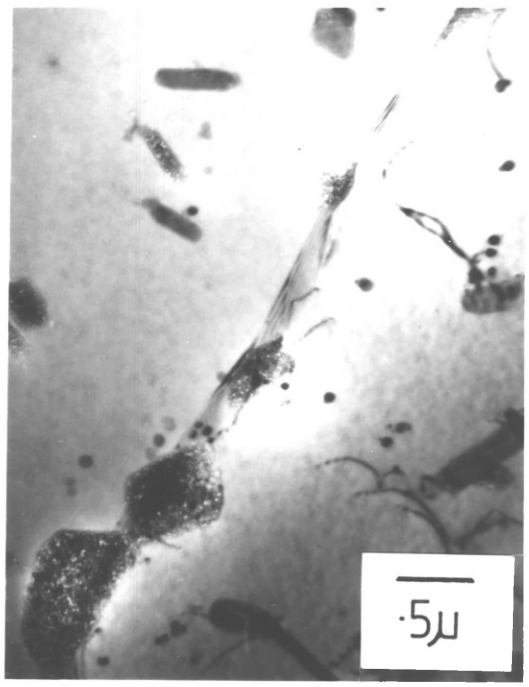
·5μ

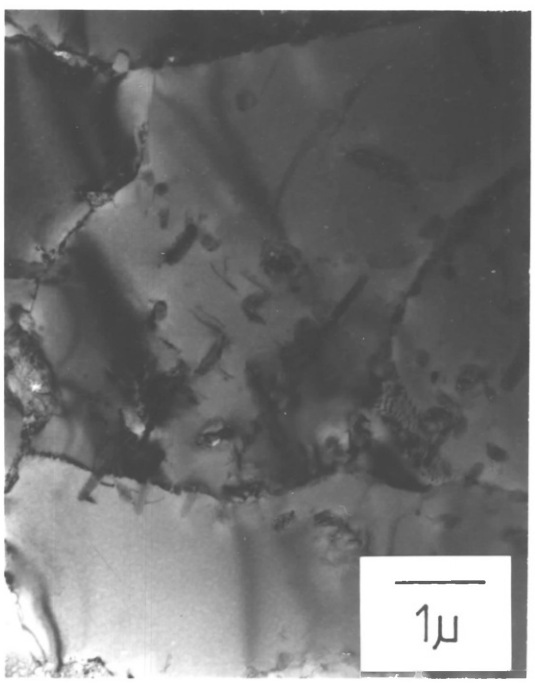
1μ

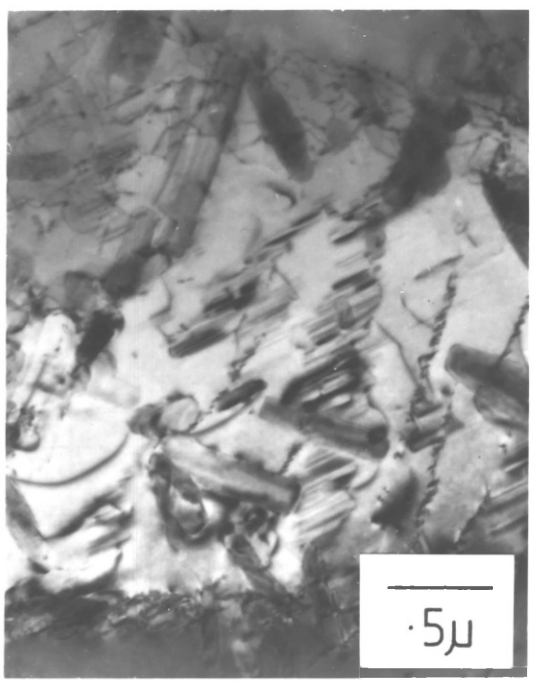
·5μ

TEM Investigation on the DSC Trace

Fig. 6.73

Fig. 6.74

Dark field micrograph with
SADP showing selected
reflections

Equilibrium precipitate exotherm peak

Al-Li-Mg-Cu

T6 Tensile Specimens Strained to Failure
at Room Temperature

Fig. 6.75

Fig. 6.76

Al-Li-Mg

Al-Li-Mg-Cu

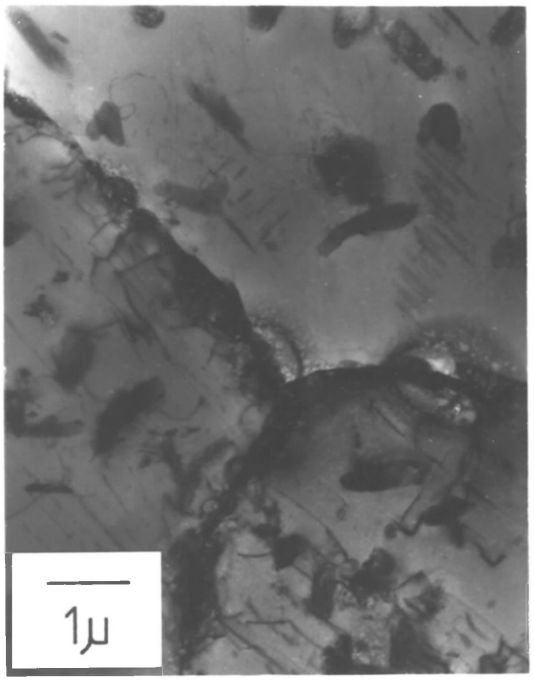
1μ

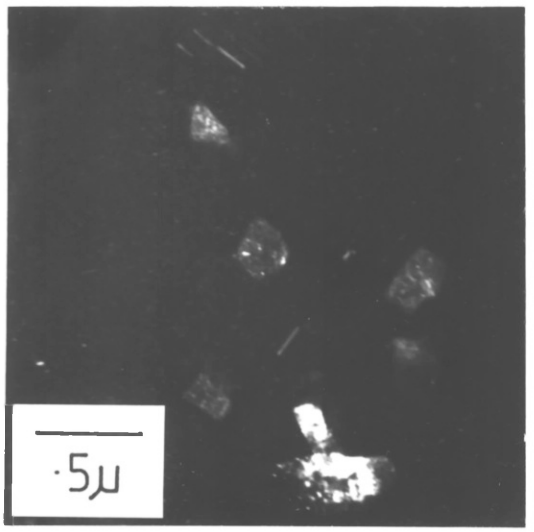
·5μ

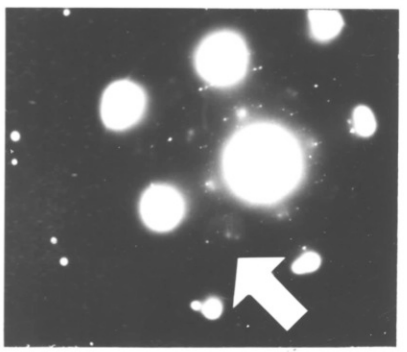

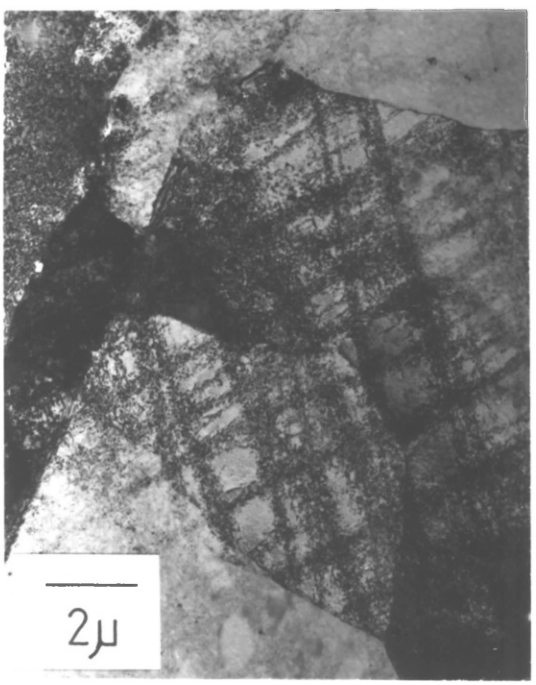
2μ

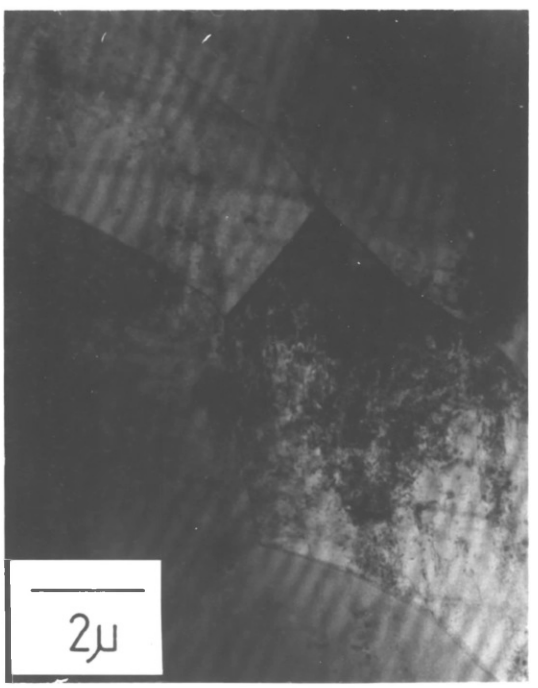
2μ

this should not be thought of as the general level of possible precipitation in this alloy.

At the peak position (Fig. 6.73) there was less S phase and it was probably beginning to dissolve whereas the Al_2MgLi particles continued to coarsen. Fig. 6.74 is a dark field micrograph containing both Al_2MgLi and S phase. In the diffraction pattern three types of reflection can be distinguished, aluminium <100>, Al_2MgLi and S.

Finally, the overall solvus temperature was significantly raised in this alloy by approximately 50°C.

To summarise then, the addition of copper to the ternary alloy appears to influence δ' precipitation as well as the high temperature equilibrium reactions. The Al_2MgLi precipitation sequence is still produced but additional precipitation in the form of the S phase from the Al-Cu-Mg system can also occur. However, the results can not be related directly to isothermal 170°C ageing, as extensive Al_2MgLi precipitation has been observed there with very little evidence of the S phase.

6.5.5 The Effect of Ageing on Room Temperature Plastic Deformation

The tensile specimens used for the modulus measurements were strained to failure and electron microscopy samples were cut out from just behind the fracture surfaces in a longitudinal direction, in order to look at the distribution of strain. In both alloys there was a marked trend with ageing time, consistent with the work hardening behaviour observed earlier. There was little difference between the two alloys in this respect which is not surprising since the precipitate distributions were similar and S phase precipitation which is reported to disperse slip[4] did not occur until overageing in the copper containing alloy.

In the solution treated condition dislocations were well distributed in the matrix with no slip band formation. Strain localisation began to occur in the underaged condition due to the precipitation of δ'. However, slip bands were narrow and did not extend for long distances. Figs. 6.75 and 6.76 show the slip dispersion patterns found in the peak aged specimens. Thick slip bands have

formed running at 90° to each other, presumably at 45° to the tensile axis. These bands extended through grain and subgrain boundaries and by intersecting with each other enclosed areas of very low dislocation density. This effect has been observed previously and has been used to explain the low toughness of these alloys[6] since strain localisation inevitably leads to stress concentrations.

The overaged specimens showed no evidence of banding and on the contrary slip was well dispersed due to looping around the coarse Al_3Li particles.

Therefore, using a standard heat treatment for these alloys can only improve the distribution of strain by sacrificing strength, since slip localisation is associated with precipitate cutting which in turn produces strengthening.

6.6 Summary

1. Homogenisation practices were established for both alloys. The soak temperature was found to have a strong effect on the final structure and properties of the Al-Li-Mg alloy and this was optimised to retain the hot worked structure after extrusion. However, the copper containing alloy proved difficult to homogenise due to the large quantities of the low melting point S phase.

2. The as extruded product showed distinct surface and core structures. The core was partially recrystallised at all but the highest extrusion temperatures with the remainder consisting of well recovered subgrains. Recrystallisation was enhanced by low extrusion temperatures and high ratios. The surface was always fully recrystallised but the scale of the structure varied with the process conditions. The copper containing alloy generally underwent lower levels of recrystallisation than the ternary alloy but gave coarser surface structures.

3. The extruded structure was influenced by the second phase particle distribution and by the Al_3Zr dispersoids in particular.

4. The alloys were difficult to recrystallise after extrusion by thermal treatments and it was impossible to produce a fully recrystallised structure in this way. As a result the extruded structures were always retained virtually unchanged after solution treatment.

5. In the fully heat treated condition the strength and ductility were influenced by the extrusion variables. At low extrusion ratios the Al-Li-Mg alloy could be strengthened by reducing the temperature and refining the subgrain size. At high ratios the level of recrystallisation became the important factor and the strength decreased with lower temperatures and higher ratios. The Al-Li-Mg-Cu alloy also showed softening with increased ratios but the strength always increased with the working temperature, due to a combination of substructural and precipitation effects.

6. The addition of copper to the ternary alloy had little solid solution strengthening effect but it did alter the ageing response, raising the proof stress and reducing the ductility.

7. The Al-Li-Mg alloy is capable of 2014 T6 strength to weight ratios, with the same ductility, but cannot reproduce the ductility on a pure strength comparison. It is also capable of 7075 T76 strength levels when substructural strengthening is greatest. The quaternary alloy exceeds the 7075 T76 minimum strength level for all extrusion conditions but the ductility is always reduced. However, it is possible to increase this by suitable underageing treatments.

8. The Al-Li-Mg alloy has a greater capacity for work hardening than Al-Li-Mg-Cu after similar ageing treatments and this ought to be reflected in subsequent toughness measurements.

9. The modulus values of the two alloys were similar, although the addition of copper produced a slight improvement and agreed with published values. Both alloys had the same density corresponding to 90% of that for 2014.

10. The alloys were fairly insensitive to an intermediate cold stretch. The Al-Li-Mg alloy did not show any marked quench sensitivity

and could be directly aged to give the same tensile properties. The copper alloy was sensitive in this respect and a solution treatment step was necessary to achieve maximum strenthening.

11. The ageing sequence in the ternary alloy is;

SOLID SOLUTION → δ' → Al_2MgLi

Al_2MgLi forms preferentially at grain boundaries at an early stage of ageing but can form in the matrix after longer times. Extensive PFZs were found at grain boundaries and also around Al_2MgLi particles. The response of Al-Li-Mg-Cu was dominated by that of the Al-Li-Mg system but it additionally gave some S phase formation at longer times. From the tensile results this did not appear to be encouraged by cold stretching. Copper also influenced the vacancy condensation mechanisms and dislocation loops and helices were produced in this alloy. In addition the density of grain boundary precipitation was raised.

12. The DSC investigation showed that the addition of copper influences the kinetics of the δ' precipitation reaction and this may explain the strength increase it produced. It also verified that this alloy is capable of producing S phase precipitation under 'suitable' conditions.

13. Slip localisation is associated with strengthening by δ' precipitation in both of the alloys and is caused by the mode of interaction between the slip dislocations and the precipitates. The slip bands formed during room temperature deformation of the peak aged structure can extend through grain and subgrain boundaries.

CHAPTER SEVEN

THE EFFECT OF EXTRUSION AND HEAT TREATMENT VARIABLES ON FRACTURE TOUGHNESS

7.1 Experimental

Initially toughness measurements were made in the L - T direction using the crack opening displacement technique according to BS 5762 : 1979. This is similar to the plane strain fracture toughness test (BS 5447 - 1977) and if the specimen thickness is sufficient to give valid K_{1c} results then they may be presented in those terms.

Single edge notch bend specimens were used of dimensions 12 x 12 x 60 mm with a loading span of 48 mm. They were cut out of 12 mm square extruded bar corresponding to an extrusion ratio of 31:1. The notch depth was 3 mm and the width 1.5 mm. Prefatiguing was performed to give an overall crack length of approximately 6 mm before testing in three point bending using an Instrom universal testing machine.

In the more brittle specimens limited plasticity meant that K_{1c} conditions were satisfied, however, deviations from the standard during the fatigue precracking stage through lack of fatigue force control made the test invalid. As a result all the figures are quoted as K_Q values calculated from the crack tip opening displacement using the relationship :

$$K_Q = (m\sigma E\delta)^{\frac{1}{2}}$$

where σ = yield stress

δ = crack tip opening displacement

E = Youngs modulus

m = geometrical factor, assumed equal to unity.

A constant value of 78 GPa was used for the elastic modulus in all the calculations.

Testing was also carried out in the transverse - longitudinal orientation, i.e. with crack propagation occurring along the extrusion direction. For this work a bolt-loaded double cantilever beam specimen was used, of dimensions 15 x 15 x 125 mm, machined from 10:1 extrusions. Here the cracking force was applied by tightening two opposed bolts passing through the arms of the notch. Details of the specimen and the analysis used to calculate values of the stress intensity factor are given in Appendix Two.

To ensure there was a narrow sharp crack tip at the start of the test a minimum crack length of 45 mm was produced before commencing. Measurements were then made of the initial crack length and the displacement of the arms of the notch required to produce further crack growth. Clearly such values of toughness are specific to this specimen geometry and are not directly comparable with data obtained from other tests. The advantage of this test was that it was simple to perform and part of this investigation was to determine its usefulness for testing extruded material.

Finally spare COD specimens were tested using the Charpy impact test. Again these were non standard but it is useful to compare the results with those from COD testing.

7.2 COD Testing

Specimens were prepared to include extrusion and heat treatment variables. The three heat treatments UA, PA and OA established in Chapter Six were used and the extrusion temperature was varied inside the upper and lower limits for each alloy. Output from the test was in the form of load versus crack opening displacement curves and typical traces for the Al-Li-Mg alloy are given in Fig. 7.1. All the curves start off in a linear manner as the beam is elastically deformed. The load then levels off due to a combination of general yielding and slow crack growth, until instability is reached and the load begins to fall again. These curves show substantial plastic deformation with the maximum load increasing with proof stress. Surprisingly, this is limited in the underaged condition which always exhibited a load drop before the peak was reached, signifying a period of rapid unstable crack growth. This was associated with an audible click during the test. In the overaged condition the rise to the peak load was smooth but general instability occurred after only small displacements as shown in Fig. 7.1. The three lower traces here are from samples extruded at 400°C. Extrusions processed at 500°C exhibited similar types of load displacement loci for the different tempers but the load values were generally higher, corresponding to the higher yield stress of the unrecrystallised structure. This is shown for the

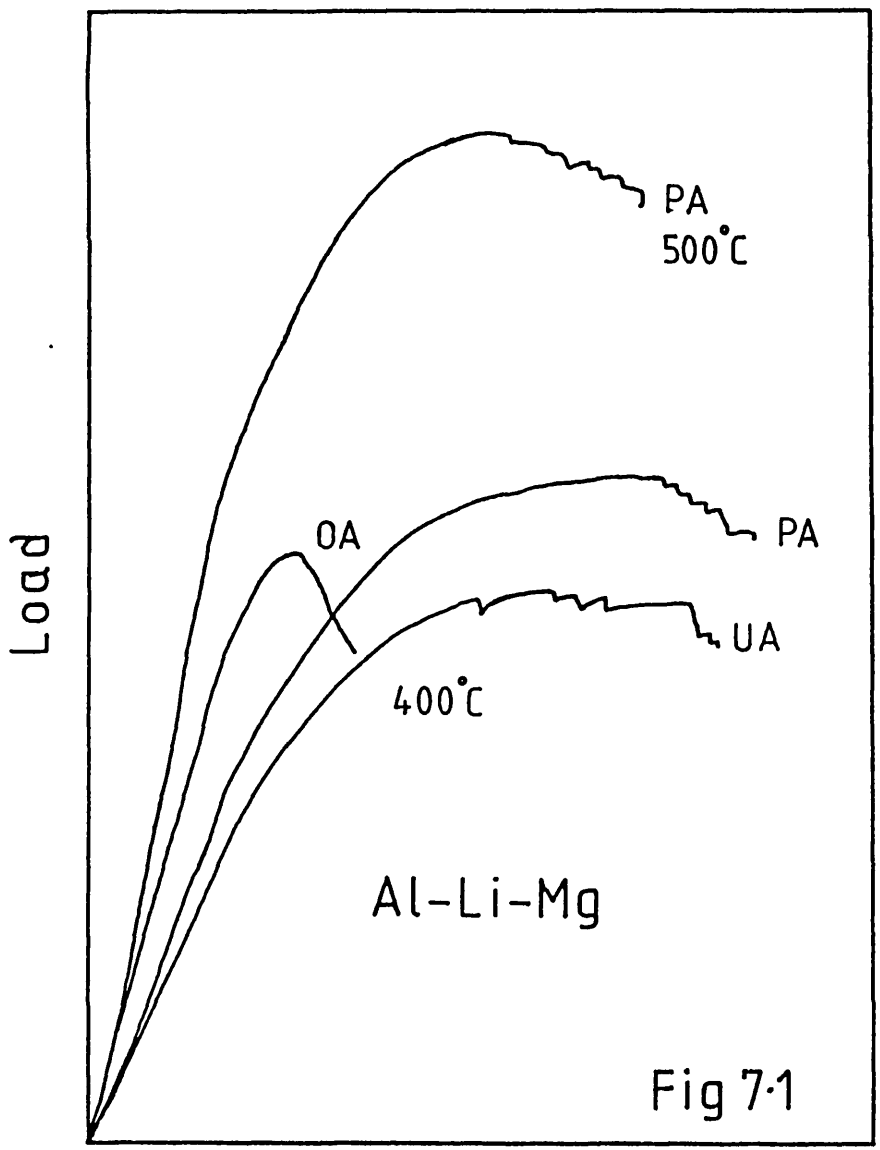

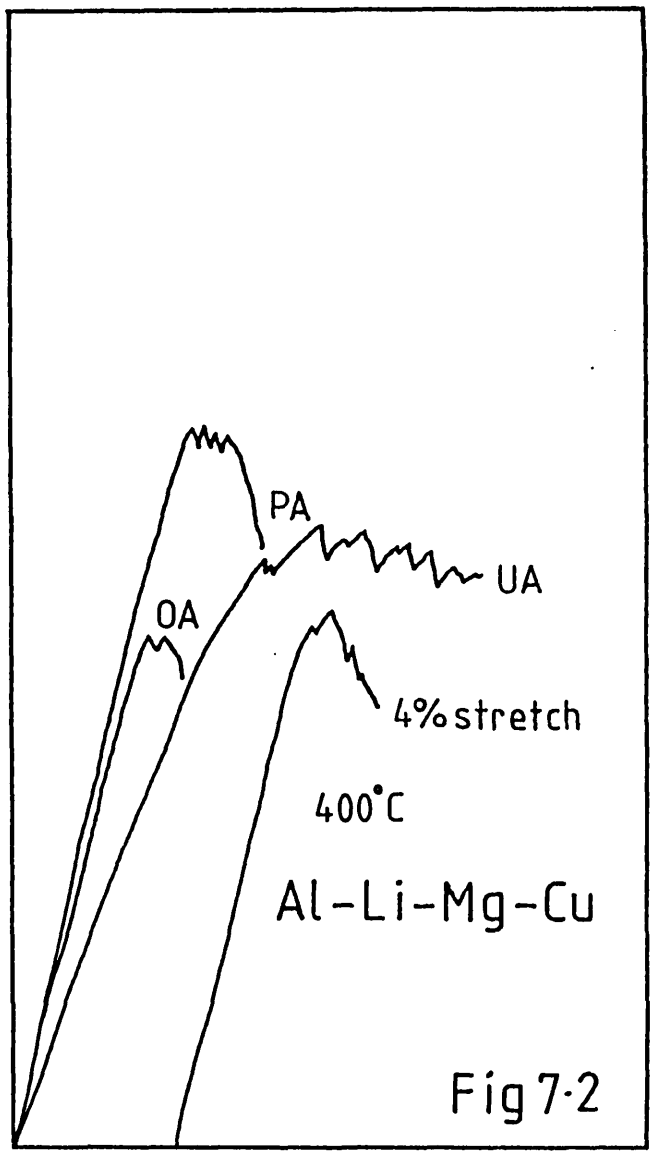

COD test traces.

peak strength condition in the upper trace of Fig. 7.1 where there is only a slight decrease in the displacement at peak load.

Fig. 7.2 contains typical traces from the Al-Li-Mg-Cu alloy tests,at the same scale. The obvious difference here is the absence of the region of plasticity and slow crack growth shown by the ternary alloy. A load drop or 'pop-in' was observed for all conditions, after very little plastic deformation, signifying rapid crack extension and this was usually quickly followed by specimen failure. These traces satisfied the plasticity criterion for plane strain fracture toughness and values could have been quoted as such if it were not for the deviations from standard practice outlined earlier. Although the proof stresses were higher than for the Al-Li-Mg alloy, failure occurred at similar values of load explaining why extensive yielding was not seen. The underaged condition now appeared to be tougher than the peak strength temper as it showed the first load drop at larger displacements and took longer for complete specimen failure. As with the first alloy the failures in the overaged temper were very rapid and in some cases specimens failed completely into two pieces before the test could be stopped. Stretching was incorporated into the heat treatment schedule for this alloy and a trace is shown for a sample given a 4% stretch prior to ageing. Clearly the load and displacement at the onset of rapid crack extension have been reduced.

The values of K_Q calculated from the load-clip gauge displacement loci are given for the two alloys in Figs. 7.3 and 7.4 which include the effects of heat treatment and extrusion conditions. The extrusion range for the square section used for these specimens was limited to 40°C for the copper containing alloy and thus extrusion temperature had little effect on these results. The Al-Li-Mg alloy, on the other hand, was extruded over a wider range and here toughness was reduced at the lowest extrusion temperature in each heat treated condition. This is initially surprising since this also corresponds to the lowest yield strength, but both effects are due to the increased level of static recrystallisation in the product. For extrusion temperatures of 500, 450 and 400°C the levels of core recrystallisation were 5,25 and 55% respectively. The higher level

of softening caused a loss in toughness due to the favourable orientation of recrystallised grain boundaries, some of which were parallel to the crack direction presenting an easy crack path. Similar trends have been reported[81] for 7000 series alloys and Thompson[28] has presented plane stress results for 7075 sheet indicating that toughness decreases with the transition from unrecrystallised, to elongated recrystallised, to equiaxed recrystallised structures.

Therefore, by suitable processing the proof stress can be raised along with the L-T toughness. The same mechanism ought to be possible in the quaternary alloy at higher extrusion temperatures although as was reported in Chapter Six this would also introduce extra precipitation hardening which is detrimental to toughness. Grain shape can also be modified by control of the homogenisation schedule, as the results in Chapter Six would indicate. Since a higher temperature treatment tends to promote static recrystallisation the choice of 500°C as a soak temperature was beneficial with regards to L-T toughness.

Turning now to the effects of heat treatment, the picture for the Al-Li-Mg alloy is somewhat confusing. Clearly, overageing to the level shown here results in serious embrittlement even though the proof stress is reduced and the matrix plasticity raised, as evidenced by the n values. Harris et al drew the same conclusion working on an almost identical alloy[18]. The confusion in the results arises from the two sets of UA data presented in Fig. 7.3; the 'pop-in' values and the maximum load values. As expected the 'pop-in' toughness results fall well below those for the peak strength temper whereas the maximum load values were only slightly lower. The problem here is which data set to compare. The load drop results are important since the accelerated crack growth at this point would probably have caused dramatic failure of a larger specimen. Once rapid crack extension had taken place the specimens were weakened and the maximum load point on the locus occurred at a lower position than if only slow crack growth had occurred. Without this feature these toughness values would probably have exceeded those for the peak strength temper. Hence, neither type of result is directly comparable with those for the peak aged condition which exhibited a smooth rise to the peak load.

One of the drawbacks of this test program was that initiation values were not measured. Whereas the initiation value of clip gauge displacement was not detectable on most of the load displacement traces, the 'pop-in' value in the UA condition was probably close to this position. Therefore, it cannot be concluded that the peak aged condition is simply tougher than the underaged condition, which would oppose the established trends for other age hardening aluminium alloys[44].

Several 2014 T6 specimens were fabricated and tested in this work for comparison purposes since these toughness results are not directly comparable with literature values. This material was extruded at 450°C, solution treated at 500°C and then aged at 160°C for 18 hours. The grain structure was unrecrystallised. The traces produced showed a smooth rise to the peak load and an average value of 46 MPa$\sqrt{m}$ was found which is plotted with the results for both alloys in Figs. 7.3 and 7.4. The higher toughness Al-Li-Mg values approach this level but it must be stressed that this is in the longitudinal-transverse orientation, usually the toughest for a directional grain structure.

The trend in toughness with heat treatment is much clearer in the Al-Li-Mg-Cu results (Fig. 7.4). All the load displacement loci for this alloy showed rapid crack growth early on in the test and toughness values calculated from this point are therefore directly comparable. Toughness increases in the order:

$$OA < PA < UA$$

so that the overaged condition is still more brittle than the peak strength temper and as expected from yield stress considerations the underaged condition is the toughest. However, the values are much lower than for the Al-Li-Mg alloy and are centred around the overaged values for this composition. In the peak strength temper the difference is 18 MPa$\sqrt{m}$, a drop of 45%.

Averaged results for both alloys are compared in Fig. 7.5 on a proof stress basis, together with the figure for 2014 T6. Usually this type of plot is drawn for strength variations due to age hardening but this figure also includes substructural hardening effects in each temper. Again two sets of results are included for

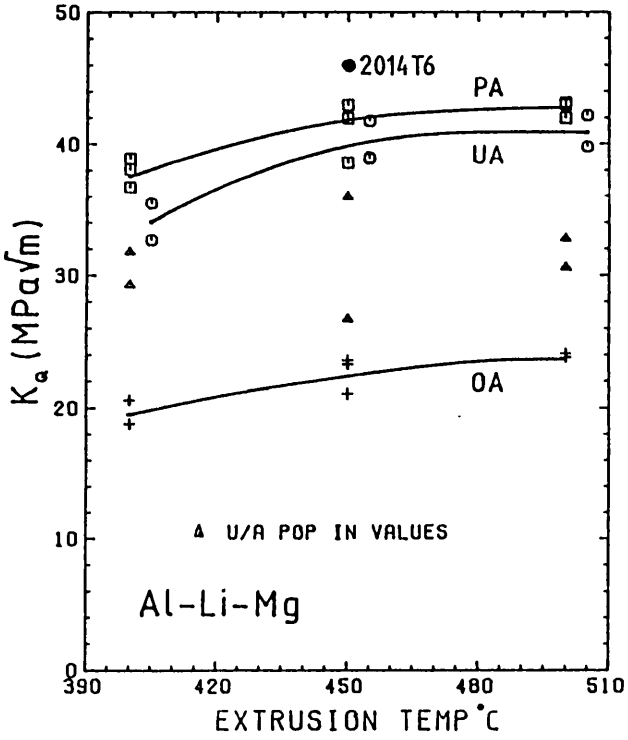

Fig 7.3

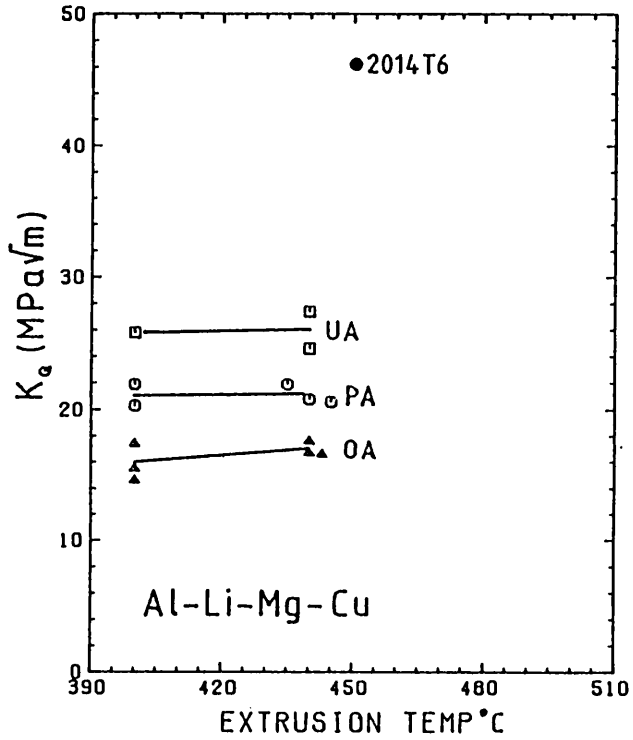

Fig 7.4

Variation in L-T toughness with extrusion and heat treatment conditions (COD results).

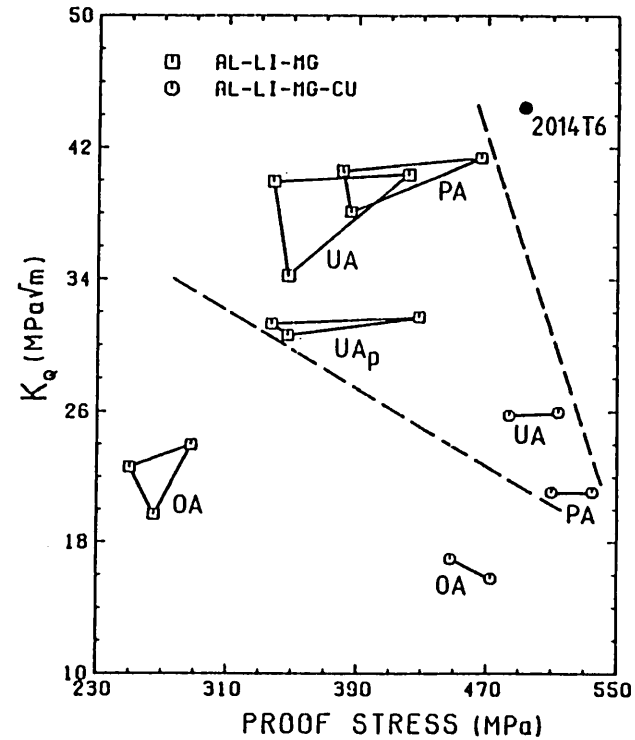

Fig 7.5

L-T toughness vs. proof stress.

the Al-Li-Mg alloy in the UA condition.

For 2000[45] and 7000[46] series alloys plots of this kind usually show a decrease in toughness to peak strength followed by a return on a slightly lower path on overageing. However, as has already been shown for both alloys,here overageing produces a further toughness drop and the trend follows a 'dog-leg' path. This must be due to the high levels of Al_2MgLi precipitation observed in this condition counteracting the softening and increased work hardening capacity indicated by tensile test results. Considering only the UA and PA conditions a band can be drawn containing the results from both alloys showing toughness decreasing with increasing proof stress and this has been constructed in Fig. 7.5. This would tend to suggest that the lower toughness in the Al-Li-Mg-Cu alloy is primarily due to the increased yield stress and reduced crack tip ductility. Any additional precipitation reactions caused by the presence of copper are not having a beneficial effect which is to be expected from the very low precipitate densities seen in the structural investigation. However, if the copper were influencing the δ' precipitation reaction, as suspected, it would support this trend.

The maximum toughness condition for the ternary alloy falls just short of the strength and toughness of the 2014 T6 sample tested. Vierod investigated the effect of extrusion temperature on the strength and toughness of 2014 T6 using the same testing techniques[3] and obtained some improvement in toughness and strength with higher extrusion temperatures. His toughness results increased from 35-45 $MPa\sqrt{m}$ for a proof stress range of 400 to 500 MPa so that the results here represent the upper end of this range. The ternary alloy is therefore capable of most of this property range and this could be extended to higher strength levels on a strength:weight ratio basis.

In Chapter Six the effects of an intermediate cold stretch on the heat treated tensile properties of the Al-Li-Mg-Cu alloy were reported. Toughness tests were also performed on this alloy using similar treatments to investigate whether any precipitation reactions, particularly that producing S phase, were being promoted and affecting toughness. In other Al-Li-Mg-Cu alloys improved toughness has been reported in stretched and aged material due to the strain dispersing effect of this phase[16]. The results are presented in Table 7.1 in

comparison with T6 values. Both levels of stretching gave similar figures but rather than improving toughness, these treatments were detrimental, giving a 4-5 MPa√m loss corresponding to a reduction of 25% under the T6 values. This agrees with the reduced ductility and work hardening capacity found after these treatments, which are clearly not beneficial in these alloys and it is doubtful whether significant S phase precipitation can be promoted. With the highest level of stretching there can be no lack of nucleation sites and S phase formation is probably not thermodynamically favourable with high magnesium:copper ratios.

	Toughness MPa√m		
Extrusion Temp.	T6	T8 (2%)	T8(4%)
400°C	20.3/21.9	15.4/16.5	15.2
440°C	20.8/21.9/20.6	15.6	16.2/16.5/16.9

Table 7.1 The Effect of Stretching on the Toughness of the Al-Li-Mg-Cu Alloy

7.2.1 Fracture Surfaces

Crack extension in commercial high strength aluminium alloys normally takes place by a fibrous transgranular mode. Voids are nucleated at inclusion particles within the plastic zone ahead of the crack tip which subsequently grow until the material between them ruptures. In precipitation hardening alloys the structural changes during ageing can influence the fracture process. These changes can be summarised for the two alloys in question as follows:

1. Growth of δ' precipitates and resultant changes in the proof stress and deformation mode.
2. Formation of coarse equilibrium grain boundary precipitates and at later times matrix precipitates.
3. Formation of precipitate free zones at high angle boundaries.

As the proof stress is raised the extent to which plastic deformation at the crack tip can relieve the stress concentration is reduced, giving the usual inverse relationship with toughness.

Coarse equilibrium precipitates can act as sites for void nucleation but overageing does not normally lead to reduced toughness as this is compensated for by increased matrix plasticity. Clearly the alloys here oppose this trend. Precipitation on grain boundaries can make them low energy fracture paths, leading to intergranular fracture, and this has been reported[46] to occur in 7075. However, this transition does not take place in most commercial alloys due to easy void nucleation within the grains at dispersoid particles. The effect of PFZ formation on toughness and fracture mode is unclear as experiments to vary this feature are accompanied by other structural changes and results are conflicting[28]. The usual argument against them is that they are sites for preferential deformation, and promote crack formation at triple points leading to intergranular fracture.

Fracture surfaces were examined just below the fatigue crack in the early stages of crack growth. The effects of ageing time on the appearance of the Al-Li-Mg fractures will be discussed first.

In the underaged condition (Fig. 7.6) failure was initially transgranular and occurred by extensive shearing. Most of the fracture surface consisted of relatively smooth shear facets, as shown in the extreme left of the figure, which were probably the result of failure at slip bands. Other areas contained evidence of large void formation and here the material separating the dimples showed extensive plasticity indicative of the high work hardening capacity in this temper. However, after a short amount of crack growth in this manner the crack front was suddenly redirected at right angles down the extrusion direction, as shown in Fig. 7.7. The reason for this was unclear by examination of the transition point and on some portions of the crack front it occurred directly below the fatigue crack. The new surface was the result of a completely brittle separation of the extruded grain boundaries which were smooth and free of any signs of plastic deformation. This increment of crack growth took place very rapidly giving rise to the click heard during the test and was responsible for the 'pop-in' observed on the load displacement trace. Further

COD Fracture Surfaces

Fig. 7.6

Al-Li-Mg UA

Extrusion temp = 500°C

Fig. 7.7

Al-Li-Mg UA

Extrusion temp = 500°C

Fig. 7.8

Al-Li-Mg PA

Extrusion temp = 500°C

Fig. 7.9

Al-Li-Mg PA

Extrusion temp = 400°C

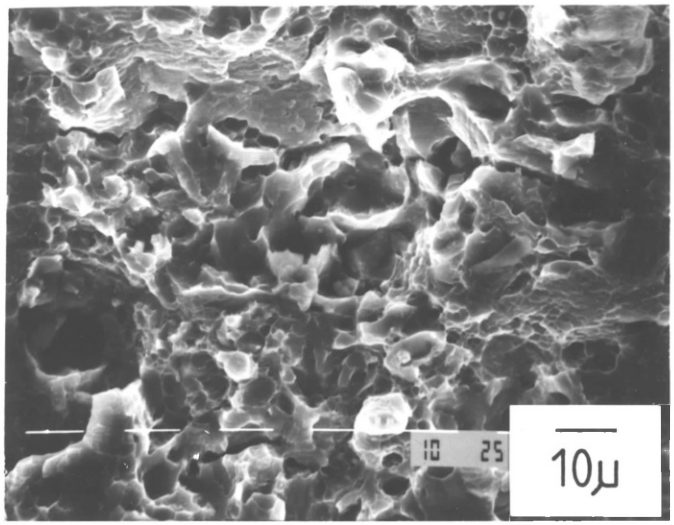
10
25
10μ

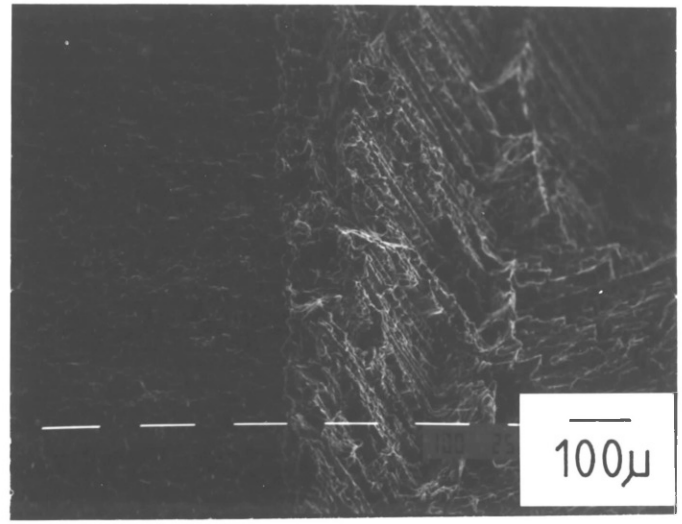
100μ

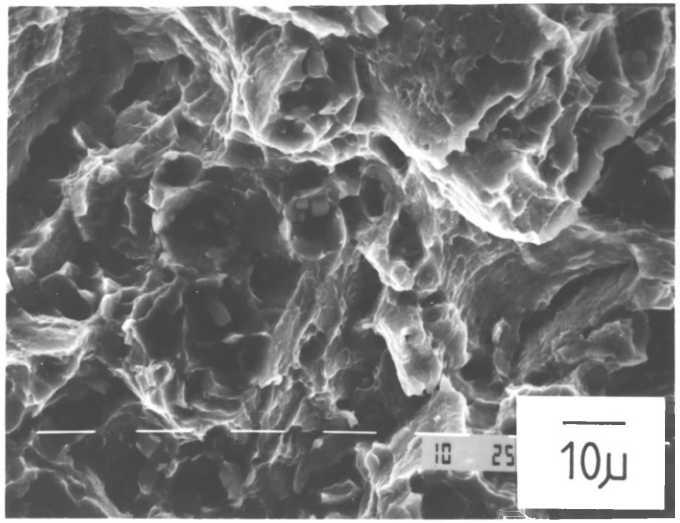
10
25
10μ

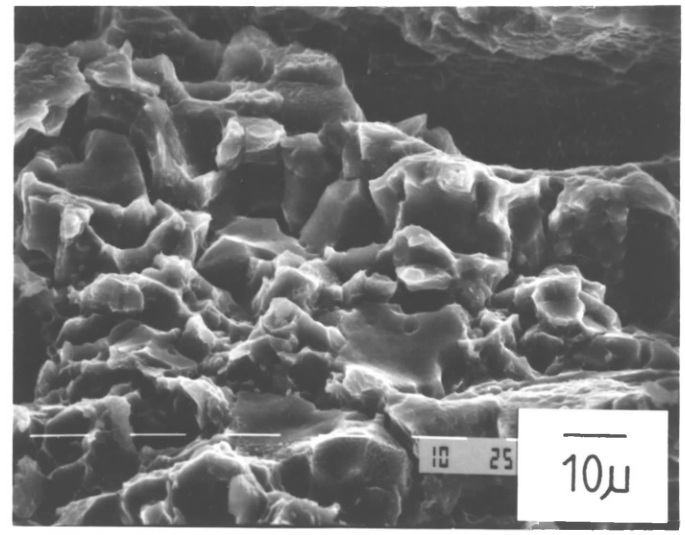
10
25
10μ

loading gave rise to repeated cycles of slow transgranular fracture, followed by rapid intergranular splitting.

In the peak strength condition, shown in Fig. 7.8, the failure was similar to that in the UA condition, except that the splitting mechanism did not take place. Although secondary cracking was observed the crack front was not redirected. The fracture surface was less extensively sheared than that in the UA temper due to the reduced matrix plasticity. The particles in the dimples shown were identified as being iron containing stringers but it is possible that at this stage some of the equilibrium precipitates were large enough to give void nucleation.

The structures in Figs. 7.6 and 7.8 are from the highest temperature extrusion which was almost fully recovered. The effect of producing a partially recrystallised structure is brought out in Fig. 7.9. This sample was heat treated to give peak strength and failure occurred by two mechanisms. Void nucleation and coalescence still took place but recrystallised grain boundaries parallel to the crack direction separated in a brittle manner analagous to the separation of the extruded grain boundaries in the UA temper. Such areas were also seen in the other tempers for this extrusion and therefore the reduction in toughness at low extrusion temperatures can be attributed to introduction of this low energy path. The intergranular areas were generally smooth but showed some cavity formation due to the grain boundary precipitates. However, these were not the cause of failure along this path because of their absence in the UA temper. Also the influence of PFZs on this fracture path can be dismissed due to the limited plasticity seen on the grain surfaces.

Fig. 7.10 shows the fracture surface of the low Z extrusion in the overaged condition. Failure has taken place in a completely transgranular manner but the surface is covered with cavities roughly 1 μ in diameter, associated with the coarse Al_2MgLi precipitate distribution produced by this heat treatment. Due to the frequency of these precipitates any beneficial effect of the high n value for this temper is being negated by the ease of void nucleation and coalescence, which explains the continued decrease in toughness after attaining peak strength. In the high Z extrusions areas of inter-

granular fracture were still observed, although they were covered in voids due to the high density of boundary precipitates. This mechanism was probably not as important here due to the general low level of toughness which is why the toughness decrease with extrusion temperature was less severe for this heat treatment.

Failures in the Al-Li-Mg-Cu alloy were very similar in appearance to those of the ternary alloy and similar trends were encountered on increasing the ageing time. Although all the tempers showed a load drop on the COD trace the splitting mechanism still only took place in the underaged testpieces and in the other conditions rapid crack growth took place in the transgranular mode. In the areas of the underaged fracture where the crack did propagate in the 'correct' direction the surface again consisted of shear facets and cavities but the extension of the ligaments between the voids was severely reduced. In addition the density of the voids was increased due to the action of the S phase stringer particles. All the extrusions were partially recrystallised as a result of the low extrusion temperatures and brittle intergranular fracture also occurred, as shown in Fig. 7.11 for the PA condition. This partly contributed to the low toughness in this alloy but from this study it would appear that the increased yield strength and reduced work hardening capacity were the major factors.

The disturbing feature to come out of this investigation is the propensity for intergranular fracture in both alloys and in particular the surprising behaviour in the UA condition. Here intergranular failure is preferred to the transgranular transverse mode activated by the maximum principle stress. It would appear that high angle boundaries have an inherent weakness not associated with the products of ageing and this would tend to suggest embrittlement by solute segregation. However, this still does not explain why splitting should only occur in the UA condition, usually the toughest, when the effects of continued ageing might be expected to produce even further grain boundary weakening. Fig. 7.14 outlines a possible explanation for this behaviour. The energy required to activate the transgranular fracture mode in these alloys has already been shown to decrease with ageing time. In comparison, the energy to cause splitting will be a weaker function of ageing time and ought to be

COD Fracture Surfaces

Fig. 7.10

Al-Li-Mg OA

Extrusion temp = 500°C

Fig. 7.11

Al-Li-Mg-Cu PA

Extrusion temp = 400°C

DCB Fracture Surfaces

Fig. 7.12

Al-Li-Mg UA

Extrusion temp = 325°C

Fig. 7.13

Al-Li-Mg UA

Extrusion temp = 325°C

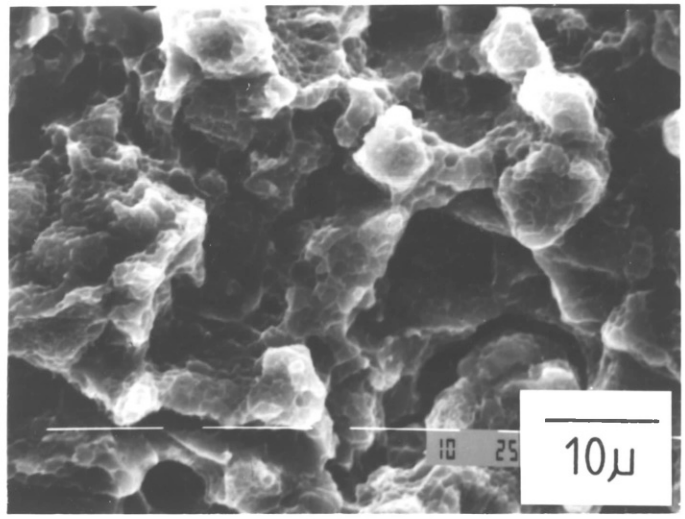
10μ

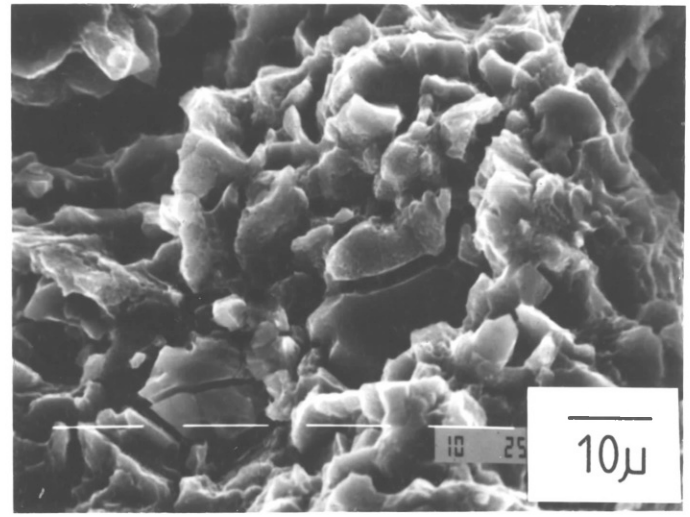
10μ

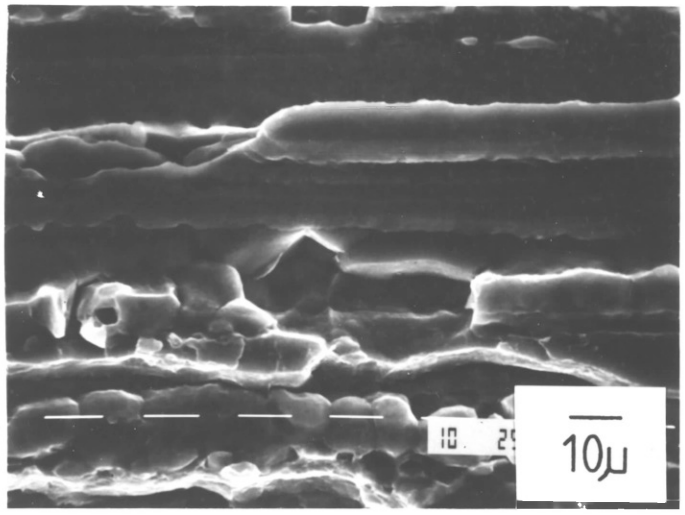
10μ

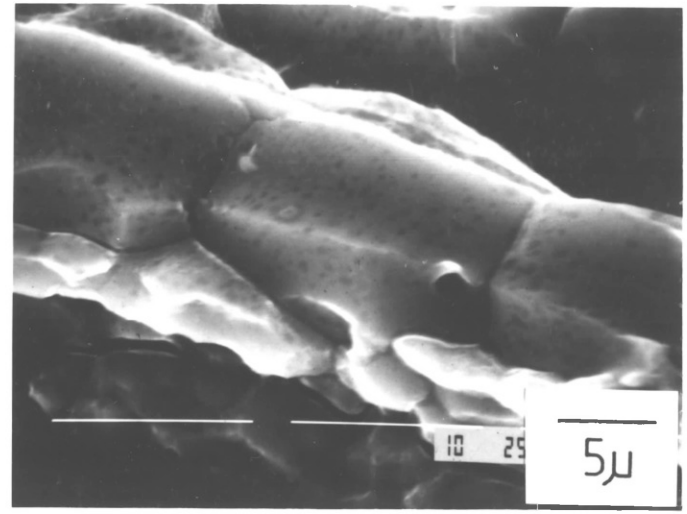
5μ

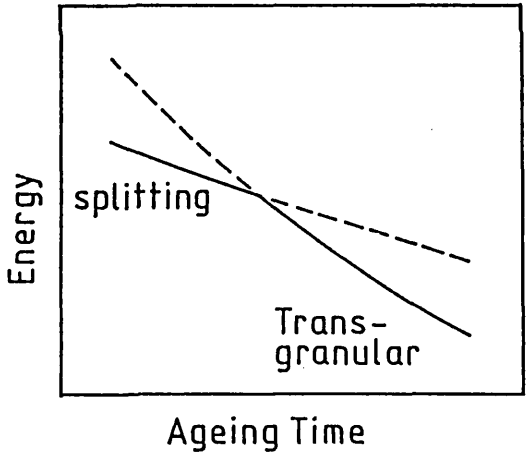

Fig 7.14

Model for grain boundary splitting.

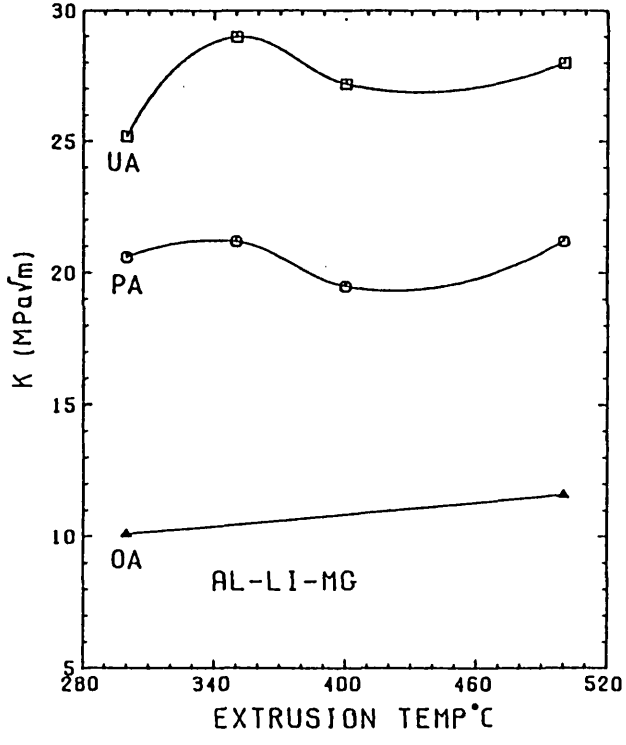

Fig 7.15

Variation in T-L toughness with the extrusion and heat treatment conditions (DCB results).

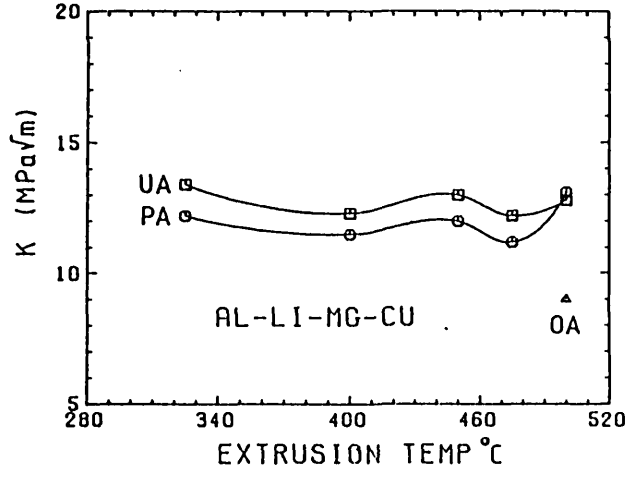

Fig 7.16

higher than that for ductile failure due to the orientation effect. However, it is possible that in the UA condition the resistance to fibrous failure is sufficiently high to allow grain boundary splitting to take place. Unfortunately, in this test the rapid crack extension associated with this mode of failure is easily detected whereas slow crack growth is not.

If the grain boundary embrittlement is due to solute segregation then possible elements causing this are sodium and potassium brought in with the lithium additions, although their bulk concentrations were low. Alternatively the fluxes used in the casting operation may be contaminating the melt. Various authors attribute conflicting significance to the presence of alkali metals and the literature on this topic was reviewed in section 1.4.1.1. The segregating species ought to be easily identifiable using Auger spectroscopy, since this technique relies on characteristic auger electrons which are of such a low energy that they can only escape if produced within the first five atom layers from the surface. Unfortunately, such equipment, with an situ fracture facility, was not readily available for this work.

7.3 DCB Testing

In this test crack propagation occurs in the longitudinal direction which ought to favour the grain boundary splitting mechanism seen in the COD test. To provide sufficiently large specimens 10:1 extrusions were used and this meant that variations in grain structure were not as marked as in the COD test. The test was designed to give a rapid method of toughness determination and no measurement of load was made. Instead this was calculated from the displacement of the notch arms. The test was stopped when an increment of crack growth was observed (or heard) and so the test is really measuring the load required to cause rapid crack extension. Obviously the values of toughness produced are only directly comparable with other results obtained using the same specimen.

The results for the two alloys are presented in Figs. 7.15 and 7.16 which show the effects of ageing time and extrusion temperature.

In both cases the toughness decreased with ageing time and no anomalous effects were found in the UA condition. This mode of loading should initiate the splitting mechanism which was thought to be independent of ageing time. However, to initiate cracking the ability to accommodate plastic deformation at the crack tip is still an important factor and so the deformation mode and precipitate distribution will affect the results. It is worth noting the macroscopic characteristics of fracture in the three tempers. In the underaged condition the displacement of the arms to cause cracking was the greatest and when cracking occurred it was very rapid and extensive due to the greater amount of stored energy available. Peak ageing gave crack extension after smaller displacements and the length of crack produced was reduced. Finally, in the overaged specimens the amount of crack extension was so small that it was difficult to detect visually.

The results for the Al-Li-Mg-Cu alloy (Fig. 7.16) are again centred around the values for the ternary alloy in the overaged temper, showing less variation with ageing time. In the PA condition the toughness of the copper containing alloy was roughly half that of the previous alloy, agreeing with the level of embrittlement found in the COD test. Therefore, similar mechanisms are responsible for failure here, although grain boundary separation is being promoted.

The effects of extrusion temperature on toughness are negligible in this direction, since the levels of recrystallisation were low and when it occurred the grains were banded in the extrusion direction anyway. Variations in subgrain size had no influence on the results because they are not involved in the fracture path. The insensitivity of toughness to process conditions shown here does mean that strength increases can be achieved by control of the extrusion temperature without damaging this property.

In this test it is important to produce a straight crack and this was facilitated by the grain boundary weakness in this direction. Some 2014 T6 specimens were produced for comparison purposes, but crack initiation proved difficult and they failed by transverse cracking at the root of the notch, indicating that in this alloy the boundaries do not offer a substantial reduction in the fracture energy.

Any further work with this type of test ought to use a modified specimen with a reduced notch width, possibly using a narrow saw cut to initiate the crack. In the toughest condition for these alloys (Al-Li-Mg UA) the arms were deflected so much that it was difficult to maintain symmetry. A narrower slit would increase the arm thickness and reduce the amount of bending required.

7.3.1 Fracture Surfaces

The fracture surfaces of the two alloys were again very similar for each heat treatment. In the UA and PA ternary, brittle intergranular fracture was preceded by periods of slow crack growth, similar in appearance to the COD failures, consisting of areas of shear and areas of void nucleation and coalescence. Such a region would appear to be necessary to nucleate grain boundary fracture and this explains the trend in toughness seen with ageing time. This section will consider the nature of the fast fracture surfaces and the effect of grain boundary features on this path.

Figs. 7.12 and 7.13 show the Al-Li-Mg alloy in the UA temper. The fracture is clearly intergranular and as this sample was taken from a partially recrystallised, low temperature extrusion, recrystallised boundary facets can be seen. Separation has occurred at high angle boundaries with almost no evidence of void formation. At high magnification, in Fig. 7.13, the grain boundaries are shown to be covered in dark patches, presumably the fine Al_2MgLi precipitates, but these have not given rise to voids. This is because they are below the critical size for this process. In the peak aged condition, Fig. 7.17, the crack path is still intergranular but the grain boundary precipitates are now large enough to nucleate voids, reducing the resistance of this route further.

On overageing, the path route was changed in both alloys and some specimens had to be rejected because the cracks did not propagate longitudinally. Fig. 7.18 shows the Al-Li-Mg fracture surface. As in the COD test it is dominated by the voids formed at the coarse grain boundary and matrix precipitates. Although this crack did propagate in the general direction of extrusion, considerable lateral

DCB Fracture Surfaces

Fig. 7.17

Al-Li-Mg PA

Extrusion temp = 325°C

Fig. 7.18

Al-Li-Mg OA

Extrusion temp = 325°C

Fig. 7.19

Al-Li-Mg-Cu PA

Extrusion temp = 325°C

Fig. 7.20

Al-Li-Mg-Cu PA

Extrusion temp = 325°C

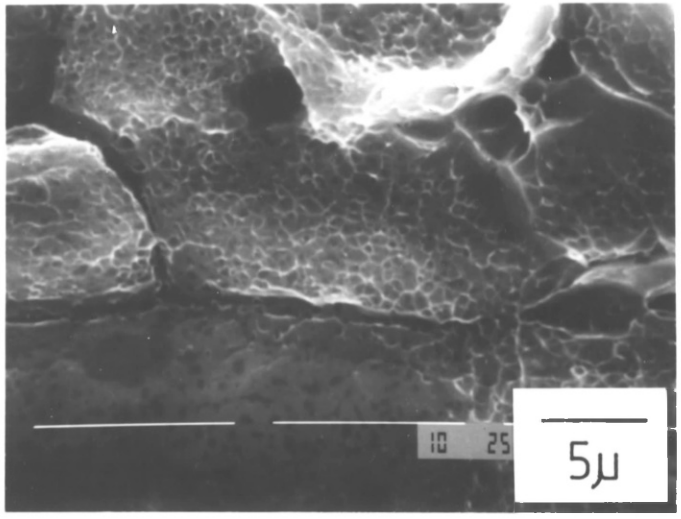
5μ

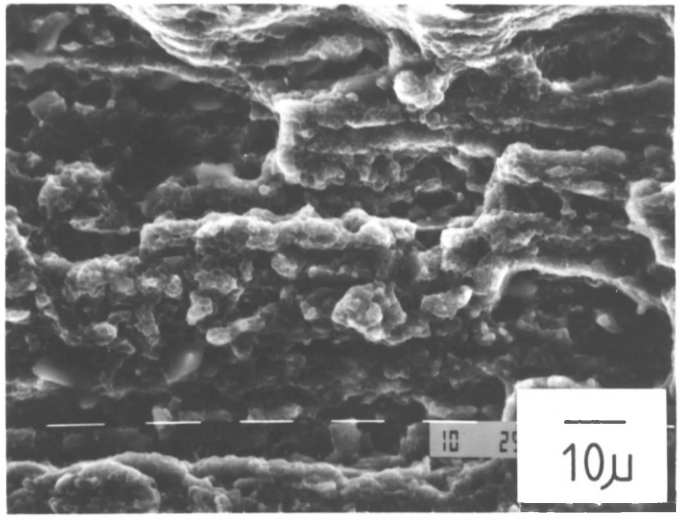
10μ

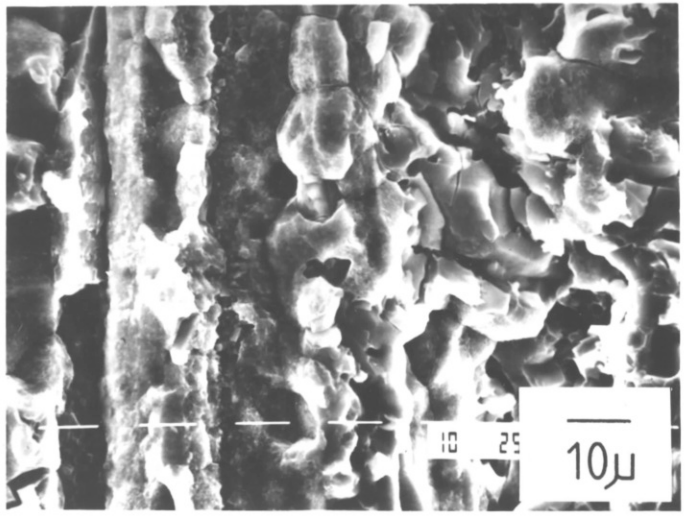
10μ

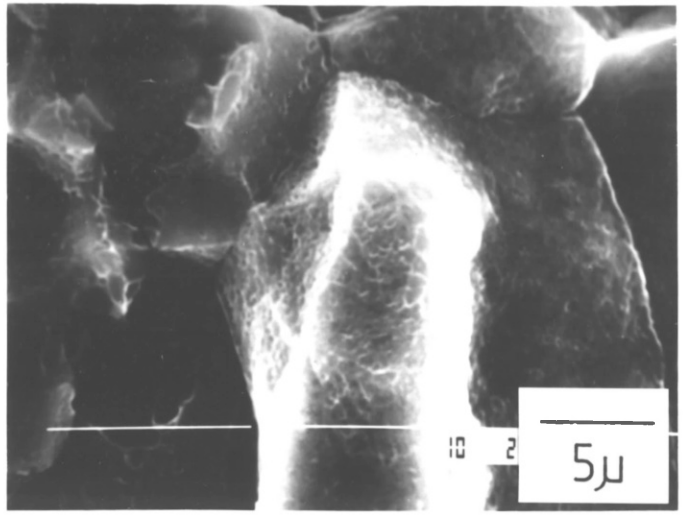
5μ

spreading has occurred indicating that void coalescence can offer a low energy path to match that at the boundaries. Individual crack extensions were small in this condition and it was not possible to distinguish between regions of slow and fast crack growth.

The fracture surface of the Al-Li-Mg-Cu alloy in the peak strength condition is shown in Figs. 7.19 and 7.20. Here again high angle boundary failure is dominant and void formation has occurred at precipitates formed on these sites but the plasticity associated with them is severely reduced.

In summary then, the grain boundary weakness found in both alloys is not the result of changes brought about by ageing. Overageing does offer an alternative failure path, but this requires an even lower fracture energy.

7.4 Impact Testing

The specimens used for this work were non standard and therefore results are not comparable with literature values.

Table 7.2 contains results for both alloys in the peak aged condition, together with the effect of stretching on the copper containing alloy. A figure for 2014 T6 is also included for comparison. Generally the trends here follow those for the COD results, although the impact resistance of 2014 T6 is significantly higher than that of Al-Li-Mg T6.

The values for the quaternary alloy are about half of those for the ternary and stretching appears to reduce the resistance to fracture even further, in agreement with previous results.

Fig. 7.21 illustrates the effects of heat treatment and extrusion conditions for the Al-Li-Mg alloy. Using this measure of toughness, the values increase in the order OA < PA < UA. Failure is therefore occurring by the transgranular mode in the UA condition rather than by intergranular splitting. The drop in toughness due to the onset of recrystallisation is greater here but then the test is measuring the energy for the entire fracture path. In the OA temper this factor again had little effect due to the ease of void nucleation and coalescence.

Alloy	T_1 (°C)	Impact Energy (Joules) T6	T82%	T84%
2014	450	32	-	-
Al-Li-Mg	450	22	-	-
Al-Li-Mg	400	9	-	-
Al-Li-Mg-Cu	440	9	10	7
Al-Li-Mg-Cu	400	10	8	9

Table 7.2 Impact Test Results

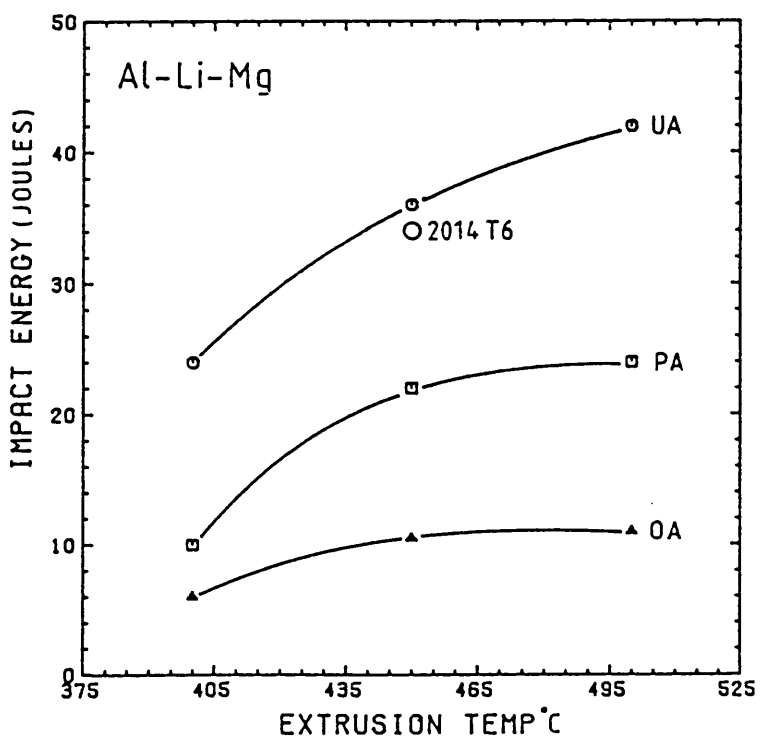

Fig. 7.21 Impact Test Results for Al-Li-Mg

Therefore the trends shown here do support those from the COD test apart from in the UA condition and impact testing could be used to establish basic behaviour in similar alloys.

7.5 Tensile Test Fractures

7.5.1 Longitudinal Tensile Tests

This section discusses the fracture surfaces of the longitudinal tensile tests used to give the property results reported in Chapter six. As with the fracture toughness tests, the effects of extrusion temperature and ageing time are reflected in the mode of failure.

Beginning with the influence of ageing time, the usual trend in heat treatable alloys is a transition from 45° failure in the underaged condition to 90° failure on overageing due to the formation of coarse precipitates. The important factors in these alloys will be the level of hardening and strain localisation due to δ' precipitation and the extent of Al_2MgLi formation. In the solution treated condition ductile failure occurred at 45° to the tensile axis on the plane of maximum shear stress. The surface consisted of large deep voids with considerable extension of the intervoid ligaments. However, some smooth extruded grain boundaries were in evidence confirming that the grain boundary weakness was present at this stage and therefore was not a product of ageing. Splitting down the extruded boundaries will be a high energy failure mode in this orientation as the maximum principal stress is parallel to the boundaries and the other stresses are negligible. Some necking is necessary to give the necessary triaxial stress system which is possible in the more ductile conditions.

Underageing still gave a 45° failure on the macroscopic scale but on closer examination the surface had a stepped appearance as shown in Fig. 7.22. This micrograph is for the Al-Li-Mg alloy but the other alloy gave the same features. The tensile axis here is from the bottom left to top right. On top of the 'steps' the structure was the result of fibrous fracture, consisting of areas of void formation, together with lateral grain boundary splitting, as

this extrusion was quite heavily recrystallised. The sides of the steps were the result of the brittle separation of extruded grain boundaries analagous to the pop-in effect seen in the UA COD tests. Failure is therefore due to a combination of these two mechanisms on the plane of maximum shear stress. If void nucleation and growth is taking place along this plane then with the onset of necking these regions could connect via the extruded boundaries giving rise to the observed structure. In the peak aged condition the same extrusion failed at 90° to the tensile axis by the mode shown in Fig. 7.23. Fracture has now occurred by a combination of ductile tearing and separation of recrystallised grain boundaries. This type of failure is promoted by the ease of void nucleation now, due to the higher yield stress and the presence of coarse Al_2MgLi precipitates. On prolonged ageing the equilibrium precipitate distribution again became the dominant factor and the fracture was covered in small cavities nucleated at these sites.

The copper containing alloy gave similar types of tensile failures with increasing ageing time but 90° failure occurred at lower levels of age hardening due to the higher levels of inclusions present and the higher proof stress.

Extrusion conditions influenced the type of failure through the level of recrystallisation produced in the extrudate. So far the structures considered have been recrystallised to a large extent, typical of high extrusion ratios and low temperatures. At low ratios and particularly at high temperatures almost fully recovered structures were produced and Fig. 7.24 shows the type of failure associated with them. Fracture took place at 45° to the tensile axis by a predominantly shear mechanism with very little evidence of void formation. The strong texture and strain localisation were responsible for this. The Al-Li-Mg-Cu alloy rarely exhibited this type of failure because of the difficulty in extrusion at high temperatures. However, in both alloys the transition from this type of structure to a highly recrystallised condition gave rise to mixed mode fracture surfaces containing regions of 45° shear and regions of 90° void and grain boundary failure. Although recrystallised structures failed in a partly brittle manner due to the grain boundary weakness, they had improved ductility over structures failing by the shear mode primarily due to the reduction in yield stress. This outlines the conflict between ductility and toughness data as

Tensile Test Failures

Fig. 7.22

Al-Li-Mg UA
Extrusion temp = 380°C
Extrusion ratio = 50:1

Fig. 7.23

Al-Li-Mg PA
Extrusion temp = 380°C
Extrusion ratio = 50:1

Fig. 7.24

Al-Li-Mg PA
Extrusion temp = 475°C
Extrusion ratio = 30:1

Fig. 7.25

Al-Li-Mg PA
Transverse direction

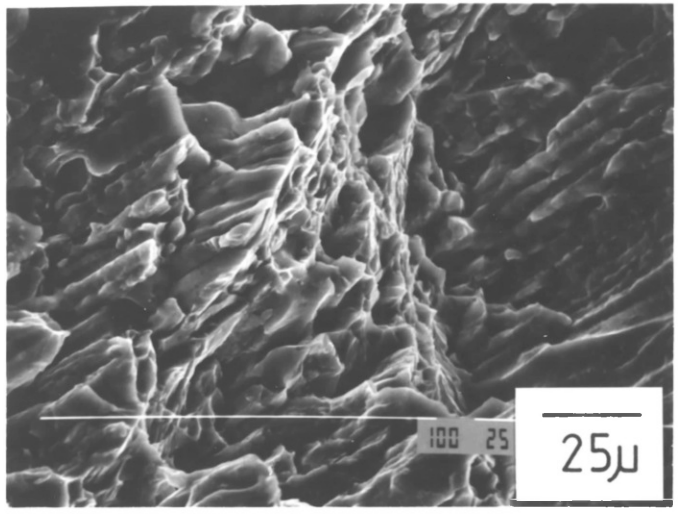
25µ

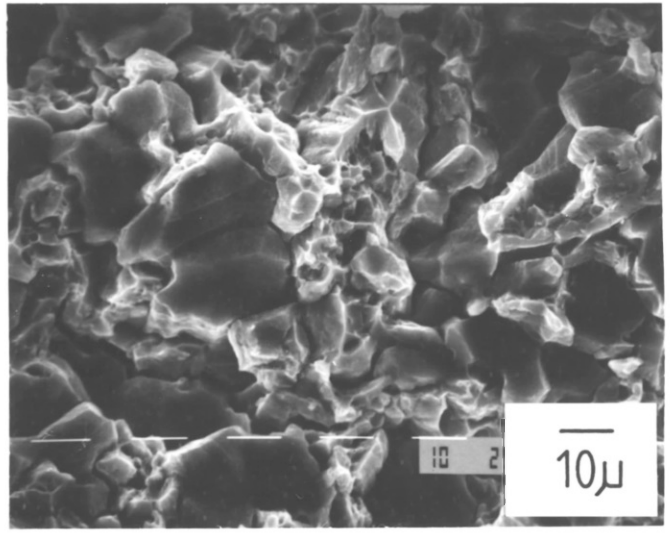
10µ

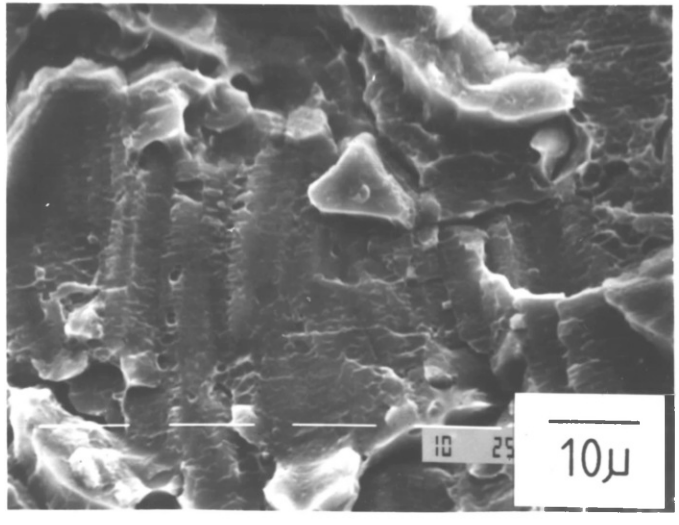
10µ

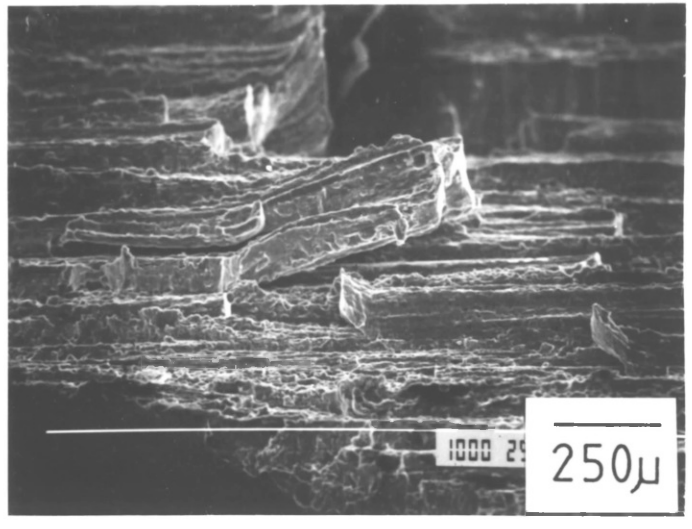
250µ

the highest L-T toughness results were obtained for unrecrystallised extrusions.

7.5.2 Transverse Tensile Tests

Using the 54 mm diameter Al-Li-Mg extrusion provided by Alcan, tensile specimens were produced in the transverse direction in order to investigate the behaviour of the extruded grain boundaries when directly stressed. The solution treated condition was the only one to show 45° shear failure and although this was generally ductile in appearance some smooth grain boundary areas were present. In the UA, PA and OA conditions the fractures were planar due to completely brittle separation of the extruded boundaries as shown in Fig. 7.25. Although the level of grain boundary precipitation increased with time, this caused little cavity formation and particles appeared to be pulled out of the grain boundaries with little or no plastic deformation. Even the OA condition, where splitting was superseded by void nucleation and coalescence in the DCB specimens, showed the same effect.

Specimens were also tested in the longitudinal direction for comparison of the tensile properties. These failures were by 45° shear due to the recovered nature of the bar. The results for the two directions are given in Table 7.3, where the most striking point is the considerable softening in the transverse direction. This is of the order of 150 MPa for each heat treatment and is presumably due to the lack of fibre and texture strengthening. Ductilities are very similar in the two orientations, apart from at the longest ageing time but the lower proof stress in the transverse direction gives artificially high values for this orientation.

Sample	PS (MPa)	UTS (MPa)	EL%
S Treated (T)	126	284	2 1
3 Hours (T)	247	359	5.4
3 Hours (L)	392	461	5.3
16 Hours (T)	275	387	4.1
16 Hours (L)	418	479	4.1
96 Hours (T)	303	382	6.2
96 Hours (L)	453	527	2.3

Table 7.3 Transverse Tensile Properties

7.6 Summary

1. In both alloys toughness decreases with increasing ageing time. The decrease to peak strength is due to the yield stress effect, together with strain localisation, whilst further embrittlement on overageing is due to excessive stable precipitate formation. PFZs had no noticeable effect on this trend.

2. Both alloys showed a propensity for intergranular fracture under a suitable stress system in all conditions and this was not due to structural changes at the boundaries caused by ageing. However, the effect was encountered more often in the heat treated condition due to the formation of stress concentrations associated with reduced matrix plasticity. When stressed directly across the grain boundaries, as in the DCB and transverse tensile tests, failures were almost completely intergranular.

3. COD tests in the L-T orientation gave transgranular failure except in the UA condition where crack propagation down the extruded grain boundaries occurred at right angles to the preferred direction. This was found in both alloys and was attributed to the grain boundary weakness and the high transgranular fracture energy in this temper. The rapid crack extension associated with this feature gave misleadingly low toughness results for this heat treatment.

4. The onset of static recrystallisation reduced the L-T toughness and impact energy of the ternary alloy and would have done so for the copper containing alloy if a wider extrusion range had been possible. This was due to the low energy fracture path presented by lateral recrystallised grain boundaries. As a result the toughest extrusion also possessed the highest proof stress.

5. The Al-Li-Mg alloy was tougher than the Al-Li-Mg-Cu in all conditions in all the tests used. This was attributed partly to the higher inclusion content of the latter but was mainly due to the higher proof stress, as the fracture surfaces were very similar. Any extra precipitation reactions occurring are

therefore not beneficial to this property. In the COD tests the Al-Li-Mg-Cu alloy showed limited plasticity and always gave a load drop, whereas the ternary alloy always gave a maximum load point (apart from in the UA temper).

6. The Al-Li-Mg alloy in the peak aged condition approached the strength and toughness levels of the 2014 T6 samples tested.

7. Cold stretching prior to ageing reduced the toughness of the Al-Li-Mg-Cu alloy. This would indicate that significant S phase precipitation, which can act as a slip dispersing agent, is not being promoted by this treatment.

8. The toughness in the longitudinal crack propagation direction, as measured by the DCB test, is independent of the level of recrystallisation and the subgrain size, as the fracture path is completely intergranular. Therefore toughness in this direction is independent of the level of substructural strengthening.

9. The DCB and impact tests gave the expected improvement in toughness for the UA temper because the splitting mode of failure did not occur in the Charpy test and in the DCB test it occurred in both the UA and PA conditions.

10. The DCB test using this specimen size and geometry is not suitable for more ductile alloys and only worked in this study because of the inherent grain boundary weakness found in these alloys.

11. The change in fracture mode in the tensile tests can be explained in terms of two trends:
    (i) Recovered to recrystallised structure; 45° - 90° failure, due to increased grain boundary fracture.
    (ii) UA to OA temper; 45° - 90° failure, due to increased void nucleation.

12. The transverse properties of the extrusions can be expected to show reduced strength and toughness.

CHAPTER EIGHT

THE EFFECT OF EXTRUSION AND HEAT TREATMENT VARIABLES ON CORROSION RESISTANCE

The experimental work in this section utilised accelerated corrosion tests established to predict long term outdoor behaviour of existing alloy systems. Strictly the test results for the lithium containing alloys ought to be correlated in a similar way, but understandably there is a lack of documented data on the corrosion of these alloys in natural environments. Clearly such a test program was not practical in this study due to the time scale involved and therefore caution should be exercised in comparison of these results with those for conventional systems.

Heat treatable aluminium alloys generally undergo corrosion by an intergranular mode where a narrow path is corroded out preferentially at the grain boundaries. The mechanism is electrochemical, depending on the presence of local cells at the boundaries caused by second phase particles and PFZs. Therefore, in these alloys a variation in corrosion susceptibility with ageing is to be expected. In this investigation a test was used to investigate general intergranular corrosion attack, along with a separate test for exfoliation susceptibility. The latter form of corrosion still takes place by an intergranular mode, but the extruded grain boundaries parallel to the metal surface are selectively attacked. With the generation of corrosion products at these sites the grains are forced apart to give lifting of the surface layers.

8.1 Intergranular Corrosion

8.1.1 Experimental

The susceptibility to intergranular corrosion was studied using the NAWLT (Nitric acid weight loss test) method described in ASTM G67-80. This is a simple test which consists of totally immersing the specimen in concentrated nitric acid (reagent grade) at 30°C for 24 hours. A measure of the level of attack is then obtained by determining the weight loss per unit area. The standard is aimed at 5000 series alloys, where the mode of attack is grain boundary precipitate dissolution but the method of attack should be similar for these two alloys.

Specimens were prepared from 50:1 extrusions to include process and heat treatment variables. They were cut to 100 mm lengths and the ends were ground to remove the worked layer. Prior to testing, the samples were immersed in a 30% nitric acid solution for five minutes to remove the oxide layer formed during heat treatment which would otherwise have given increased weight losses. Finally, the testpieces were dried and the initial dimensions and weight were recorded before immersion. Two testpieces were used for each data point. For some of the tests the surface layer was machined off to a depth of 1 mm and then ground on silicon carbide paper, again to remove any worked layer before testing.

8.1.2 Corrosion of the Extruded Surface

The variation in weight loss with ageing time for the samples with the extruded surface intact is shown in Fig. 8.1. The results here cover a range of process conditions for the Al-Li-Mg alloy, but all the quaternary results were obtained using a 425°C extrusion as the working limits were very narrow at this ratio. All the extrusions showed an increase in weight loss with longer ageing times even on overageing. This suggests that the prime factor in determining the corrosion susceptibility is the level of grain boundary precipitation. Although matrix precipitation of the stable phase is stimulated in these alloys at long ageing times, it does not appear to promote electrochemical homogeneity. Here again these alloys differ in their behaviour from 2000 and 7000 series alloys where corrosion susceptibility can be reduced by slight overageing as a result of the more even precipitate distribution within the grains[82].

It was somewhat surprising to find that the copper containing alloy showed improved corrosion resistance over the ternary alloy when the structural study indicated that grain boundary precipitation was made more extensive by this addition. To explain this conflict it is necessary to examine more closely the mode of attack at the extrudate surface. In both cases the extrusions were heat treated in air, producing a surface layer, approximately 25 μ deep, depleted in solute and hence low in precipitation, due to the oxidation reaction.

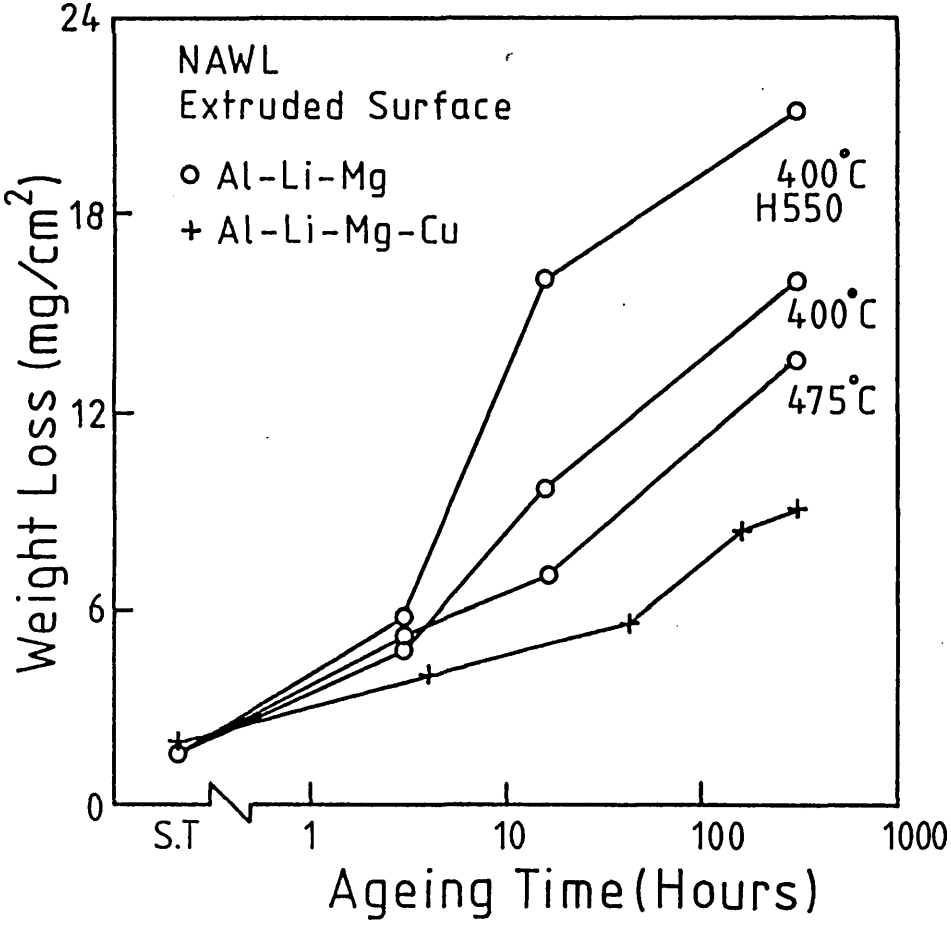

Fig 8.1

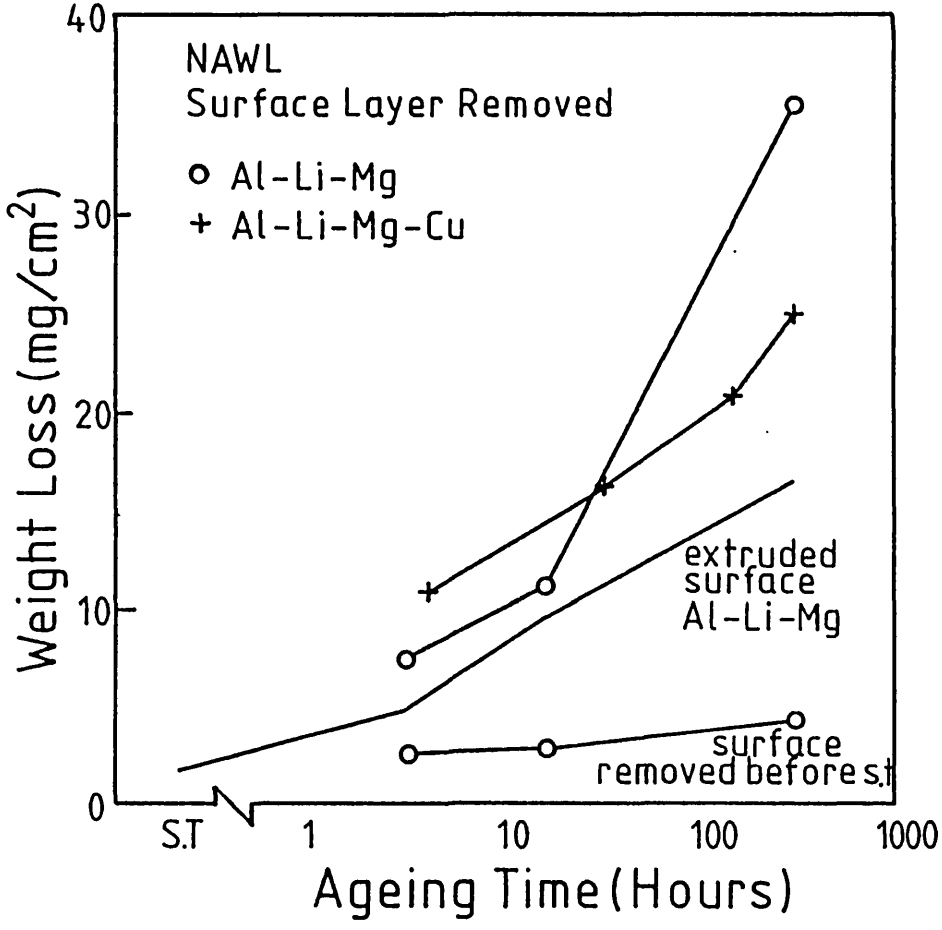

Fig 8.2

Variation in weight loss with the extrusion and heat treatment conditions (NAWLT results).

This zone rendered some passivity to the specimens and grain boundary attack here was slow compared to the more severe penetration at the exposed ends of the testpieces. There the surface layer remained raised above the core after the test. However, the contribution from these regions to the total weight loss was minimal when the entire specimen area was taken into account. Figs. 8.3 and 8.4 show the change in the appearance of the exposed testpieces with ageing time on the macroscopic scale. Both alloys were relatively free from attack in the solution treated condition and this was verified by SEM which revealed minor grain boundary attack with very little loss of material. In the underaged condition the ternary alloy testpieces showed surface markings at this scale associated with sites of preferential attack. In the PA and OA conditions these sites became progressively deeper and wider and the surface layer began to fall away, leaving the fibrous core exposed. In comparison the surface of the Al-Li-Mg-Cu testpieces remained intact until the overaged condition and even then the attack was not as severe. The nature of the attack on an Al-Li-Mg PA sample in an area where the surface remained intact can be seen in Fig. 8.5. There are two types of corrosion site here; grain boundaries and individual pits within the grains. Preferential attack at the boundaries has occurred as a series of overlapping pits presumably at precipitates, with the deepest pitting occurring at boundary triple points. The pitting within the grains was extensive and was quite deep in some cases. However, the problem with this type of test is that after 24 hours immersion it is difficult to detect the particles that originally caused such local attack. It is unlikely that sufficient stable precipitates have formed at this stage, particularly in the matrix, to account for this level of pitting but it may be due to the high density of broken down inclusion particles in this region or possibly it is occurring at δ' - Al_3Zr composite precipitates with their associated PFZs. In a similar temper the surface of the copper containing alloy contained the same features but exhibited less pitting within the grains.

The weight loss due to the above form of attack is low as material is being dissolved rather than being removed as entire grains. Fig. 8.6 shows the nature of the attack in the same sample

Fig. 8.3

Exposed NAWLT Specimens

Al-Li-Mg

Fig. 8.4

Exposed NAWLT Specimens

Al-Li-Mg-Cu

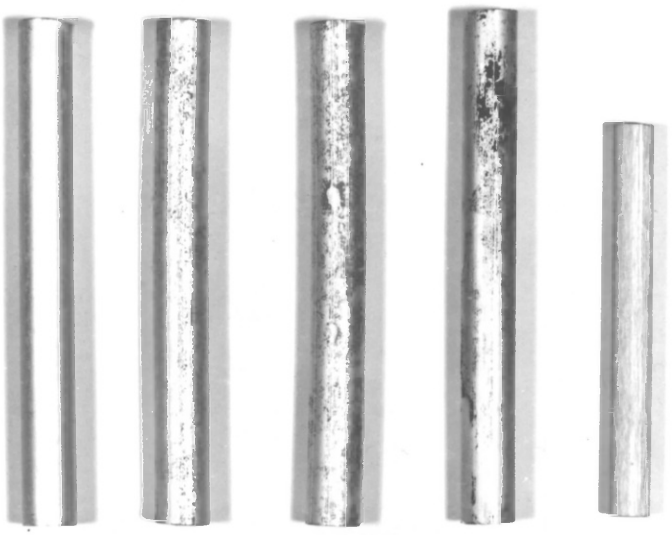

ST UA PA OA PA

AL-LI-MG

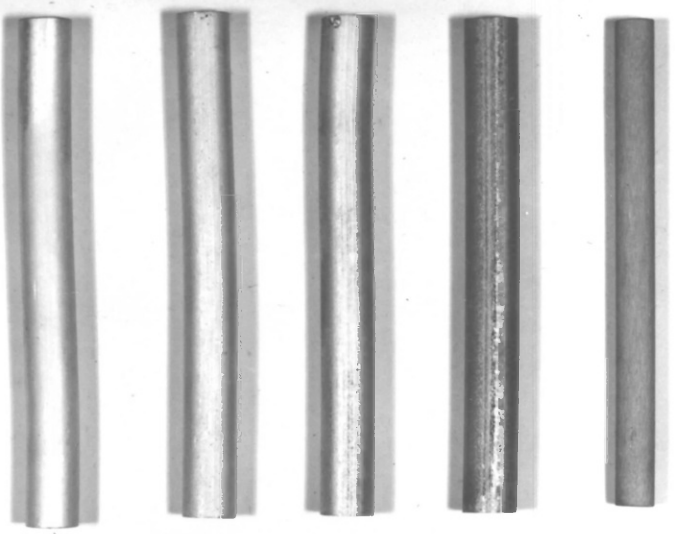

ST UA PA OA PA

AL-LI-MG-CU

as Fig. 8.5, but this time in a region where corrosion has taken place below the surface layer. This transverse section indicates how the surface zone, low in precipitation, has been penetrated and how the fine recrystallised structure beneath has come under attack. The corrosion front has travelled laterally, undercutting the surface, as well as towards the centre of the extrusion. As the growth of such pits continues a stage is reached where the surface material can no longer be supported and it falls away. Similar areas will also coalesce to give the removal of large portions of the surface and correspondingly high weight losses.

The reason why this mechanism did not take place until later ageing times for the Al-Li-Mg-Cu specimens and even then to a lesser extent, is connected with the difference in the surface recrystallised grain sizes between the two alloys. Whereas the surface of the ternary alloy was composed of a band of equiaxed recrystallised grains of the order of 10 μ in diameter, those in the copper alloy were roughly 150 μ in diameter at the surface and 70 μ thick, often in a layer 2-3 grains deep. Such grains therefore extended well past the solute depleted layer. Thus, assuming the rates of attack along high angle boundaries are similar in the two cases, then it will take longer for corrosion to reach a lateral grain boundary path in the Al-Li-Mg-Cu alloy to allow undercutting of the surface. In the ternary alloy this can occur as soon as the solute depleted layer is penetrated due to the high density of grain boundaries. Once undercutting has been initiated in the quaternary the rate of weight loss ought to be higher due to the large bulk of each grain but this situation was not reached in the 24 hour test period, except in the overaged temper.

The effect of processing conditions on the susceptibility to corrosion of the ternary is quite marked, producing differences greater than that between the two alloys and this is also a surface grain size effect. On raising the extrusion temperature from 400 to 475°C the surface grain size was reduced slightly from 10 to 6 μ along with the level of weight loss. The extrusion given the alternative high temperature homogenisation had an increased suface grain size of 20 μ and this gave the upper trace in Fig. 8.1. Thus, the level of corrosion attack is greater as the surface grain size is

Fig. 8.5

Exposed NAWLT specimen
Al-Li-Mg PA
Extruded Surface

Fig. 8.6

Exposed NAWLT specimen
Al-Li-Mg PA
Transverse section
Kellars Reagent

Fig. 8.7

End of exposed Exco specimen
Al-Li-Mg-Cu PA
longitudinal section
Kellars reagent

Fig. 8.8

Surface of exposed Exco specimen
Al-Li-Mg-Cu PA
longitudinal section
Kellars reagent

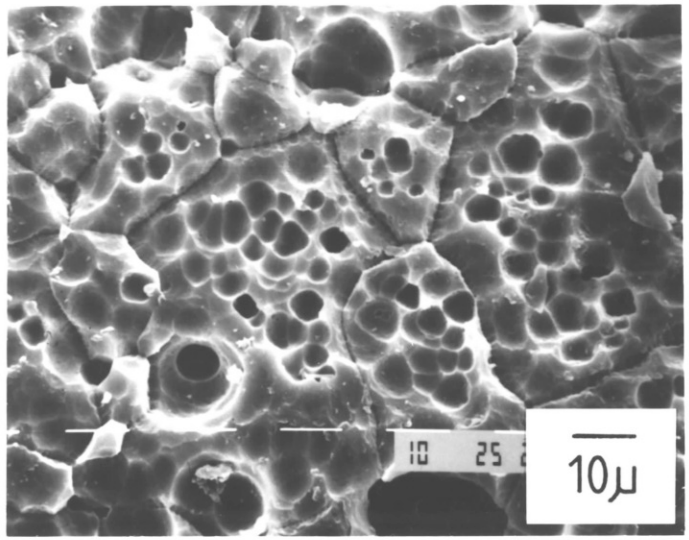
10μ

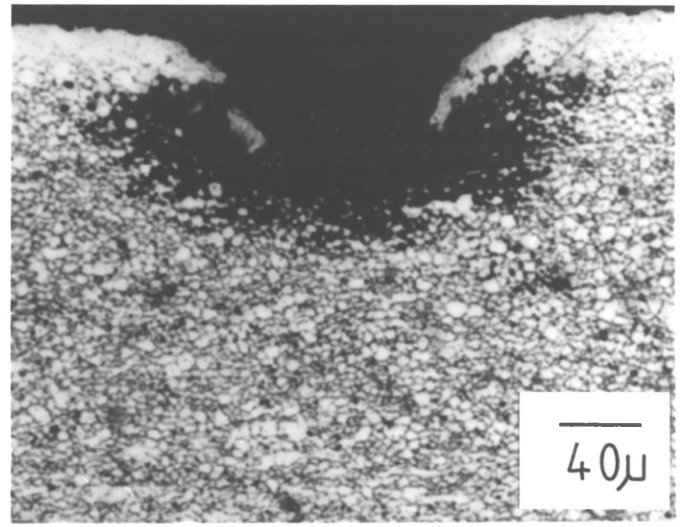
40μ

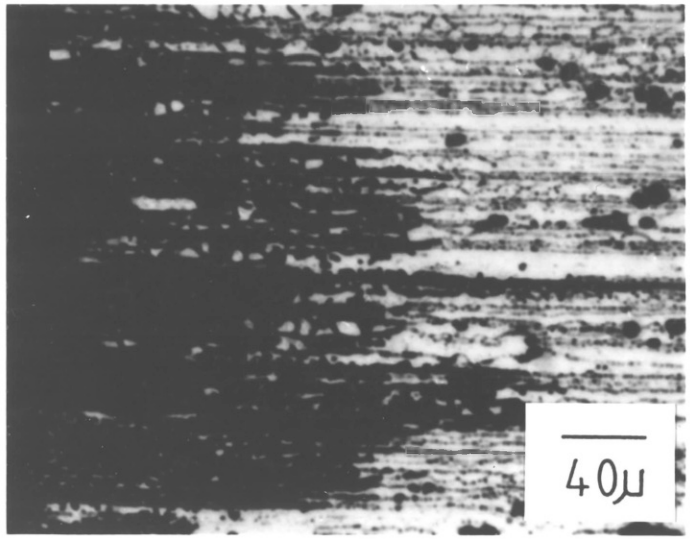
40μ

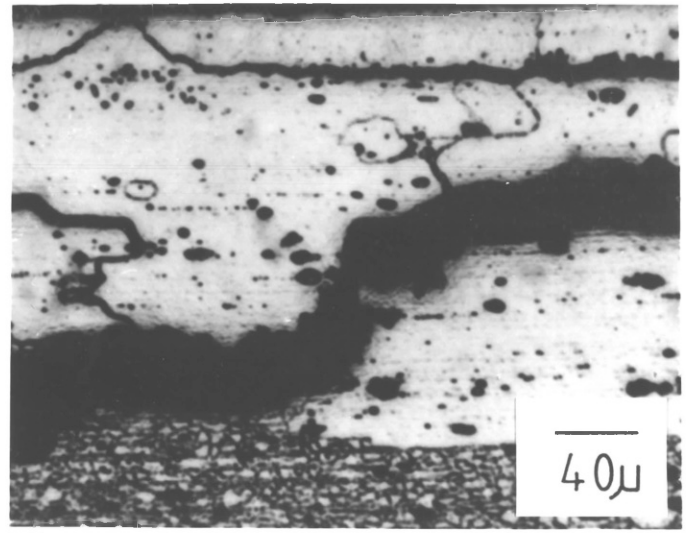
40μ

raised. All these structures were much finer than those for the copper alloy extrusion and were generally equiaxed, extending inwards in a band until the fibrous core structure was reached. Therefore, undercutting could still occur easily with the coarser grain sizes, but now the weight loss increased with the size of the grains being removed. This effect only became prominent in the peak aged condition when corrosion could advance a sufficient distance down the boundaries.

8.1.3 Extrudate Core Attack

In order to compare the two alloys in terms of the effects of ageing without the complication of the surface structures, a series of tests were run where the specimen surface was machined away to a depth of 1 mm. The results are presented in Fig. 8.2 along with the Al-Li-Mg 400°C extrusion 'surface' values for comparison. Now the copper containing alloy showed enhanced attack up to the peak strength temper, as expected from the increased boundary precipitation but the ternary composition still gave higher losses on overageing. It is possible that in the Al-Li-Mg-Cu alloy the heavier level of matrix precipitation at long ageing times tended to give reduced electrochemical heterogeneity. In addition, the sparse S phase distribution may have been beneficial in this respect. Compared with the results for the 'extruded surface specimens' the weight losses are higher due to the action of the protective surface layer. The macroscopic appearance of this form of attack is shown for peak aged samples on the right of Figs. 8.3 and 8.4. These are darkened and show uniform attack.

The lower data line in Fig. 8.2 is made up of results from tests where the specimens were heat treated after the surface layer had been removed, giving a solute depleted layer again. Here the level of attack is much lower than for the extruded surface and shows little increase with ageing time. This suggests that the surface layer is very stable here with no corrosion path through it. Consequently, the extruded surface must contain defects, possibly due to the high concentration of broken up inclusion particles in this region, that permit corrosion to penetrate this layer.

8.1.4 Variation in the Rate of Attack with Time

To further compare the behaviour of the two alloys, tests were run whereby samples were removed at intervals to follow the change in the rate of weight loss during the 24 hour test period. Peak aged samples were used. The results are shown in Fig. 8.9 for samples with an extruded surface and in Fig. 8.10 for those with the surface layer removed. Again the 400°C Al-Li-Mg extrusion was used. When the solute depleted layer was present the alloys initially showed similar attack rates to each other and this continued up to approximately 9 hours immersion time. After this period the copper free composition underwent accelerated attack and the difference between the two alloys increased as the test progressed to give the final trend seen in the full NAWLT results. Microscopy showed that the divergence of the two traces after nine hours corresponded to the penetration of the surface layer in the ternary alloy, so that at this point the loss of large areas of surface material began to occur. Paths across the solute depleted layer appeared to be in the vicinity of surface pores, probably formed by gas evolution. However, such features were observed in SEM on the surfaces of both alloys and the solute depleted depths were almost identical, indicating that the presence of such voids was not the causal factor. The surface grain size is still the important feature here. Pore sizes were small, although they penetrated the solute depleted layer, when compared with the recrystallised grain size in the copper containing alloy, and hence they merely extended the corrosion path length slightly. This type of attack was observed in metallographic sections but it was never advanced enough to loosen entire grains in this alloy, whereas in the ternary alloy it provided an easy path to the fine recrystallised grains beneath the surface.

When the surface layer was removed, (Fig. 8.10), both alloys underwent a more rapid rate of attack. Initially the copper containing samples showed higher weight losses but after 12 hours the rates of attack were similar and this alloy gave a consistently higher level of attack. Again this behaviour is directly related to the precipitate distribution produced by ageing as the mechanism of corrosion is grain boundary attack and subsequent grain removal from an early stage.

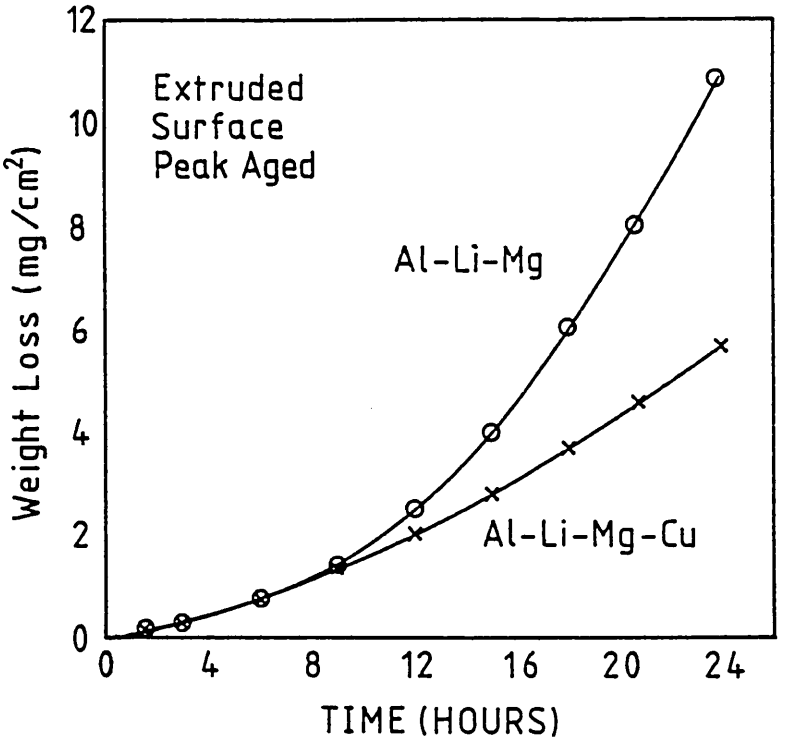

Fig 8.9

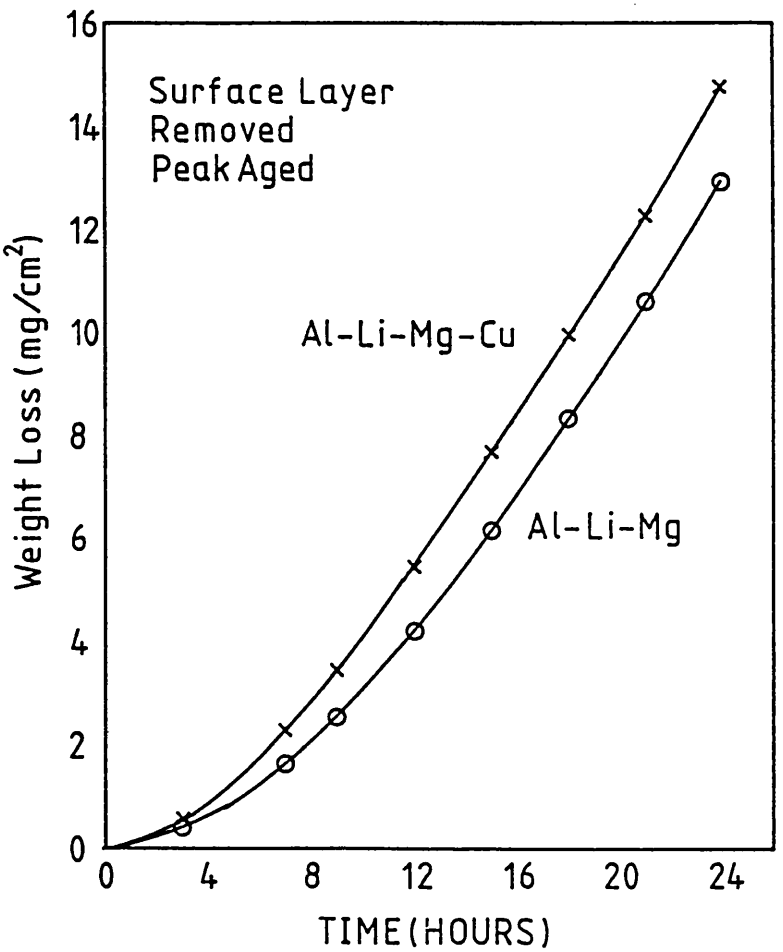

Fig 8.10

Variations in weight loss with exposure time (NAWLT).

8.2 Exfoliation Corrosion

8.2.1 Experimental

Exfoliation corrosion testing was performed according to ASTM G34-79, the EXCO test, which is a standard method for measuring the susceptibility of 2000 and 7000 series alloys to this form of attack. Samples were continuously immersed in a solution containing 4M sodium chloride, 0.5 M potassium nitrate and 0.1 M nitric acid at 25°C for a test period of 96 hours. The level of attack was then graded on a visual scale by comparison with standard photographs. The alloys were tested separately as the standard dictates that copper bearing alloys should not be placed in the same environment as copper free samples.

Round bar extrusions are unsuitable for this test as the exfoliated flakes tend to fall away from the specimen as soon as they are produced. For this reason extruded strip, 30 x 5 mm in section, was used and this was processed at 400°C. Specimens were made by cutting out 90 mm lengths but half of the sample was milled to a depth of 1 mm on one face to give exposure to the core structure as well as the extruded surface. In addition, the sides of the specimens were also machined away to remove any protective surface layer. Finally the back of the testpieces were coated in laquer to prevent attack at this site, providing a stable base for any corrosion products.

At the end of the test period the samples were removed and graded whilst still wet before cleaning in concentrated nitric acid and washing.

8.2.2. Variations with Ageing Time

Process variables were not included in this study as the extrusion limits were very narrow for the strip section used. The extruded structures were partially recrystallised in the centre with a recrystallised surface layer. Again the grain sizes were much coarser in this region for the Al-Li-Mg-Cu extrudate. Thus the ageing time was the only variable and the heat treatments established in

Chapter six were utilised. Solution treating was performed in air, giving a solute depleted zone at the extruded surface again.

The test specimens after exposure and cleaning are shown in Figs 8.11 and 8.12 for the copper free and copper containing alloys respectively. The Exco performance ratings made immediately after the test are listed in Table 8.1.

Alloy	ST	UA	PA	OA
Surface Al-Li-Mg	N	N	N	N
Core	N	N	N	N
Surface Al-Li-Mg-Cu	N	N	EA	EB
Core	P	EA	EB	EC

N	No appreciable attack
P	Pitting
EA-ED	Exfoliation

Table 8.1 Exco Test Ratings
96 Hour Exposure

Clearly, the Al-Li-Mg alloy was resistant to this form of attack in all tempers, regardless of the type of surface presented to the environment. Other workers have also reported that Al-Li-Mg alloys in sheet form show good resistance[24, 51]. However, Evancho[51] also used the more severe SWAAT test and did encounter some mild exfoliation at worked surfaces. Some reaction was observed here during the test, producing gas evolution and this became increasingly vigorous with longer ageing times. This attack was very general in nature and did not lead to any signs of exfoliation. Longitudinal sections revealed that attack had occurred along grain boundares at the specimen ends but this was not very extensive. As extruded surfaces were virtually unattacked due to the low precipitate density and these were slightly undercut by reaction

Fig. 8.11 Exposed Al-Li-Mg Exco Specimens

Extruded Surface

ST UA PA OA

Surface Layer Removed

Fig. 8.12 Exposed Al-Li-Mg-Cu Exco Specimens

Extruded Surface

ST UA PA OA

Surface Layer Removed

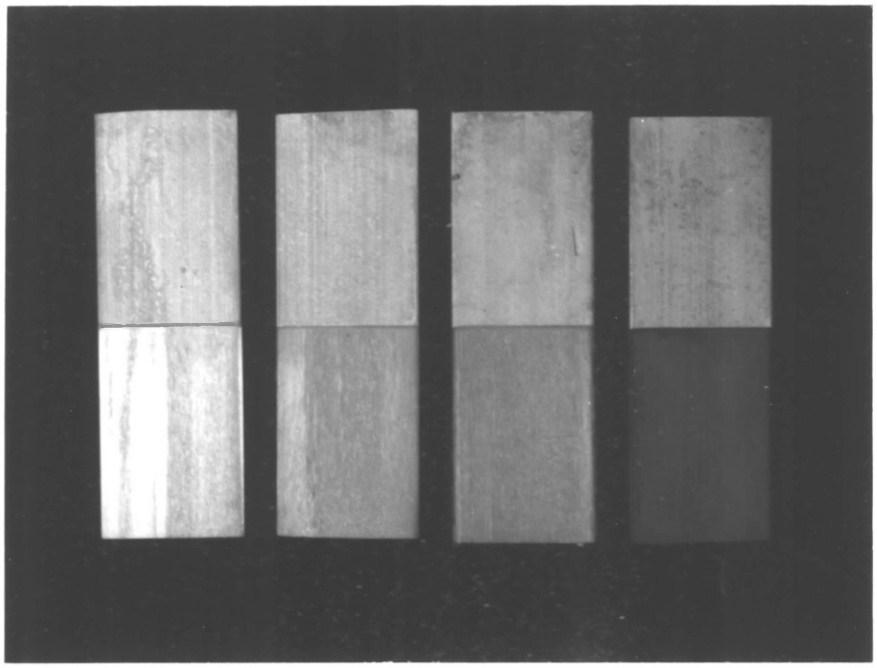

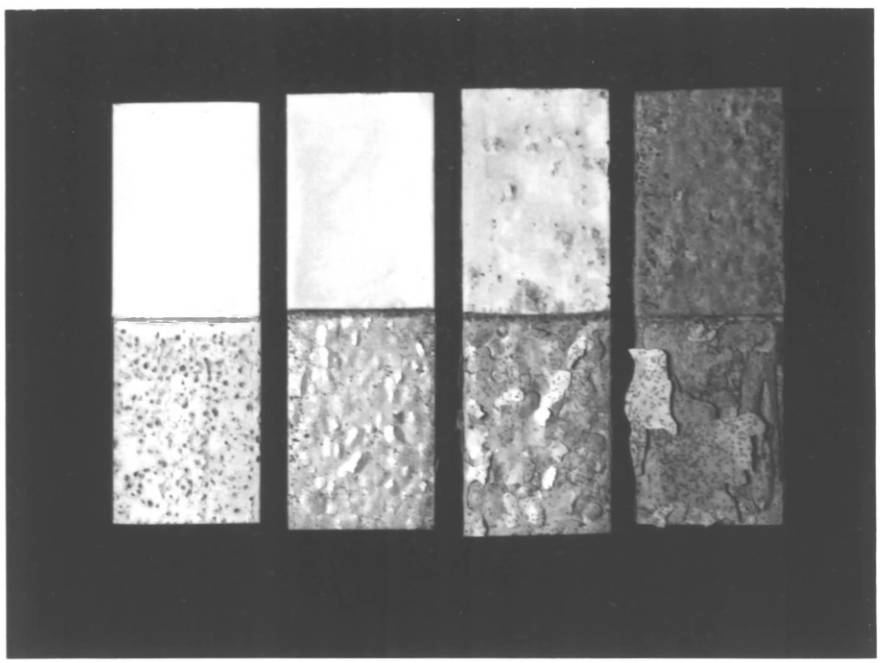

at the specimen sides and edges. In the peak aged temper, loss of grains can be seen in Fig. 8.11, but this only occurred at the specimen corners and is not strictly exfoliation.

The Al-Li-Mg-Cu alloy exhibited considerably greater susceptibility to this form of corrosion and this increased with the ageing time, as evidenced in Fig. 8.12. Now exposed extruded boundaries were severely attacked deep into the specimen as shown in Fig. 8.7. Better resistance was shown by the extruded surfaces but even these exfoliated in the PA and OA tempers due to penetration from the sides. Here the flakes of exfoliated material were produced by lifting of the recrystallised surface layer, as shown in Fig. 8.8 for the PA sample. Once the surface layer was machined away exfoliation occurred in all the aged tempers as attack could now take place directly into the specimen surface. Severe pitting was produced in the solution treated testpiece but this could not be classified as exfoliation.

The onset of exfoliation in this alloy can partly be attributed to the increase in the level of high angle boundary precipitation promoting attack between the extruded grains. Aluminium alloys containing copper are generally regarded as being susceptible to this form of attack due to copper containing precipitate formation but resistance can usually be imparted by slight overageing to promote precipitation within the grains. From these results this technique would appear not to work for this alloy and overageing reduces the resistance even further. The increased level of attack over the ternary alloy in the solution treated condition does suggest that the presence of copper has another effect. It is possible that the increased inclusion content it causes is responsible for this behaviour, or it may be due to segregation of copper in solution setting up an electrochemical cell. Miller et al[24] also reported the onset of exfoliation susceptibility when copper additions of the order of 1% were made to Al-Li-Mg alloys and their results for the DTDXXXA alloy, in sheet form, showed similar performances to this alloy as the ageing time was increased. Since their alloy was adequately homogenised the detrimental effect of inclusion particles raised above can be discounted.

8.3 Summary

1. Corrosion attack in the NAWL test occurred by a predominantly intergranular mode in these alloys with the level of susceptibility increasing with the ageing time used.

2. The intergranular corrosion of these alloys in the extruded form is strongly influenced by the structure at the wrought surface. This is due to two features at this location; the solute depleted zone and the fully recrystallised layer.

3. The ternary alloy showed higher weight losses compared to the copper containing alloy when extruded surfaces were exposed to attack. This was due to corrosion occurring beneath the surface, made possible by the fine recrystallised grain size, which led to the loss of surface material. The quaternary alloy was more resistant to this form of attack because of the much coarser surface grain structure.

4. Variations in the extrusion process conditions influenced the level of attack at wrought surfaces through their effect on the recrystallised grain size. Slight increases in the grain size here raised the weight losses because of the larger mass associated with each grain lost.

5. When the surface layer was removed, allowing more uniform attack, the addition of copper increased the level of corrosion, apart from at the longest ageing times when the ternary alloy became more susceptible.

6. The exfoliation resistance of the Al-Li-Mg alloy as determined by the Exco test was very good in all tempers. This was the case for wrought and machined surfaces.

7. The addition of copper to the ternary alloy induced susceptibility to exfoliation in all age hardened conditions and the level of this attack increased with ageing time.

8. The Al-Li-Mg-Cu alloy also showed minor pitting in the solution treated condition during the Exco test, indicating that the decrease in the resistance tc this form of attack, caused by the copper addition, is not simply due to its influence on grain boundary precipitation during ageing.

9. Solution treatment of these alloys in air produces a solute depleted layer at the surface and this can impart some corrosion resistance to the product.

CHAPTER NINE

A FURTHER INVESTIGATION INTO THE EFFECTS OF COPPER ADDITIONS TO THE Al-Li-Mg ALLOY

The results obtained using DC cast material in the preceeding chapters would indicate that whilst the addition of 1% copper increases the strength of the base alloy, it is detrimental to ductility, toughness and corrosion resistance. This Chapter presents the results of an experimental program carried out to further study the influence of this element, particularly at lower concentrations. Copper additions to the ternary alloy were made, ranging from 0.1 to 2 wt.% and two zirconium free compositions were also included. The properties investigated included tensile properties, toughness, corrosion resistance and stress corrosion resistance.

9.1 Experimental

Eight alloys were prepared by the British Alcan Aluminium Company in the form of small scale chill cast blocks and the compositions of these are given in Table 9.1, together with hydrogen analyses. All material was given a standard homogenisation treatment of 16 hours at 500°C followed by a forced air cool. From each block two billets were machined for extrusion and rolling which were carried out using the facilities at the British Alcan Aluminium Research Centre at Chalfont Park. The extrusion billets were 66 mm in diameter and 195 mm long. An extrusion ratio of approximately 7:1 was used to give an extrudate diameter of 25.4 mm. Billets were given a 30 minute preheat at 480°C in an air circulating furnace before extrusion at a nominal ram speed of 2 mm/s with a container temperature of 460°C. However, the delay time before extrusion was such that the initial temperature would have been considerably lower than this. The press capacity was only 300 tons and due to the high frictional contribution in this set up all the billets stuck initially, but were able to be extruded when a sufficient temperature rise was generated. All extrusions were allowed to air cool. 30 cm was discarded from either end of the extrudate to remove any back end defect or underdeveloped structure. The extruded rods were used for all the property determinations except corrosion testing where rolled sheet was used.

The sizes of the rolling blocks varied slightly but they were all approximately 40 mm in thickness. They were given a 1 hour

	Weight Percent									
Alloy	Li	Mg	Cu	Zr	Fe	Si	Cr	Ti	Na	H_2ppm
RGF	2.49	3.72	L .01	L.01	.06	.04	L.01	.004	L.001	0.74
RGG	2.31	3.74	L .01	.14	.06	.04	L.01	.003	L.001	0.44
RGH	2.47	3.98	.10	.10	.07	.04	L.01	.002	L.001	0.62
RGL	2.52	3.99	.25	.08	.07	.04	L.01	.004	L.001	0.56
RGK	2.36	3.81	.44	.14	.07	.04	L.01	.005	L.001	0.36
RGN	2.44	3.63	.86	.14	.07	.03	L.01	.019	L.001	0.49
RGO	2.46	3.95	2.02	.16	.09	.04	L.01	.002	L.001	0.36
RGP	2.54	3.84	1.90	L.01	.07	.04	L.01	.002	L.001	0.28

Table 9.1 Chill Cast Alloy Compositions

preheat in an air circulating furnace at 500°C before rolling for a series of 4 passes with a reduction of 0.6 to 1.2 mm per pass. In between every four passes the rolled product was given a 15 minute reheat. The final sheet thickness was 2.5 mm.

Properties were evaluated using tests described in previous chapters. All the extruded material used for specimens was given a 2% cold stretch prior to ageing. Toughness was measured using the DCB test and corrosion resistance was assessed by the NAWL test. Specimens for the latter were stamped out of sheet to the dimensions 100 x 25 mm and the sheared surfaces were dressed with a file. Stress corrosion testing, which was not performed on the DC cast alloys, was carried out using the C-ring test (ASTM G38-79). This is an alternate immersion test in a 3.5% NaCl solution.

9.2 Hot Working

All the alloys were extruded successfully after initially sticking, giving an acceptable surface finish. The surface of the rolled sheet was poor as there was insufficient material available to optimise the rolling conditions. Apart from alloys RGH, RGL and RGK (0.1, 0.25, 0.44%Cu) which gave minor surface crazing, all the others exhibited very severe transverse cracking in the early passes. As a result, most of the sheet contained subsurface cracks with entrapped oxide layers. At the higher copper levels the onset of cracking was probably due to melting of the coarse S-type phases, indicating too high a rolling temperature. The copper free alloy also cracked but this may have been simply due to the low ductility of this alloy during hot working which was reported in the hot torsion ductility tests (section 5.5).

9.3 Grain Structures

All the extruded structures of the Zr containing alloys were partially recrystallised after extrusion but this was not extensive due to the low extrusion ratio and high temperature used. Increasing the level of the copper addition had no specific effect on the grain

structure in the core, but it did lead to coarsening of the recrystallised periphery. These structures were stable during solution treatment.

In the zirconium free alloys the structures were completely recrystallised after extrusion. They underwent further grain growth during heat treatment to give final grain sizes of the order of 100 μ, indicating the importance of zirconium as a recrystallisation inhibitor in these alloys.

The coarse S type particles seen in the DC cast quaternary alloy were also present in the copper bearing alloys here. Their size and density increased with the copper content and at the 2% level stringers up to 50 μ long were present. However, little of this phase was in evidence at low copper levels below 0.44%.

The rolled sheet had similar structures to the extrusions which were all partially recrystallised, except for the two zirconium free alloys which were again fully recrystallised. The levels of recrystallisation were generally higher though, ranging from 50 to 80% recrystallised, due to the high reductions given. At the surface the solute depleted layer was deeper than that found in the extrusions because of the several reheats used during processing. These structures were stable on heat treatment.

9.4 Ageing Response and Tensile Properties

9.4.1 Solution Treated Properties

A standard solution treatment of one hour at 510°C followed by water quenching was used for all the alloys. This temperature was adopted because it was the highest attainable in the high copper alloys without causing second phase liquation. Fig. 9.1 shows the change in the hardness of the solution treated extrusions with varying copper content. Two lines have been drawn for the zirconium containing and zirconium free alloys. Both of these showed an increase in hardness with copper to approximately the same extent but the recrystallised structures were roughly 10 Hv softer due to the lack of any retained hot worked structure. The addition of 2% copper to the base alloy raised the hardness by 13 Hv through solid solution strengthening. A linear fit to these results gave a rate of hardening of 6.8 Hv/wt.%

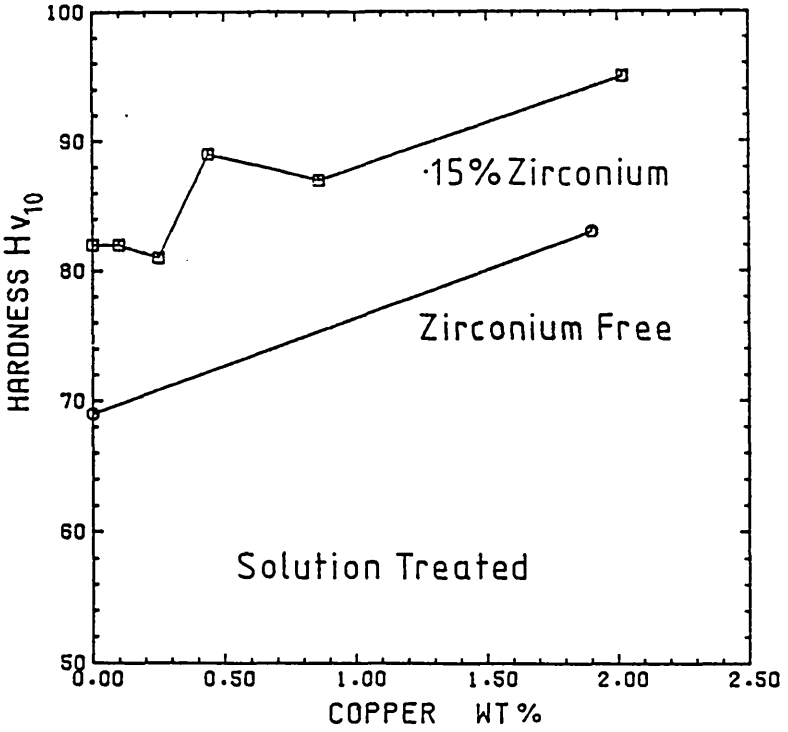

Fig 9.1 Effect of copper on solution treated hardness.

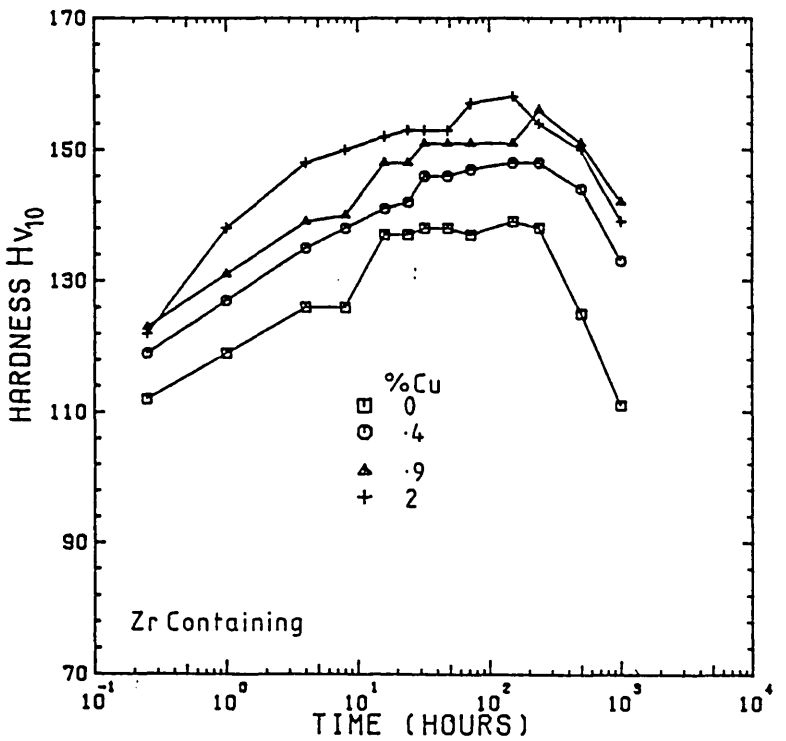

Fig 9.2 Effect of copper on the ageing response.

copper. At low copper levels there was no detectable hardness increase up to 0.25% simply due to the ineffectiveness of such low concentrations at solution strengthening.

9.4.2 Ageing Curves

The response to ageing at 170°C, after solution treatment, was followed for all the alloys using the hardness test. Material for this work was taken from the extrusions but it was not stretched prior to ageing.

The effect of copper on the form of the hardness v time curve is demonstrated in Fig. 9.2 for the zirconium containing alloys. The obvious trend here is the increase in peak hardness with increasing copper content. At the 2% Cu level this was raised by roughly 20 Hv over the base alloy but from the previous section it can be seen that half of this increase was present in the solution treated condition. However, copper is still producing a further strength increment during the precipitation treatment, as was observed for the DC cast alloys. All the curves are of a similar shape, with a broad peak, where the hardness slowly increases with time. Overageing began after similar times in all cases but the rate of hardness loss was highest for the Al-Li-Mg base alloy, i.e. the reverse of the trend seen in the DC cast material

Ageing curves for the zirconium free alloys, RGF and RGP, are presented in Fig. 9.3 along with those for the corresponding Zr containing compositions. The curves for the recrystallised extrusions start off lower than the others due to the lack of substructural strengthening but instead of showing a plateau in the region of peak hardness, they exhibit a continuous rise in hardness. In the case of the copper free alloy the final hardness was higher than that for the corresponding Zr containing composition. The addition of 2% Cu to these alloys had a similar effect in both cases. Although all the alloys began to overage after similar times, those containing Zr showed a more rapid property loss. This behaviour is probably due to the lack of suitable sites for Al_2MgLi formation in the recrystallised alloys as the grain boundary area is reduced. Consequently, less solute is lost

to this phase. The flat peaks seen in the Zr containing alloys are therefore probably due to a combination of δ' growth balancing lithium loss to stable precipitates and the increased rate of over-ageing is consistent with rapid Al_2MgLi formation. Another possible influence on this behaviour is the formation of the composite δ' - Al_3Zr precipitates. In an earlier chapter, these were reported to form δ' PFZs and will therefore contribute to the softening of the matrix.

The hardness - time plots were used to establish subsequent heat treatment practices to give peak strength and 80% UA tempers. These times are listed in Table 9.2 and were used for the remaining work in this chapter.

	Time (Hours)	
Alloy	80% UA	PA
RGF	8	64
RGG	3	16
RGH	6	32
RGL	6	32
RGK	3	32
RGN	4	32
RGO	2	16
RGP	2	16

Table 9.2 Heat Treatment Schedules

9.4.3 Peak-Aged Tensile Properties

The longitudinal tensile properties in the peak aged condition are shown for the eight alloys in Fig. 9.4. Separate lines have again been drawn for the Zr free compositions. The destruction of the hot worked structure by static recrystallisation in these two alloys gave reduced strengths. The difference in proof stress with the addition of 2% Cu was roughly 20MPa. However, these results are slightly

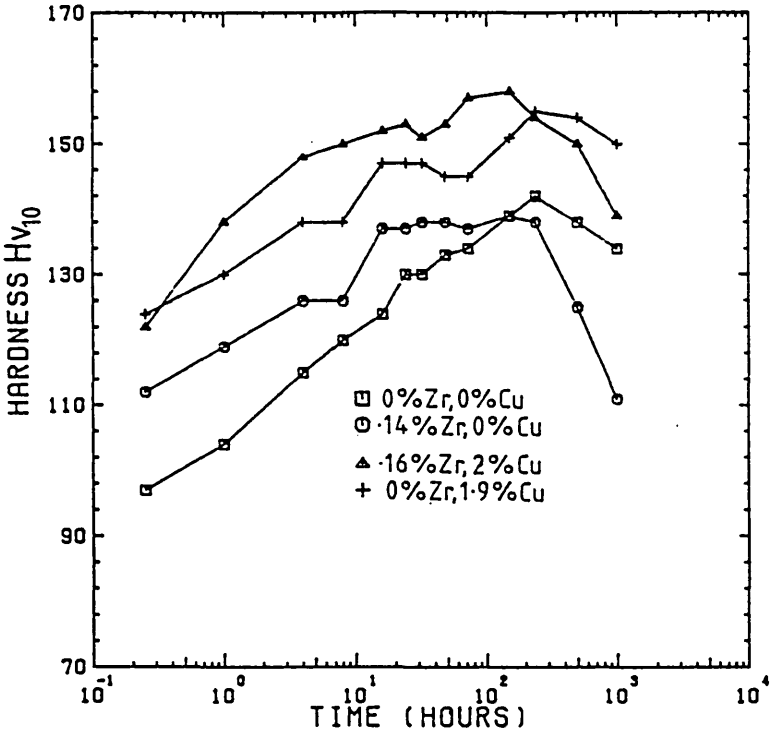

Fig 9.3 Effect of zirconium on the ageing response.

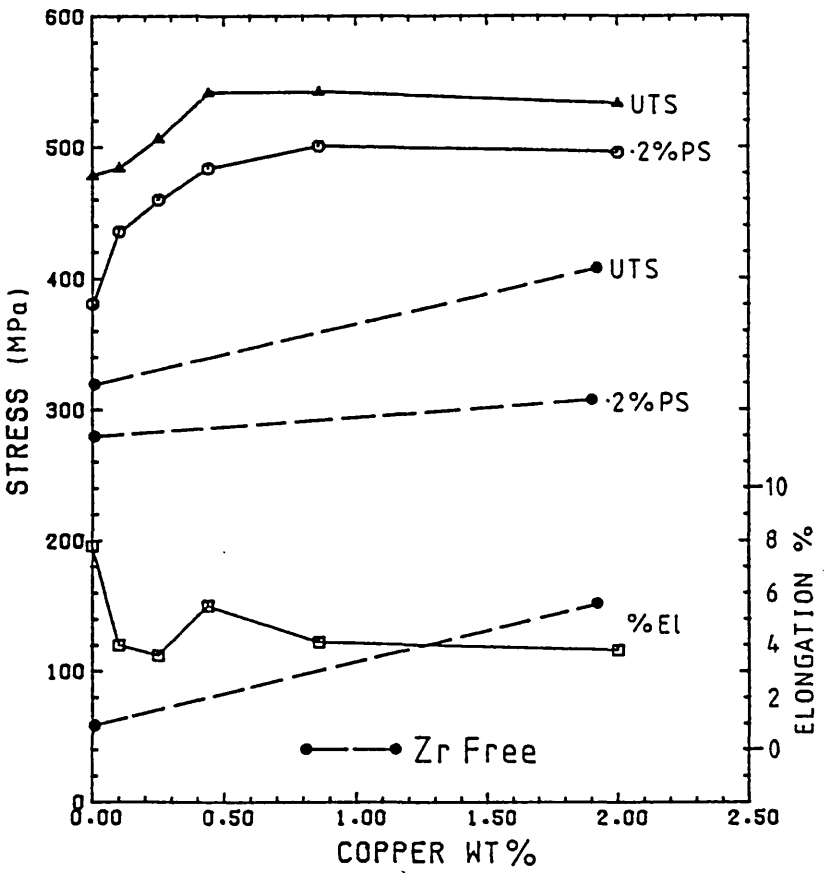

Fig 9.4 Effect of copper on the peak aged tensile properties.

misleading, particularly for the 2% Cu alloy, because in the preliminary hardness investigation with times up to 100 hours, their full hardening potential was not realised. This led to the improved ductility at the high copper level. The copper free alloy was given a longer ageing treatment and strengthening was probably closer to the maximum possible. Although the proof stress was lower here than for the corresponding Zr containing alloy, the elongation was also reduced due to the brittle separation of favourably orientated grain boundaries.

Turning now to the effects of copper additions to the Al-Li-Mg-Zr base alloy, clearly the proof stress and UTS are raised as the copper concentration is increased. Strengthening is most rapid at the lower levels of addition, with the first 0.1% giving a proof stress increment of 60 MPa. At 0.9% Cu the trend begins to level off so that increasing the concentration to 2% does not produce any further effect. There is no marked trend in the elongation results, apart from the decrease as soon as copper is added. Increasing the level of addition did not produce any further reduction and all the values were between 3 - 4%,apart from at 0.44% Cu but this was an effect carried over from the solution treated condition.

In search for a mechanism to explain the influence of copper on the proof stress,solid solution strengthening can be disregarded. Although it may make a contribution at the higher copper levels, it would be ineffective at concentrations of 0.1 and 0.25% where the most rapid hardening was produced. This is confirmed by the solution treated hardness results in section 9.4.1 where no hardening was observed until the 0.44% level. Copper is therefore affecting the precipitation reaction during ageing; either by causing copper containing phases to coprecipitate along with δ', or by altering the kinetics of the δ' formation reaction itself. The latter would seem to be the more likely, as at concentrations of the order of 0.1 and 0.25% it is doubtful whether significant amounts of copper bearing phases could be formed. At higher copper levels where such phases are more likely to form, no further hardening is produced on exceeding 0.8% Cu and this would also tend to disregard the effect of such precipitation. Thus, copper is acting as a 'trace' addition in these alloys. Possible mechanisms by which this may be occurring will be discussed further in section 9.6.

9.5 Peak Aged Structures

A TEM investigation was carried out on selected alloys in the peak aged condition - in order to study the changes in matrix and grain boundary precipitation. Unstretched extruded material was used for this work.

Apart from the Zr free alloy, all the structures were partially recrystallised, consisting of areas of elongated original grains containing a substructure, together with areas of banded recrystallised grains. As expected at the low copper levels there was no evidence of S phase precipitation in the matrix, or any other extra hardening phase, supporting the theory that the strength increase came from another source. S phase was observed at the high copper levels, formed on dislocations but as shown for the 2% Cu alloy in Fig. 9.8 this was very sparse. Even if its formation was enhanced in stretched material it was not responsible for significant strengthening as the tensile results in the previous section indicated. Bands of dislocation loops, similar to those observed in the Al-Li-Mg-Cu DC cast alloy, were also seen at the higher copper levels and in the zirconium free alloy they were accompanied by helical dislocations up to 10 μ long. Their presence again indicates that copper may be influencing the concentration and mobility of vacancies and this forms part of one of the mechanisms put forward in a later section to explain the strengthening action of this element.

Preferential grain boundary precipitation of the stable phase occurred in all the alloys but there was a tendency towards more continuous networks as more copper was added. At the 2% Cu level (Fig. 9.6) the precipitates were 'elongated' along the boundary as opposed to the coarse equiaxed morphology in the Al-Li-Mg ternary alloy. The precipitate distribution in the 0.25% Cu alloy is shown in Fig. 9.5. Here the equilibrium precipitates are fairly coarse, up to 2 μ in diameter, but have formed in the matrix as well as on the boundaries so that their density on the latter is reduced. They have a regular morphology, not observed in the Al-Li-Mg alloy, but it is unlikely that new phases could be formed at this copper level.

Stable precipitation in the Zr free alloys was again restricted to high angle boundaries as shown for the ternary in Fig. 9.7, but the particle densities at these sites were high.

Effect of Copper on the Peak Aged Structures

Fig. 9.5

Alloy RGL

0.25 wt.% Cu

Fig. 9.6

Alloy RGO

2 wt.% Cu

Fig. 9.7

Alloy RGF

0% Zr, 0% Cu

Fig. 9.8

Alloy RGO

2 wt.% Cu


2μ

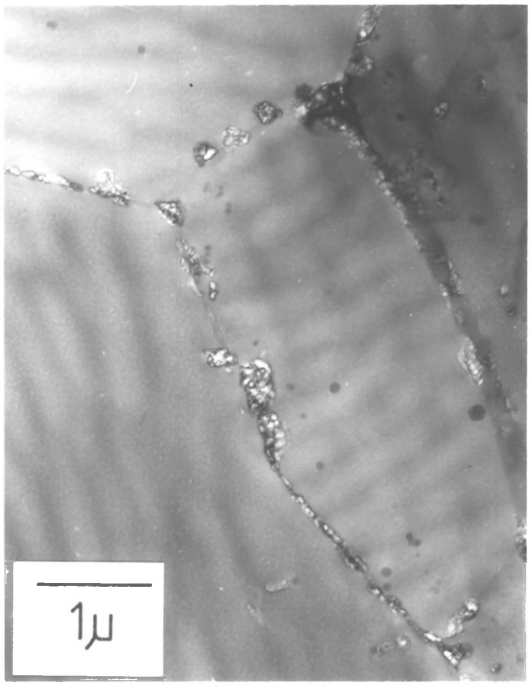
1μ

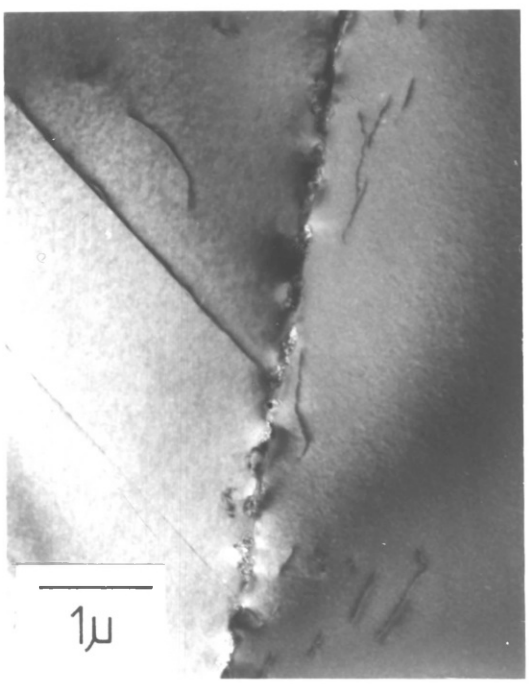
1μ

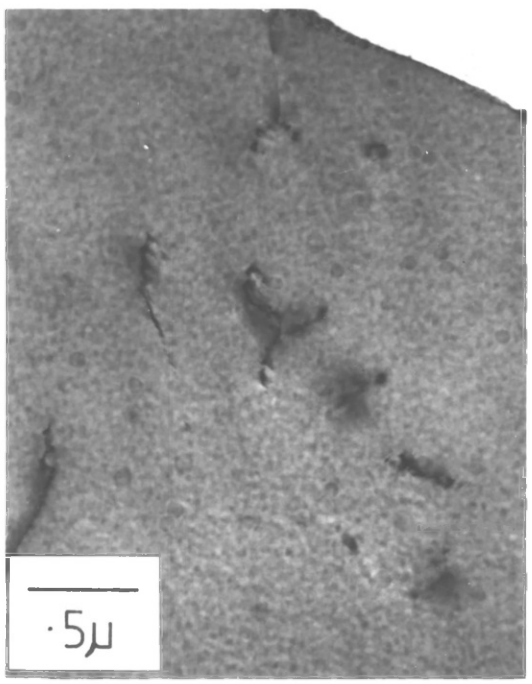
·5μ

9.6 Differential Scanning Calorimetry

9.6.1 DSC Traces

As with the DC cast alloys, there is still some doubt after examining the peak aged structures as to the cause of the strength increase accompanying the addition of copper. It was though that with the gradual increase in the copper content of the chill cast alloys that DSC might provide an explanation for this behaviour. The experimental technique used has already been fully described in section 6.5.4. Samples of extrudate were solution treated 48 hours before the test.

The effect of the addition of copper on the form of the DSC trace is shown in Fig. 9.9 for three of the alloys (0, 0.1 and 0.9% Cu). The changes that have taken place in the form of the low temperature δ' precipitation reaction and the higher temperature stable precipitation sequence are similar to those already reported for the DC cast material.

In the Cu free alloy the equilibrium precipitation reaction occurred over a wide temperature range ($\sim$ 100°C) with little heat evolution. Even with the addition of only 0.1% copper the form of this reaction was drastically changed giving a marked, sharp exotherm. This began at similar temperatures but was complete within approximately 50°C. At the 0.25% level the form of this portion of the trace was almost identical but above this concentration a step was produced on the low temperature side of the exotherm, indicating two overlapping precipitation reactions. The 0.9% copper alloy trace in Fig. 9.9 shows this feature well. TEM was not performed in this section of work, but based on the DSC results on the DC cast alloys (section 6.5.4) the precipitation reactions responsible for this type of peak are those forming Al_2MgLi and S-phase. However, this does not explain the single sharp reaction peak produced in the low solute alloy where copper containing phases are unlikely to be formed to any great extent. This feature may tie up with the peculiar form of precipitation observed in the peak aged 0.25% copper alloy where coarse, regular shaped particles were formed at grain boundaries and in the matrix. TEM on samples held at the exotherm temperature is really necessary to clarify this point.

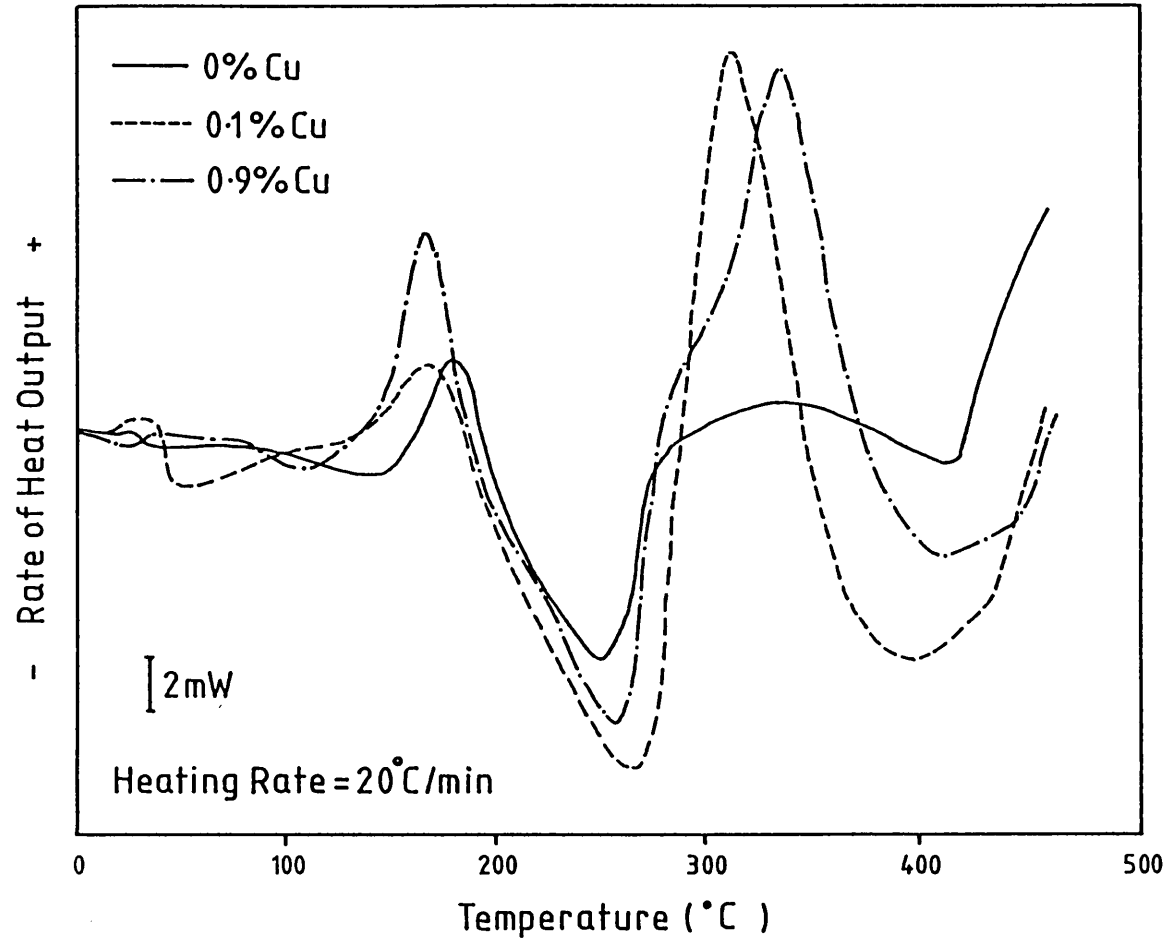

Fig 9.9 Effect of copper on the form of the DSC trace.

Again it must be stressed that the DSC technique will tend to give close to the maximum amounts of any possible phases. What is clear from the structural investigation on peak aged material is that apart from Al_3Li any extra precipitation was sparse and unlikely to cause any substantial strength increment. This points to changes in the Al_3Li reaction as being responsible for the mechanical property changes.

The main effect of copper on the kinetics of the δ' reaction was a downward shift in the peak temperature. Fig. 9.10 is a plot of the peak exotherm temperature with copper concentration. The largest drop occurs with the introduction of 0.1% copper, approximately 10°C, but after this the decrease is more gradual up to the 2% level, apart from the anomalous result at 0.44% Cu. Structurally, the change in the reaction temperature indicates that precipitation is being made easier at lower temperatures and effectively the activation energy is reduced. Translating this into isothermal ageing terms, the δ' distribution should be finer, as more stable nuclei are able to form and this is probably the reason for the strength improvements seen. Possible mechanisms for the effect of copper on the reaction kinetics are discussed in the next section.

9.6.2 Mechanisms for the Effect of Copper Additions on the δ' Reaction Kinetics

In these alloys the strong influence of even 0.1% copper on the δ' reaction would indicate that it is acting as a trace element. Although this study was not detailed enough to identify its mode of action, suggested mechanisms for the shift in reaction temperature will be discussed.

1. Vacancy Interactions

The stimulation of finer precipitation by trace additions has been reported for other alloy systems where it has been attributed to solute vacancy interactions. Vietz et al indicated that silver was able to stimulate finer precipitation of the hardening phase in Al-Zn-Mg alloys and implied an interaction between silver atoms and vacancies or silver atoms and magnesium atoms[83]. Recent work using

the DSC technique showed that the addition of 0.63% Cu to the same system can reduce its quench sensitivity by retention of a higher vacancy supersaturation[84]. Here again it was proposed that solute-vacancy complex formation was responsible.

This would appear to be a plausible explanation for the alloy behaviour in the present work, especially since in the high copper alloys, the products of vacancy condensation, were introduced for the first time, implying a higher vacancy concentration. Copper containing solute-vacancy complexes may be acting as nucleation sites for precipitation. The reduction in activation energy produced would then give a finer dispersion during isothermal ageing and would also allow the reaction to proceed at lower temperatures during the DSC test. However, there is an argument against this mechanism; if such complexes were promoting precipitation then a narrowing of PFZs at grain boundaries should have been seen in the copper containing DC cast alloy, which was not the case. Possibly grain boundary precipitation had a stronger influence on PFZ formation than initially thought.

2. Changes in Interfacial Energy

Copper atoms may be segregating to the Al_3Li/matrix interface reducing the surface energy of the precipitate. If this were the case then it would again reduce the activation energy for stable precipitate growth together with a reduction in the critical nucleus size. This mechanism is more unlikely than the solute-vacancy interaction model, since the Al_3Li precipitates already have an inherently low interfacial energy[9]. However, it may explain the change in the mode of stable precipitate growth in the low copper alloys.

The above mechanisms predict that the strength increase produced by the addition of copper is due to the promotion of a finer δ' dispersion. This was not verified by the TEM investigation on the DC cast alloy, where little difference between the two precipitate populations was observed. Further work is therefore required on this point.

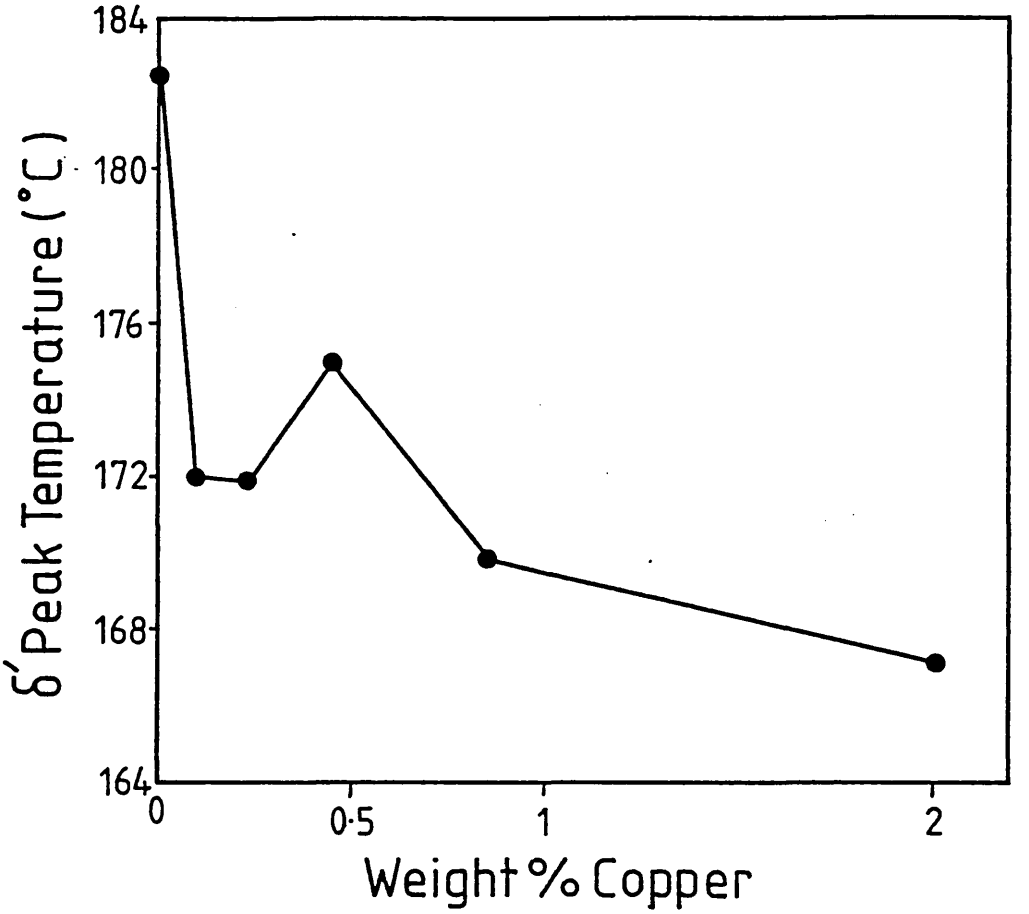

Fig 9.10 Effect of copper on the position of the delta prime exotherm.

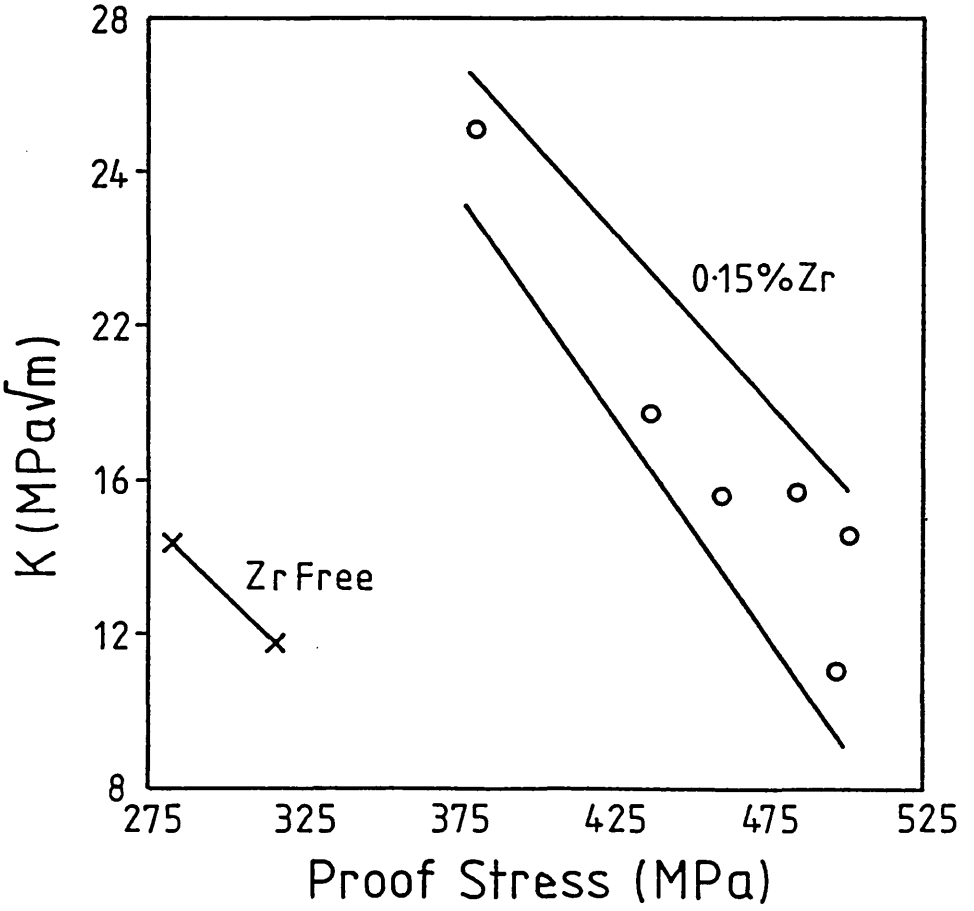

Fig 9.11 Toughness vs. proof stress.

9.7 Toughness

Toughness testing was performed on all the alloys using the DCB test described in section 7.1, with crack propagation occurring down the extrusion direction. Testpieces were machined from T8 extruded material. A minimum of three test results were obtained for each alloy and the averages of these values are presented in Fig. 9.11 where they are plotted against proof stress.

The data forms two bands as shown, distinguishing between the Zr containing and Zr free alloys. In both of these the toughness decreases as the proof stress is raised, coinciding with increasing copper content. Although the Zr free alloys had the lowest proof stresses, they also possessed low toughness, comparable with that of the copper and zirconium containing alloys which had a proof stress some 200 MPa higher. These two alloys were fully recrystallised and it proved difficult to maintain a straight crack due to the lack of directionality in the structure. Their fracture surfaces were totally intergranular and were covered in very fine dimples associated with Al_2MgLi precipitates. However, since the direction of crack growth was down the extrusion direction, i.e. down the grain boundaries in unrecrystallised material, the presence of recrystallised grain boundaries was not detrimental. Possible causes of embrittlement could be the larger grain size, allowing large dislocation pile ups to form, and also the lack of Al_3Zr precipitates which are thought to inhibit planar slip.

Returning to the zirconium containing alloys the decrease in toughness wih proof stress is almost linear. The largest drop in toughness occurs for the addition of 0.1% Cu which also gives the greatest strength increment. Fracture surfaces were almost entirely intergranular over the entire range of alloys indicating that the grain boundary weakness found in all the DC cast alloys is also present here. Figs. 9.12 and 9.13 show the fractures of the 0% and 2% Cu alloys respectively. Although the micrographs are at different magnification, the fracture paths appear similar, i.e. along recrystallised and original grain boundaries. The tendency towards more continuous boundary precipitation with higher copper levels did not appear to play a significant role on the fracture surfaces. Therefore the reduction in toughness with increasing copper content can be attributed

DCB Fracture Surfaces

Fig. 9.12

Alloy RGG 0% Cu

Fig. 9.13

Alloy RGO 2% Cu

Stress Corrosion Crack Paths

Fig. 9.14

Alloy RGN 0.86% Cu
Transverse section
Kellars reagent

Fig. 9.15

Alloy RGN 0.86% Cu

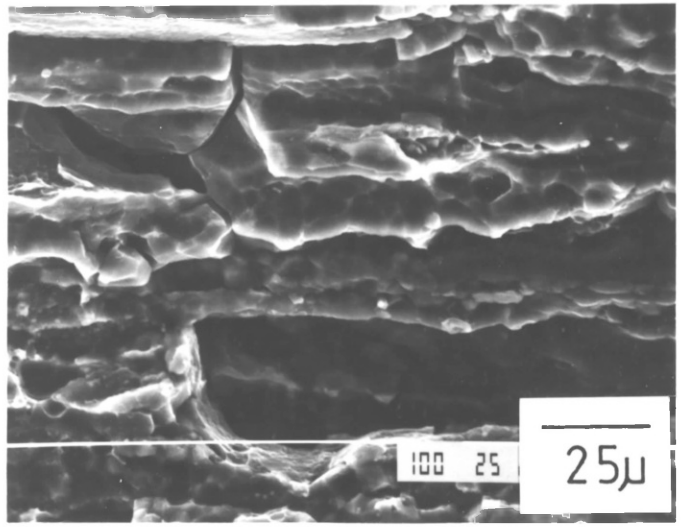
100 25
25µ

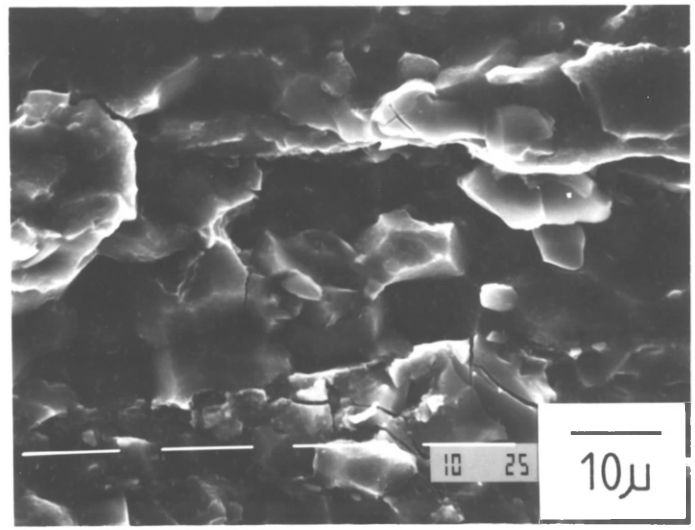
10 25
10µ

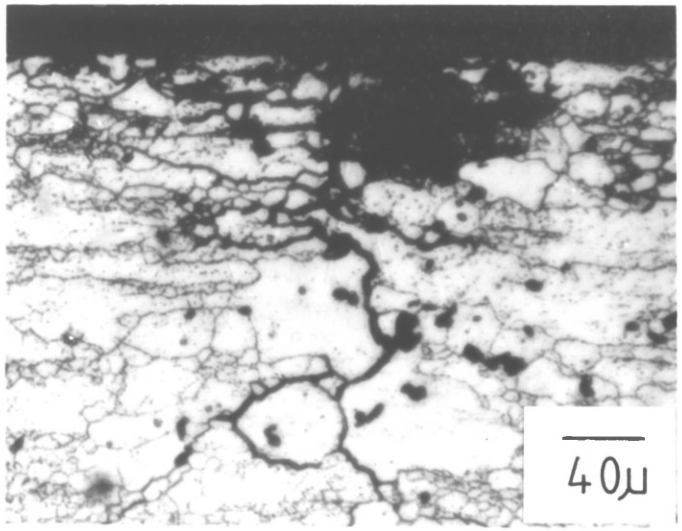
40µ

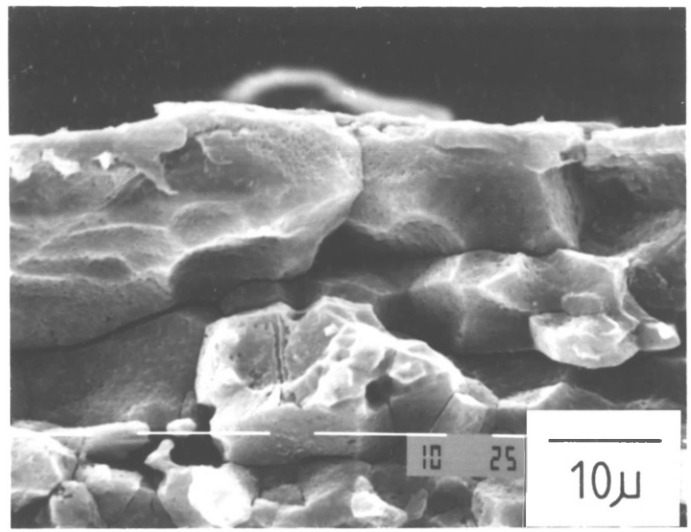
10 25
10µ

to the hardening it produces and the resulting reduction in crack tip plasticity. Again, any S phase precipitation occurring in these alloys is not improving this property.

The trends with proof stress shown here support the results obtained earlier for the DC cast alloys and would probably be the same in the L-T direction.

9.8 Corrosion Resistance

Corrosion testing was carried out on rolled sheet from all eight alloys using the NAWL test. The quality of the sheet was poor, apart from the low copper alloys, 0.1, 0.25 and 0.4% Cu, and contained longitudinal subsurface cracks with entrapped oxide. This condition was the most severe in the 0.86% Cu alloy and the zirconium free compositions. The test procedure was the same as that used previously on extruded specimens except that an initial 30 second dip in a 30% NaOH solution was given in an attempt to remove any loose surface areas. Samples were tested in the solution treated, 80% UA, PA and 300 hour aged conditions.

The results of all the tests are presented in Fig. 9.16 where the weight loss per unit area is plotted against the level of copper addition. Looking at the data overall, there are two general trends;

1. The weight loss increases as the ageing time is raised for each alloy.
2. In each temper the level of attack increases with the level of copper addition.

This behaviour relates to the results of the structural study reported earlier, as these factors promote further grain boundary precipitation. Increasing the copper level also raised the level of attack in the solution treated condition so there must be a contribution to susceptibility from either the coarse copper bearing inclusions or possibly copper segregation effects at the boundaries.

The Al-Li-Mg-Zr alloy showed the lowest susceptibility to this form of corrosion with very little increase in the rate of attack occurring until the overaged condition. This contradicts the results

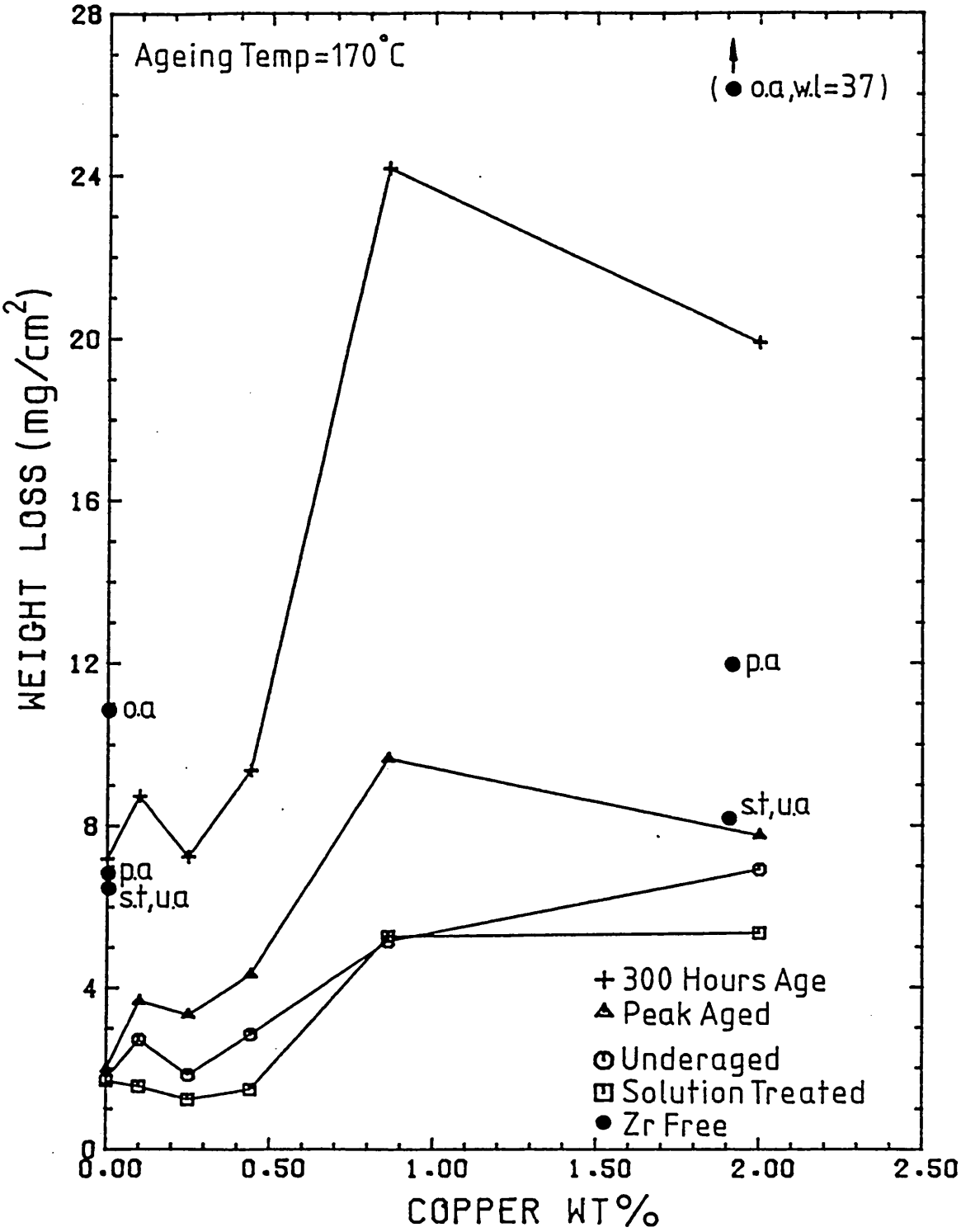

Fig 9.16 NAWL corrosion results for the chill cast alloys.

obtained on extruded DC cast material where a continuous increase in weight loss was observed. No undercutting of the sheet surface took place and this, in conjunction with the deeper solute depleted layer on the sheet, was probably responsible for the insensitivity to ageing. Alloy RGN (0.9% Cu) and the corresponding DC cast alloy did show similar trends.

There was a marked difference between the low copper (< 0.44%) and high copper alloys in all the tempers. This was only partly due to the good surface quality of the former (which gave lower weight losses than the ternary alloy in the ST condition). The increase in this difference with longer ageing times can be attributed to the change in the form of grain boundary precipitation. Whereas stable precipitate formation was limited in the low solute compositions, at high concentrations the precipitate densities on the grain boundaries were very high. Therefore the strength increase at low levels of copper addition can be achieved without a significant loss of corrosion resistance.

The high level of attack shown by the 0.9% Cu alloy was again partly due to poor sheet quality, when from a structural point of view the weight losses should have been lower than for the 2% Cu alloy. The same effect was also partly to blame for the high weight losses shown by the Zr free alloys but the large increase in susceptibility on ageing indicates that the high precipitate densities on grain boundaries was the major factor. Therefore an unrecrystallised (or, as in this case, partially recrystallised) structure is preferable to a coarse fully recrystallised one.

On completion of the tests, solutions from specimens in the UA and PA tempers were analysed for Al, Mg, Cu and Li in order to follow the levels of dissolution of the various elements. The concentrations of all of them increased with ageing time and with the copper content as the general attack rate increased. The magnesium:copper ratio was always consistent with the alloy composition and this would indicate that neither element is being preferentially dissolved and that the attack is taking place by the removal of entire grains. The magnesium: lithium ratio was constant at roughly 3:1 which is higher than the 1.5:1 ratio in the alloy. This may be due to the formation of insoluble corrosion products containing lithium.

9.9 Stress Corrosion Resistance

Susceptibility to stress corrosion cracking (SCC) in aluminium alloys can be strongly influenced by alloy composition and heat treatment although there is no strong correlation between strength or toughness and this property.

SCC is usually intergranular and general features affecting this mode of attack are grain boundary precipitates, PFZs and deformation mode. The 2000 and 7000 series alloys are susceptible to this type of attack but resistant tempers can be produced by overageing[58]. If aluminium-lithium alloys are to be considered as a replacement for these systems then they must also be capable of resisting stress corrosion.

Testing was performed on underaged and peak aged extruded material using the C ring test (ASTM G38-79), which is a constant strain alternate immersion method, using 3.5% NaCl solution. All of the extrusions were given a 2% stretch prior to ageing but an overaged temper was not included due to lack of material. The rings used were 20 mm in diameter meaning that 2 mm had been removed from the extruded surface. In this test the ring is deflected by means of a bolt passing through the centre, giving a maximum tensile stress at the periphery. Here the rings were deflected so as to set this stress level at 75% of the proof stress. Once on test specimens were inspected daily and the criteria used for failure was the initiation of a crack. Table 9.3 lists the test lives of all the specimens. In some cases only one out of 4 or 5 specimens failed within the maximum test period of 245 days, but to be classed as an SCC failure here, at least half of the samples had to fail.

The alloys containing less than 0.44% Cu did not fail in the test period used, and this alloy only failed in the peak strength temper. Lives of the specimens that failed are plotted in Fig. 9.17 in the form of copper content against median life. The main trend here is a decrease in test life with increasing copper concentration. Extending the ageing time from the UA to the PA temper had the same effect, although this trend was reversed at the 0.86% Cu level. Structurally, both of these factors have similar effects at the grain boundaries, and promote more continuous precipitation which accounts for the increased susceptibility. In addition, they also raise the

Alloy	Life in Days UA	PA
RGF (0 Cu, 0 Zr)	5 > 245	4 > 245, 111
RGG (0 Cu, 0.14 Zr)	5 > 245	5 > 245
RGH (0.1 Cu, 0.1 Zr)	5 > 245	5 > 245
RGL (0.25 Cu, 0.08 Zr)	4 > 245, 34	3 > 245
RGK (0.44 Cu, 0.14 Zr)	4 > 245, 14	2 > 245, 14, 20
RGN (0.86 Cu, 0.14 Zr)	6, 9, 13, 2 x 14	2 x 13, 15, 27
RGO (2.02 Cu, 0.16 Zr)	2 x 6, 2 x 7, 10	4 x 6, 8
RGP (1.9 Cu, 0 Zr)	5 x 11	3, 4 x 6

Table 9.3 Stress Corrosion Lives

stress level (figures are shown in parentheses in Fig. 9.17 for the PA temper) and reduce toughness, both of which may affect the stress distribution at the crack tip. The change in deformation mode between the two tempers is also likely to be detrimental in this respect.

All the stress corrosion failures were intergranular and a typical crack is shown in Fig. 9.14 which is a transverse section through a 0.9% Cu alloy specimen. Lateral branching has occurred and also the crack appears to pass through several coarse S type particles which may also enhance susceptibility. The large pit at the surface is caused by general corrosion along the crack path. Fig. 9.15 is an SEM micrograph of the same sample showing the crack surface. The path is clearly intergranular, but the pitting on the boundaries at precipitates might have been a result of general corrosion, although such particles were probably involved in the mode of SCC attack. The grain boundary weakness observed in all the toughness tests probably assisted in this form of attack but it was not the causal factor as the low copper alloys exhibited good resistance.

The effect of zirconium on the SCC behaviour is unclear as only one of the two Zr free alloys failed. The life of this alloy exceeded that of the corresponding high copper alloy but this may have been due to the slightly reduced copper content and not necessarily

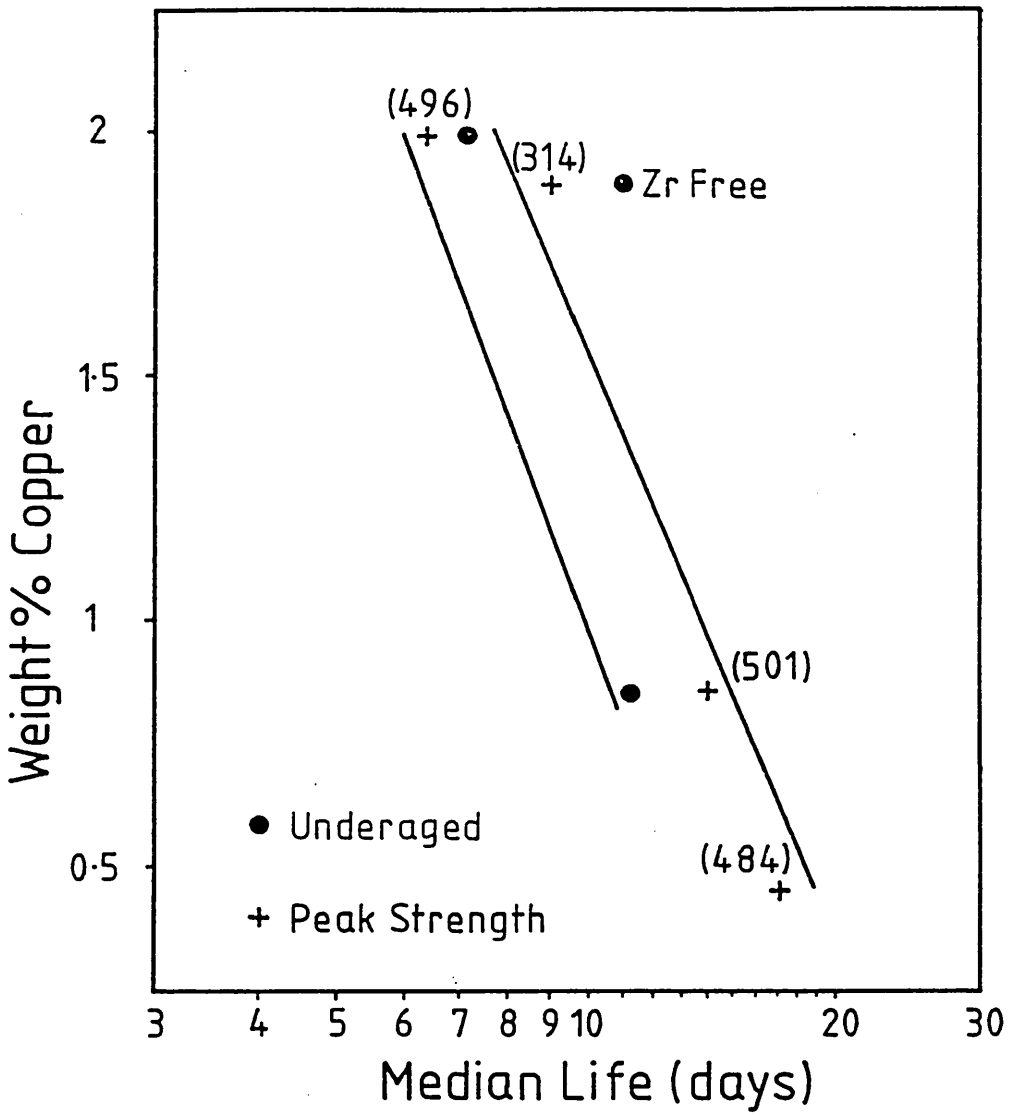

Fig 9.17 Effect of composition and heat treatment on stress corrosion resistance.

a result of the recrystallised grain structure. However, the short transverse direction is the worst test direction with regard to this property for unrecrystallised product, whereas equiaxed structures show the same properties in all directions.

Some mechanisms to explain SCC involve hydrogen embrittlement[57] but the hydrogen contents of these alloys, which are listed in Table 9.1, show no correlation with the test results.

To summarise, the ternary alloy and the low copper alloys showed good resistance to SCC using this test, but increasing copper levels led to susceptibility. Therefore an improvement in strength can be achieved by small copper additions without encountering this form of attack. Finally, although the overaged temper was not tested the trends shown here and in the toughness and corrosion sections indicate that this treatment would probably be detrimental to stress corrosion behaviour.

9.10 Summary

1. Copper additions to the ternary alloy produced solid solution hardening at the rate of 6.8 Hv/weight % copper. The effects of this were insignificant except at the higher copper levels.

2. The presence of copper produced a marked strength increase over the ternary alloy upon ageing. This was large even at the 0.1% Cu level (60 MPa) and increased with further additions up to 0.9% copper. Elongation values followed the reverse trend to the proof stress.

3. DSC testing indicated that the addition of copper was responsible for changes in the nature of the Al_3Li and stable precipitation reactions. The lack of coprecipitation observed in TEM pointed to the changes in the δ' reaction as being responsible for the strengthening effect. Increasing the copper level progressively shifted the δ' exotherm to lower temperatures. This was thought to correspond to a reduction of the activation energy for precipitation, giving a refined δ' dispersion during isothermal ageing.

4. A model was proposed to explain the hardening produced by copper additions whereby δ' nucleation is stimulated by copper containing solute-vacancy complexes, resulting in a finer dispersion.

5. Increasing the copper concentration promoted more continuous grain boundary precipitation and at the higher levels sparse S phase precipitation was also produced in the matrix.

6. The ageing response was modified in the zirconium free alloys; instead of showing a plateau at peak hardness, the hardness time curves showed a continual increase. On overageing softening occurred more slowly than for the Zr containing alloys.

7. Toughness decreased as copper was added principally due to the increased proof stress. Fracture was again intergranular and the grain boundary weakness observed in the DC cast alloys was also present here. The zirconium free alloys showed reduced strength and low toughness possibly due to the effect of the large grain size and lack of Al_3Zr precipitates on the slip distribution.

8. Intergranular corrosion resistance was decreased by longer ageing times and higher copper levels due to increased high angle boundary precipitation. The low copper alloys only exhibited slightly higher susceptibility than the ternary alloy but there was a large increase above the 0.4% Cu level. The attack was general in nature with no element being selectively removed.

9. The Al-Li-Mg alloy and the low copper alloys (< 0.4%) were not susceptible to stress corrosion cracking and therefore some strength improvement is possible here without loss of resistance. In the alloys that failed, susceptibility increased as the ageing treatment was extended from the UA to the PA temper and also with increasing copper content. Increased grain boundary precipitation was thought to be the reason for these trends. The effect of zirconium on this property was unclear.

CHAPTER TEN

CONCLUSIONS AND SUGGESTIONS FOR FURTHER WORK

Conclusions

1. The extrusion limits of the two DC cast alloys were established and simple expressions to predict the extrusion pressure were derived. The pressure requirements were similar in both cases. The addition of copper reduced the working range due to the onset of hot shortness caused by liquation of S-type phases. A similar effect was observed in the hot torsion tests. Increasing the ram speed and extrusion ratio reduced the temperature range over which extrusion was possible in both alloys.

2. Using the torsion test, the flow stress characteristics of the two alloys were characterised by determining the constants in the hot working equation. The addition of copper to the ternary alloy reduced the activation energy for recovery processes and gave lower steady state torques at all but the highest strain rates. A theory was proposed to explain this behaviour, whereby interactions between copper atoms and vacancies alter the overall vacancy concentration and assist recovery at low strain rates.

3. Homogenisation practices were established for the two alloys but the treatment given to the copper containing alloy was inadequate due to the presence of low melting point phases. The ternary alloy was capable of withstanding higher soak temperatures and increasing this factor was observed to promote static recrystallisation immediately after extrusion.

4. The extrusions were partially recrystallised at all but the highest extrusion temperatures. The remainder consisted of a recovered subgrain structure. Dynamic recovery was the operative softening mechanism during extrusion and static recrystallisation took place after deformation. The extent to which the latter occurred was related to the extrusion conditions and was promoted by lower extrusion temperatures and higher ratios. Full recrystallisation was never observed.

5. The extruded structures were stable during solution treatment due to the presence of Al_3Zr dispersoids. Thus the fully heat treated

properties were related to the extrusion parameters, with high temperatures and low ratios promoting higher strength. This was purely a grain structure effect in the ternary alloy, where increased static recrystallisation lead to softening. In the quaternary alloy higher extrusion temperatures gave strengthening due to a combination of substructural and precipitation effects.

6. The addition of copper to the ternary alloy gave very little solid solution hardening in the as extruded condition but it did increase the response to artificial ageing, giving increased strength and reduced ductility. The Al-Li-Mg alloy was capable of 2014 T6 strength levels but not ductility unless on a strength to weight ratio basis. The higher strength Al-Li-Mg-Cu alloy was capable of 7075 T76 strength levels but never achieved the same ductility levels.

7. The use of an intermediate cold stretch did not enhance the age hardening response in either alloy and precipitation would appear not to be dislocation nucleated.

8. Al_3Li was the main product of artificial hardening in both alloys. The ageing sequence in the ternary alloy was;

$$SSS \rightarrow Al_3Li \rightarrow Al_2MgLi .$$

Al_2MgLi precipitation took place preferentially at grain boundaries, but occurred in the matrix at longer ageing times. Al_3Li PFZs were formed at high angle boundaries and at Al_2MgLi precipitates.

The ageing response of the quaternary alloy was very similar and was dominated by the products of the Al-Li-Mg system. Indeed the density of grain boundary precipitation was increased in this alloy. Sparse dislocation nucleated laths of S phase were found after long ageing times, but this did not appear to give any strength contribution. T8 tensile results indicated that cold stretching did not promote their formation.

9. The DSC investigation indicated that the addition of copper influenced the kinetics of the Al_3Li precipitation reaction and depressed the exotherm to a lower temperature.

Work on the chill cast alloys, where six different copper levels were studied, supported this and the exotherm was consistently depressed

to lower temperatures. Copper was considered to be acting as a trace addition here since the largest drop occurred with the addition of 0.1 wt.% Cu. The proof stress increased with copper content in a corresponding manner. This was due to changes in the Al_3Li distribution and not solid solution hardening as the latter would have been insignificant at the lower copper levels. A model was proposed to explain this behaviour whereby copper containing vacancy complexes act as nucleation sites for Al_3Li, so reducing the activation energy and refining the dispersion. The idea of copper atom-vacancy interactions also ties in with the increased number of vacancy condensation products observed in the copper containing alloys.

10. Toughness was measured using several tests and was found to decrease with ageing time in both DC cast alloys. The decrease up to peak strength was due to the increase in the yield stress, whereas the further drop on overageing was due to the formation of coarse equilibrium precipitates. The Al-Li-Mg-Cu alloy possessed significantly lower toughness than the ternary as a result of the higher proof stress. The inclusion of a cold stretch in the heat treatment of this alloy produced a further decrease in toughness indicating that any S phase precipitation promoted by this treatment was not having any significant effect on this property.

11. A grain boundary weakness was in evidence in all the DC and chill cast alloys tested. Grain boundaries failed in a completely brittle manner when stressed normal to their length and showed only slight ductility in the vicinity of stable ageing precipitates. This feature was even in evidence, to some extent, on the fracture surfaces of longitudinal tensile tests on solution treated material. The most likely explanation is solute segregation at the boundaries, but the segregating species was not identified.

12. L-T toughness, measured by the COD test, was related to the extrusion conditions. The onset of static recrystallisation at low extrusion temperatures gave rise to reduced toughness due to the introduction of brittle grain boundaries parallel to the crack path. Toughness as measured in the T-L orientation was unaffected as all the

grain boundaries were aligned in the crack direction anyway.

13. The decrease in toughness produced by the addition of 0.8% Cu to the DC cast ternary alloy was supported by the trend in the chill cast alloy results. Toughness decreased with increasing copper content primarily due to the increased proof stress and the relationship with the latter was almost linear.

14. In the toughest condition for the L-T orientation, the Al-Li-Mg alloy approached 2014 T6 strength and toughness levels.

15. The susceptibility of the extrusions to intergranular corrosion increased with longer ageing times due to further grain boundary precipitation. Attack at the extrudate surface was complicated by the solute depleted zone and the fully recrystallised layer. The former imparted some resistance to corrosion but once penetrated this was severly undercut in the ternary alloy, leading to heavy attack. The quaternary alloy had a much coarser surface grain structure and this mechanism did not take place, giving a lower level of damage. However, once the surface layer was machined away the copper containing alloy suffered heavier attack due to the increased precipitate density on the grain boundaries.

16. The extrusion conditions had some influence on the corrosion resistance of the ternary alloy due to their effect on the nature of the surface grain structure.

17. The chill cast alloys showed increased corrosion susceptibility with increased copper content, but up to 0.25% Cu the level of attack was low. Therefore at these levels of addition a strength increase over the ternary alloy can be acheived without a significant loss of corrosion resistance.

18. The exfoliation resistance of the DC cast Al-Li-Mg alloy was very good in all tempers. However, the addition of 0.8% Cu led to susceptibility, the level of which increased with ageing time. This alloy also exhibited heavier attack in the solution treated condition so this effect was not simply due to increased grain boundary precipitation.

19. The chill cast ternary alloy together with the low copper compositions, were not susceptible to SCC in the UA and PA tempers at the stress level used in this work. Above 0.25 wt.% Cu failures did occur and the susceptibility was raised at higher copper levels and by extending the ageing treatment. Again the low copper compositions appeared attractive, combining increased strength with SCC resistance.

20. The tests performed on zirconium free material would indicate that this element can have an influence on the ageing response as well as the grain structure.

Suggestions for Further Work

Further work on the two initial alloy compositions ought to include the following:

1. An improved homogenisation schedule for the copper containing alloy to remove the large quantities of low melting point phases and to extend the working range. This may be possible by soaking closer to the liquation point, or by the use of a two stage treatment whereby the initial soak alters the liquation point of the particles allowing the temperature to be raised further.

2. The use of lower ageing temperatures or a two stage ageing treatment (a low temperature 'nucleating' age followed by a short high temperature 'growth' age) to attempt to prevent stable precipitate formation at high angle boundaries.

3. The use of alternative ageing treatments in an attempt to promote more S phase precipitation in the Al-Li-Mg-Cu alloy. Although this work did not indicate that significant formation of this phase was likely a two stage heat treatment combined with cold working may be beneficial in this respect.

4. An investigation into the effect of copper on the Al_3Li precipitation reaction to verify that the distribution of this phase is being affected. The quench sensitivity of the alloys ought to be studied in order to determine whether the addition of copper alters this property which might support the proposed vacancy interaction mechanism.

5. In situ fracture studies using Auger analysis to identify any species segregating to the grain boundaries and causing embrittlement.

It would also be worthwhile studying an Al-Li-Mg-Cu alloy with a copper content in the range 0.1 to 0.25 wt.%. These compositions showed promise in the areas of corrosion and stress corrosion resistance whilst offering a significant strength improvement over the base alloy. Workability ought not to be such a problem here as the number

of S-phase inclusions should be lower and the full effect of varying the extrusion parameters could be established.

References

1. P.A. Tunnicliffe, Ph.D. Thesis, Univ. London (1979)
2. S.J. Paterson, Ph.D. Thesis, Univ. London (1981)
3. R.P. Vierod, Ph.D. Thesis, Univ. London (1983)
4. C.S. Peel et al, Proc. 2nd Int. Al-Li Conf., Met. Soc. AIME, 363 (1984)
5. W.E. Quist et al, IBID, 313
6. E.A. Starke et al, J. Met., 33, (8), 24 (1981)
7. W.R.D. Jones, P.P. Das, J.I.M., 88, 435 (1959/60)
8. J.M. Silcock, IBID, 88, 357 (1959/60)
9. B. Noble, G.E. Thompson, J. Met. Sci., 5, 114 (1971)
10. D.B. Williams, J.W. Edington, IBID, 9, 529 (1975)
11. G.E. Thompson, B. Noble, J.I.M., 101, 111 (1973)
12. R. Nozato, G.N. Nakai, Trans. J.I.M., 18, 679 (1977)
13. D.B. Williams, Proc. 1st Int. Al-Li Conf., Met. Soc. AIME, 89 (1981)
14. B. Noble et al, J. Mat. Sci., 17 (2), 461 (1982)
15. K. Dinsdale et al, Proc. 1st Int. Al-Li Conf., Met. Soc. AIME, 101 (1981)
16. P.J. Gregson, Ph.D. Thesis, Univ. London (1983)
17. D.W. Levinson, D.J. McPherson, Trans. ASM, 48, 689 (1956)
18. S.J. Harris et al, Proc. 2nd Int. Al-Li Conf., Met. Soc. AIME, 219 (1984)
19. H.K. Hardy, J.I.M., 84, 429 (1955/56)
20. H.K. Hardy, J.M. Silcock, IBID, 84, 423 (1955/56)
21. E.A. Starke, F.S. Lin, Met. Trans., 13A, 2259 (1982)
22. F.S. Lin et al, IBID, 13A, 401 (1982)
23. B. Noble, G.E. Thompson, J. Met.Sci., 6, 167 (1972)
24. W.S. Miller et al, Proc. 2nd Int. Al-Li Conf., Met. Soc. AIME, 335 (1984)
25. I.G. Palmer et al, IBID, 91 (1984)
26. R.J. Kav et al, IBID, 255 (1984)
27. I.J. Polmear, Light Alloys, Arnold (1981)
28. D.S. Thompson, Met. Trans., 6A, 671 (1975)
29. A.J. Bryant, Met. Tech., 2, 21 (1975)
30. J.J. Jonas et al, Int. Met. Rev., 14, 1 (1969)

31. H.J. McQueen, J. Met., 20 (4), 31 (1968)
32. C.M. Sellars, W.J. McTegart, Int. Met. Rev., 17, 1 (1972)
33. H.J. McQueen, Met. Trans., 8A, 807 (1977)
34. R.J. McElroy, A.C. Scopiak, Int. Met. Rev., 17, 175 (1972)
35. D.J. Abson, J.J. Jonas, J. Met. Sci., 4, 24 (1970)
36. M.G. Tutcher, Ph.D. Thesis Univ. London (1979)
37. P.J.E. Forsyth, C.A. Stubbington, Met. Tech., 2, 158 (1975)
38. A. Kelly, R.B. Nicholson, Prog. Mat. Sci., 10 (3) (1963)
39. J.W. Martin, Precipitation Hardening, Pergamon Press (1968)
40. J.W. Martin, Micromechanisms in Particle Hardened Alloys, Cambridge Univ. Press (1980)
41. T.V. Strichegoleva, O.F. Rybalko, Phys. Met. Metall., 43 (3), 83 (1976)
42. B. Noble et al, J. Met. Sci., 16, 425 (1982)
43. D. Hull, An Introduction to Dislocations,Pergamon Press (1975)
44. G.T. Hahn, A.R. Rosenfield, Met. Trans., 6A, 653 (1975)
45. G.G. Garett, J.F. Knott, IBID, 9A 1187 (1978)
46. I. Kirman, IBID, 2A, 1761 (1971)
47. F.S. Lin, Scripta Met., 16, 1295 (1982)
48. T.H. Sanders et al, Mat. Sci. Eng., 43, 247 (1980)
49. T.H. Sanders, Alcoa Report, NADC Contract No. N62269-76-C-0271 (1979)
50. W.X. Feng et al, Met. Trans., 15A, 1209 (1984)
51. J.W. Evancho, Alcoa Report, NADC Contract No. N62269-73-C-0219 (1974)
52. K.J. Gardner, R. Grimes, J. Met. Sci., 13, 216 (1979)
53. Y.M. Vaynblat et al, Phys. Met. Metall, 42 (5), 103 (1976)
54. A.K. Vasudevan et al, Proc. 2nd Int. Al-Li Conf., Met. Soc. AIME, 181 (1984)
55. D. Webster, Met. Trans., 18A, 1913 (1979)
56. D.P. Hill, D.N. Williams, Proc. 2nd Int. Al-Li Conf., Met. Soc. AIME, 201 (1984)
57. J. Kruger, Stress Corrosion Cracking, Pub Freund (1980) pp5
58. M.O. Speidel, Met. Trans., 6A, 631 (1975)
59. A.W. Thompson, I.M. Bernstein, Stress Corrosion Cracking, Pub. Freund (1980) pp 193.
60. P.P. Pizzo et al, Proc. 2nd Int. Al-Li Conf. Met. Soc. AIME, 627 (1984)

61. J.G. Rinker at al, IBID, 597
62. P.P. Pizzo, NASA Contractor Report, 3578 (1982)
63. P. Niskanen et al, Corr. Sci., 22 (4), 283 (1982)
64. T. Sheppard, D. Raybould, J.I.M., 89, 225 (1960/61)
65. D.S. Wright, T. Sheppard, Met. Tech., 6, 224 (1979)
66. T. Sheppard, D.S. Wright, IBID, 6, 215 (1979)
67. J.G. Tweedale, M.Sc. Thesis, Univ. London (1974)
68. D.S. Wright, Ph.D. Thesis, Univ. London (1978)
69. C.E. Pearson, R.N. Parkins, The Extrusion of Metals, Chapman and Hall (1960)
70. W.J. McTegart, Ductility, ASM Seminar (1967) pp 133
71. A. Sendorek, A.W. Pearson, J.I.M., 19, 33 (1971)
72. N. Ryum, Acta Met., 17, 269 (1969)
73. L.F. Mondolfo, Aluminium Alloys, Structure and Properties, Butterworths (1976)
74. F.J. Humphreys, Met. Sci., 3, 136 (1979)
75. H.J. McQueen et al, Can. J. Phys., 45 (2.2.3), 1225 (1967)
76. G.E. Dieter, Mechanical Metallurgy, McGraw Hill (1976)
77. C.Q. Chen, J.F. Knott, J. Met. Sci., 15, 357 (1981)
78. T.H. Sanders, Alcoa Report, NADC Contract No. N62269-74-C-0438 (1976)
79. F.W. Gayle, J.B. Van der Sander, Scripta Met., 18, 473 (1984)
80. E.S. Balmuth, Scripta Met., 18, 301 (1984)
81. J.T. Staley, Properties Related to Fracture Toughness, ASTM, STP 605, pp 71
82. W.A. Anderson, Precipitation From Solid Solution, AIME, (1957) pp 150
83. J.T. Vietz et al, J.I.M., 92, 327 (1963/64)
84. R.J. Livak, J.M. Papazian, Scripta Met., 18, 483 (1984)

APPENDIX ONE

EXTRUSION DATA

The following tables list the extrusion variables for all the experimental runs, together with calculated temperature rises, strain rates and measured extrusion pressures.

Coding

The first letter of the run codes gives details of the extrudate surface finish. Any characters after this describe deviations from normal procedure.

A	Acceptable surface finish
B	Slight cracking at points on the length and periphery
C	Cracking along entire extrusion
ST	Billet stuck due to insufficient press capacity
AC	Extrusion air cooled
NR	No extrusion data recorded
500	Alternative homogenisation practice
COD	Square die used for COD testpieces
STR	Strip die used

Temperature Rises

Peak temperature rises were calculated assuming adiabatic conditions.

Final temperatures were calculated using an integral profile computer model, further details of which can be found in reference 2.

Al-Li-Mg

RUN CODES	EXT RATIO	FURNACE TEMP	INITIAL TEMP	PEAK TEMP	FINAL TEMP	BILLET LENGTH	CTNR TEMP	RAM SPEED	STRAIN RATE	MAX PRESSURE	MIN PRESSURE
		DEG.C	DEG.C	DEG.C	DEG.C	MMS	DEG.C	MMS/S	-1 SEC	2 MN/M	2 MN/M
01A	10.0	300.0	295.0	316.6	446.6	75.0	250.0	14.0	6.86	893.13	640.53
02A	10.0	300.0	295.0	322.7	444.2	75.0	250.0	14.0	6.86	915.69	624.74
03A	10.0	350.0	344.0	360.5	470.8	75.0	300.0	14.0	6.86	744.28	554.83
04A	10.0	400.0	394.0	409.2	509.5	75.0	350.0	14.8	7.25	629.25	579.64
05A	10.0	400.0	394.0	405.2	506.1	75.0	350.0	14.0	6.86	617.98	539.04
06A	10.0	450.0	440.0	451.2	525.0	75.0	400.0	14.0	6.86	505.21	412.74
07B	10.0	500.0	487.0	495.7	556.5	75.0	450.0	14.0	6.86	392.44	385.67
08A	10.0	500.0	487.0	490.3	529.4	75.0	450.0	4.7	2.30	331.54	327.03
09A	10.0	500.0	487.0	494.8	529.2	75.0	450.0	4.3	2.11	354.10	354.10
10A	10.0	525.0	508.0	513.5	541.2	75.0	475.0	3.9	1.91	302.22	302.22
11A	10.0	550.0	530.0	532.3	552.7	75.0	500.0	3.9	1.91	232.31	232.31
12A 550	10.0	300.0	295.0	317.0	456.3	75.0	250.0	14.8	7.25	911.18	703.68
13A 550	10.0	500.0	487.0	493.0	526.6	75.0	450.0	4.7	2.30	331.54	320.27
14A	20.0	325.0	318.0	336.5	505.0	75.0	275.0	13.7	8.62	1019.44	778.11
15A	20.0	350.0	344.0	358.0	471.2	75.0	300.0	5.1	3.21	866.07	636.02
16A	20.0	350.0	344.0	360.3	489.5	75.0	300.0	14.8	9.31	899.90	505.21
17A	20.0	350.0	346.0	351.2	479.8	75.0	300.0	4.7	2.96	859.30	687.89
18A	20.0	400.0	394.0	410.6	523.6	75.0	350.0	13.3	8.37	687.89	658.57
19A	20.0	450.0	440.0	448.8	511.4	75.0	400.0	4.3	2.71	543.55	442.06
20A	20.0	450.0	442.0	451.5	525.4	75.0	400.0	4.8	3.02	588.66	498.44
21A	20.0	500.0	487.0	492.5	555.6	75.0	450.0	4.7	2.96	457.84	457.84
22A	20.0	500.0	487.0	490.6	551.1	75.0	450.0	4.5	2.83	442.06	424.01
23A	20.0	500.0	490.0	496.7	547.7	75.0	450.0	4.9	3.08	412.74	412.74
24A	20.0	525.0	510.0	512.9	559.4	75.0	475.0	4.7	2.96	354.10	354.10
25C NR	20.0	550.0	535.0	0	0	75.0	500.0	4.7	2.96	0	0
26A 550	20.0	500.0	483.0	488.2	546.9	75.0	450.0	4.7	2.96	430.78	424.01
27A 550	20.0	350.0	346.0	360.0	471.4	75.0	300.0	5.1	3.21	866.07	624.74
28A 475	20.0	350.0	344.0	353.1	480.4	75.0	300.0	5.1	3.21	899.90	658.57
29A 475	20.0	500.0	488.0	495.1	550.2	75.0	450.0	5.3	3.34	442.06	401.46
30A	30.0	350.0	345.0	360.2	525.4	75.0	300.0	14.8	13.54	945.01	762.32
31A	30.0	360.0	354.0	368.9	490.0	75.0	310.0	5.0	4.57	922.45	658.57
32A	30.0	400.0	392.0	404.8	510.1	75.0	350.0	4.9	4.48	796.15	613.47
33A AC	30.0	400.0	394.0	409.5	507.3	75.0	350.0	4.7	4.30	771.34	636.02
34A	30.0	400.0	394.0	411.8	508.5	75.0	350.0	5.1	4.67	802.92	595.42
35A	30.0	425.0	405.0	417.8	530.6	75.0	375.0	13.6	12.44	633.76	611.21
36A	30.0	450.0	438.0	449.2	530.3	75.0	400.0	4.9	4.48	617.98	539.04
37A	30.0	475.0	469.0	472.3	551.4	75.0	425.0	5.1	4.67	543.55	480.40
38A	30.0	500.0	486.0	497.2	553.1	75.0	450.0	5.3	4.85	464.61	446.57
39A	30.0	500.0	487.0	494.7	557.9	75.0	450.0	4.9	4.48	480.40	457.84
40A	30.0	500.0	488.0	495.7	547.4	75.0	450.0	3.3	3.02	480.40	437.55
41A	30.0	520.0	509.0	516.4	560.7	75.0	470.0	3.0	2.74	457.84	408.23
42 ST	50.0	375.0	370.0	0	0	75.0	325.0	5.0	7.38	945.01	0
43A	50.0	380.0	374.0	397.7	550.8	75.0	330.0	13.3	19.64	978.84	755.56
44A	50.0	400.0	394.0	405.9	525.4	75.0	350.0	5.1	7.53	841.26	669.85
45A	50.0	400.0	394.0	403.2	572.1	75.0	350.0	13.3	19.64	915.69	744.28
46A	50.0	400.0	395.0	412.3	555.2	75.0	350.0	14.0	20.67	859.30	699.17
47A	50.0	425.0	417.0	431.4	540.3	75.0	375.0	5.1	7.53	796.15	654.06
48A	50.0	430.0	420.0	428.1	544.6	75.0	380.0	5.1	7.53	802.92	606.70
49A	50.0	450.0	443.0	451.7	555.3	75.0	400.0	4.7	6.94	717.21	624.74
50A	50.0	475.0	464.0	474.1	561.7	75.0	425.0	4.7	6.94	629.25	579.64
51A	50.0	475.0	467.0	478.9	564.5	75.0	425.0	5.1	7.53	658.57	543.55
52A	50.0	500.0	481.0	492.9	561.0	75.0	450.0	3.9	5.76	539.04	539.04
53C	50.0	525.0	508.0	515.7	574.5	75.0	475.0	3.5	5.17	480.40	469.12
54A 550	50.0	400.0	394.0	406.0	557.7	75.0	350.0	14.0	20.67	852.54	699.17
55B NR	60.0	375.0	368.0	0	0	75.0	325.0	14.0	25.62	0	0
56B	60.0	380.0	373.0	394.7	560.2	75.0	330.0	14.0	25.62	978.84	773.60
57B	60.0	380.0	373.0	400.5	547.2	75.0	350.0	12.5	22.87	911.18	762.32
58B	60.0	400.0	393.0	414.9	562.1	75.0	350.0	13.0	23.79	904.41	721.72
59A	60.0	450.0	439.0	446.0	544.5	75.0	400.0	3.6	6.59	692.40	584.15
60A	80.0	450.0	440.0	455.4	564.4	75.0	400.0	4.3	9.95	848.03	640.53
61A	100.0	450.0	440.0	455.2	563.5	75.0	400.0	4.1	12.36	836.75	654.06
62A	100.0	450.0	440.0	451.7	577.2	75.0	400.0	4.3	12.96	829.98	762.32
63B	100.0	475.0	458.0	463.8	568.4	75.0	425.0	3.9	11.76	717.21	581.89
64B COD	40.0	400.0	393.0	409.9	548.0	75.0	350.0	14.0	16.74	841.26	669.85
65A COD	40.0	400.0	394.0	402.2	508.5	75.0	350.0	4.3	5.14	814.20	566.10
66A COD	40.0	450.0	440.0	453.3	530.9	75.0	400.0	4.3	5.14	658.57	525.51
67A COD	40.0	500.0	487.0	494.0	551.8	75.0	450.0	3.5	4.19	496.19	446.57
68 ST	30.0	350.0	344.0	0	0	75.0	300.0	14.0	12.81	0	0
69A STR	30.0	400.0	394.0	419.3	494.5	75.0	350.0	4.5	4.12	784.88	554.83
70A STR	30.0	400.0	394.0	406.5	504.3	75.0	350.0	4.7	4.30	778.11	572.87

Al-Li-Mg-Cu

RUN CODES	EXT RATIO	FURNACE TEMP	INITIAL TEMP	PEAK TEMP	FINAL TEMP	BILLET LENGTH	CTNR TEMP	RAM SPEED	STRAIN RATE	MAX PRESSURE	MIN PRESSURE
									-1	2	2
		DEG.C	DEG.C	DEG.C	DEG.C	MMS	DEG.C	MMS/S	SEC	MN/M	MN/M
01 ST	10.0	300.0	296.0	0	0	75.0	250.0	11.0	6.86	956.29	0
02A	10.0	325.0	319.0	333.6	478.0	75.0	275.0	14.8	7.25	904.41	636.02
03A	10.0	325.0	322.0	335.0	484.9	75.0	275.0	14.8	7.25	922.45	647.30
04B	10.0	400.0	390.0	398.6	484.0	75.0	350.0	12.8	6.27	534.53	457.84
05A	10.0	400.0	394.0	397.4	464.3	75.0	350.0	3.3	1.62	566.10	469.12
06A	10.0	450.0	438.0	443.8	495.4	75.0	400.0	3.5	1.71	475.89	405.97
07A	10.0	475.0	461.0	467.5	503.8	75.0	425.0	3.1	1.52	405.97	354.10
08A	10.0	500.0	480.0	484.4	519.7	75.0	450.0	3.1	1.52	360.86	327.03
09A	10.0	500.0	485.0	489.0	521.0	75.0	450.0	3.5	1.71	327.03	320.27
10C	10.0	525.0	510.0	511.7	537.9	75.0	475.0	3.3	1.62	279.67	279.67
11A	10.0	400.0	393.0	406.6	513.6	100.0	350.0	14.0	6.86	692.40	487.16
12A	10.0	400.0	391.0	400.4	479.6	95.0	350.0	4.7	2.30	654.06	435.29
13A	10.0	400.0	391.0	402.5	476.8	95.0	350.0	4.7	2.30	658.57	412.74
14A	10.0	400.0	392.0	403.2	488.2	95.0	350.0	4.7	2.30	703.68	469.12
15A	10.0	400.0	393.0	403.1	477.2	95.0	350.0	4.7	2.30	636.02	424.01
16A	10.0	400.0	394.0	403.4	481.0	95.0	350.0	4.7	2.30	654.06	430.78
17A	20.0	325.0	317.0	333.4	504.7	75.0	275.0	15.0	9.44	1014.93	751.04
18B	20.0	350.0	344.0	357.1	491.3	75.0	300.0	12.4	7.80	811.94	651.81
19B	20.0	350.0	344.0	351.3	508.9	75.0	300.0	10.0	6.29	908.92	712.70
20B AC	20.0	350.0	344.0	0	0	100.0	300.0	10.0	6.29	169.15	0
21A	20.0	375.0	368.0	379.4	482.9	75.0	325.0	4.7	2.96	807.43	584.15
22C	20.0	400.0	392.0	401.8	503.9	75.0	350.0	11.0	6.92	611.21	563.85
23A	20.0	400.0	393.0	409.1	492.9	75.0	350.0	4.7	2.96	728.49	554.83
24A	20.0	425.0	412.0	419.7	504.0	75.0	375.0	4.7	2.96	640.53	498.44
25A	20.0	450.0	437.0	442.5	516.7	75.0	400.0	3.5	2.20	545.80	545.80
26A AC	20.0	450.0	437.0	0	0	75.0	400.0	3.5	2.20	0	0
27A	20.0	450.0	438.0	445.1	523.0	75.0	400.0	4.5	2.83	588.66	498.44
28A	20.0	450.0	438.0	445.1	521.4	75.0	400.0	4.3	2.71	584.15	498.44
29A	20.0	450.0	440.0	447.8	518.1	75.0	400.0	4.5	2.83	554.83	480.40
30C	20.0	475.0	460.0	464.1	535.5	75.0	425.0	5.1	3.21	505.21	435.29
31C	20.0	500.0	485.0	488.5	545.3	75.0	450.0	4.5	2.83	430.78	390.18
32 ST	30.0	350.0	344.0	0	0	75.0	300.0	10.0	9.15	1030.71	0
33A	30.0	375.0	366.0	377.1	502.3	75.0	325.0	4.7	4.30	915.69	654.06
34A	30.0	400.0	394.0	406.8	486.2	75.0	350.0	2.7	2.47	791.64	550.32
35A	30.0	425.0	417.0	427.6	526.8	75.0	375.0	4.7	4.30	751.04	579.64
36A	30.0	440.0	429.0	436.9	509.0	75.0	390.0	3.1	2.84	654.06	475.89
37C	30.0	450.0	438.0	443.9	525.9	75.0	400.0	4.0	3.66	586.40	545.80
38B	40.0	400.0	391.0	398.9	504.6	75.0	350.0	3.3	3.95	789.39	658.57
39B	40.0	380.0	370.0	384.6	506.0	75.0	330.0	4.0	4.78	906.67	728.49
40 ST	50.0	380.0	363.0	0	0	75.0	330.0	4.0	5.91	0	0
41B	50.0	400.0	393.0	409.3	524.0	75.0	350.0	4.3	6.35	899.90	676.62
42B	50.0	400.0	394.0	406.7	550.7	75.0	350.0	4.7	6.94	899.90	890.88
43A	50.0	425.0	416.0	427.1	537.7	75.0	375.0	5.6	8.27	784.88	595.42
44A	50.0	440.0	422.0	432.0	537.1	75.0	390.0	3.1	4.58	825.47	617.98
45C	50.0	440.0	429.0	438.3	531.1	75.0	390.0	3.1	4.58	766.83	579.64
46C	50.0	450.0	439.0	447.9	537.0	75.0	400.0	3.7	5.46	733.00	516.48
47C	80.0	430.0	422.0	435.5	533.5	75.0	380.0	3.1	7.17	836.75	629.25
48C	80.0	430.0	420.0	432.4	553.3	75.0	380.0	4.7	10.87	877.35	647.30
49C	100.0	420.0	410.0	420.6	536.1	75.0	370.0	3.1	9.35	877.35	699.17
50C	100.0	430.0	420.0	433.5	534.1	75.0	380.0	3.1	9.35	836.75	640.53
51A COD	40.0	400.0	394.0	407.1	493.1	75.0	350.0	3.1	3.71	814.20	543.55
52A COD	40.0	400.0	394.0	406.9	495.6	75.0	350.0	3.1	3.71	802.92	584.15
53A COD	40.0	425.0	416.0	424.5	511.7	75.0	375.0	3.5	4.19	703.68	554.83
54A COD	40.0	440.0	428.0	439.3	518.7	75.0	390.0	3.1	3.71	699.17	550.32
55A COD	40.0	440.0	429.0	437.0	518.4	75.0	390.0	3.3	3.95	665.34	539.04
56A STR	30.0	400.0	395.0	403.2	496.7	75.0	350.0	3.1	2.84	818.71	550.32

Al-Li-Mg 2" Diameter

RUN CODES	EXT RATIO	FURNACE TEMP	INITIAL TEMP	PEAK TEMP	FINAL TEMP	BILLET LENGTH	CTNR TEMP	RAM SPEED	STRAIN RATE	MAX PRESSURE	MIN PRESSURE
		DEG.C	DEG.C	DEG.C	DEG.C	MMS	DEG.C	MMS/S	-1 SEC	2 MN/M	2 MN/M
01A	6.0	225.0	223.0	267.2	512.4	100.0	175.0	14.0	4.44	1827.43	894.19
02A	6.0	250.0	248.0	277.3	429.3	100.0	200.0	12.0	3.80	1210.18	605.24
03 ST	23.0	250.0	248.0	0	0	100.0	200.0	14.0	14.14	1776.67	0
04A	23.0	275.0	273.0	302.2	561.2	100.0	225.0	14.0	14.14	1612.67	1038.67
05A AC	23.0	275.0	272.0	310.2	548.9	100.0	225.0	15.0	15.15	1581.43	995.71
06A 500	23.0	275.0	273.0	318.9	542.2	100.0	225.0	15.0	15.15	1518.95	1058.19
07A	23.0	300.0	298.0	333.0	505.8	100.0	250.0	5.0	5.05	1448.67	902.00
08A	23.0	350.0	348.0	374.5	504.4	100.0	300.0	5.0	5.05	1097.24	761.43
09A	23.0	400.0	396.0	412.2	523.0	100.0	350.0	5.0	5.05	894.19	636.48
10A	23.0	450.0	444.0	453.7	554.2	100.0	400.0	5.0	5.05	714.57	632.57
11A AC	23.0	450.0	438.0	449.5	535.8	100.0	400.0	5.0	5.05	636.48	585.71
12B	23.0	500.0	485.0	490.2	575.4	100.0	450.0	5.0	5.05	574.00	523.24
13B AC	23.0	500.0	482.0	489.1	565.6	100.0	450.0	5.0	5.05	523.24	515.43
14B 500	23.0	500.0	485.0	493.8	574.0	100.0	450.0	5.0	5.05	585.71	523.24
15A	35.0	350.0	347.0	366.6	517.0	100.0	300.0	5.0	7.35	1179.24	738.00
16A	35.0	450.0	438.0	451.3	558.7	100.0	400.0	5.0	7.35	800.48	616.95
17A NR	58.0	350.0	347.0	0	0	100.0	300.0	5.0	11.65	0	0
18A	58.0	450.0	432.0	448.2	574.5	100.0	400.0	5.0	11.65	894.19	687.24

2014

RUN CODES	EXT RATIO	FURNACE TEMP	INITIAL TEMP	PEAK TEMP	FINAL TEMP	BILLET LENGTH	CTNR TEMP	RAM SPEED	STRAIN RATE	MAX PRESSURE	MIN PRESSURE
		DEG.C	DEG.C	DEG.C	DEG.C	MMS	DEG.C	MMS/S	-1 SEC	2 MN/M	2 MN/M
01A	10.0	300.0	296.0	309.3	420.3	95.0	250.0	14.0	6.86	699.17	527.76
02A	10.0	500.0	487.0	488.0	529.5	95.0	450.0	5.0	2.45	304.48	297.71
03A STR	30.0	400.0	393.0	401.7	484.3	95.0	350.0	5.0	4.57	606.70	487.16
04A COD	40.0	450.0	438.0	0	0	95.0	400.0	5.0	5.98	0	0

APPENDIX TWO

THE DERIVATION OF THE STRESS INTENSITY FACTOR FOR THE DCB SPECIMEN

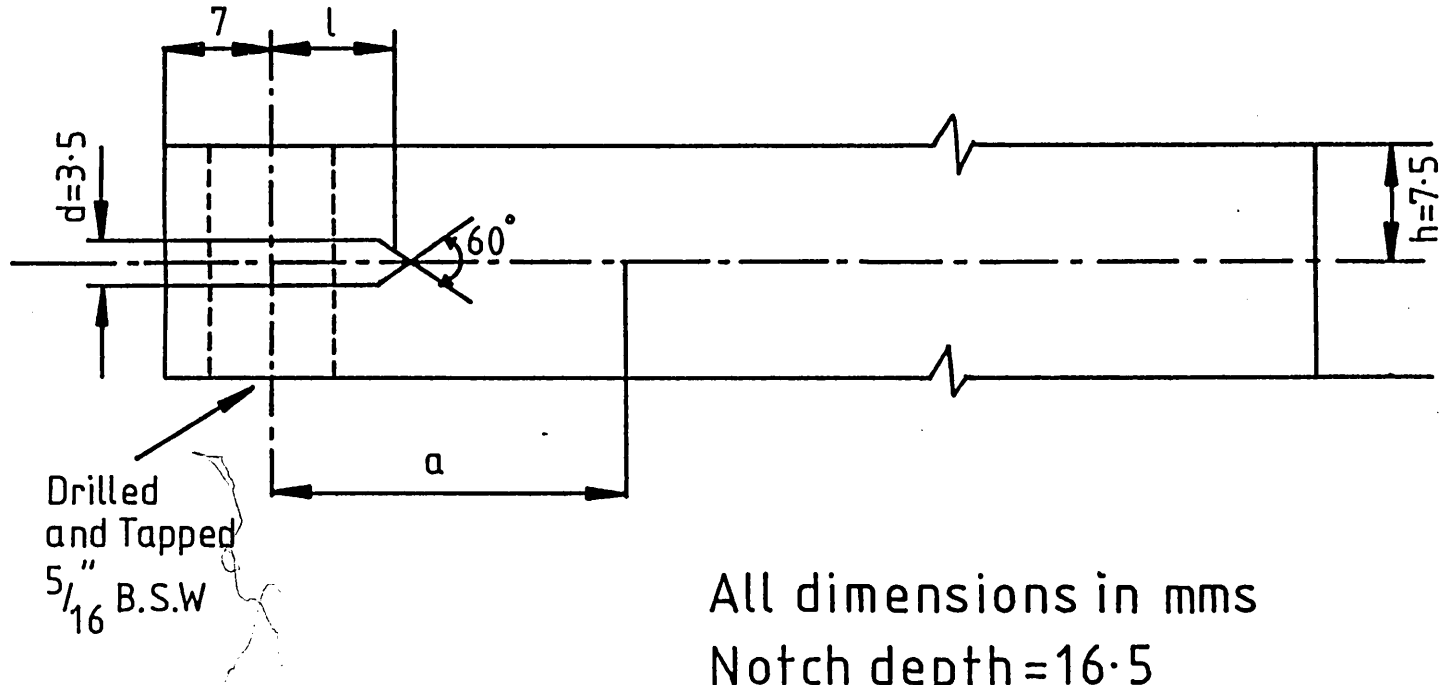

All dimensions in mms
Notch depth = 16·5
Length = 125

Fig A1 The D.C.B specimen

The stress intensity factor at the tip of a loaded DCB specimen may be calculated using the following standard equations:

$$K_1 = (GE)^{\frac{1}{2}} \qquad \text{(A-1)}$$

$$G = (P^2/2b)dc/da \qquad \text{(A-2)}$$

where

- G = strain energy release rate
- E = elastic modulus
- P = load
- b = specimen thickness
- a = crack length measured from load point
- c = specimen compliance for crack length a.

The term dc/da may be calculated from a compliance versus crack length curve or alternatively a standard expression for the compliance of a DCB specimen can be used;

$$c = (2/3EI)[(a + a_o)^3 + h^2a] \qquad \text{(A-3)}$$

where

- I = moment of inertia of one of the testpiece arms $= (bh^3/12)$
- h = half the test piece height
- a_o = empirical rotation correction $= 0.6h$

The load P is given by:

$$P = (v/c) \qquad \text{(A-4)}$$

where v is the total deflection of the two arms of the testpiece at the load point.

Now by substitution into equation (A-1) K_1 can be written:

$$K_1 = (v/c)[(E/2b)dc/da]^{\frac{1}{2}} \qquad \text{(A-5)}$$

In the case of the DCB specimen used here (Fig. A1) the slit width d is very wide compared to the arm thickness and v will be greater than for specimens with narrow slits, giving erroneously high K_1 values. Therefore it is necessary to include an expression to take account of the slit dimensions.

The effective arm length is a, but this consists of two portions; the first of length 1 and height 5.9 mm, and the second of length a - 1 and height 7.5 mm. In order to determine the contribution of each portion to the total deflection v, it was assumed that each half was of height h but of modulus E for the wider portion and E_1 for the other.

Simple beam theory for a rectangular section cantilever beam indicates that:

$$E_1 = \frac{Eh_1^3}{h^3} = 0.49\ E = nE. \qquad \text{(A-6)}$$

By assuming the arms are in uniaxial tension an effective average modulus can be calculated by addition of the two strain terms giving

$$E' = naE/[1(1.0-n) + na] \qquad \text{(A-7)}$$

For this specimen $n \sim 0.5$
so this may be approximated to:

$$E' = aE/(a + 1) \qquad \text{(A-8)}$$

Substituting E' for E in equation (A-3) gives

$$c = (2/3EI)[a^3 + (3a_o + 1)a^2 + (3a_o\ (a_o + 1) + h^2)a + 1a_o{}^3a^{-1.0} + a_o{}^3 + 1(h^2 + 3a_o{}^2)] \qquad \text{(A-9)}$$

Differentiating gives:

$$dc/da = (2/3EI)[3a^2 + 2a\ (3a_o + 1) + 3a_o\ (a_o + 1) + h^2 - a_o{}^3\ 1a^{-2}] \qquad \text{(A-10)}$$

Now equations (A-9) and (A-10) may be substituted into equation (A-5) to yield K_1.

Acknowledgements

I should like to express my sincere thanks to Professor T. Sheppard for initiating the project and for his subsequent advice and guidance throughout the work.

I am grateful to my industrial sponsors, Alcan International, for their financial support and supply of materials. I am also indebted to the staff at Chalfont Park and Banbury laboratories for their advice and assistance with experimental work. In particular, I wish to thank Mr A. Gray for his help with the corrosion work and Dr W. Miller for his help with the work on the chill cast alloys.

Many thanks to all members of the John Percy Group, technical staff and students, for their advice and assistance with practical work, and finally thanks to all JPDC members.